Characterisation of mycobacterial amidases and their role in bacterial growth and physiology

Sibusiso Senzani (0603371N)

A thesis submitted to the Faculty of Health Science, University of the Witwatersrand, Johannesburg, in fulfilment of the requirements for the degree of Doctor of Philosophy on medicine.

Johannesburg, 2018

DECLARATION

I, Sibusiso Senzani declare that this Thesis is my own work. It is being submitted for the Degree of Doctor of Philosophy in Medicine at the University of the Witwatersrand, Johannesburg. It has not been submitted before for any degree or examination at this or any other University.

Sibusiso Senzani

4th day of June 2018

DEDICATIONS

I would like to dedicate this to 8 very important people in my life. My parents, Mahudi Senzani and Alpheus Senzani, for allowing me to be myself and never pressure me to follow the grain. My little sister Mbali Senzani, and cousin, 'Hloni' Segonyane for always reminding me that there are more important things in life than work. Finally my four closest friends Qiniso Pitse, Philane Ndaba, Mntimande Mbatha and Mawabo Msingaphantsi (collectively known as QPiTSM), You guys have been with me since the beginning of high school, and to this day, regardless of any life problems and issues, whenever we get together it seems like we are back in high school again and for that I thank you. Without any of these people I would not be where I am right now.

PRESENTATIONS FROM THIS DISSERTATION

Conference	: 4th biennial South African TB Conference
Presentation	: Oral
Year	: 2014
Achievement	: Discovery Health Clinical Excellence Award

Conference	: Wits University Cross-Faculty symposium
Presentation	: Oral
Year	: 2014
Achievement	: Best Research across All Faculties

Conference	: Wits University Health Sciences Research Day
Presentation	: Poster
Year	: 2014
Achievement	: Best poster presentation by a student

Conference	: Wits University Molecular Biosciences Research Thrust Symposium
Presentation	: Oral
Year	: 2014
Achievement	: First prize for an oral presentation

Conference	: Wits University Health Sciences Research Day
Presentation	: Oral
Year	: 2016
Achievement	: Best Oral presentation

ACKNOWLEDGEMENTS

I would like to thank my entire family for supporting me throughout this PhD

I would like to thank the South African Medical Research Council and the University of the Witwatersrand for the financial support offered throughout my studies, allowing me the opportunity to do this PhD

I would like to thank the South African National Research foundation, The Howard Hughes Medical Institute and the Swiss National Science Foundation for financial support and allowing me the opportunity to travel outside the country, not only expanding my understanding of science, but also my view of the world.

I would like to thank Prof Eric Betzig for hosting me and allowing me the opportunity to work at his lab. Dr Dong Li for all your help using the TIRF microscope and analysing data

I would like to thank Prof John McKinney and Dr Neeraj Dhar for hosting me at your lab and all your help; offering advice on how to conduct fluorescent microscopy, offering strains and vectors to advance the study to a level at which it would be difficult to take on my own, all the help conducting live cell microscopy and willingness to conduct movies for us as, it would not be reasonable to fly to Switzerland every time a new strain was made.

I would like to thank the Microscopy and Microanalysis Unit at the University of Cape Town for always having you doors open for us. Whenever I need to conduct Scanning or Transmission electron microscopy you always made the equipment available and allowed me the ability to work after hours for as long as I needed to get my work done.

I would like to thank Prof Bavesh Kana for your guidance, support, supervision and patience. I am not the most forthcoming with regards to reporting the work I am conducting and you understood that and allowed me to ‘do my thing’, thank you.

I would like to thank the senior staff and my colleagues at the CBTBR for the support, assistance and laughter, it made this process more enjoyable and offered me the opportunity to meet a group of people I am sure I will remain friends with fro a long time.

Finally I would like to thank Nicole ‘Nikki” Cardoso, you have been someone I can bounce all my crazy ideas off and you never shut them down. We’ve had some stimulating scientific

conversations and many ideas we never had the chance to implement. I would also like to thank you for being a friend and someone who was down in the trenches with me during this long battle. There have been many times I thought this was not worth it but you helped me keep going.

ABSTRACT

The genus *Mycobacterium* represents a complex family containing a number of clinically significant pathogens such as *Mycobacterium ulcerans*, *Mycobacterium leprae* and *Mycobacterium tuberculosis* (Mtb), the latter known to be the etiological agent of tuberculosis (TB). TB remains a global health issue, claiming approximately two million lives annually, with much of this burden being carried in the developing world in countries such as India and South Africa. The emergence of drug-resistant strains of Mtb and the synergistic relationship between TB and HIV/AIDS has crippled efforts to eradicate this disease by rendering many of the current therapeutics ineffective. This has created an urgent need for new drugs with novel modes of action and in this regard, peptidoglycan (PG)-associated enzymes constitute attractive targets for drug development. This study focused on a group of PG hydrolysing enzymes, the *N*-acetylmuramyl-L-alanine amidases (amidases), which have been linked to a number of essential cellular processes including cell division, antibiotic tolerance and pathogenicity in other organisms. Using the gene sequences of previously characterised cell wall amidases as queries, our bioinformatics analysis revealed that Mtb and *Mycobacterium smegmatis* contained 4 amidases, designated *ami1-ami4*. Analysis of an *ami1* deficient *M. smegmatis* strain highlighted a role for this enzyme in cell division, cell elongation, cell shape maintenance and antibiotic tolerance. Deletion of *ami1* resulted in the formation of chains consisting of 3 to 8 cells in approximately 20 % of the bacterial population assessed. Growth in these chains was characterised by ectopic mis-localisation of DivIVA, which resulted in the formation of lateral branches and Y-formed cell division. Single-cell localisation of the β-sliding clamp (DnaN) and ParB, required for chromosome segregation, revealed that these ectopic branches were able to coordinate chromosome replication and partitioning. Additionally, increased cell permeability was noted in the Δ*ami1* strain, which was associated with increased antibiotic susceptibility. These cell division defects were not observed in the Mtb Δ*ami1* mutant. However, in this case, lateral growth appendages were observed under nutrient limited conditions. Deletion of *ami1* in Mtb also resulted in a reduction in bacterial persistence upon challenge with isoniazid. In contrast, loss of *ami4* in Mtb did not appear to have an impact on bacterial growth or survival rather, the mutant displayed increased survival under oxidative stress. The *ami2* gene has been predicted to be essential, a hypothesis that was confirmed herein through the generation of a merodiploid strain wherein *ami2* could be deleted. As such, characterisation of the role of Ami2 was conducted using a previously generated gene depletion

strain. Depletion of Ami2 resulted in retarded growth, altered colony morphology, defective sliding motility, the formation of short cells and cells which contain bulges at the pole. Single-cell time lapse microscopy revealed that depletion of *ami2* resulted in cessation of growth. Analysis of the localisation pattern of Ami2 revealed a polar localisation pattern, confirming a role for this enzyme in bacterial elongation. Collectively, these data highlight novel, specialist functions for mycobacterial amidases in cell elongation and division. The essentiality of Ami2 for mycobacterial growth also validates this enzyme as a possible drug target for TB.

PUBLICATIONS FROM THIS THESIS

MACHOWSKI, E. E., SENZANI, S., EALAND, C. & KANA, B. D. 2014. Comparative genomics for mycobacterial PG remodelling enzymes reveals extensive genetic multiplicity. *BMC Microbiology,* 14**,** 75.

SENZANI, S., LI, D., BHASKAR, A., EALAND, C., CHANG, J., RIMAL, B., LIU, C., KIM, S. J., DHAR, N. & KANA, B. 2017. An Amidase_3 domain-containing *N*-acetylmuramyl-L-alanine amidase is required for mycobacterial cell division. *Scientific Reports,* 7**,** 1140.

TABLE OF CONTENTS

LIST OF FIGURES

LIST OF TABLES

NOMENCLATURE

Δ	: Delta
µ	: Micro
Ω	: ohm
AAP	: Antarctic Alkaline Phosphatase
AIDS	: Acquired Immunodeficiency Syndrome
Ami	: Amidase
Amp	: Ampicillin
AmpK	: 5′ Adenosine monophosphate-activated protein kinase
Amp^R	: Ampicillin resistance
ATc	: Anhydrotetracycline
atg	: autophagy-related gene
b	: Bases
bp	: Base pairs
cDNA	: Complementary Deoxyribonucleic acid
CFU	: Colony Forming Units
CPS	: Chemiluminescent Peroxidase Substrate
CR	: Complementary Receptors
CSPD	: Disodium 2-chloro-5-(4-methoxyspiro (2-dioxetane-3,2 (2-dioxetane-3,2′-(5′-chloro)-tricyclo[3.3.1.1. 3, 7.]decan)-4-yl)-1-phenyl phosphate
CTAB	: Cetyltrimethylammonium bromide
DAP	: Diaminopimelic acid
DCO	: Double cross over
DDSA	: Dodecenyl Succinic Anhydride
DiG	: Alkali-labile digoxigenin
DMF	: Dimethylformamide
DMP	: Tris-2,3,6-(dimethylaminomethyl)phenol
DNA	: Deoxyribonucleic acid
dNTP	: Nucleoside triphosphates
DOTS	: Directly Observed Treatment Short course
EDTA	: Ethylenediaminetetraacetic acid
EMB	: Ethambutol
F	: farad
$FeSO_4.7H2O$	: Iron sulfate
Flu	: Influenza
g	: Grams
GlcNAc	: *N*-acetylglucosamine
GTP	: Guanosine triphosphate
h	: Hour
H_2O	: dihydrogen monoxide (water)
HCl	: Hydrochloric acid
HIV	: Human Immunodeficiency Virus
Hyg	: Hygromycin
Hyg^R	: Hygromycin resistant
INH	: Isoniazid
IRAK	: Interleukin-1 Receptor-Associated Kinase

Kan : Kanamycin
Kan^R : Kanamycin resistant
kb : kilobases
kbp : kilobase pairs
KOH : Potassium hydroxide
kV : kilovolts
l : litres
LA : Lysogeny Agar
lacZ : Gene encoding galactosidase
LB : Lysogeny Broth
LTBI : Latent tuberculosis infection
M : Molar
mA : milliamps
MAP : Mycolic acid-Arabinogalactan-PG
MDR : Multidrug-resistant
mg : milligrams
$MgCl_2$: Magnesium Chloride
MIC : Minimum Inhibitory Concentration
min : minutes
mJ : millijoules
ml : millilitres
MOPS : 3-(N-Morpholino) propanesulfonic acid
mRNA : messenger Ribonucleic acid
Mtb : *Mycobacterium tuberculosis*
mTOR : mammalian Target Of Rapamycin
MurNAc : *N*-acetylmuramic acid
n : nano
NaCl : Sodium Chloride
NaOH : Sodium hydroxide
nm : nanometres
NOD : Nucleotide-binding Oligomerisation Domain
OD : Optical density
PBP : Penicillin-binding Proteins
PBS : Phosphate Buffered Saline
PCR : Polymerase Chain Reaction
PGRP : PG Recognition Proteins
PNK : Polynucleotide Kinase
PVDF : Polyvinylidene fluoride
PZA : Pyrazinamide
qPCR : quantitative Polymerase Chain Reaction
R : Resistant
RBS : Ribosomal Binding Site
RD1 : Region of Difference 1
RIF : Rifampicin
RNA : Ribonucleic acid
RNI : Reactive Nitrogen Intermediates

ROI : Reactive Oxygen Intermediates
rpf : resuscitation promoting factor
rpm : Revolutions per minute
rsEGFP : reversibly switchable Enhanced Green Fluorescence Protein
rt : reverse transcriptase
sacB : Gene encoding levansucrase
SCO : Single cross over
sdH2O : Sterile distilled water
SDS : Sodium Dodecyl Sulfate
SEM : Scanning Electron Microscopy
SLR : Sequestosome 1/p62 Like Receptor
SSC : Saline Sodium Citrate
TB : Tuberculosis
TBE : Tris-Borate-EDTA
TBS : Tris-buffered saline
TBST : Tris-buffered saline with Tween20
TE : Tris-EDTA
TEM : Transmission Electron Microscopy
TIRAP : TIR domain-containing Adaptor Protein
TiRF : Total internal Reflection Fluorescence
TLR : Toll-Like Receptor
TNF : Tumor Necrosis Factor
TRAF : TNF Receptor Associated Factors
Tris : Tris (hydroxymethyl) aminomethane
Tween : Polyoxyethylene sorbitan monooleate
TY : Tryptone, Yeast Extract
U : Enzyme Unit
UTP : Uridine triphosphate
UV : Ultraviolet
V : Volts
v/v : Volume per volume
vanc : Vancomycin
VBNC : Viable but non culturable
w/v : Weight per volume
WHO : World Health Organisation
XDR : Extensively Drug-resistant
XDR-TB : Extensively Drug-resistant Tuberculosis
X-gal : 5-bromo-4-chloro-3-indolyl-D-thiogalactopyranoside

Chapter 1

1 The Tuberculosis (TB) Epidemic

1.1 Mankind's TB history

Throughout the existence of humanity, there has always been an invisible threat to the livelihood and survival of the race in the form of infectious diseases caused by fungi, viral agents or bacteria. This is evident by the numerous epidemics and pandemics, which have plagued mankind at one point or another (Karlen, 1996, Gottfried, 2010, Patterson and Pyle, 1991). Two such documented historic epidemics include the bubonic plague and the Spanish flu, which individually wreaked havoc in Europe in the 1300s and 1918-1920, respectively (Gottfried, 2010, Patterson and Pyle, 1991). Though these ultimately claimed millions of lives, both were cured and today remain effectively eliminated (Patterson and Pyle, 1991, Gottfried, 2010). In recent times, the emergence of the HIV/AIDS epidemic has garnered much attention as the latest in a long line of persistent threats. As before, humankind has managed to respond to these threats by mobilising global resources and cooperation. However, tuberculosis (TB) stands out as the one disease which has persisted throughout human history, with little hope of eradication.

TB, which is caused by infection with the bacterial agent *Mycobacterium tuberculosis* (Mtb), is an extremely successful infectious disease, which still claims approximately 1.5 million lives annually (WHO, 2016a). Early evidence of this disease has been confirmed through DNA analysis of bone samples belonging to the pre-pottery Neolithic civilisation, dating back 9 000 years (Hershkovitz et al., 2008). Furthermore, analysis of fauna from the Pleistocene age has indicated the presence of corrosive TB-type disease, suggesting the possible existence of TB for more than 20 000 years (Rothschild and Martin, 2003). These studies support the hypothesis that Mtb has co-evolved with human kind over centuries, which contributes towards its success as a pathogen today (Hershkovitz et al., 2008, Rothschild and Martin, 2003). One of the contributing factors to the current global burden of TB is the ability of the tubercle bacillus to generate diverse clinical outcomes in patients, ranging from active disease to latent infection (Lin and Flynn, 2010). Latent infection is an asymptomatic form of TB wherein the bacteria have been hypothesised to remain quiescent in the host, until conditions become favourable for growth. An example of this would be compromised host immunity (Lin and Flynn, 2010, Wayne, 1994). However, this hypothesis has been recently challenged by emerging data that suggest a dynamic host immune response during latent infection, suggesting that this form of disease is the result of a complex interplay between the bacterium and the host (Barry et al., 2009). Furthermore, the responsiveness of latently infected

individuals to isoniazid therapy also points to dynamic growth heterogeneity in the prevailing bacteria during latent infection (Semu et al., 2017).

Despite decades of effort to control TB through the use of combination chemotherapy and sanatoria, the World Health Organisation (WHO) was compelled to declare TB a global health emergency in 1993 (WHO, 2016a). This lead to increased basic and translational research and the introduction of policies, such as the directly observed treatment short course (DOTS), which aided in curbing the epidemic throughout the world (WHO, 2016a). Though globally successful, these policies have not had the desired effect in developing countries, primarily Africa and some parts of Asia, where the TB burden still remains unacceptably high (WHO, 2016a, WHO, 2016b). This can be attributed to a number of factors including a lack of infrastructure, shortage of trained staff, poor diagnostics, inadequate linkage to care, and the paucity of drugs. This prompted African nations to view TB as an emergency on the continent, in an attempt to increase political will and strengthen health systems to more effectively deal with TB (Chudi, 2010).

Another factor which has hampered the elimination of TB in Africa is the synergistic relationship between TB and HIV/AIDS. It is currently estimated that 1/3 of the world's population is infected with latent TB (WHO, 2016a, Lin and Flynn, 2010). In HIV-negative individuals, this poses a 5 – 10 % lifetime risk of reactivation to cause active TB disease (Aaron et al., 2004, McShane, 2005). In HIV-positive individuals, however, this risk increases exponentially to an annual risk of 7 to 10 % (McShane, 2005, Aaron et al., 2004). This is alarming, as currently Africa has the highest prevalence of incident HIV infection, with 4.5 % of the adult population (aged 15 - 49) currently infected with HIV/AIDS; significantly more than the second highest region (the Americas) and the global prevalence, at 0.5 and 0.8 %, respectively (Figure 1.1) (WHO, 2016b). As a result, the African HIV/AIDS problem has created a reservoir of people with a high risk of progressing to active TB, which will lead to an increase in incidence and mortality. Also, HIV-infected individuals have a greater risk of getting infected with TB due to their weakened immunity. Considering this, a more granular understanding of how these two diseases synergise will be important for the development of novel therapeutic interventions.

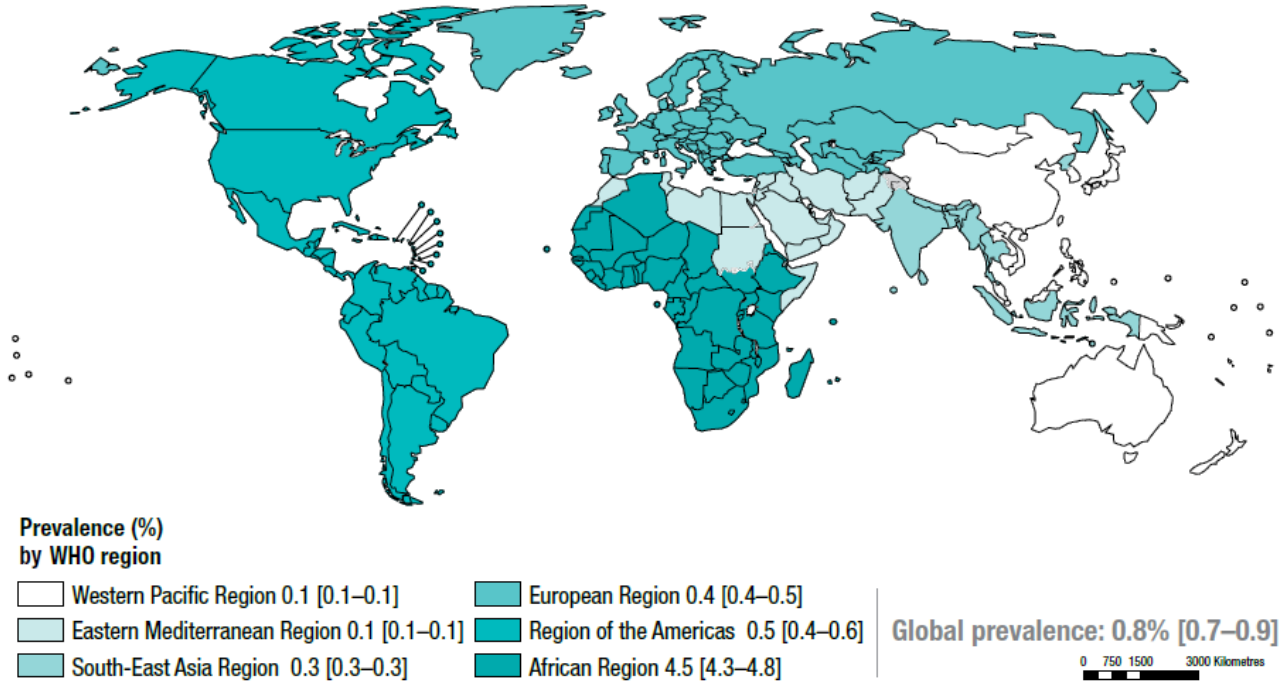

Figure 1.1: Global prevalence of HIV in individuals aged 15 – 49 years (taken from WHO, 2016b)**.**

1.2 Mtb infection, development of TB and the eternal arms race

One of the key components required for the elimination of TB is an understanding of how Mtb infects susceptible individuals and the processes that follow, ultimately resulting in disease. A vast amount of research has been conducted to try and answer this question. Infection by Mtb is a consequence of the inhalation of aerosolised droplets, which contain tubercle bacilli (Wells, 1934, WHO, 2016a, Smith, 2003). These bio-aerosols are expelled by individuals presenting with active TB disease through coughing, talking or heavy breathing (Jones-López et al., 2013). The precise parameters, with regards to the inoculum size (which include the aerosol size and the number of bacilli), necessary to yield successful infection are still unclear. Much attention has been directed to defining the size of an effective bio-aerosol. Research conducted in the 60's and 70's suggested the optimal size for an aerosol destined for the alveolar space is smaller than 5 µm, containing 1 to 3 bacilli (Grosset, 2003, Wells, 1934). The production of such aerosols containing Mtb was further confirmed in the 21st century (Jones-López et al., 2013, Wurie et al., 2016). Furthermore, an increase in the production of aerosols in the optimal range was observed in individuals with active pulmonary TB, when compared to individuals with latent TB (Wurie et al., 2016). The minimum size of these aerosols and diversity of clinical outcomes associated with them has been

difficult to replicate in most small animal models (Orme and Gonzalez-Juarrero, 2007). A recent study assessing transmission of TB through aerosols in households was able to identify a culturable Mtb concentration threshold required for the transmission of TB in the household. It was shown that individuals expelling 10 or more colony forming units (CFU) per cough were more likely to transmit TB to their close contacts when compared to individuals with less than 10 (Jones-López et al., 2013). The question of whether repeated exposure to bio-aerosols is required, or determines trajectory of infection and disease, remains unanswered.

Once these aerosols reach the intended location, the bacilli are released and phagocytised by alveolar macrophages (Smith, 2003). This process is regulated by interactions between Mtb and a number of essential macrophage borne cell surface receptors (Smith, 2003, Houben et al., 2006, Schlesinger, 1993, Gaynor et al., 1995, Ferguson et al., 1999). These receptors have been shown to either promote or repress the phagocytosis of foreign elements. In the case of Mtb, adhesion and subsequent phagocytosis appears to be regulated by mannose receptors, complementary receptors (CR1, CR3 and CR4), human toll-like receptor 2 (TLR2) and surfactant protein A and D. With the exception of surfactant protein D, these receptors have been shown to promote adhesion (Smith, 2003, Houben et al., 2006). Inhibition of the mannose and complementary receptors resulted in a significant reduction of the adhesion potential of Mtb (Schlesinger, 1993). Additionally, the mannose receptors appear to promote the adhesion of virulent strains of Mtb, as repression of this receptor did not affect the phagocytosis of the avirulent H37Ra or that of heat-killed mycobacterial strains (Schlesinger, 1993). Surfactant protein A, functions as an enhancer for Mtb adhesion. Elevated levels of this glycopeptide led to an increase in phagocytised Mtb. However, the removal of this protein did not diminish phagocytosis, indicating it is not an essential adhesion protein and that this is a multifactorial process (Gaynor et al., 1995). Furthermore, the lack of a mannose receptor in the presence of elevated surfactant protein A, phenocopied the mannose receptor suppression phenotype, indicating surfactant protein A activity is dependent on the mannose receptor and suggesting that it enhances the activity of the receptor (Gaynor et al., 1995). This, however, seems to have an antagonistic function to that of surfactant protein D, which reduces the level of adhesion, by binding directly to Mtb lipoarabinomannan, preventing the association of bacilli with mannose receptors (Ferguson et al., 1999). Another receptor which plays an important role not only in the adhesion of Mtb but also the immunological cascade which follows is the TLR2 receptor, which will be discussed in-depth, later.

Following phagocytosis, Mtb is enclosed within a lipid containing vacuole called a phagosome, which serves to contain the infecting agent (Smith, 2003). Under ordinary conditions, this combines with a secondary vacuole (the lysosome), containing lytic enzymes, to form the phagolysosome (Fairn and Grinstein, 2012). This combined vacuole exerts unfavourable conditions on the invading bacilli, possessing elements such as toxic reactive oxygen and nitrogen intermediates (ROI and RNI) and lytic enzymes, which serve to eliminate bacteria (Ehrt and Schnappinger, 2009, Fairn and Grinstein, 2012). In the case of Mtb, it is well-accepted that the bacterium prevents the maturation of the phagosome and the ultimate production of the phagolysosome, by inhibiting the fusion of the phagosome to the lysosome (Ehrt and Schnappinger, 2009). This results in formation of moderately acidic conditions, containing ROI, wherein Mtb can survive and propagate (Ehrt and Schnappinger, 2009). Whilst it is generally accepted that tubercle bacteria replicate in the arrested phagosome, recent studies have shown the presence of Mtb in the cytosolic space, suggesting that bacteria escape the phagosomal vacuole (van der Wel et al., 2007, Smith et al., 2008). It was previously thought the bacterium continues to propagate, resulting in the ultimate eruption of the phagosome and subsequent release of the bacterial agents into the cytoplasm. In addition, secreted factors such as ESAT-6 and CFP-10 have been shown to be important for colonisation of the macrophages (Smith et al., 2008).

ESAT-6 and CFP-10 are immunogenic, virulence factors located in the Region of Difference 1 (RD1) (Guinn et al., 2004, Tan et al., 2006). These are released by the bacterium and play a crucial role in the pathogenicity of mycobacteria (Xu et al., 2007, Guinn et al., 2004). Previously, it was postulated that these components produce nano pores on the phagosome membrane, creating channels which can be used for the extrusion of signalling molecules and recruitment of nutrients required for growth (Smith et al., 2008). This hypothesis was proven incorrect as this pore forming activity was shown to be a by-product of residual detergent remaining from the enzyme preparation (Conrad et al., 2017). Subsequent work has revealed a more elaborate network of processes controlled by these components, which leads to the release of infectious mycobacterial agents in the alveolar space, primed for the infection of healthy macrophages (Smith et al., 2008, Derrick and Morris, 2007). The first step of this model requires the release of mycobacteria from the phagosome to the cytosol. The exact mechanism through which ESAT-6 and CFP-10 exert this function is unknown. However, it has been shown that the absence of either results in abrogation of cytosolic translocation (Smith et al., 2008). It is currently unclear whether mycobacteria

continue to propagate in the cytoplasm. The presence of the bacterial agents in the cytoplasm leads to apoptosis and ultimately the release of infectious agents into the alveolar space (Derrick and Morris, 2007). This apoptotic process seems to be reliant on the release of ESAT-6 and CFP-10 into the cytoplasm (Derrick and Morris, 2007). It has been shown that treatment of macrophage cells with exogenous ESAT-6 leads to the increased expression of various caspases and ultimate death of the cell (Derrick and Morris, 2007). Though escape to the cytoplasm prevents any phagosome associated killing of Mtb, there are mechanisms which the macrophage can use to kill cytosolic bacilli, an example of these is autophagy.

Autophagy is the process responsible for the delivery of cytosolic elements to the lysosome for degradation (Deretic, 2014). This process is generally utilised as a quality and quantity control mechanism, tasked with the removal of defective elements such as misfolded proteins, deficient mitochondria and protein aggregates (Deretic, 2014). Autophagy can be further classified into two standard forms; bulk and selective. Bulk autophagy is a process that primarily occurs during starvation (Deretic, 2014, Bento et al., 2016). This results in the bulk degradation of cellular components, leading to the release of energy, through lipolysis and amino acids, which can be used for protein synthesis (Deretic, 2014, Bento et al., 2016). Selective autophagy, as the name indicates, is driven by the tagging of substrates, sequestered for degradation (Deretic, 2014, Deretic et al., 2013, Zaffagnini and Martens, 2016). In the case of bacteria, autophagy is initiated by the ubiquitination of the bacterial element by the E3 ligase; this is followed by the recognition of ubiquitin by Sequestosome 1/p62 like receptors (SLRs) (Ponpuak et al., 2010, Bento et al., 2016, Zaffagnini and Martens, 2016). This results in the recruitment of autophagy-related gene (*atg8*) product, LC3, leading to further recruitment of subsequent *atg* gene products responsible for the formation of a lipid membrane (Ponpuak et al., 2010, Deretic et al., 2013, Bento et al., 2016, Zaffagnini and Martens, 2016). This is followed by fusion of the autophagosome and lysosome, producing the autophagolysosome and subsequent degradation of the bacterial agent (Deretic et al., 2013, Ponpuak et al., 2010, Bento et al., 2016, Zaffagnini and Martens, 2016).

Like many other host-derived antimicrobial processes, mycobacteria have devised mechanisms to evade autophagy. One of these mechanisms is the activation of mTOR. The initiation of the autophagy process is regulated by two essential kinases (AMPK and mTOR) through the phosphorylation of the autophagy-initiating kinase Ulk1 (Kim et al., 2011). Phosphorylation of

Ulk1 by AMPK leads to the initiation of autophagy and phosphorylation by mTOR leads to the inhibition of autophagy (Kim et al., 2011). The second mechanism utilised by Mtb to avert autophagy is the accumulation of intracellular lipid droplets. Infection of host macrophages leads to reprogramming of cellular processes, which results in an increase in the production of lipid droplets (Russell et al., 2009). These can be used by Mtb as a nutrient source. The influx of lipids can also serve a secondary function, which is the inhibition of the macrophage autophagy pathway (Singh et al., 2009). These and relates studies illustrated that although the human immune system has devised methods to deal with Mtb, it appears the pathogen has developed specific countermeasures to inhibit these. This metabolic flexibility in the pathogen has made the development of drugs to combat this bacterium challenging. As such, the history of TB drug development is filled with short term successes, which are constantly threatened by the emergence of drug-resistant TB.

1.3 The history of TB and drugs

Drug development for TB can be described as a never-ending arms race as the tubercle bacillus is able to readily evolve resistance to current and newer treatments. Since the discovery of antibiotics, the search for the elusive "magic bullet" to try to solve this age-old problem has been ongoing. Currently, the treatment of drug-susceptible TB is a six month antibiotic regimen, which consists of 4 antibiotics (WHO, 2016a). The regimen involves the administration of rifampicin (RIF), isoniazid (INH), pyrazinamide (PZA) and ethambutol (EMB) for two months, followed by treatment with RIF and INH for a further four months. This long term treatment duration, together with the toxicity of some of the drugs, has created concerns regarding patient non-compliance (WHO, 2016a, Chudi, 2010). In developing countries, the lack of efficient health care systems, inappropriate infrastructure and poverty contribute to a lack of compliance to the TB treatment regimen as patients cannot access drugs and effective support systems (Chudi, 2010, Raviglione and Sulis, 2016). These issues contribute to the emergence and transmission of drug-resistant Mtb strains. Drug resistance TB remains a major problem, predominantly in the developing world (Figure 1.2) (WHO, 2016a). The occurrence of drug-resistant TB can be dated back to the introduction of the first TB drug, streptomycin in 1944 (Keshavjee and Farmer, 2012). Four years later streptomycin resistant Mtb was isolated from relapse patients treated with streptomycin (Crofton and Mitchison, 1948). This led to the discovery and introduction of new drugs into the regimen, resulting in the current combination treatment program for TB (Keshavjee and Farmer,

2012). Administration of multiple drugs reduces the chance for composite drug resistance to occur however, it's important to note that Mtb isolates resistant to individual drugs in the regimen have been identified since the introduction of these drugs into the clinical setting.

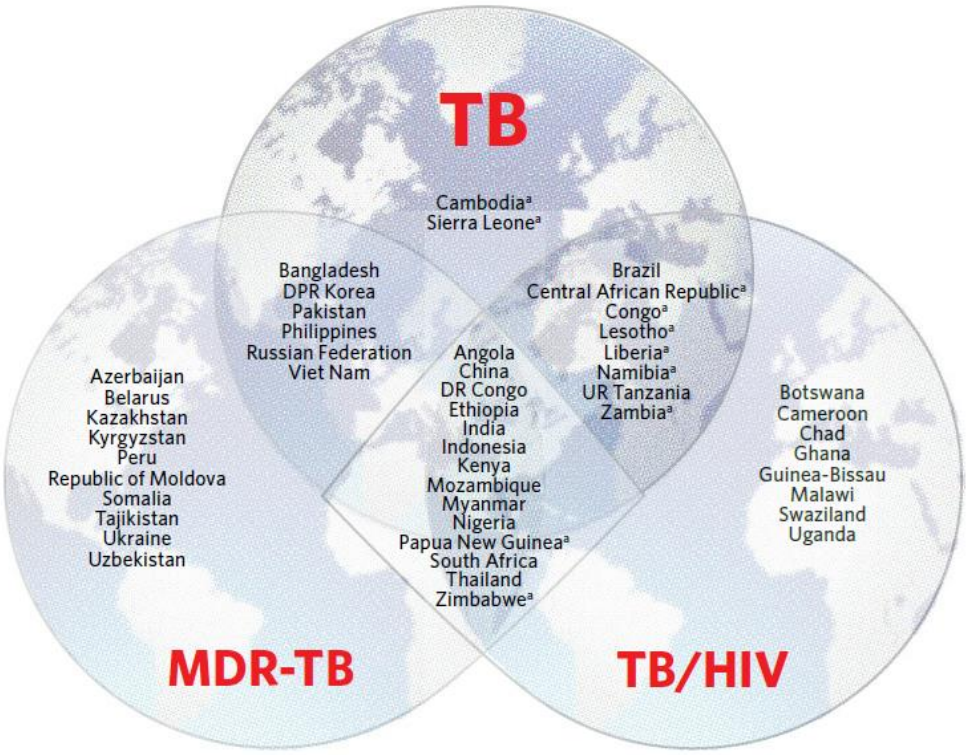

Figure 1.2: Venn diagram depicting countries with high burden TB infection as well as high burden MDR-TB and TB/HIV co-infection (Taken from WHO, 2016a).

In addition to mono-resistance, there has been a rapid emergence of strains resistant to two or more TB drugs, including multi-drug-resistant (MDR) and extensively drug-resistant (XDR) TB. This form of TB is characterised by infection with Mtb strains that are resistant to RIF and INH (MDR) or RIF, INH, an aminoglycoside and a fluoroquinolone (XDR) (WHO, 2016a). Given that RIF and INH are rendered ineffective, the treatment of MDR essentially involves the introduction of more drugs (including aminoglycosides and fluoroquinolone) initially not used due their low efficacy or high toxicity (WHO, 2016a). This highly toxic regimen is administered for 9 – 12 months, with significant compliance challenges (WHO, 2016a). XDR-TB presents further limitations in therapeutic options and treatment in this case is somewhat individualised with a variety of drugs that have limited efficacy (Zumla et al., 2013). Together, these challenges underscore the urgent

need for the development of novel TB treatments that have a shorter duration of treatment, a reduced pill burden and negligible side effects (WHO, 2016a).

The first new drug to be developed for TB over the past 60 years is bedaquiline, which has shown some promise in the treatment of MDR TB (Keshavjee and Farmer, 2012, Diacon et al., 2014). Furthermore, the repurposing of drugs, initially developed for the treatment of other conditions such as mental disorders and anti-inflammatory medications, for TB treatment has shown promising results (Zumla et al., 2013, Zumla et al., 2012). The repurposing of drugs is advantageous as limited new research is required to determine the toxicity effects, which reduces time and cost that would have been spent on the development and assessment of the drug (Zumla et al., 2012, Zumla et al., 2013). The success of bedaquiline has been followed by the identification of other agents that show promise in TB drug development initiatives, especially for treatment of drug-resistant TB (Keshavjee and Farmer, 2012).

1.4 Mechanisms of antibiotic tolerance in Mtb

An important factor that hampering the development of new TB drugs is the inherent tolerance of Mtb to external compounds, which makes it difficult to kill using antimicrobial agents. This is primarily because the tubercle bacillus is equipped with mechanisms to either avoid or eliminate drugs and antibiotics. These systems include mechanisms such as efflux pumps and the inherent complexity of the cell wall that limits diffusion of drugs.

Efflux pumps are transporter proteins that are usually embedded in the inner membrane (Lomovskaya et al., 2001). These are found in both gram positive and gram negative bacteria and have been shown to play an important role in the removal of a wide range of cytoplasmic antibiotics (Lomovskaya et al., 2001, Vila et al., 2007, Webber and Piddock, 2003). The active efflux of drugs by these pumps necessitates that more drug is required in order to overwhelm these pumps and increase effective cytosol concentrations of drug in the bacterium (Lomovskaya et al., 2001). To address this issue, a number of efflux pump inhibitors have been developed with the intent of using them in combination with antibiotics in order to reduce the amount of antibiotic required to kill the pathogen. As an illustration, verapamil (an efflux pump inhibitor), in combination with bedaquiline has been used for clinical trials in order to determine whether the combination leads to a reduction in the amount of effective bedaquiline required to achieve functional cure (Gupta et al., 2014). This study confirmed that combining drugs with efflux pump

inhibitors has the potential to reduce the minimum inhibitory concentration of the drug (Gupta et al., 2014). However, an important limitation with this approach is the toxicity of efflux pump inhibitors but this may be offset if the effective drug concentration required is reduced to a point where TB drug related toxicities become negligible. This will reduce the overall toxicity of the regimen, which may provide a substantive benefit in the longer-term.

The other notable physical barrier to the development of new TB drugs is the cell wall. The mycobacterial cell wall is a uniquely complex structure consisting of multiple layers, including the capsule, mycolic acid, arabinogalactan, peptidoglycan (PG) and plasma membrane, with the inherent ability of not only protecting the organisms from host derived stresses but also preventing the penetration of antibiotics (Jarlier and Nikaido, 1994). Unlike the gram negative capsule, the mycobacterial capsule is shrouded in mystery. The exact structural composition is unclear and the ability to detect this structure is highly dependent on the manner in which the sample is prepared (Daffe and Etienne, 1999). Extensive research conducted on the capsule has identified the basic structural composition, primarily comprising polysaccharides and proteins as well as small amounts of lipids (Daffe and Etienne, 1999). The capsule, in addition to serving as a barrier against the diffusion of compounds, forms a niche for the settlement of enzymes, such as peroxidase and superoxide dismutases which play an important role in the scavenging of harmful radicles, thus protecting mycobacteria in the macrophage environment (Daffe and Etienne, 1999).

The next layer is generally classified as one large polymer, referred to as the MAP (mycolic acid, arabinogalactan and PG) layer and accounts for the impermeable nature of mycobacteria (Jarlier and Nikaido, 1994, Liu et al., 1996). The mycobacterial mycolic acid layer consists of various forms of mycolic acids with varying sizes and numerous studies have demonstrated the importance of this layer in pathogenicity and antimicrobial tolerance (Liu et al., 1996, Nataraj et al., 2015, Marrakchi et al., 2014, Jarlier and Nikaido, 1994). The limited permeability of the mycolic acid layer has been associated with the length of mycolic acids as it has been demonstrated that the corynebacterial mycolic acid layer (which contains shorter mycolic acids) is far more permeable than that of mycobacteria (Liu et al., 1996). The arabinogalactan layer is made up of long, branch-like structures consisting of arabinan and galactan subunits and serves an important structural role whereby it is thought to anchor the mycolic acid layer to the PG layer (Jarlier and

Nikaido, 1994). A diagrammatic description of the mycobacterial cell wall, and how it differs from that found in other bacteria, is given in Figure 1.3.

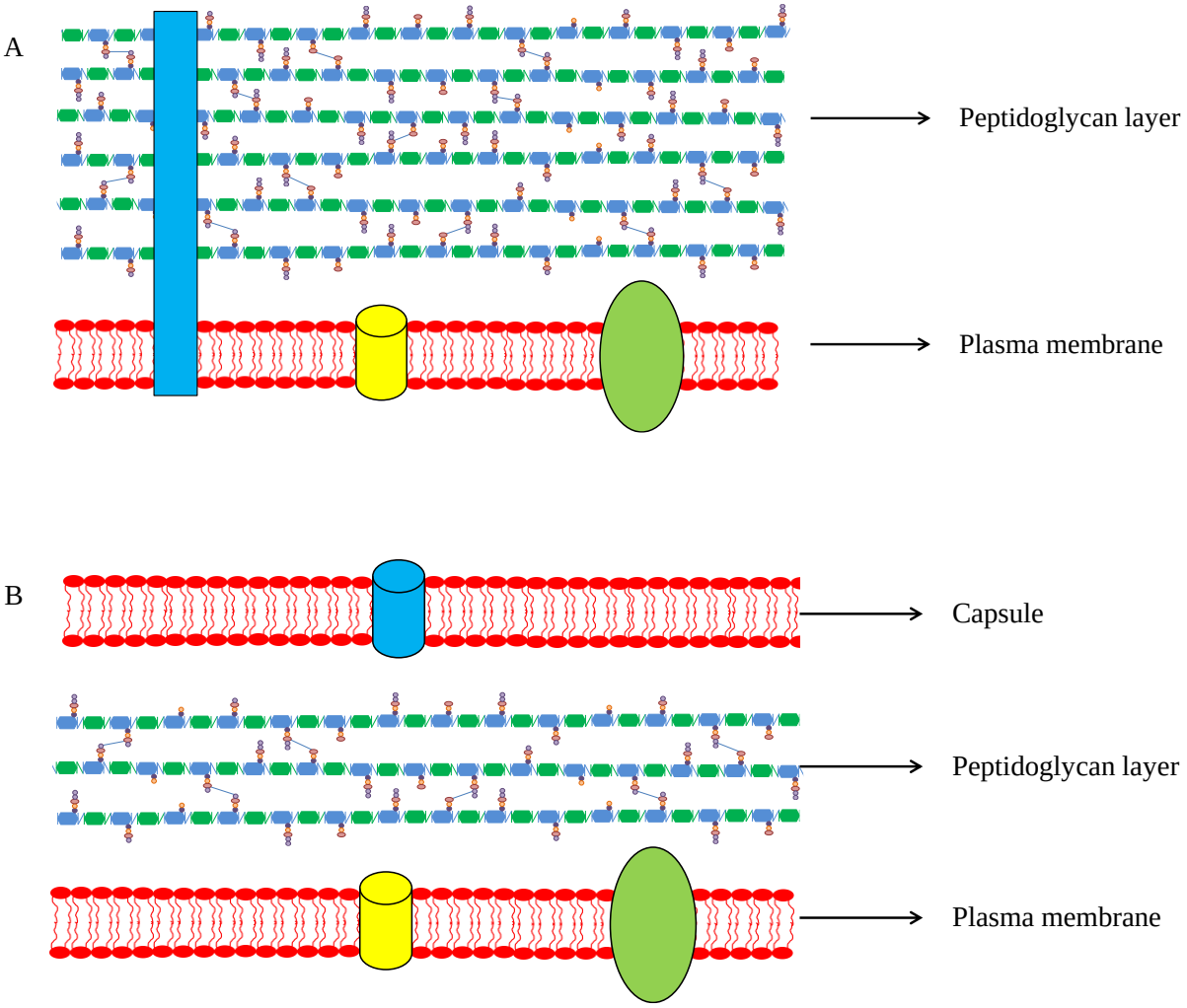

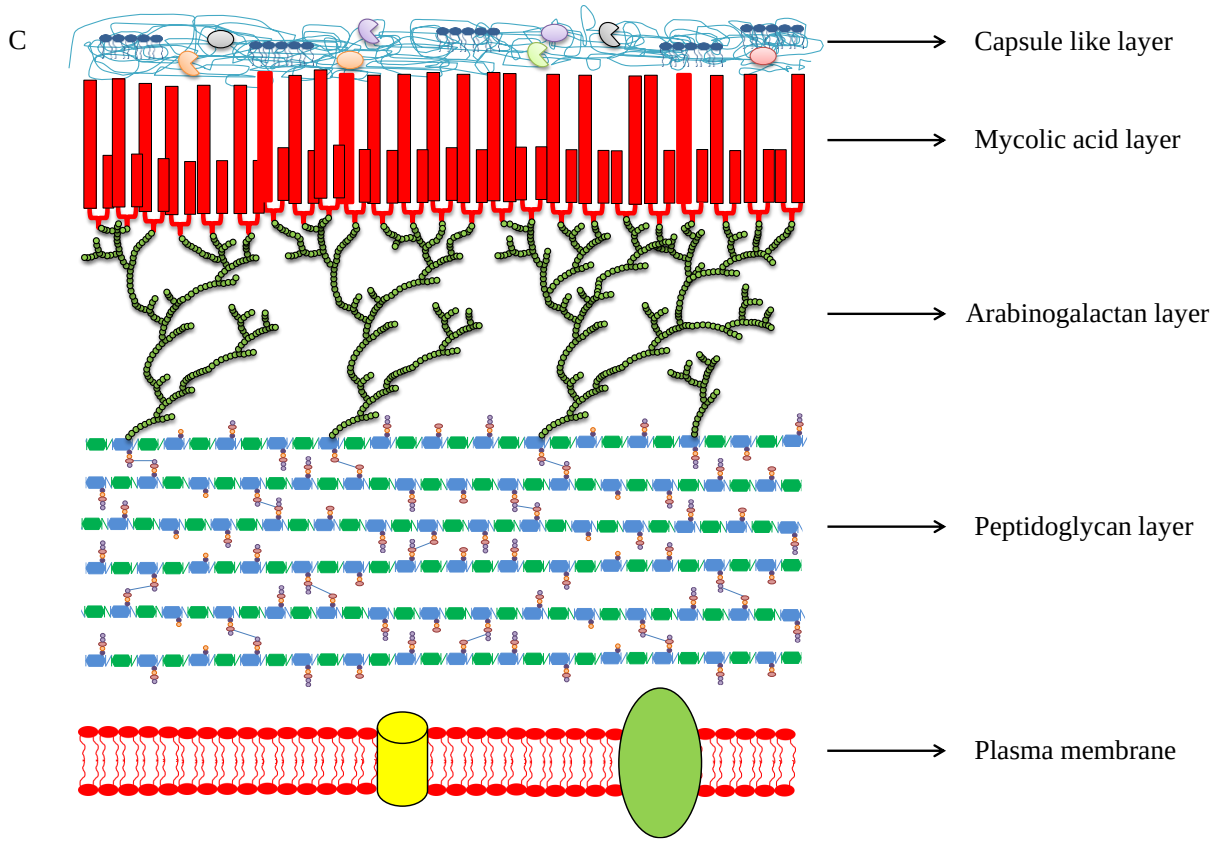

Figure 1.3: Diagrammatic representation of the cell wall of various classes of bacteria. (A) Shown is the gram positive cell wall, which consists of a plasma membrane and a thick PG layer, (B) The gram negative cell wall consisting of a plasma membrane, thin PG layer and a capsule layer and (C) the complex mycobacterial cell wall consisting the plasma membrane, thick PG, arabinogalactan, mycolic acid and capsule like layers (adapted from Hett and Rubin, 2008, figure drawn by S. Senzani).

The final layer of the MAP complex is the PG layer. PG is a complex, essential bacterial macromolecule consisting of long saccharide chains with alternating *N*-acetylmuramic acid (MurNAc) and *N*-acetylglucosamine (GlcNAc) residues linked via a β-1, 4-glycosidic bond (Brennan, 2003). These sugar chains are linked by crosslinks that form between adjacent stem peptides, which are covalently attached to the muramic acid residues (Brennan, 2003). This structure plays a crucial role in a variety of cellular processes including the determination of cell shape, as organisms lacking PG exhibit an amoeboid form, lacking any form or structure (Weibull, 1953). PG also plays an essential role in protecting the cells from osmotic pressure (Rayman and MacLeod, 1975). This intrinsically allows PG containing organisms the ability to survive under conditions of varying salt concentration as opposed to their PG deficient counterparts (Sumaryati et al., 1992, Rayman and MacLeod, 1975). In pathogenic organisms such as Mtb, PG plays an

essential role in modulating host immune systems to allow for pathogen evasion of host immune responses, as well as a number of other essential functions which will be discussed later.

PG is an extremely dynamic molecule, which is continuously remodelled to allow for bacterial growth, insertion of extracellular structures, including pilli or porins, as well as to allow for various growth switches that can occur under different growth conditions, such as the switch from vegetative growth to dormancy (Driks, 2002, Hett and Rubin, 2008, Vollmer et al., 2008). As such, this remodelling process is important and is conducted by a plethora of enzymes that are required for the synthesis of PG subunits, hydrolysis of the PG complex, insertion of PG subunits into the complex and modification of PG (Egan et al., 2016). The large number of enzymes associated with this single structure has drawn some interest with regards to the identification of novel drug targets in order to disrupt the maintenance of PG. Due to the covalently linked nature of the MAP structure, disruption of the PG layer (even in the absence of killing) could result in a cascade which would lead to disturbances in the mycolic acid layer. With this in mind, a number of antibiotics that target PG synthesis already exist, including penicillin (β-lactams), vancomycin (glycopeptides) and meropenem (carbapenems) (Caminero et al., 2010, De Lorenzo et al., 2013). The majority of these drugs unfortunately are not used for the routine treatment of TB and as such, the remodelling of the PG layer has yet to be fully exploited in mycobacteria.

In this study, we attempt to advance the knowledge on mycobacterial PG remodelling during cell division to identify enzymes that can be used for the development of new drugs. We focus on a group of PG hydrolysing enzymes termed *N*-acetylmuramyl-L-alanine amidases (hereafter referred to as amidases for simplicity) and their role in mycobacterial growth and cell division. Previous research conducted in our lab identified four mycobacterial amidases designate Ami1-Ami4 (Machowski et al., 2014). Preliminary work identified a role for Ami1 in cell division and Ami2 in cell elongation in *Mycobacterium smegmatis*. In this PhD, we further resolved these observations and establish a role for Ami1 in the degradation of septal PG (Senzani et al., 2017) We also advance the research related to the other mycobacterial amidases mentioned above. Ami1 and Ami2 were characterised in detail in *M. smegmatis*. Following this, Ami1 was studied further in Mtb, followed by an analysis of the biological role of Ami4. Due to time constraints and the focus on *M. smegmatis*, the work presented for Mtb amidases is only preliminary. The overall frame work for the dissertation research, and this dissertation report, is outlined in Figure 1.4.

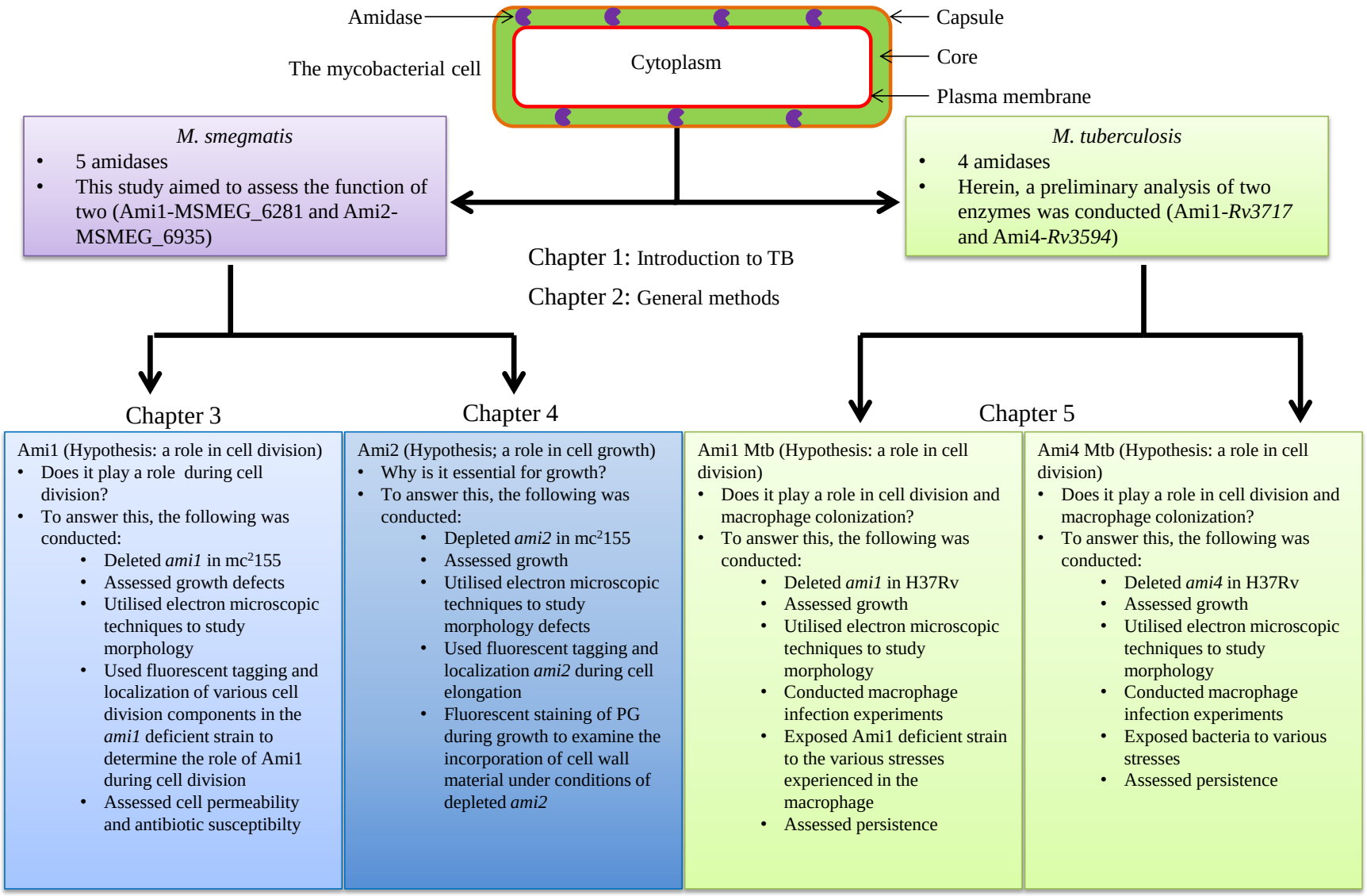

Figure 1.4: Flow chart depicting the outline of the study. Shown are the various aspects of the study indicating the chapters in which each amidase is addressed as well as the major question associated with each enzyme, and the steps taken to interrogate the question (Figure drawn by S. Senzani).

Chapter 2

2 General Methods

2.1 Bacterial strains, vectors and growth conditions

General vectors used in this study are listed in Table 2.1. Other vectors and bacterial strains are listed in the respective chapters that detail the findings. Freezer stocks for all these were stored at – 80 ˚C in liquid media containing 6.6 % (v/v) glycerol.

Table 2.1: Basic vectors used in this study

Vectors	Genotype	Reference
p2NIL	*E. coli* cloning vector; Kan^R	(Parish and Stoker, 2000)
pFLAGEM	*E. coli-Mycobacterium* episomal shuttle vector carrying a 3X FLAG epitope sequence downstream P_{myc}-*tetO*; Hyg^R	E. Machowski
pSE100	*E. coli-Mycobacterium* shuttle vector carrying P_{myc}-*tetO*; Hyg^R	(Ehrt et al., 2005b)
pGOAL17	Vector carrying *lacZ* and *sacB* genes as a *Pac*I cassette; Amp^R	(Parish and Stoker, 2000)
pMV306(H)	pMV306 derivative carrying Hyg^R marker	H. Boshoff

Kan^R: Kanamycin Resistance, Hyg^R: Hygromycin Resistance

2.1.1 Growth of *E. coli* DH5α and derivative strains

E. coli strains were grown in Lysogeny broth (LB) or agar (LA) at 37 °C, supplemented with the appropriate antibiotic (Appendix A). Antibiotic concentrations used were: Kanamycin (Kan) 50 μg/ml and Hygromycin (Hyg) 200 μg/ml. *E. coli* strains cultured in LB were grown with shaking at 250 rpm unless stated otherwise.

2.1.2 Growth of *M. smegmatis* strains

M. smegmatis strains were cultured in Middlebrook 7H9 liquid media supplemented with 0.2 % glucose, 0.5 % glycerol, 0.085 % NaCl, and 0.05 % Tween 80 containing appropriate antibiotic at 37 °C (herein referred to as 7H9S media) with shaking at 100 rpm. Where necessary, *M. smegmatis* was grown on or Middlebrook 7H10 solid media supplemented with 0.2 % glucose, 0.5 % glycerol, and 0.085 % NaCl (herein referred to as 7H10). Antibiotic concentrations used were: Kan 25 μg/ml and Hyg 50 μg/ml.

2.1.3 Growth of Mtb strains

Mtb strains were cultured in Middlebrook 7H9 liquid media supplemented with Middlebrook OADC enrichment, 0.5 % glycerol, and 0.05 % Tween 80 at 37 °C (herein referred to as 7H9T media). Where necessary, bacteria were growth on Middlebrook 7H11 solid media supplemented with Middlebrook OADC enrichment and 0.5 % glycerol containing appropriate antibiotic (herein referred to as 7H11). Antibiotic concentrations used were: Kan 25 µg/ml and Hyg 50 µg/ml.

2.2 DNA manipulation

2.2.1 Mycobacterial chromosomal DNA extraction

2.2.1.1 *Cetyltrimethylammonium bromide (CTAB) DNA extraction in M. smegmatis*

Bacterial strains were grown on 7H10 agar for 2 to 5 days, until a lawn of cells had formed on the plates. The cells were harvested by scraping the surface of the agar plate and suspending in 500 µl TE buffer. This was followed by killing of bacteria through incubation at 65 °C for 35 min. The cells were then cooled to room temperature and a 50 µl aliquot of lysozyme (10 mg/ml) was added to the sample, followed by incubation at 37 °C for 1 h. Thereafter, 70 µl of 10 % SDS and 6 µl of proteinase K (10 mg/ml) was added to the sample and incubated at 65 °C for 2 h. Following this, 100 µl of 5 M NaCl and 80 µl pre-warmed CTAB/NaCl was added, mixed and incubated at 65 °C for 10 min. An equal volume of 24:1/Chloroform:Isoamyl alcohol was added, the solution was mixed and centrifuged at maximum speed for 10 min at room temperature. The aqueous layer was transferred into a clean Eppendorf tube, followed by the addition of 0.6 volume equivalent of isopropanol and centrifugation for 20 min at room temperature. The supernatant was discarded, the pellet was washed in 70 % ethanol and dried using an Eppendorf Concentrator 5301. The DNA pellet was resuspended in 50 µl sterile distilled water (sdH_2O), quantified using NanoDrop and stored at 4 °C.

2.2.1.2 *Cetyltrimethylammonium bromide (CTAB) DNA extraction in* Mtb

Bacterial strains were grown on 7H11 agar for 3 to 4 weeks until lawn had formed on the plates, the cells were then harvested by scraping the surface of the agar plate and suspending in 500 µl of TE buffer. The bacteria were killed by incubation at 80 °C for 1 h and the cells were then cooled down to room temperature. A 50 µl aliquot of lysozyme (10 mg/ml) was added to the sample and incubated at 37 °C for 1 h. From this point, the same procedure was followed as described for *M. smegmatis*.

2.2.1.3 *Small scale DNA extraction for PCR in M. smegmatis and* Mtb

A single colony was scraped from an agar plate and resuspended in 30 µl sdH_2O. A 10 µl sample was spotted on 7H11 agar for a sample reference. The remaining suspension was incubated at 95 °C for 5 min, followed by the addition of 20 µl of chloroform. The solution was mixed, centrifuged at 16 000 × g for 5 min and the aqueous layer was transferred into a fresh Eppendorf tube. A 2 µl aliquot of this was used as template for PCR, where necessary.

2.2.2 *E. coli* vector extraction

2.2.2.1 *Bulk vector preparation using Nucleobond Xtra vector purification kit*

Vector DNA preparation using the Nucleobond Xtra kit was done as per manufacturer's instructions (Macherey Nagel). Briefly, 50 ml of *E. coli* culture was grown in LB containing appropriate antibiotic at 37 °C with shaking at 250 rpm until the OD_{600nm} was greater than 3. The cells were harvested by centrifugation at 3 900 × g for 10 min. The supernatant was discarded and the cells were resuspended in 8 ml of RES buffer containing RNAse A. Thereafter, 8 ml of the lysis buffer, LYS buffer, was added to the sample and mixed gently by inverting 10 to 15 times, followed by incubation at room temperature for 3 to 5 min. Then, 8 ml of neutralisation buffer, NEU buffer, was added to the sample, which was mixed gently by inverting the tube. The sample was placed on ice for 5 min. During the neutralisation stage, a new Nucleobond Xtra column containing the accompanying filter was equilibrated by adding 12 ml of EQU buffer into the column and allowing the buffer to flow through. The supernatant from the neutralised vector extraction was then decanted into the column and allowed to flow through. Thereafter, the column was washed with 8 ml WASH buffer and the DNA was eluted using 5 ml ELU buffer into a sterile tube. The DNA was precipitated by adding 3.5 ml of isopropanol into the tube, followed by centrifugation at 16 000 × g at 4 °C for 30 min. The resulting supernatant was discarded and the pellet was washed with 70 % ethanol. Thereafter, the pellet was dried, resuspended in 50 µl sdH_2O and quantified using the NanoDrop.

2.2.2.2 *Small scale vector preparation using QIAGEN vector purification kit*

Vector DNA preparation using the QIAGEN vector purification kit was done as per manufacturer's instructions (QIAGEN). Briefly, 5 ml *E. coli* culture was grown in LB containing appropriate antibiotics at 37 °C with shaking at 250 rpm overnight. The cells were harvested by centrifugation at 16 000 × g for 1 min. The supernatant was discarded and the cells were resuspended in 300 µl

of Buffer P1. Following this, 300 µl of the lysis buffer, Buffer P2, was added to the sample and mixed gently by inverting 10 to 15 times, followed by incubation at room temperature for 3 to 5 min. Then, 300 µl of Buffer P3 was added to the sample to neutralise the reaction, which was then mixed gently by inverting, followed by centrifuged at 16 000 × g for 10 min. The supernatant was then decanted into a QIAGEN DNA extraction column and centrifuged at 10 000 × g for 30 sec. The flow-through was discarded and the column was washed by adding 700 µl QC buffer. The flow-through was discarded and the excess QC buffer was removed through centrifugation at 10 000 × g for 2 min. The column was then placed in a fresh Eppendorf tube and DNA was eluted by adding 50 µl of sterile distilled water (equilibrated to 65 ˚C) and centrifugation at 10 000 × g for 2 min. The resulting DNA was quantified using the NanoDrop spectrophotometer.

2.2.2.3 *Vector miniprep using alkaline lysis method*

A single *E. coli* colony was grown in 2 ml LB containing appropriate antibiotics at 37 °C. A 10 µl sample was spotted on LA containing appropriate antibiotics as a reference. The remaining cells were harvested from the culture through centrifugation at 10000 × g and resuspended in 100 µl cold solution I. Thereafter, 200 µl of room temperature solution II was then added to the sample, this was mixed by inverting 10 times and placed on ice for 5 min. Following incubation, 150 µl of cold solution III was added and the sample was placed on ice for a further 10 min. The sample was centrifuged at room temperature for 10 min and the supernatant was transferred to a clean Eppendorf tube. A 300 µl aliquot of isopropanol was added, and the mixture was centrifuged at room temperature for 20 min. The supernatant was discarded, the pellet washed with 70 % ethanol and dried using an Eppendorf Concentrator 5301. The DNA pellet was then resuspended in 20 µl sdH_2O and quantified using agarose gel electrophoresis explained further in section 2.2.10.

2.2.3 Sodium acetate DNA precipitation

A one-tenth volume equivalent of 3 M sodium acetate, pH 5.2, and 2.5 volume equivalent of cold 100 % ethanol was added to the DNA solution. The sample was mixed and incubated at -20 °C for 20 min. The sample was then centrifuged at room temperature for 20 min at maximum speed, the supernatant was discarded and the pellet washed in 70 % ethanol. The pellet was dried using the Eppendorf Concentrator 5301 and resuspend in 20 µl sdH_2O.

2.2.4 DNA restriction enzyme digestion

Restriction digests were conducted using Roche (Roche Applied Sciences) and /or NEB (New England Biolab) enzymes and reactions were set up as per manufacturer's instructions. Briefly, reactions were set up in a 20 µl volume, unless stated otherwise, containing 1 × appropriate restriction buffer, 1 µg DNA, 1 U restriction enzyme and sdH_2O. Digests were incubated at the appropriate temperature for 1 h. The enzyme was heat inactivated at 65 ˚C for 10 min unless advised differently by the manufacturer.

2.2.5 Phosphorylation of DNA

Phosphorylation of DNA was conducted using Polynucleotide kinase (PNK) (Roche Applied Sciences) in 20 µl reactions containing 1 × PNK buffer, 1 µg of PCR product, 1 U of PNK and sdH_2O. This was incubated at 37 ºC for 30 min and then heat inactivated at 65 ºC for 20 min.

2.2.6 Dephosphorylation of 5′ends of vector DNA

Dephosphorylation of 5′ ends was conducted using FastAP (Fermentas) in 20 µl reactions containing 1 × FastAP buffer, 1 µg of digested DNA, 2 U of FastAP phosphatase and sdH_2O. This reaction was incubated at 37 ºC for 10 min, then heat inactivated at 65 ˚C for 20 min.

2.2.7 DNA ligation

All ligations were carried out using the Fermentas T4 Ligase (Fermentas) or Fastlink DNA ligation kit (Epicenter). For optimal ligation conditions a molar ratio of 1:1 vector:insert was used in all reactions. A constant amount of vector, 50 ng, was used for all ligation reactions and the insert mass required to make up a molar ratio of 1:1 (vector:insert) was calculated using the following equation:

$$\text{Amount of insert (ng)} = \frac{\text{Amount of vector (50 ng)} \times \text{Size of insert (bp)}}{\text{Size of vector (bp)}}$$

Either T4 DNA ligase or the Epicenter ligase was used. In the case of T4 ligase, the reactions were set up in 20 µl volumes containing 1 × ligation buffer, 50 ng vector DNA, 1 molar equivalent insert DNA, 5 U T4 ligase and sdH_2O, which were incubated at 22 ºC for 10 min. In the case of blunt

end ligations, the reaction was supplemented with one-tenth volume PEG4000 and incubated at 22 ºC for 1 h. T4 ligase was then heat inactivated at 75 ºC for 10 min.

With regards to the Epicenter ligation kit, the reactions were set up in a 15 µl volume containing 1 × Fast-link ligation buffer, 50 ng vector DNA, 1 molar equivalent insert DNA, 2 U T4 ligase and sdH_2O, which were incubated at 22 ˚C for 5 min. With blunt end ligations, the reaction was supplemented with one-tenth volume PEG4000 and incubated at 22 ˚C for 1 h. Ligase was then heat inactivated at 75 ºC for 10 min.

2.2.8 Agarose gel electrophoresis

Agarose gel electrophoresis was conducted using agarose gels containing 0.5 µg/ml ethidium bromide. Separation of high molecular weight DNA was accomplished by using 0.8 % agarose gels made in 1 × TAE buffer (40 mM Tris-acetate, 1 mM EDTA) and separation of low molecular weight DNA was conducted using 2 % agarose gels. Electrophoresis was carried out in 1 × TAE buffer at 80 – 100 V in electrophoresis tanks (Bio-Rab laboratories). Appropriated DNA molecular weight markers were separated on the same gel to indicate the molecular weight of the samples examined. Bands were visualised using a G:Box SYNGENE system in conjunction with the GeneSnap image acquisition software (Syngene).

2.2.9 Purification of DNA fragments

Purification of DNA fragments was conducted from agarose gels to extract either PCR or DNA restriction products for use in subsequent cloning steps. DNA purification was conducted using the Nucleospin PCR and Gel purification Kit (Macherey-Nagel) as per the manufacturer's instructions. In the case of PCR products, a small sample was separated on a gel to ensure the PCR amplified the desired product. Thereafter, a 2 × volume equivalent of binding Buffer was then added to the remaining product. This was loaded on the column provided and centrifuged at 11 000 × g for 30 s. The flow-through was discarded, the column was then washed using 700 µl of wash buffer at 11 000 × g for 2 min. The DNA was eluted by adding 50 µl of 65 ˚C dH_2O to the column and centrifuging at 11000 × g for 1 min. The DNA was quantified using the NanoDrop. In the case of gel extractions, the desired fragment was excised from the gel. The gel fragment containing DNA was then weighed and melted in a 2 volume equivalent of binding buffer at 42 ˚C. The DNA was loaded onto the column and purified as described above.

2.2.10 Nucleic acid quantification

All DNA and RNA was quantified either using the NanoDrop ND-1000 Spectrophotometer (NanoDrop Technologies), used in conjunction with software provided by the manufacturer (Coleman Technologies) or though gel electrophoresis by comparing the intensity of sample DNA to the various DNA marker bands.

2.2.11 DNA Sequencing

Sequencing, which was outsourced to the DNA Sequencing Facility of Stellenbosch University, was performed using the Big Dye terminator v3.1 Cycle Sequencing kit and Bioline Half Dye Mix. Finch TV version 1.4 was used to analyse the sequencing data.

2.3 Polymerase chain Reaction (PCR)

Screening for knockout mutant strains was conducted using the Roche Fast-Start kit (Roche Applied Science). Amplification of products for cloning was done using the Phusion High-Fidelity DNA polymerase (New England Biolab), which retains DNA proofreading capacity to ensure sequence fidelity, thus preventing the introduction of mutations.

2.3.1 Roche Fast-Start Taq PCR

PCR experiments were conducted in 25 µl volumes each containing 1 × PCR buffer, 2 mM $MgCl_2$, 0.2 mM dNTP, 0.5 mM forward and reverse primers, 1 × GC rich buffer, 50 ng DNA template, 1 U of Taq polymerase and sdH_2O in 200 µl PCR tubes. These reactions were incubated in a thermocycler using the following parameters: enzyme activation at 95 ºC for 4 min, then 35 cycles of denaturation at 95 ºC for 30 s, annealing temperature, which was dependent on the specific primer, set for 30 s and elongation at 72 ºC for a time period dependent on the length of the desired product (Fast start Taq amplifies 1 kbp/min). This was followed by a final elongation at 72 ºC for 10 min.

2.3.2 Phusion High-Fidelity DNA polymerase

PCR experiments were conducted in 50 µl volumes containing 1 × GC buffer, 0.2 mM dNTP, 0.5 mM forward and reverse primers, 3 % DMSO, 50 ng template, 1 U Phusion polymerase and sdH_2O in 200 µl PCR tubes. The reactions were incubated in a thermocycler using the following parameters: enzyme activation at 98 ºC for 30 s, then 35 cycles of denaturation at 98 ºC for 10 s, annealing temperature, which was dependent on the specific primer set, for 30 s and elongation at

72 ºC for a time period dependent on the length of the desired product (Phusion polymerase amplifies at 1 kbp/30 s), followed by a final elongation stage of 72 ºC for 10 min.

2.4 Transformation of bacterial cells

2.4.1 Transformation of chemically competent DH5α

Chemically competent cells were prepared using rubidium chloride. A single colony was inoculated in 5 ml LB broth then grown overnight. Thereafter, 1 ml of the overnight culture was inoculated in 100 ml LB broth and grown to an optical density $(OD)_{600nm}$ of between 0.48 - 0.55. The cells were placed on ice for 15 min and harvested by centrifugation at 3 900 × g for 5 min at 4 °C. The cells were then resuspended in 20 ml TfbI solution (30 mM potassium acetate, 100 mM rubidium chloride, 10 mM calcium chloride, 50 mM manganese chloride, and 15 % v/v glycerol - pH 5.8), and placed on ice for 15 min. The cells were then centrifuged at 3 900 × g for 5 min at 4 °C, resuspended in 2 ml TfbII solution (10 mM MOPS, 75 mM calcium chloride, 10 mM rubidium chloride and 15 % v/v glycerol-pH 6.5), 500 µl aliquots were flash-frozen in ethanol and stored at -80 °C until further use.

For transformations, *E. coli* DH5α competent cells were thawed on ice and 100 µl of the cell suspension was used per transformation. Vector DNA was incubated with the cells on ice for 20 min, heat-shocked at 42 °C for 90 s. Thereafter, 750 µl of 2 × TY was added to rescue the cells followed by incubation at 37 °C for 1 h. The cells were plated on LA media containing the appropriate antibiotics, and incubated for 1 - 2 days at 37 °C with the exception of larger vectors (>8 kb), which were incubated at 30 ºC for 2 days.

2.4.2 Electroporation into *M. smegmatis*

A 5 ml culture was grown overnight using single colony. This was then inoculated into 100 ml 7H9S media and grown to an OD_{600nm} of 0.6 - 0.8. The cells were harvested at 2 630 × g for 10 min at 4 °C and the pellet washed 4 times by gentle resuspension in successive steps of 45 ml, 20 ml, 10 ml and 5 ml of ice-cold 10 % glycerol, followed by centrifugation at 2 630 × g for 10 min at 4 °C. The final cell pellet was resuspended in 2 ml ice-cold 10 % glycerol and these competent cells were used immediately. Up to 10 µg vector DNA was added to a 400 µl aliquot of *M. smegmatis* competent cells. This was transferred to a 0.2 cm electroporation cuvette (Bio-Rad laboratories) and pulsed using the following conditions: 2.5 kV, 25 µF and 1000 Ω using the Gene PulserX cell (Bio-Rad Laboratories). The cells were rescued immediately with 800 µl 2 × TY for

at least 3 h at 37 °C and plated on Middlebrook 7H10 media containing the appropriate supplements and antibiotics, followed by incubation for 3 - 7 days at 37 °C before scoring CFUs.

2.4.3 Electroporation into Mtb

A 5 ml culture was grown to stationary phase. This was inoculated into 100 ml 7H9T media then grown to an OD_{600nm} of 1 – 1.5. The culture was then supplemented with glycine to a final concentration of 1.5 %, and then incubated at 37 ˚C for 16 h. The cells were harvested at 2 630 × g for 10 min at room temperature and the pellet washed 4 times by gentle resuspension as described above for *M. smegmatis*. The final cell pellet was resuspended in 2 ml 10 % glycerol and these competent cells were used immediately. Up to 10 µg vector DNA was UV-irradiated (100 mJ/cm2) then immediately inoculated into 400 µl aliquot of Mtb competent cells. This was transferred to a 0.2 cm electroporation cuvette (Bio-Rad laboratories) and pulsed using the following conditions: 2.5 kV, 25 µF and 1000 Ω using the Gene PulserX cell (Bio-Rad Laboratories). The cells were rescued immediately with 800 µl 7H9 for 16 h at 37 °C and thereafter plated on Middlebrook 7H11 media containing the appropriate supplements and antibiotics, followed by incubation for 3 – 6 weeks at 37 °C before scoring CFUs.

2.5 Southern blotting

2.5.1 Labelling of Probe DNA

Alkali-labile digoxigenin (DIG)-dUTP probes were constructed using a commercially available kit (PCR DIG Probe Synthesis Kit -Roche Applied Sciences) by PCR. A modified version of the manufacturer's instruction, using the Fast start Taq polymerase, was used. Briefly, two 50 µl reactions (labelled and unlabelled) were set up containing 1 × PCR buffer, 2 mM $MgCl_2$, 0.5 mM forward and reverse primers, 1 × GC rich buffer, 50 ng DNA template, 1 U of Taq polymerase and sdH_2O in 200 µl PCR tubes. The labelling reaction was supplemented with 2.5 µl PCR DIG labelling mix and 0.1 mM dNTPs, while the negative control was supplemented with 0.2 mM dNTPs only. The PCR amplification conditions were first optimised using Roche Fast-start Taq to ensure that a single, pure product was produced during the labelling reaction. The DIG-labelled and unlabelled reactions were run on the same agarose gel to confirm labelling, as incorporation of the DIG label results in a molecular weight shift on agarose gels.

2.5.2 Blotting

For restriction digests, 2 µg of chromosomal DNA was digested with 5 U of selected enzyme overnight. DNA was then separated on 0.8 % agarose gel with either Lambda pUC mix 4 Marker (Fermentas), Roche marker IV (Roche) or Roche marker III (Roche) at 80 V for 2 to 3 h. After photographing of the gel, using the G-Box SYNGENE system, the DNA was depurinated by soaking the gel in 0.2 M HCl for 15 min with gentle shaking. The depurination solution was then removed and the gel was soaked in a solution of 0.5 M NaOH and 1.5 M NaCl for 30 min to denature the DNA. The gel was then washed in 1 × TBE. The gel was then overlaid with Hybond™ -N nitrocellulose membrane, sandwiched between 4 Whitman filter papers and 2 sponges, and pre-soaked in 1 × TBE (89 mM Tris-Borate, 2 mM EDTA, pH 8.3). The sandwich was carefully placed in a gel cassette (Bio-Rad Laboratories) and transferred to an SB10 tank (Bio-Rad Laboratories) containing 1 × TBE. DNA was transferred to the nitrocellulose membrane at 600 mA for 2 h. The DNA was cross-linked to the nitrocellulose membrane by UV irradiation twice, at 2500 mJ/cm^3 in a UV Stratalinker 1800 (Stratagene). The membrane was incubated in 10 ml of DIG-EASY-HYB solution for 30 min at 42 ºC. The DIG labelled probe was added to the hybridisation solution and incubated at 42 ºC overnight. The DIG-EASY-HYB and probe mixture was decanted into a 50 ml Falcon tube and stored at -20 ºC for future use. The membrane was washed with a solution containing 2 × SSC (300 mM NaCl, 30 mM Sodium citrate) and 0.1 % SDS for 5 min at room temperature. This was followed by two washes in a solution containing 0.5 × SSC and 0.1 % SDS for 30 min at 68 ºC. The membrane was rinsed in wash buffer (0.1 M maleic acid buffer and 0.3 % Tween 20) for 5 min at room temperature and incubated in 1 × blocking solution (made by diluting 10 × blocking solution – Roche Applied Sciences - in 0.1 M maleic acid buffer) for 30 min. Thereafter, the membrane was incubated in 20 ml of antibody solution (20 ml 1 × blocking solution and 2 µl Anti-Digoxigenin-AP [Roche Applied Sciences]) for 30 min, followed by rinsing twice for 15 min in wash buffer. The membrane was placed in a hybridisation bag (Roche Diagnostics; Mannheim, Germany) DNA side facing up and 1 ml chloro-5-substituted adamantyl-1, 2-dioxetane phosphate (CSPD) substrate was aliquoted on to the DNA side of the membrane and incubated at room temperature for 10 min, the excess CSPD was then removed, the hybridisation bag was sealed and incubated at 37 ºC for 5 min. The membrane was exposed to X-ray film (Kodak Biomax Light or CL-Xposure™ Film-Thermo Scientific) for 10 min and the film was developed using an automated Axim developer.

2.6 Assessment of gene expression

Expression primer sets for genes of interest were designed to contain a forward and reverse primer pair for amplification and a second reverse primer (RT primer) for cDNA synthesis. Expression analysis was conducted in two steps, the first being cDNA synthesis from purified RNA, using RT primers, followed by real-time amplification of cDNA.

2.6.1 RNA extraction from mycobacterial cells

RNA extraction was carried out using the Nucleospin RNA purification Kit (Macherey-Nagel) as per the manufacturer's instructions. Cells were grown in 7H9S or 7H9T media containing the appropriate antibiotics to an $OD600_{nm}$ = 0.3. The cells were harvested at 3 900 × g for 10 min at 4 ºC. Pellets were resuspended in 350 µl lysis buffer and 3.5 µl β-mercaptoethanol was added to the sample. The cell suspension was transferred to lysis matrix B tubes (IEPSA) and ribolysed 3 times using the FastPrep Savant FP-120 Ribolyser for 45 s (Speed = 6), with incubation on ice for 2 min between each ribolysis. The lysate was transferred to the supplied lipid filters tubes and centrifuged at 11 000 × g for 30 s. Thereafter, 350 µl of 70 % ethanol was added to the flow-through and the solution was transferred to nucleic acid binding columns, centrifuged at 11 000 × g for 30 s and the flow-through was discarded. A 350 µl aliquot of membrane desalting buffer (MBD) was added to the column, which was centrifuged at 11 000 × g for 30 s and the flow-though was discarded. A 100 µl aliquot of the DNAse reaction mixture containing 10 µl of reconstituted rDNAse (reconstituted as per manufacturer's instruction) and 90 µl of Reaction buffer for rDNAse was added to the column, followed by incubation at room temperature for 30 min. Thereafter, the column was washed by aliquoting 200 µl of Buffer RA2 into the membrane and centrifuging for 30 s at 11 000 × g. A second and third wash was conducted using 600 µl Buffer RA3 at 11 000 × g for 30 s, followed by 250 µl Buffer RA3 at 11 000 × g for 2 min. Following the third wash, the column was placed in a fresh Eppendorf tube, 60 µl of RNAse free water was aliquoted onto the membrane, incubated at room temperature for 10 min and RNA eluted by centrifugation at 11 000 × g for 1 min. The RNA was then quantified using the NanoDrop spectrophotometer.

2.6.2 Reverse Transcriptase PCR (RT-PCR)

RT-PCR was carried out using the Superscript III reverse transcriptase [RT] (Invitrogen). Reactions were set up in 25 µl volumes containing 1 µg of DNA free RNA and 0.2 mM reverse

primer mix consisting of the *sigA* mRNA conversion primer and the necessary gene-specific mRNA conversion primers. The *sigA* gene is a housekeeping gene, which is generally expressed at a consistent level throughout different growth phases and is used for normalisation for differential RNA amounts isolated or used in the analysis. Primers were annealed to the RNA by incubation at 94 ºC for 90 s, 65 ºC for 3 min and 57 ºC for 3 min, followed by incubation on ice. The nucleic acid mix was split into two 12.5 µl aliquots, one for the RT reaction and another to serve as an RT free reaction control, to confirm the absence of any contamination/residual DNA in these samples. To the RT conversion sample, the following was added: 5 µl 5 × first strand buffer, 4 µl of 25 mM $MgCl_2$, 2 µl of 0.1 mM Dithiothreitol, 1 µl of 10 mM dNTP and 0.5 µl Superscript III reverse transcriptase (SSIII). The RT free control contained the same components; however, the SSIII was substituted by sterile nuclease free water. These reactions were incubated at 50 ºC for 50 min, followed by heat inactivation of the enzyme at 85 ºC for 5 min. The cDNA was then used for qPCR.

2.6.3 Quantitative real-time PCR (qPCR) amplification

Using either genomic or cDNA, qPCR amplification was conducted using the Biorad SsoFast Evergreen Supermix (Bio-Rad Laboratories). In this case, 20 µl reactions containing 10 µl Supermix, 0.25 mM qPCR forward primer and the qPCR reverse primer, 2 µl template cDNA and sterile distilled nuclease free water were set up and incubated in the CFX96 Real-Time PCR detection system (Bio-Rad Laboratories). The following parameters were used: enzyme activation step of 95 ºC for 30 s, followed by a ten cycle touchdown stage consisting of 3 steps; denaturation at 95 ºC for 10 s, annealing beginning at 65 ºC for 10 s and gradually decreasing by 0.5 ºC after each cycle, elongation at 72 ºC for 10 s, followed by SYBR Green quantification at the end of each cycle. The touchdown was followed by a 35 cycle stage consisting of a 95 ºC denaturation step for 10 s, a 60 ºC annealing step for 10 s and a 72 ºC elongation step for 10 s, followed by SYBR Green quantification at the end of each cycle. Melt curve analysis was conducted beginning at a temperature of 50 ºC, then gradually increasing by 0.5 ºC every 0.05 s to 95 °C, SYBR Green quantification was conducted continuously throughout this stage. Raw data was then processed using the Biorad CFX Manager 2.1 software (Bio-Rad Laboratories).

2.7 Analysis of bacteria growth

2.7.1 Growth rate analysis

Bacterial growth analysis of wild type and mutant strains was conducted using growth curve experiments. Pre-cultures for each strain were set up in 10 ml culture volumes using either 1 ml frozen stocks or a single colony. These were grown at 37 ˚C, shaking at 100 rpm in the case of *M. smegmatis*, until they reached stationary phase ($OD_{600nm} \approx 2$). The pre-cultures were then diluted to a final $OD600_{nm}$ = 0.05 in 50 ml 7H9S or 7H9T containing appropriate antibiotic, when necessary, and incubated at 37 ºC, with shaking at 100 rpm for *M. smegmatis*. Growth was determined by recording $OD600_{nm}$ measurements at 3 h intervals for *M. smegmatis* or daily for Mtb. Ten-fold serial dilutions were also set up for each time point and plated on 7H10 or 7H11, containing appropriate antibiotics and incubated at 37 ˚C for 3 - 5 days in the case of *M. smegmatis* or 4 to 6 weeks for Mtb. The colonies that emerged were then counted to determine the colony forming units per ml (CFU/ml). Data were displayed as a scatter plot.

2.7.2 Fluorescence microscopy

Cells were grown in 10 ml 7H9S containing appropriate antibiotics to an $OD600_{nm}$ = 0.8, followed by harvesting and washing twice in PBS. Cells were then resuspended in 1 ml of 7H9S containing appropriate antibiotics. Thereafter, 0.2 µl of 5 mg/ml vancomycin and 1 µl of 1 mg/ml BODIPY-fluorescent vancomycin (Invitrogen) were added to the culture, followed by incubation at 37 ºC for 1.5 h. The cells were then washed twice in 7H9 and resuspended in 50 µl 7H9S. Agarose pads were then prepared by spotting 500 µl of molten 2 % agarose, dissolved in dH_2O, on a slide then placing a second slide on the spot to flatten the agarose. This was allowed to set for 5 min, the top slide was removed, and 5 µl of sample was spotted on the agarose pad and left at room temperature for 2 min. A cover slip was placed on the agarose pad and the slides were then viewed using an Axio Observer Z1 base microscope (Zeiss). Images were taken using an AxioCam HRm camera and processed using the Zen blue Ver 5.1.2600 (Zeiss) or ImageJ Ver 1.48. Any image manipulation was applied to the entire image.

2.7.3 Time-lapse microscopy

A 5 ml culture was grown in 7H9S or 7H9T, containing appropriate antibiotics, to an OD_{600nm} = 0.8. This was centrifuged at 500 × g for 5 min to remove clumps. The pellet was discarded and the cell suspension was passed through a 5 µm filter to remove remaining bacterial

clumps. A 10 µl sample was then spotted and gently spread on a cellulose membrane, followed by incubation for 2 min at room temperature to allow the bacteria to settle on the membrane. The slide was then placed a microfluidic device. The bacteria were then imaged using a Delta vision Personal DV imaging system (GE HealthCare Life Sciences), using a 100x objective (Olympus Plan Semi Apochromat, 1.3 NA). The images were acquired at 10 or 15 min intervals using a CoolSnap HQ2 camera. Images were acquired on FITC (GFP fluorescent reporter strains; excitation 490/20 nm; emission 528/38 nm); TRITC/Cy5 (FM4-64 staining; excitation 542/27 nm ; emission 676/34 nm). Either 7H9S of 7H9T medium was circulated through the device at a flow rate of 25 µl/min. Images were analysed and processed using Softworx 4.1 (Applied Precision, GE HealthCare) or ImageJ v 1.48.

2.8 Scanning electron microscopy (SEM)

A 50 ml culture was grown in 7H9S or 7H9T containing appropriate antibiotic to an OD_{600nm} of 0.8. The cells were harvested by centrifugation, washed twice with PBS and resuspended in 2.5 % gluteraldehyde in PBS overnight at 4 °C. The cells were then washed twice with PBS and resuspended in 100 µl of 2 % osmium tetraoxide in PBS and incubated at room temperature for 1 h. Cells were then washed twice with PBS and dehydrated by submerging in a series of ethanol concentrations for 2 min at each concentration beginning with 30 % then 50 %, 70 % and twice at 100 % ethanol, followed by storage in 100 % ethanol. Cells were spotted on a filter, coated twice with carbon and viewed using the FEI Nova NenoSEM 230.

2.9 Transmission electron microscopy (TEM)

A 50 ml culture was grown in 7H9S or 7H9T containing appropriate antibiotic to an OD_{600nm} of 0.8. The cells were harvested by centrifugation and washed twice in 1 ml PBS. Cells were resuspended in fixing solution containing 0.1 mM HEPES, 2 % (v/v) formaldehyde, 2.5 % (v/v) gluteraldehyde and 0.05 % (w/v) ruthenuim red and incubated at room temperature for 1 h. The cells were then harvested and resuspended in 100 µl of 2 % osmium tetraoxide in PBS and incubated at room temperature for 1 h. The samples were then washed twice in PBS and dehydrated by submerging in a series of ethanol concentrations for two min at each concentration beginning with 30 % then 50 %, 70 % and twice at 100 % ethanol. The dehydrated samples were then washed in propylene oxide twice and incubated for 1 h in a solution made up of 50 % propylene oxide and 50 % resin mixture, which consists of 5.62 g araldite, 7.75 g epon 812 and 15 g DDSA. The

propylene oxide resin mixture was then removed and the cells were resuspended in 100 % resin mixture and incubated at room temperature overnight. Cells were harvested, the resin mixture was removed and fresh resin mixture containing DMP 30 at a ratio of 1:40 (g: g) of DMP 30 to resin mixture was added to the cells and incubated at 60 °C for 48 h. The solidified resin was sectioned using a Relchert Ultracut Ultramucrotome (Circa) and viewed using a Tecnai F20 TEM.

2.10 Antibiotic susceptibility assays

The concentration of antibiotic required to inhibit the growth of various mycobacterial strains was determined using a microtiter assay. Briefly, bacterial strains were grown to an OD_{600nm} = 0.3. The microtiter plates were then set up using 96 well plates containing 12 rows. Antibiotic stocks, containing 4 × the initial concentration required for the first row in the plate, were set up and 100 µl of the stock was inoculated into the first row. Thereafter, 50 µl of media was inoculated into rows 2 to 12, then a 50 µl aliquot of the antibiotic stock from row 1 was inoculated into row 2, mixed and 50 µl was removed from row 2 and inoculated into row 3. This was done through to row 12 and a 50 µl aliquot was removed from the last row and discarded. Bacterial cultures were diluted 10 000 fold and a 50 µl aliquot was added to each well. These plates were sealed and incubated at 37 ˚C for 3 – 7 days at which point, growth was examined to determine the antibiotic minimum inhibitory concentration (MIC).

2.11 Ethidium bromide diffusion assay (EtBr)

A 20 ml culture was grown in 7H9 containing appropriate antibiotic to an OD_{600nm} equal 0.8. The cells were harvested by centrifugation at 3900 × g for 10 min, washed twice with PBS and resuspended in 1 ml PBS containing 0.4% glucose. The cell density was adjusted to an OD_{600nm} of 0.4. A 95 µl aliquot of the adjusted bacterial sample was placed into flat, clear bottom, black 96-well plates, followed by addition of EtBr to final concentration of 8 µg/ml. Fluorescence was measured with an excitation and emission wavelength of 530 nm and 585 nm, respectively, every 60 seconds for 60 min at 37 °C.

Chapter 3

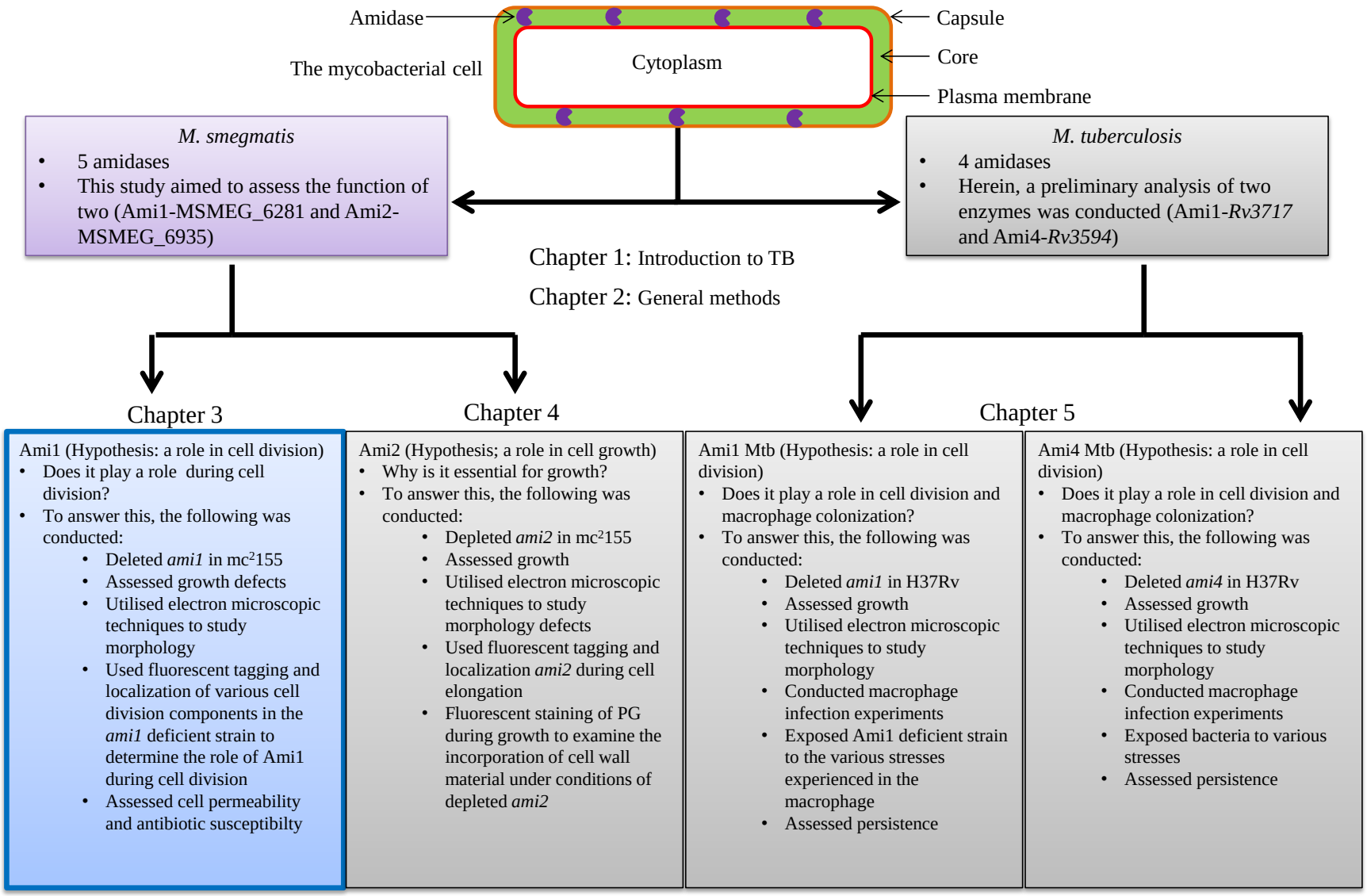

Figure 3.1: Flow chart highlighting the focus of chapter 3. Highlighted is the portion of the study which will be addressed in the following chapter (Figure drawn by S. Senzani).

3 The role of MSMEG_6281 (Ami1) in mycobacterial cell division

3.1 Introduction

3.1.1 Bacterial cell division

Cell division is an essential process occurring in all living organisms ranging from highly complex multicellular organisms down to single-cell life-forms (Khalilgharibi et al., 2012). Though mechanistically complex, cell division can be broken down into two vital processes. The first involves the duplication and partitioning of genetic material into two identical copies, also known as karyokinesis, followed by the division of cytoplasmic material into two similar (or dissimilar) daughter cells (cytokinesis) (Khalilgharibi et al., 2012). Owing to the complex nature bacterial cell division, this process is regulated and facilitated by complex multiprotein elements, which play a vital role in ensuring correct progression and ultimate completion of the process (Egan and Vollmer, 2013). In bacteria, a key element required for cell division is the protein FtsZ.

FtsZ is a tubulin-like bacterial protein, which possesses GTPase activity and is found in almost all bacteria (RayChaudhuri and Park, 1992, Wang and Lutkenhaus, 1993). It is central to cell division as it is believed to be the key component driving bacterial cytokinesis (Ortiz et al., 2016). FtsZ conducts two crucial functions during cell division, the first being an anchor for the recruitment of various cell division components, resulting in the formation of the cell division complex called the divisome (Ortiz et al., 2016, Mukherjee et al., 2001). The second is the provision of contractile force to drive the constriction of the inner cell membrane resulting in the formation and separation of the two daughter cells (Mukherjee et al., 2001). Both functions depend on the formation of the FtsZ-ring (Z-ring) (Mukherjee et al., 2001).

3.1.1.1 *The assembly of the ring*

The Z-ring is a ring-shaped complex consisting of multiple FtsZ polymers, bound to the circumference of the cell membrane at the site of cell division (Ortiz et al., 2016). Assembly of the ring begins with the polymerisation of FtsZ monomers with the aid of GTP (Scheffers and Driessen, 2002). The *N*-terminal GTPase region of FtsZ possesses a GTP binding pocket (Löwe and Amos, 1998). Binding of GTP results in further association of an adjacent C-terminal region with the GTPase domain of another FtsZ monomer, resulting in polymer formation (Scheffers and Driessen, 2002). These structures are not stable as GTP hydrolysis leads to dissociation of the C-terminal regions, leading to breakdown of the polymer. Consequently, there are components

which stabilise the Z-ring by inhibiting GTPase activity (Scheffers and Driessen, 2002). These include the bi-functional proteins ZapA, ZapB, ZapC and ZapD (Scheffers and Driessen, 2002, Low et al., 2004, Galli and Gerdes, 2012, Ortiz et al., 2016). These are somewhat functionally redundant proteins as they are individually non-essential. They stabilise FtsZ polymers and also play a role in the connection of neighbouring FtsZ polymers to form the ultimate structure of the Z-ring (Durand-Heredia et al., 2012). Deletion of multiple Zap components results in the formation of cellular filaments, which are unable to divide or form a Z-ring, indicating the collective essentiality of these proteins in the maturation and stabilisation of the Z-ring (Durand-Heredia et al., 2012). This extensive complement of *zap* genes is only found in γ-proteobacteria. In other organisms only ZapA is conserved and, in some instances, including actinomycetes, the *zap* genes are absent. The lack of clear *zap* homologues suggests alternate methods capable of stabilizing the Z-ring in actinomycetes. These mechanisms however remain currently unknown (Hale et al., 2011, Ebersbach et al., 2008, Marteyn et al., 2014). In addition to the Zap components, there are two other proteins that play an essential role in the maturation of the Z-ring, these are FtsA and ZipA. Though FtsZ retains the ability to interact with various cell division elements, it cannot bind to the cell membrane and requires FtsA and ZipA for this (Hale and de Boer, 1997).

FtsA is an actin-like ATP binding protein which retains ATPase activity. The main function of FtsA is to anchor the Z-ring to the site of cell division (van den Ent and Löwe, 2000, Hale and de Boer, 1997). FtsA activity is dependent on the binding of ATP (van den Ent and Löwe, 2000). The interaction between FtsA and ATP leads to conformational changes, which result in the attachment of FtsA to the plasma membrane and polymerisation of FtsA components forming membrane associated protofilaments (Szwedziak et al., 2012, van den Ent and Löwe, 2000, Osawa et al., 2008, Chen et al., 2017). These interact with the Z-ring, anchoring it to the cell membrane (Osawa et al., 2008, Cabré et al., 2013). ZipA conducts a similar function with one exception; ZipA does not form filaments and interacts directly with individual FtsZ monomers within the Z-ring filaments (Cabré et al., 2013, Loose and Mitchison, 2014, Chen et al., 2017). This protein, like the Zap complement of proteins, is only found in γ-proteobacteria (RayChaudhuri, 1999). ZipA also protects the Z-ring from ClpX protease degradation (Pazos et al., 2013). Association of ZipA inhibits interaction between ClpX and the Z-ring, thus preventing Z-ring degradation. This function cannot be conducted by any other cell division component (Pazos et al., 2013).

The localisation of the Z-ring is determined by various proteins that promote or inhibit assembly of the ring at the incorrect sites (Liu et al., 1999, Addinall and Lutkenhaus, 1996). These include multiple mechanisms such as the Min system, the Nucleoid Occlusion System (Noc) and other distinct components in organisms which do not possess clear homologues of these proteins. Alternate mechanisms include EzrA, which prevents FtsZ localisation at incorrect locations and SepF, MapZ, PomZ, SsgA and SsgB, which localise at sites of future septum formation prior to FtsZ and function to recruit FtsZ to these sites (Singh et al., 2007, Gola et al., 2015, Fleurie et al., 2014, Treuner-Lange et al., 2013, Willemse et al., 2011). Deletion or reduction of these components results in multiple cell division defects including, misplacement of septa, leading to mini-cells and anucleate cells, as well as the formation of filaments as a result of the inability to recruit FtsZ (Singh et al., 2007, Gola et al., 2015, Fleurie et al., 2014, Treuner-Lange et al., 2013, Willemse et al., 2011).

Following the assembly and maturation of the Z-ring, a number of Fts components are then recruited to the septum, the first being FtsE and FtsX, which play an important role in the activation of cell wall amidases in *E. coli* and other cell wall hydrolases in *Bacillus* species (Yang et al., 2011, Meisner et al., 2013, Egan and Vollmer, 2013). This is followed by the recruitment of FtsK, a DNA binding protein which plays a crucial role in the last phases of chromosome segregation by shuttling DNA to neighbouring daughter cells, ensuring that the complete genome is present in both daughter cells (Massey et al., 2006). Next is FtsQ, FtsB and FtsL, which appear to be recruited as a complex. However, the exact function of this carefully coordinated sequence of events currently remain unclear (Egan and Vollmer, 2013). This is followed by recruitment of FtsW, which functions as a lipid II transporter. Following this, FtsI, a penicillin-binding protein responsible for the synthesis of septal PG, is recruited to the septum (Mohammadi et al., 2011, Egan and Vollmer, 2013). The last component recruited is FtsN, which initiates septum synthesis and membrane constriction. FtsN is also essential for the septal recruitment of the cell division amidase, AmiC, and the penicillin-binding protein, PBP1B, in *E. coli* (Rico et al., 2010, Peters et al., 2011). This complex, termed the divisome, forms the core machinery driving cell division and separation in bacteria, shown in Figure 3.2. This dissertation focused on amidase function in cell division in mycobacteria.

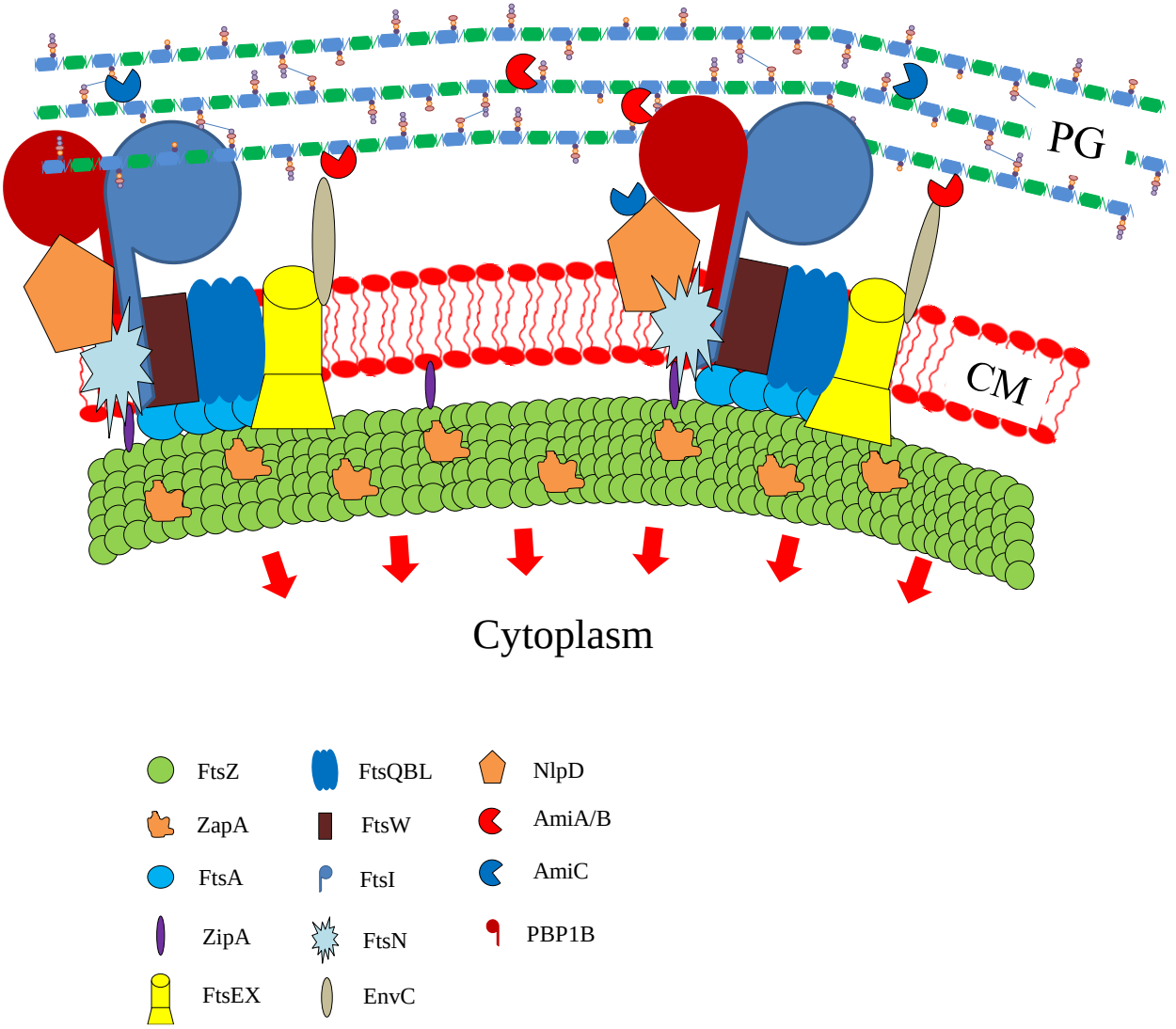

Figure 3.2: Cross sectional diagrammatic representation of a bacterial septum indicating two divisomes formed at adjacent sites of the Z-ring. Shown are the various components which make up the bacterial divisome and the direction of Z-ring constriction depicted by the red arrows. CM: cell membrane and PG: PG. Figure was drawn by S. Senzani using microscoft PowerPoint 2012.

3.1.2 The function of cell wall amidases

Cell wall amidases have different roles in a wide variety of organisms. Many organisms encode a multiplicity of these genes and though they catalyse the same reaction, their fundamental physiological role in different organisms varies, mainly due to the expression patterns and subcellular localisation. The most extensively studied group of cell wall amidases to date are those found in the gram-negative *E. coli* and the gram positive *B. subtilis*. These are discussed further below.

3.1.2.1 *Cell wall amidase function in the model organisms*

A majority of the work conducted to understand the function of cell wall amidase during cell division has been conducted in the model species *E. coli*, which encodes 5 distinct cell wall amidases [designated as AmiA, AmiB, AmiC, AmiD and AmpD (Heidrich et al., 2001, Korsak et al., 2005)].

AmiA is a periplasmic, amidase_3 domain-containing amidase. Deletion of this enzyme pointed to a possible role in cell division, as strains lacking AmiA displayed septation defects which were illustrated by the formation of cellular chains consisting of three to four cells attached by division septa (Korsak et al., 2005, Heidrich et al., 2001). The mechanism through which AmiA conducts this role is still unknown, as fluorescence-based localisation of AmiA has shown the enzyme localises diffusely throughout the cell. Furthermore, interaction between AmiA and elements localizing at the division septa has not been demonstrated (Bernhardt and de Boer, 2003). Analysis of the domains contained within this enzyme indicates AmiA is comprised of only the amidase_3 domain, containing no putative PG binding domains. This suggests the enzyme interacts with additional components in order to associate with the PG substrate.

AmiC is a periplasmic, amidase_3 domain containing amidase. AmiC is hypothesised to function as the major septation amidase, as analysis of *E. coli* strains lacking AmiC displayed significant septation defects as depicted by the formation of cellular chains consisting of three to 6 cells attached by division septa in 20 to 30 % of the cellular population (Heidrich et al., 2001, Korsak et al., 2005). Analysis of the cellular localisation of AmiC amidase has demonstrated that the enzyme localises exclusively at the division septa, supporting the hypothesis that it is a septal division enzyme (Bernhardt and de Boer, 2003). Analysis of the domains contained within this enzyme indicates AmiC is comprised of an amidase _3 domain and an AMIN domain, which is a PG binding domain hypothesised to play an important role in the correct septal localisation of AmiC (Rocaboy et al., 2013).

AmiB is a periplasmic, amidase_3 domain containing amidase (Peters et al., 2011). Analysis of *E. coli* strains lacking AmiB yielded no defects in cell division; however, deletion of this enzyme in combination with AmiA or AmiC resulted in exacerbation of the AmiA or AmiC deletion phenotype (Korsak et al., 2005, Heidrich et al., 2001). Like AmiC, AmiB localises at the division septa and this localisation is also dependent of FtsN (Peters et al., 2011). This suggests AmiB

functions synergistically with AmiC to hydrolyse septal PG. Analysis of the domains contained within this enzyme indicates AmiB is comprised of an amidase_3 domain, containing no putative PG binding domains, suggesting interaction with additional components in order to interact with septal PG.

Further analysis of these amidases revealed the presence of amidase activators, designated as EnvC and NlpD (Uehara et al., 2010). These are non-catalytic Peptidase_M23 domain-containing proteins that possess the ability to enhance AmiA, AmiB or AmiC mediated PG hydrolysis (Uehara et al., 2010). The amidase activator EnvC activates AmiA and AmiB (Uehara et al., 2010). EnvC localises at the division septum and this recruitment is dependent on the ABC transporter complex, FtsEX, which forms part of the divisome (Yang et al., 2011, Peters et al., 2011). EnvC interaction with the FtsEX complex is facilitated through the trans-membrane protein FtsX. Both EnvC and FtsX possess coiled coil domains that may play a role in interaction. NlpD is responsible for the activation of AmiC and also localises to the division site however, NlpD recruitment is FtsN dependent (Yang et al., 2011, Peters et al., 2011). Direct interaction between NlpD and FtsN has not been demonstrated. The mechanism through which these proteins activate amidases is unknown. Currently, the proposed model of activation suggests that the native conformation of the three amidases consists of a closed active site preventing PG attachment. The interaction with activator is expected to lead to conformational alterations in the amidase which would result in an open active site (Uehara et al., 2010).

3.1.2.2 *Cell wall amidases in Chlamydia*

Organisms in the genus *Chlamydiales* do not possess any genes coding for FtsZ and a number of components belonging to the Fts complement are not present. Thus, lack the central component required for cell division in other bacteria suggests a divergent mechanism of cell division (Pilhofer et al., 2013). Initially, it was proposed that the absence of FtsZ did not affect cell division primarily due to the hypothesis that *Chlamydiales* do not possess the classical bacterial cell wall containing PG, subsequent studies have shown that these organisms do retain genes required for PG synthesis and revealed synthesis of septal PG during cell division, suggesting that other components compensate for the lack of FtsZ (Pilhofer et al., 2013). Two proposed candidates for this role are MreB and RodZ, which localise to future septal sites and appear to play a role in the

constriction of the inner membrane, similar to the Z-ring. The ability of these components to recruit other Fts elements however is unclear (Ouellette et al., 2012).

Though lacking FtsZ, *Chlamydiales* retain a gene coding for a bi-functional amidase, AmiA (Klöckner et al., 2014). The *Chlamydiales* AmiA is unique in the sense that it possesses both amidase and carboxypeptidase activity (Klöckner et al., 2014). Furthermore, it has been shown to be an active amidase as complementation of the amidase deficient *E. coli* mutant with AmiA from Chlamydia reversed the chaining phenotype, indicating that the enzyme can function as a septal amidase (Klöckner et al., 2014). It is postulated that AmiA is responsible for the processing of lipid II material prior to incorporation into the cell wall, as well as cleavage of cell wall material at the septum resulting in cell separation (Klöckner et al., 2014).

As illustrated above, amidases play important and sometimes non-redundant roles in bacterial cell division. Their biological function in mycobacteria has yet to be fully unravelled. Preliminary data obtained in our lab identified and bio-infomatically characterised two mycobacterial amidase_3 containing proteins in Mtb and their *M. smegmatis* homologues (Appendix D, Figure D1) (Senzani, 2014 [MSc dissertation], Machowski et al., 2014). As one of these, MSMEG_6281 (herein referred to as Ami1), was predicted to be non-essential for growth, this protein was deleted in the mc^2155 background and preliminary analysis indicated a possible role for the mycobacterial amidase. Herein, we aimed to expand on these observations.

Hypothesis: Ami1 plays a central role in cell division and deletion thereof will result in division defects and changes in the mycobacterial cell wall. We also expect that these defects will result in morphological changes in the mycobacterial cell.

Preliminary work prior to this PhD. As part of an MSc study (Senzani, 2014) an Ami1 defective mutant was generated and a preliminary phenotypic characterisation was carried out.

Aims and objectives: The main aim of this section was to carefully characterise the existing Ami1 defective mutant to establish a biological function for this enzyme. As such, the specific objectives included:

1. An *ami1* defective mutant was constructed in an MSc study (Senzani, 2014) and herein, the first objective was construction of a genetically complemented derivative, Δ*ami1*::pSEami1.
2. Confirming previously identified phenotypic defects in the Δ*ami*1 mutant through microscopy.
3. Assessing individual bacterial growth through single cell microscopy.
4. Construction of a reporter strain, mc^2155::pAmi1GFP to assess cellular localisation of Ami1GFP.
5. Confirming Ami1GFP functionality through genetic complementation of the Δ*ami1* strain.
6. Construction of strains, mc^2155::pFtsZGFP and Δ*ami1*::pFtsZGFP for cellular localisation of FtsZGFP in both mc^2155 and the *ami1* deficient strains.
7. Construction of a Δ*ami1*::ParBM-DnaNG strain for localisation of DnaN and ParB in the *ami1* deficient strain.
8. Assessing antibiotic susceptibility and cell wall permeability of the Δ*ami1* strain.

3.2 Methods

3.2.1 Construction of the *ami1* complementation derivative, Δ*ami1*::pSEami1

Primers were designed; *ami1*pSECF and *ami1*pSECR listed on Table 3.3, to amplify the *ami1* gene as well as 400 bp upstream the transcriptional start codon. PCR amplification of the respective fragments was carried out using Phusion polymerase, using an annealing temperature of 60 °C for *ami1* and an elongation time of 1 min to allow for complete amplification of the *ami1* fragment, which is 1245 bp. The PCR products were purified using the Nucleospin PCR purification Kit. Thereafter, 3 µg of pSE100 and the PCR products were digested with *Hind*III and *Xba*I, removing the P_{mcy}-tet. The pSE100 restriction product was then treated with FastAP phosphatase for 30 min. The restriction products were separated on a 0.8 % agarose gel and the respective bands (5172 bp for pSE100 and 1239 bp for *ami1*) were excised from the gel and purified using the Nucleospin gel purification kit. These were then quantified using the NanoDrop and ligations were set up containing 50 ng of pSE100 and varying molar ratios of *ami1*. The fragments were ligated using Fermentas T4 ligase for 10 min, transformed into DH5α cells and plated on LA_{Hyg200}.

Ten possible clones were selected and screen by restriction with *Eco*RI, which would yield two fragments, a 4105 bp and a 2306 bp band. A single positive clone was grown in 50 ml LB_{Hyg200} overnight and bulk vector extraction was carried out using the Nucleobond bulk vector extraction kit. Extracted vector DNA was quantified and digested with a variety of enzymes to profile the *ami1* complementation vector (pSEami1). The vector was also sent for sequencing to check for the presence of mutations within the amplicon. Following this, 1 µg of pSEami1 was electroporated into electrocompetent Δ*ami1* cells, plated on $7H10_{Hyg50}$ and incubated at 37ºC for 5 days to create the Δ*ami1*::pSEami1 strain. Subsequently, 5 colonies were selected and PCR was conducted on these using the *ami1*pSECF and *ami1*pSECR primers which would yield a 489 bp band for the Δ*ami1* strain and both a 1240 bp band representing the pSEami1 copy and the 489 bp Δ*ami1* band respectively

A single clone was selected (Δ*ami1*::pSEami1), cultured and qPCR was conducted on the WT, Δ*ami1* and Δ*ami1*::pSEami1 strains to compare the levels on *ami1* transcription. The *sigA* gene was included to serve as a normaliser for RNA amounts.

Table 3.1: Bacterial strains created/used in this study

Strain	Genotype	Reference
Escherichia coli DH5α	*SupE44* Δ*lacU169 hsdR17 recA1 endA1 gyrA96 thi-1 relA1*	Promega, Madison, WI
mc^2155	High frequency transformation mutant of *M. smegmatis* ATCC 607	(Snapper et al., 1990)
Δ*ami1*	Derivative of mc^2155 carrying an unmarked, out-of-frame deletion in *ami1*	Senzani, 2014
Δ*ami1*::pMVami1	Derivative of Δ*ami1* carrying pMVami1 integrated at the bacterial *attB* phage attachment site, Hyg^R	Senzani, 2014
Δ*ami1*::pSEami1	Derivative of Δ*ami1* carrying episomal pSEami1, Hyg^R	This study
mc^2155::pAmi1GFP	Derivative of mc^2155 carrying an episomal pSAmi1GFP vector, Hyg^R	This study
mc^2155::pFtsZGFP	Derivative of mc^2155 carrying pMFtsZGFP integrated at the *attB* bacterial phage attachment site, Hyg^R	This study
mc^2155::plS220	Derivative of mc^2155 carrying plS220 integrated at the bacterial *attB* phage attachment site, Hyg^R	This study
mc^2155::pMAmi1GFP	Derivative of mc^2155 carrying pMAmi1GFP integrated at the *attB* bacterial phage attachment site, Hyg^R	This study
Δ*ami1*::pFtsZGFP	Derivative of Δ*ami1* carrying pMFtsZGFP integrated at the *attB* bacterial phage attachment site, Hyg^R	This study
Δ*ami1*::plS220	Derivative of Δ*ami1* carrying plS220 integrated at the bacterial *attB* phage attachment site, Hyg^R	This study
Δ*ami1*::pAmi1GFP	Derivative of Δ*ami1* carrying episomal pAmi1GFP, Hyg^R	This study
mc^2155::ParBM-DnaNG	Derivative of mc^2155 in which *parB* and *dnaN* are replaced with *parB-mCherry* and *dnaN-gfp*, respectively	Santi and McKinney (2015)
Δ*ami1*::ParBM-DnaNG	Derivative of mc^2155::ParBM-DnaNG, containing an out of frame deletion in *ami1*	This study
Δ*ami1*::pAmi2GFP	Derivative of Δ*ami1* carrying episomal pAmi2GFP, Hyg^R	This study

Kan^R: Kanamycin Resistance, Hyg^R: Hygromycin Resistance

3.2.2 Construction of the Ami1 localisation strain, mc^2155::pAmi1GFP

Localisation of Ami1 was conducted using the rsEGFP fluorescent tag. The approach involved PCR amplification of the rsEGFP tag, and fusion to the *ami1* gene by three-way cloning of the

Table 3.2: Vectors created and/or used in this study

Vectors	Genotype	Reference
pSEAmi1	Derivative of pSE100(H) carrying a functional *ami1* gene and the upstream native promoter region Hyg^R	This study
pAmi1GFP	Derivative of pSE100 carrying the *ami1-rsEGFP* fusion gene downstream the P_{myc}-tet Hyg^R	This study
pFtsZGFP	Derivative of pMV306(H) carrying the *ftsZ-rsEGFP* fusion gene downstream the *ftsZ* native promoter Hyg^R	This study
pIS220	Derivative of pMV361 carrying a DivIVA-GFP fusion under the regulation of the *hsp60* promoter, Hyg^R	(Santi and McKinney, 2015)
pFtsZGFP	Derivative of pMV306(H) carrying the *ftsZ-rsEGFP* fusion gene downstream the *ftsZ* native promoter Hyg^R	This study

Kan^R: Kanamycin Resistance, Hyg^R: Hygromycin Resistance, Amp^R: Ampicillin Resistance

Table 3.3: list of primers used in the *M. smegmatis*, *ami1* study

Gene	primers	Amplicon
*ami1*pSECF	GCGCGCTCTAGACTGCGCCATGATCGTCAC	1240 bp *ami1* amplicon including 400 bp upstream the *ami1* start codon
*ami1*pSECR	GCCGCCAAGCTTGGAGAACCTCAAGAAGCA	
*ami1*RTF	CCGGAATGATCGTGTTCCT	qPCR product, a 106 bp region within the *ami1* ORF
*ami1*RTR	CTCTCCTGGCAGTTCTTGGT	
*ami1*RTR2	GTCCCACGTGAAGCTGTGTT	RT-PCR conversion primer
SigARTF	GGGCGTGATGTCCATCTCCT	qPCR product, a 122 bp region within the *sigA* ORF
SigARTR	GTATCCCGGTGCATGGTC	
*ftsZ*pSELF	CGCGCGTCTAGACGCGTCGATCACGTTGAC	1586 bp *ftsZ* amplicon including 400 bp upstream the *ftsZ* start codon and excluding the transcriptional stop codon
*ftsZ*pSELR	GGCGGCGAATTCGTGCCGCATGAAGGGCGG	
*ami1*pSELF	GCGCCGCCGCATGCCGCGACGCGGCTACCGTG	825 bp *ami1* amplicon excluding the transcriptional stop codon
*ami1*pSELR	GCGCGCGCGAATTCACGCACGGGGCTGACGGC	
rsEGFPF	CGCGCGGAATTCATGGTGAGCAAGGGCGAGGA	720 bp *rsEGFP* amplicon
rsEGFPR1	GCGCGCCTGCAGAGGAGTCCAAGCTCAGCTAA	
rsEGFPRF	GCGCGCCCATGGAGGAGTCCAAGCTCAGCTAA	
MsmAmi1SF	GCCGCCGGATCCCAGGTACAGCCCGATGCT	1704 bp *ami1* amplicon including 31 bp of the 5′ end region of the *ami1* gene and 1673 bp of the region upstream the transcriptional start site
MsmAmi1SR	GCCGCCGAATTCGCAGACAGGCTGGGACTC	

*red: restriction endonuclease site

ami1 and rsEGFP fragments into pSE100, downstream the Tet operator. This resulted in a construct wherein the Tet operator regulates the expression of *ami1* which contains a C-terminal rsEGFP tag.

Primers were designed, *ami1*pSELF and *ami1*pSELR, for *ami1* and rsEGFPR and rsEGFPR1, for *rsEGFP*, listed in Table 3.3, to amplify the full-length *ami1* gene and *rsEGFP* tag. In the case of

the amidase primers, these were designed to amplify a product which does not contain the transcriptional stop codon allowing for the fusion of the reading frame with the C-terminus of the *rsEGFP* tag. PCR amplification of the fragments was carried out using Phusion polymerase, using an annealing temperature of 60 ºC and an elongation time of 1 min to allow for complete amplification of the *ami1* fragment. The PCR products were purified using the Nucleospin PCR purification Kit. Thereafter, pSE100 was digested with *Sph*I and *Pst*I, the *ami1* fragment was digested with *Sph*I and *Eco*RI and the rsEGFP fragment was digested with *Eco*RI and *Pst*I. The digested pSE100 was then treated with FastAP phosphatase for 10 min. The restriction products were separated on a 0.8 % agarose gel and the respective bands (5498 bp for pSE100, 803 bp for *ami1* and 698 bp for *rsEGFP*) were excised and purified using the Nucleospin gel purification kit. Thereafter, these were quantified using the NanoDrop spectrophotometer and ligations were set up containing 50 ng of pSE100 and varying molar ratios of the *ami1* and rsEGFP fragments. The fragments were ligated using Fermentas T4 ligase for 10 min, transformed into DH5α cells and plated on LA_{Hyg200}. Following the emergence of bacterial colonies, 10 possible clones were selected and screen by restriction with *Eco*RI, which would yield four fragments, a 2461 bp, 2306 bp, 1538 bp and a 732 bp band. A single positive clone (pAmi1GFP) was grown in 50 ml LB_{Hyg200} overnight and bulk vector extraction was carried out using the Nucleobond bulk vector extraction kit. Vector DNA was quantified and digested with a variety of enzymes to profile the rsEGFP tagged Amidase 1 vector. The vector was also sent for sequencing to check for mutations, which might have occurred during PCR amplification. Following confirmation, 1 µg of the vector was then electroporated into electrocompetent mc^2155 cells, plated on $7H10_{Hyg50}$ and incubated at 37ºC for 5 days to create the mc^2155::pAmi1GFP. Clones were selected and assessed by PCR screening using the *ami1*pSELF and the rsEGFPR primers to determine whether they possess the full length *ami1-rsEGFP* fusion fragment. The PCR was run on 0.8 % agarose gel.

3.2.3 Construction of the FtsZ localisation strains, mc^2155::pFtsZGFP and Δ*ami1*::pFtsZGFP

Localisation of FtsZ was conducted using the rsEGFP fluorescent tag. As with Ami1, the approach involved PCR amplification of the rsEGFP tag and the *ftsZ* gene including 400 bp upstream the transcriptional start site. The amplification would be followed by three way cloning of the ftsZ and rsEGFP fragment into the integrating vector pMV306(H).

Primers, *fts*ZpSELF and *fts*ZpSELR for *ami1*, and rsEGFPR and rsEGFPRF for rsEGFP, listed in Table 3.3, were used to amplify the *rsEGFP* tag and *ftsZ* fragment. The *ftsZ* primers were designed to amplify a product which does not contain the transcriptional stop codon allowing for fusion to the C-terminus of the *rsEGFP* tag. PCR amplification of the respective fragments was carried out using Phusion polymerase, using an annealing temperature of 60ºC and an elongation time of 1 min to allow for complete amplification of the *ftsZ* fragment, which is 1586 bp. The PCR products were purified using the Nucleospin PCR purification kit and 3 µg of pMV306(H) and the PCR products were digested for cloning. The pMV306(H) vector was digested with *Nco*I and *Xba*I, the *ftsZ* fragment was digested with *Xba*I and *Eco*RI and the *rsEGFP* fragment was digested with *Eco*RI. Thereafter, pMV306(H) was treated FastAP phosphatase for 30 min and the *rsEGFP* fragment was phosphorylated with PNK. The digested products were separated on a 0.8 % agarose gel and the respective bands (4262 bp for pMV306, 1564 bp for *ftsZ*, 706 bp for *rsEGFP*) were excised and purified using the Nucleospin gel purification kit. The resulting DNA was quantified using the NanoDrop spectrophotometer and ligations were set up containing 50 ng of pMV306(H) and varying molar ratios of *ftsZ* and *rsEGFP* fragment. The fragments were ligated using Fermentas T4 ligase for 10 min, transformed into DH5α cells and plates LA_{Hyg200}. Several, possible clones were selected and analysed by restriction with *Eco*RI, which would yield three fragments, a 2858 bp, 2943 bp, and a 743 bp band. One positive clone was grown in 50 ml LB_{Hyg200} overnight, followed by bulk vector extraction using the Nucleobond bulk vector extraction kit. Vector DNA was profiled with a variety of restriction enzymes to confirm integrity. The vector was also sent to Inqaba biotech, for sequencing to confirm that no mutations occurred during PCR amplification. Once confirmed, 1 µg of the vector was then electroporated into electrocompetent mc^2155 and Δ*ami1* cells, plated on $7H10_{Hyg50}$ and incubated at 37ºC for 5 days to create the mc^2155::pFtsZGFP and Δ*ami1*::pFtsZGFP. Clones were selected and assessed by PCR screening using the *fts*ZpSELF and the rsEGFPR primers to determine whether clones possess the full length *ftsZ-rsEGFP* fusion fragment. PCR products were run on a 0.8 % agarose gel.

3.2.4 Construction of the Δ*ami1*::ParBM-DnaNG strain

To construct the Δ*ami1*::ParBM-DnaNG strain, the native *ami1* gene was knocked out using homologous recombination in a strain background that contained chromosomal derivatives of *parB* and *dnaN* that carry fusions to fluorescent proteins (Santi et al., 2013). This strain was kindly provided by N. Dhar. This technique involves the use of a suicide vector carrying a

truncated/deleted non-functional version of the gene of interest and a substantial amount (1200 bp - 1500 bp) of the 5′ and 3′ regions to create areas of homology. Also included are selectable and counter-selectable markers. The vector was inserted into mycobacterial cells and plated on antibiotic, which drives the integration of the non-replicating suicide vector into the mycobacterial genome using the 5′ or 3′ homologous regions, resulting in the production of a single crossover (SCO) strain that retains both the wild type and mutant allele. The second homologous recombination event is induced by using a counter-selectable marker on the vector, in this case the *sacB* gene, which encodes Levane Sucrase that converts sucrose to a toxic metabolite, resulting in the death of bacterial cells (Reyrat et al., 1998). Thus, plating on media containing sucrose drives the occurrance of the second recombination event, removing the vector to abrogate the lethality of the *sacB* gene. The second crossover can occur in the same homologous region as the first crossover, resulting in the regeneration of the wild type strain, or it can occur in the homologous region opposite to that of the first crossover, resulting in the production of a mutant strain.

Using the p2ΔAmi1G19 vector generated previously (Senzani, 2014), 1, 3 and 5 µg of DNA was electroporated into electrocompetent mc^2155::ParBM-DnaNG cells and plated on 7H10 containing Kan, Hyg and 0.004 % X-gal, then incubated at 37 ˚C for 5 days to create SCOs. A single blue colony was then cultured in 2 × TY supplemented with Kan and Hyg at 37 ºC, then sub-cultured in 2 × TY without antibiotic. The resulting cells were subjected to sucrose counter selection by plating 100 µl of a 10-fold serial dilution series onto media containing sucrose and X-gal. The plates were incubated for 3 - 5 days until blue and white colonies emerged. White colonies represent strains which have undergone the second cross over event to yield either a reversion to wild type or a mutant strain and blue colonies represent strains that have incurred a mutation in *sacB* to render them resistant to the toxic effects of sucrose. Subsequently, 10 white colonies were selected and PCR screening was conducted on these using the *ami1*pSECF and *ami1*pSECR primers which would yield a 1240 bp band in the case of wild type and a 489 bp band for the Δ*ami1*::ParBM-DnaNG strain.

Figure 3.3 illustrates the basic outline of the research undertaken in this chapter, with reference to the specific methods.

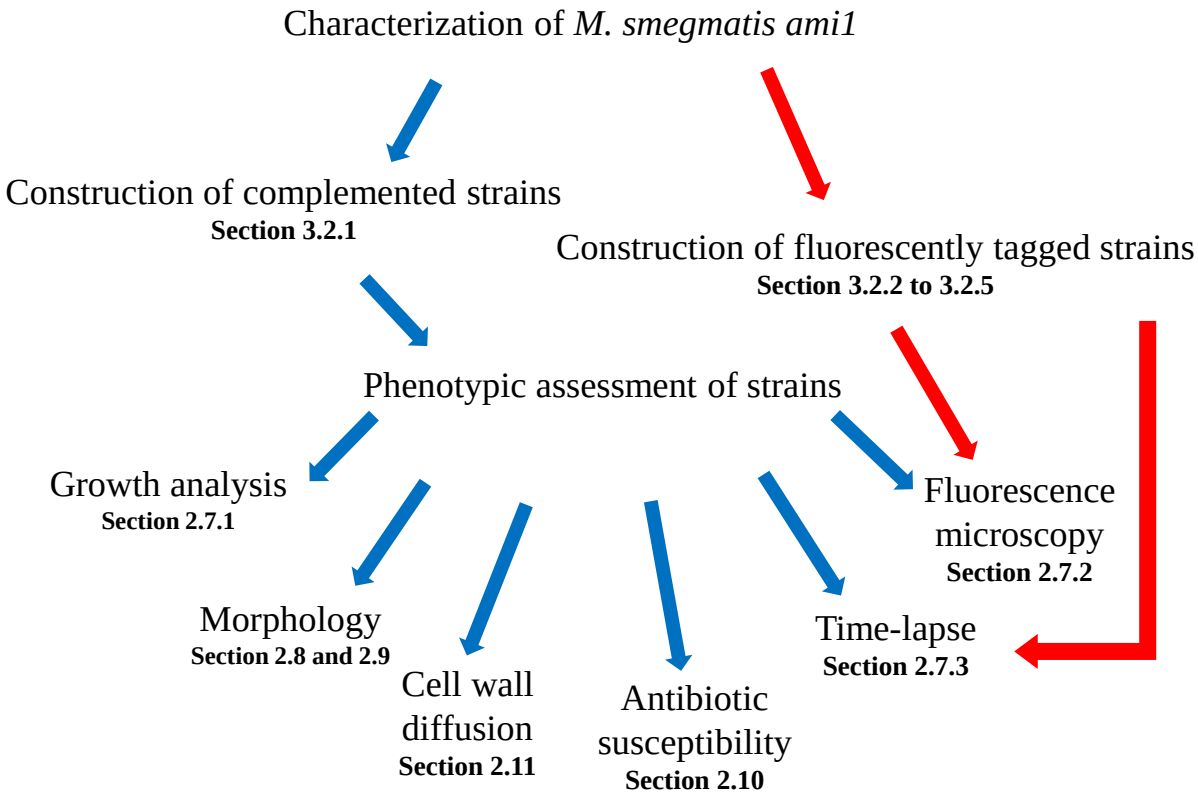

Figure 3.3: Flow chart depicting the experimental layout for the work undertaken to study *M. smegmatis ami1*, described in this chapter.

3.3 Results

3.3.1 Construction of the Ami1 complementation strain

During an MSc study (Senzani, 2014), a Δ*ami1* mutant was constructed and genotypic characterisation of this strain can be found in Appendix D, Figure D2. Thereafter a genetically complemented derivative of the Δ*ami1* mutant was constructed. However, this strain did not display the expected reversion to the wild type phenotype. Hence, a new strain was constructed herein. The approach adopted involved the introduction of an episomal variant of *ami1,* in which expression would be driven of the native promoter as opposed to the integrating pMVami1 vector.

3.3.1.1 *Construction of the pSEami1 vector*

PCR amplification was conducted to amplify the *ami1* gene and 400 bp upstream the transcriptional start codon. The fragments were then cloned into pSE100 and clones were screened by restriction digest with *Eco*RI. A single positive clone was then selected and the genetic integrity of the vector was confirmed by extensive restriction profiling, which is shown in Figure 3.4.

In all cases, with the exception of the *Sma*I restriction digest, which did not cleave the vector DNA, all the fragment sizes observed corresponded to the vector map and expected sizes, confirming the genetic integrity of the vector (Figure 3.4). The genetic integrity of the vector was then further confirmed by sequencing of the cloned region, which revealed that no mutations had occurred during PCR and cloning processes (data not shown). This vector was then used for construction of the Δ*ami1*::pSEami1 strain.

3.3.1.2 *Construction and screening of the Δami1::pSEami1 strain*

The pSEami1 vector was electroporated into the mc^2155 strain (section 2.4.2); the transformation efficiency obtained from the electro-competent cells was 8.4×10^3 CFU/µg vector DNA (determined using the pSE100 control vector). Five clones were selected and screened by PCR, Figure 3.5A. Clone 1 was selected and RT-qPCR was conducted to determine whether the full length variant of the gene was being expressed at similar levels to the mc^2155 copy, Figure 3.5B.

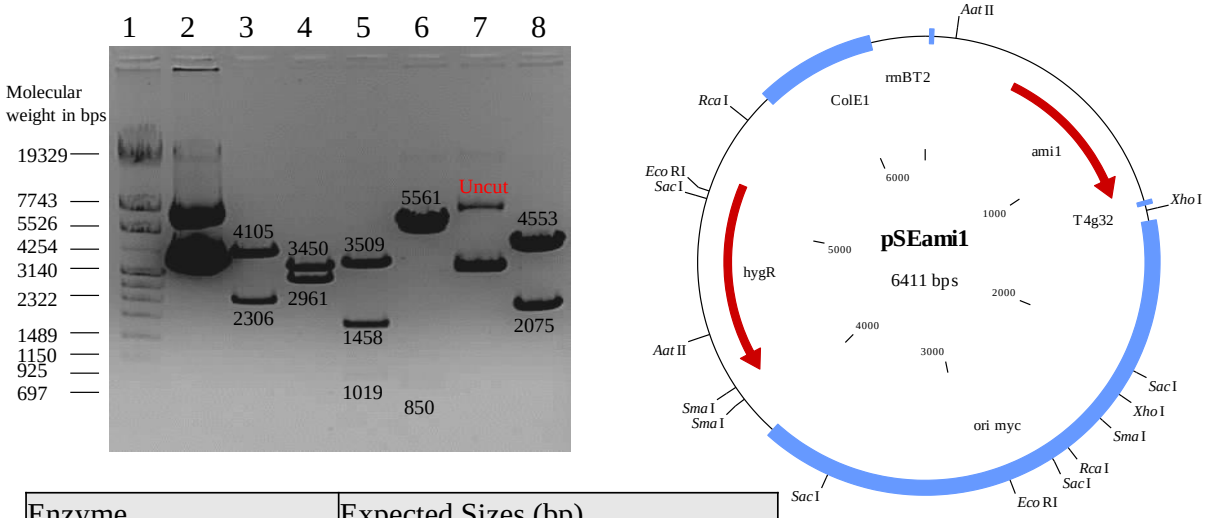

Enzyme	Expected Sizes (bp)
*Eco*RI	4105, 2306
*Rca*I	3450, 2961
*Sac*I	3409, 1458, 1019, 525
*Xho*I	5561, 850
*Sma*I	4553, 1792, 66
*Aat*II	4336, 2075

Figure 3.4: Restriction profile of pSEami1. Shown are the different restriction nucleases used and the expected sizes in a table, which result from restriction digests of the pSEami1 vector. The predicted vector map of pSEami1 vector and agarose gel depicting the products of restriction digest of pAmi1GFP are also shown. In the agarose gel, Lane 1: Roche Marker IV, Lane 2: Uncut, Lane 3: *Eco*RI, Lane 4: *Rca*I, Lane 5: *Sac*I, Lane 6: *Xho*I, Lane 7: *Sma*I, Lane 8: *Aat*II.

3.3.2 Ami1 is essential for bacterial cell division and cell shape maintenance

Preliminary work conducted in *M. smegmatis* depicted a possible role for Ami1 in cell division as shown by the formation of chains consisting of three or more cells attached by cell division septa (Senzani, 2014). At the time, we did not conduct an in-depth analysis of the observed phenotypes to determine the robustness of the data. As such, one of the initial tasks in this PhD was to assess the cell division defects observed in the preliminary analysis. Thus, high resolution SEM was conducted on the mc^{2}155, Δ*ami1* and Δ*ami1*::pSEami1 strains and representatives of the resulting micrographs are given in Figure 3.6. We noted numerous defects including the formation of cellular chains, lateral budding and abnormal septa, Figure 3.6. To further quantify this, various parameters including cell length, width, percentage of chains and percentage of cells containing abnormal septa were measured to get a better understanding of the phenotypes, Figure 3.7 and Figure 3.8.

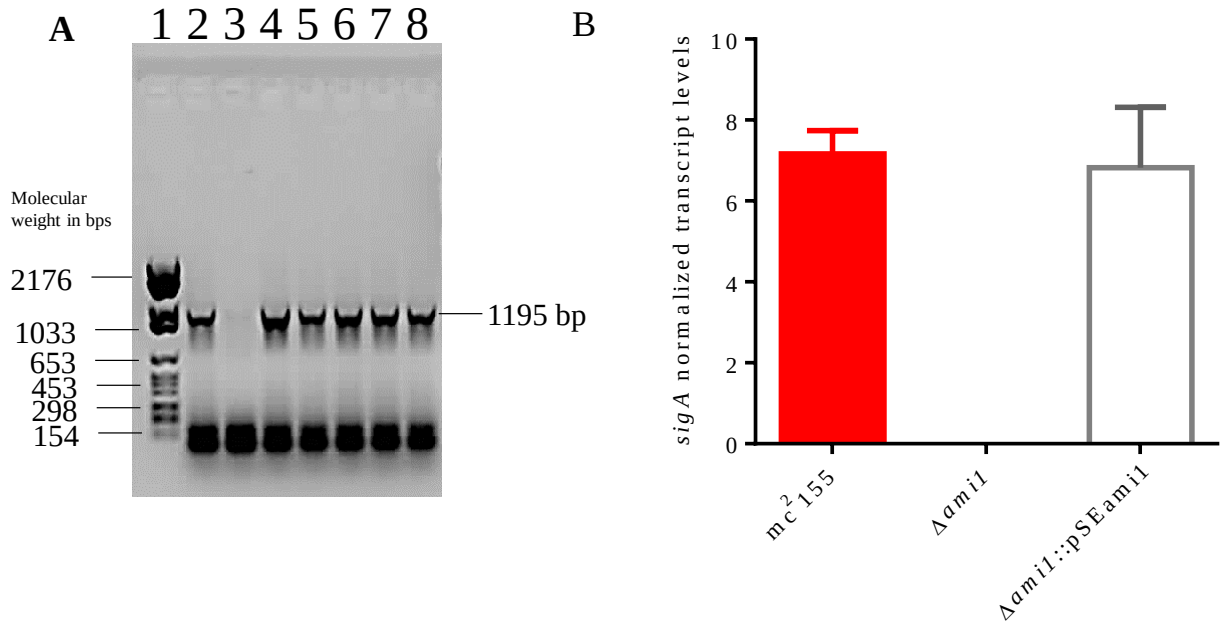

Figure 3.5: PCR screen and RT-qPCR of the Δami1::pSEami1 strain. (A) Shows the PCR screen for the five possible Δ*ami1*::pSEami1 clones showing the expected PCR product size (1195 bp) represent the full length *ami1* and the 400 bp 5′ region; Lane 1: Roche Marker VI, Lane 2: mc^{2}155, Lane 3: no template control and Lanes 4 to 8: clone 1 to 5. (B) Shows a bar graph representing the normalised log phase expression levels of *ami1* in the mc^{2}155, Δ*ami1* and Δ*ami1*::pSEami1 strains. Data are the average of three independent experiments.

From the ~ 400 cells analysed per strain, 20 % of the Δ*ami1* population were in the form of chains, while only 1.4 % and 3.7 % of the mc^{2}155 and Δ*ami1*::pSEami1 strains displayed this phenotype, respectively. A more prominent observation was the presence of septa in 94 % of the Δ*ami1* population as opposed to the 18 % and 16 % found in the mc^{2}155 and Δ*ami1*::pSEami1 strains respectively. This indicated that the Δ*ami1* mutant was arrested at the late stages of cell division, at the cell separation stage. Furthermore, 22 % of the Δ*ami1* population displayed the presence of abnormal septa, Figure 3.7. Further analysis of bacterial cell length and width revealed that the Δ*ami1* strains was longer and thinner when compared to the mc^{2}155 and Δ*ami1*::pSEami1 counterparts. The Δ*ami1* mutant strain also displayed a broader range with regards to cell length and width when compared to the wild type and genetically complemented counterparts. The Δ*ami1* displayed lengths of between 3 µm to 16 µm with a mean and median of 7.85 µm and 8.16 µm respectively, Figure 3.8. Cells from the mc^{2}155 and Δ*ami1*::pSEami1 strains fell within a cell length range of 2 µm to 9 µm with a mean and median of 4.76 µm and 4.82 µm with a mean and median of 0.48 µm and 0.48 µm respectively. The difference between the mc^{2}155 and Δ*ami1*::pSEami1 cell widths was marginal, ranging between 0.49 µm and 0.54 µm, with a mean

and median of 0.51 µm and 0.52 µm for the mc^{2}155 population and ranging between 0.47 µm and 0.54 µm with a mean and median of 0.51 µm and 0.52 µm for the Δ*ami1*::pSEami1 population.

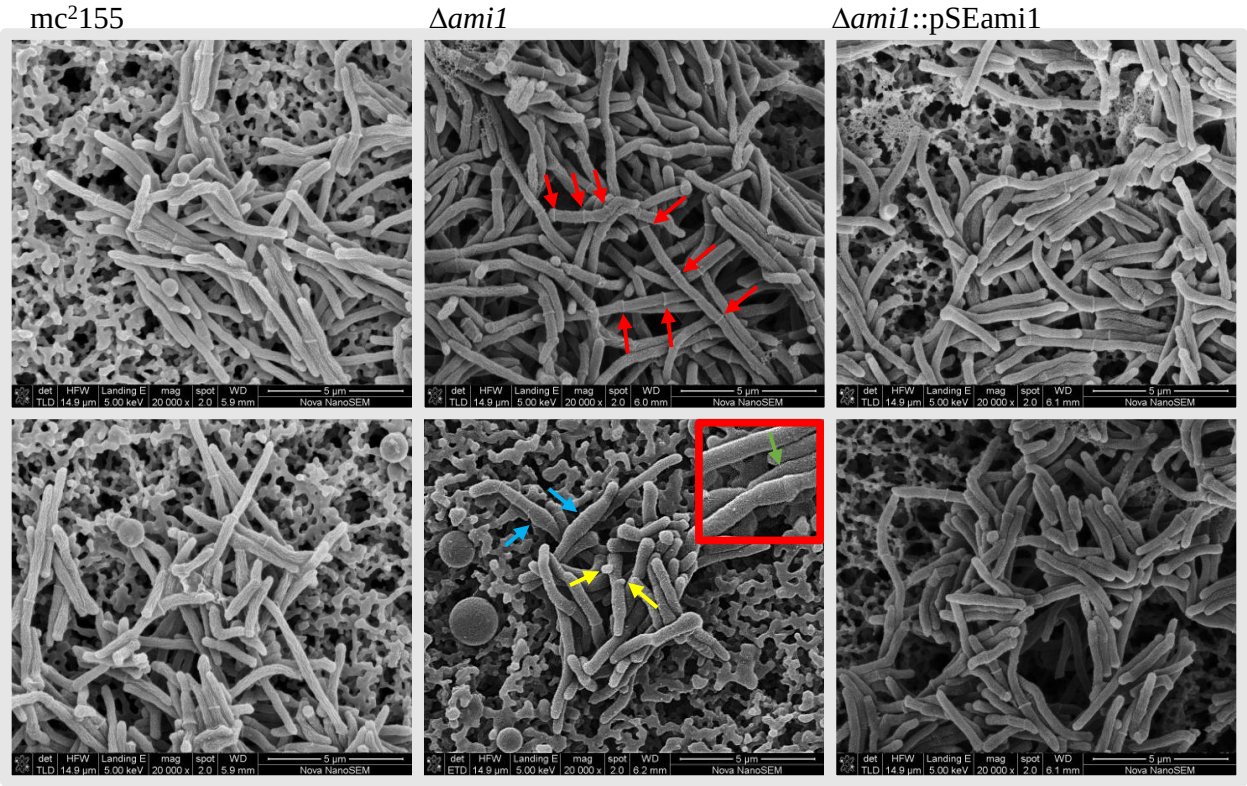

Figure 3.6: Microscopic analysis of the mc2155, Δami1 and Δami1::pAmi1GFP strains. Shown are SEM images of the mc^{2}155, Δ*ami1* and Δ*ami1*::pAmi1GFP strains. Strains were grown in 7H9 to log phase then fixed, dehydrated, carbon coated and imaged using high resolution SEM. Red arrows depict multiple septa found in Δ*ami1* cell chains, Blue arrows indicate cell bulges found in the Δ*ami1* strain, yellow arrows indicate ectopic buds and the insert and green arrow depict an abnormal septum.

3.3.3 Ami1 does not affect septal PG synthesis

In addition to high resolution SEM, fluorescence microscopy was conducted. This was done to evaluate the potential role of Ami1 during PG synthesis. To do this, the mc^{2}155, Δ*ami1* and Δ*ami1*::pSEami1 strains were stained with BODIPY-vanc. This is a green fluorescent probe which binds to the terminal D-ala-D-ala moiety, found predominantly in newly synthesised PG and can be used to spatially monitor sites of new PG synthesis. Fluorescence microscopy was then conducted to assess spatial distribution of the BODIPY signal, Figure 3.9A.

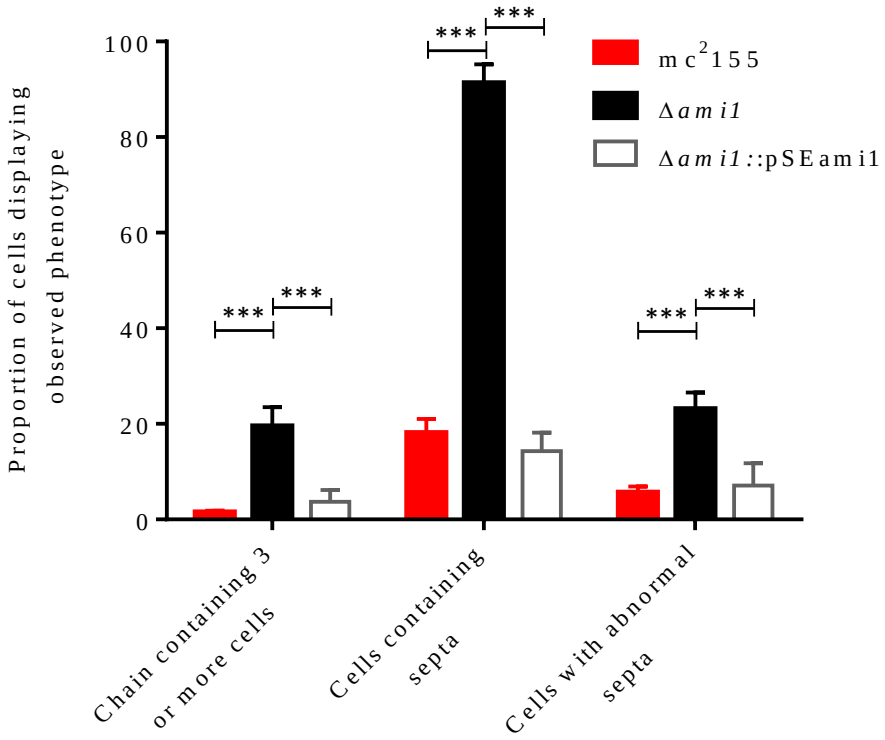

Figure 3.7: Histogram showing the quantification of the various Δ*ami1* associated phenotypic defects out of approximately 400 cells per strain. Displayed are the three distinctive phenotypes which emerged as a result of *ami1* deletion and the proportions in which they were observed in the mc^{2}155, Δ*ami1* and Δ*ami1*::pSEami1 strains from three biological replicates, p-values were obtained using the student's *t* – test. ***: $p < 0.001$.

All three strains displayed a similar staining pattern, with BODIPY-vanc localizing primarily at the cell pole and division septum, suggesting Ami1 does not play a role in directing PG synthesis to these sites. Following this, analysis of the intensities of BODIPY staining in the individual cells was conducted, using ImageJ, to determine whether specific regions of the cell are undergoing elevated levels of PG synthesis as depicted by increased levels of BODIPY-vanc localisation and subsequent fluorescence, Figure 3.9B. This analysis revealed that in all three strains stain equally well at the poles and the septum. We also noted that staining intensity at both poles was not equal as one pole fluoresced more brightly, Figure 3.9B. These data confirmed the observations from a recent seminal study that reported that mycobacterial growth occurs through the greater incorporation of cell wall material at one pole (Botella et al., 2017). The chaining phenotype in the Δ*ami1* mutant was confirmed as demonstrated by the presence of multiple septa that stained with BODIPY-vanc. This confirmed that new PG was being incorporated at the septum in the mutant and that Ami1 played no role in this process Furthermore, in Δ*ami1* chains, one septum appeared to fluoresce more than the others regardless of the number of septa suggesting the various septa

are synthesised in a successive manner. To further understand these findings, two parameters were quantified in these populations, the first being the proportion of cells displaying polar BODIPY-vanc staining and the second evaluating the proportion of cells, within the polar staining population, which exhibit septal staining in addition to polar staining as an indicator of the proportion of cell undergoing cell division, Figure 3.10.

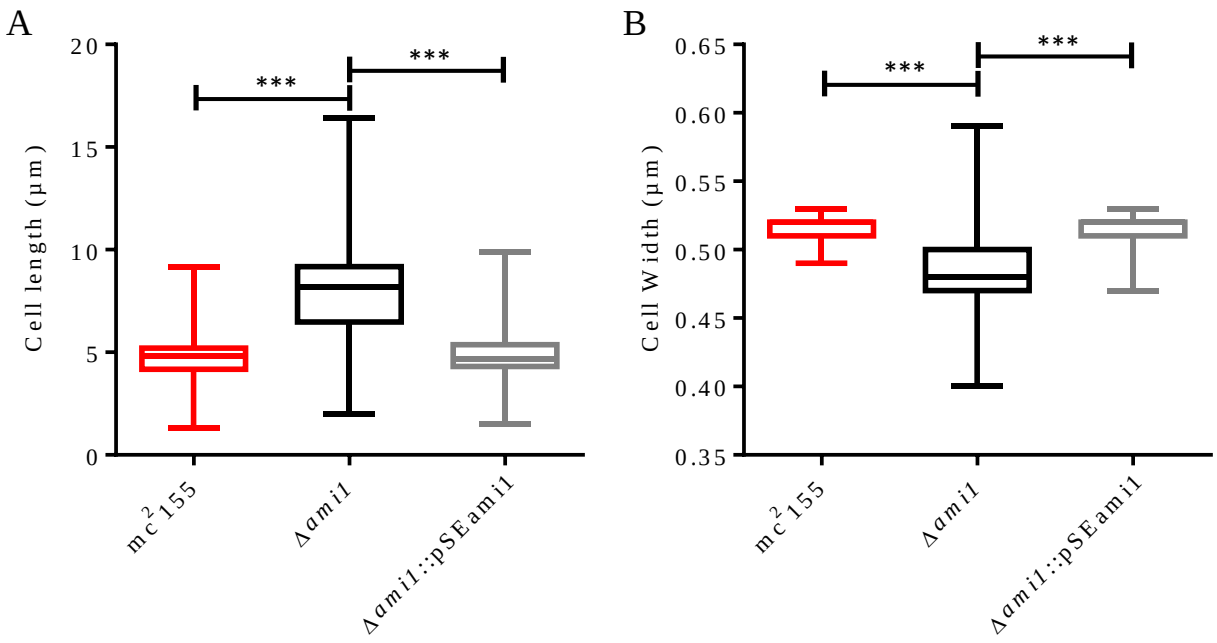

Figure 3.8: Box-and-whisker analysis of the mc^{2}155, Δ*ami1* and Δ*ami1*::pSEami1 strains, showing the cell length and width of approximately 350 cells. (A) Comparison of the variation in cell length demonstrating a change in the distribution of mycobacterial cell length in the absence of Ami1. (B) Comparison of the variation in cell width depicting a change in the distribution of mycobacterial cell width in the absence of Ami1, p-values were obtained using the student's *t* – test. ***: $p < 0.001$. Data represent three independent experiments.

Analysis of ~ 200 cells indicated that 80 to 90 % of the cells displayed polar staining, with minor insignificant variations between the three strains. However, significant differences were observed when quantifying the proportion of cells displaying both polar and septal staining. In both the mc^{2}155 and Δ*ami1*::pSEami1 populations 19 % and 16 %, respectively displayed septal staining; however, 90 % of the Δ*ami1* population displayed septal staining confirming a high proportion of cells undergoing cell division. This is consistent with the high resolution SEM data which showed 94 % of the Δ*ami1* population contained cells with septa.

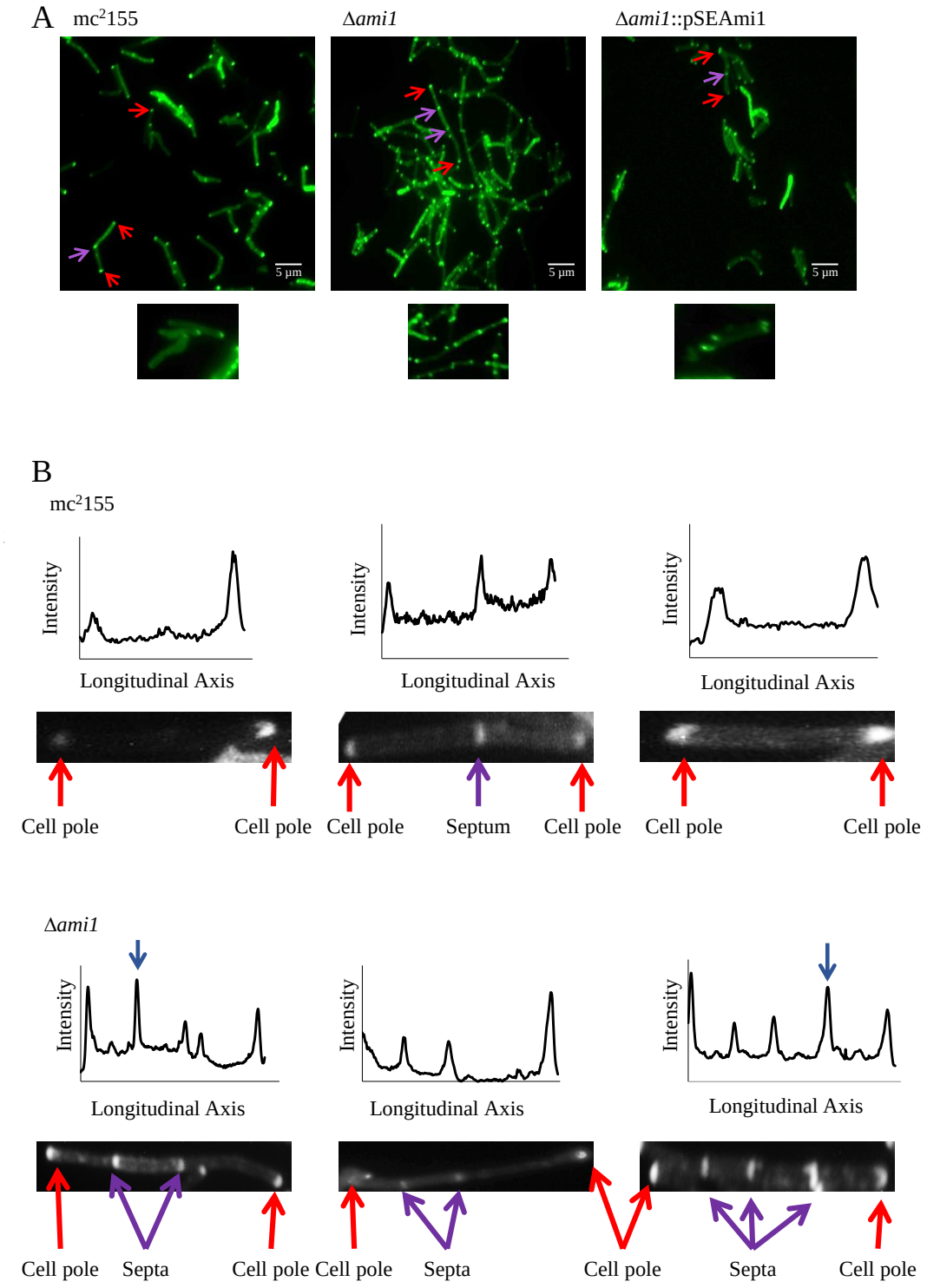

Figure 3.9: Microscopic analysis of the fluorescent BODIPY-vanc stained mc²155, Δ*ami1* and Δ*ami1*::pSEami1 cells. A: Shown are the mc²155, Δ*ami1* and Δ*ami1*::pSEami1 cells depicting the various staining patterns. B: Analysis of the BODIPY-vanc staining patterns in mc²155 and Δ*ami1* through the quantification of fluorescence intensity in individual cells to elucidate sites of new PG synthesis. Red arrows indicate the cell poles, Purple arrows indicate cell septa and the blue arrows show the highly fluorescent septum in the Δ*ami1* cell chain.

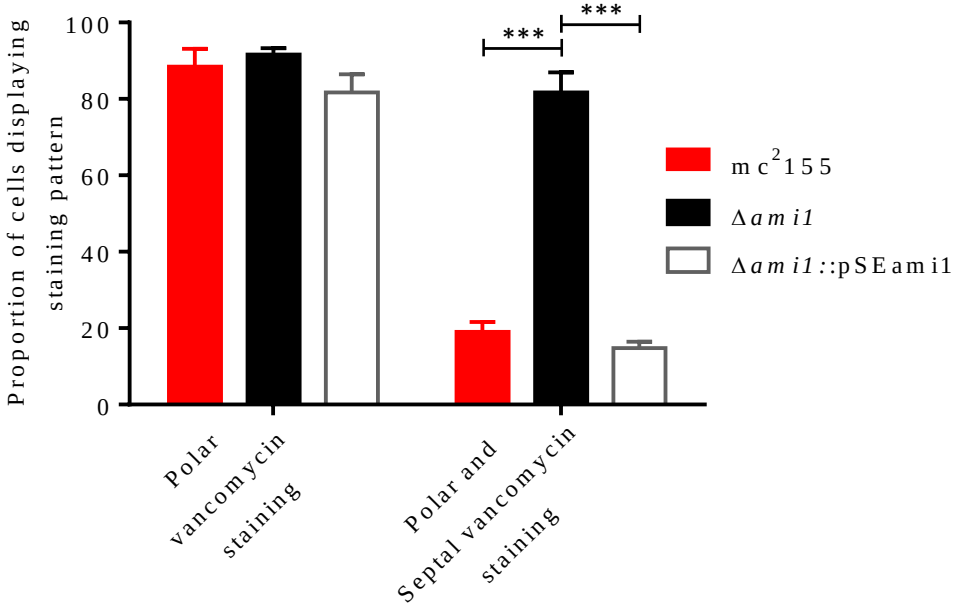

Figure 3.10: Histogram depicting the analysis of the fluorescent BODIPY-Vanc staining patterns. Shown is the proportion of bacterial cells that exhibit polar staining out of approximately 200 cells per strain, as well as the proportion of cells within the polar staining population which displays septal BODIPY-Vanc staining. p-values were obtained using the student's *t* – test. ***: $p < 0.001$. Data represent three independent experiments.

3.3.4 Δ*ami1* can bypass stalled division through lateral growth

Although the Δ*ami1* strain exhibits significant division defects, the strain grew at the same rate as both mc^{2}155 and Δ*ami1*::pSEami1 (data not shown). Thus to understand how this growth occurred, time lapse microscopy of the mc^{2}155 and Δ*ami1* strains was conducted. These strains were sent to the École polytechnique fédérale de Lausanne (EPFL) in Laussane, Switzerland where single cell time-lapse analysis was done. Thereafter, detailed analysis of the videos was conducted in this PhD, Figure 3.11.

Time lapse microscopy of mc^{2}155 revealed a typical growth pattern whereby the individual cells grow to a particular point followed by cell division resulting in the formation of two daughter cells. The Δ*ami1* mutant cells displayed a number of deviations from the normal growth pattern. The most prominent defect in this mutant was the formation of viable lateral buds, which continue to elongate and function as new single cells. The lateral buds, led to branches that underwent cell division and appeared to function independent of the stalled 'mother cell'. Furthermore, in some instances, these branches continue to form further aberrant buds, which then form branches resulting in a tree like form, Figure 3.11 and Appendix E, movies 3.1 to 3.6. Another notable defect

was the release of cell wall material from the septum, Figure 3.11 and Appendix E, movies 3.7 to 3.9.

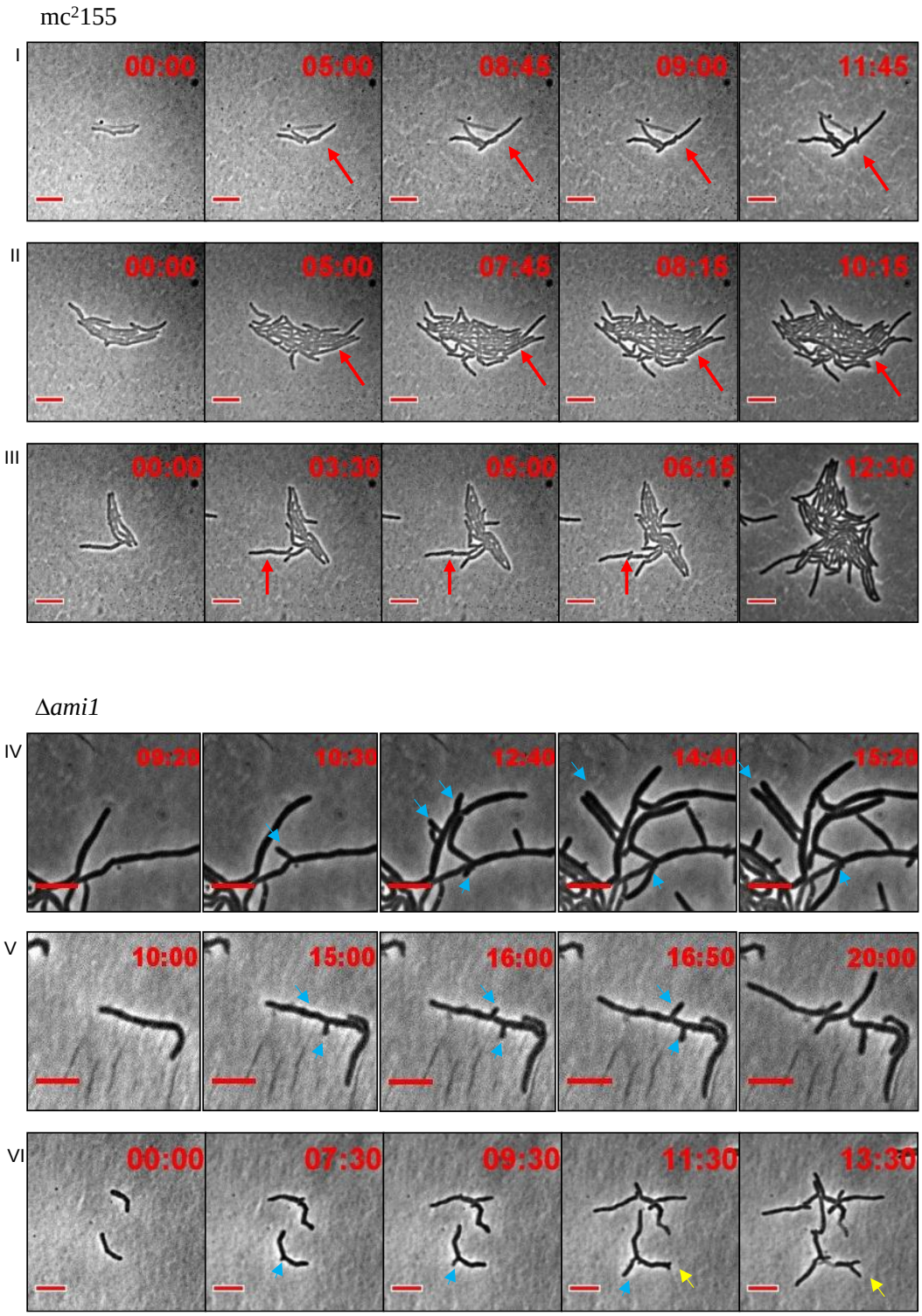

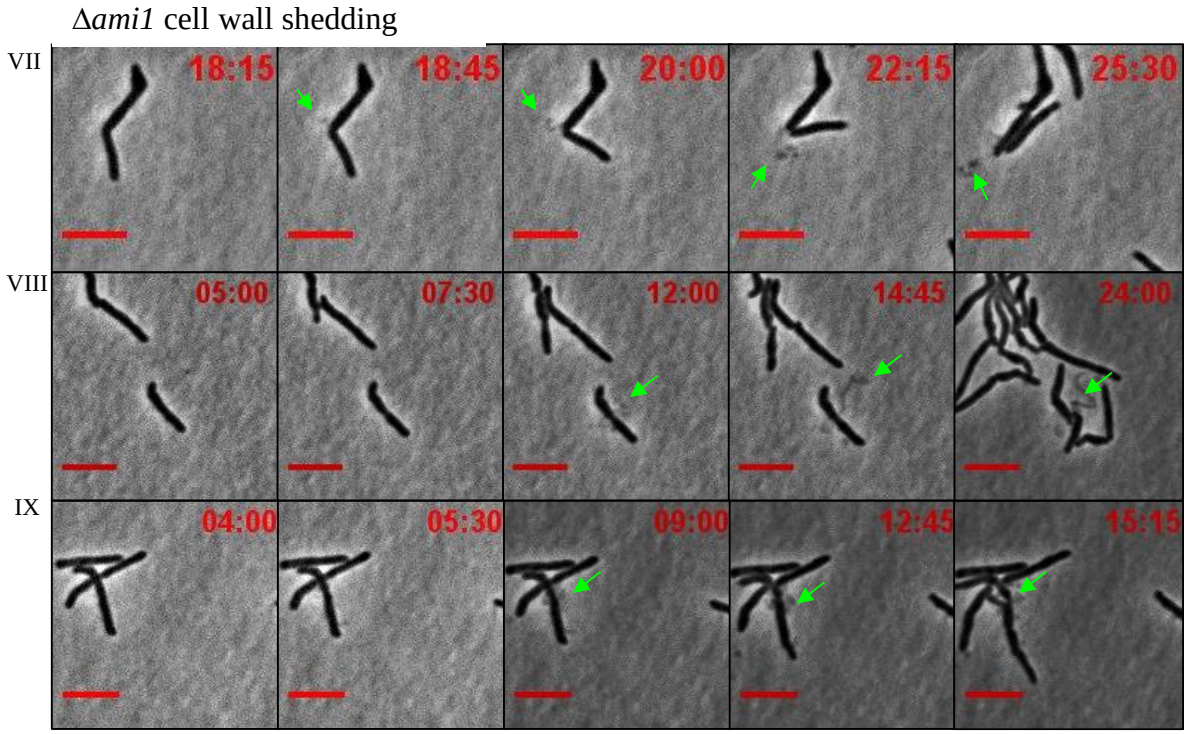

Figure 3.11: Time-lapse microscopic analysis of the mc^{2}155 and Δ*ami1* strains. Cells were grown and imaged in 7H9S media. I-III depicts three representative mc^{2}155 micro-colonies, IV-VI depicts three representative Δ*ami1* micro-colonies showing cell budding and branch formation and VII-IX depicts three representative Δ*ami1* micro-colonies showing the release of cell wall material form the bacterial septum. Red arrows depict sites of cell division, blue arrows depict lateral budding and branch formation, yellow arrows depict polar budding and green arrows show cell wall material secretion. Movies were generated by N. Dhar then processed and analysed by the student (Senzani et al., 2017).

3.3.5 Localisation of mycobacterial Ami1

We next turned our attention to cellular localisation of Ami1. To assess cellular localisation, an Ami1-rsEGFP fusion protein was inserted into the mc^{2}155 strain. The approach involved cloning of the *ami1-rsEGFP* fusion product downstream of the P_{myc}-tet promoter (for constitutive expression of the fusion product), followed by the introduction of the vector into mc^{2}155 and fluorescence microscopy.

3.3.5.1 *Construction of the pAmi1GFP vector*

PCR amplification was conducted to amplify the *ami1* gene without the stop codon and the *rsEGFP* gene. The fragments were then cloned into pSE100 and clones were screened by restriction with *Eco*RI. A single positive clone was then selected and the genetic integrity of the vector was confirmed by extensive restriction profiling, shown in Figure 3.12. In all cases, all the fragment sizes observed corresponded to the vector map and expected sizes, confirming the genetic

integrity of the vector. The genetic integrity of the vector was then further confirmed by sequencing of the cloned region, which revealed that no mutations had occurred during PCR and cloning processes (data not shown). This vector was then used for construction of the mc^{2}155::pAmi1GFP strain.

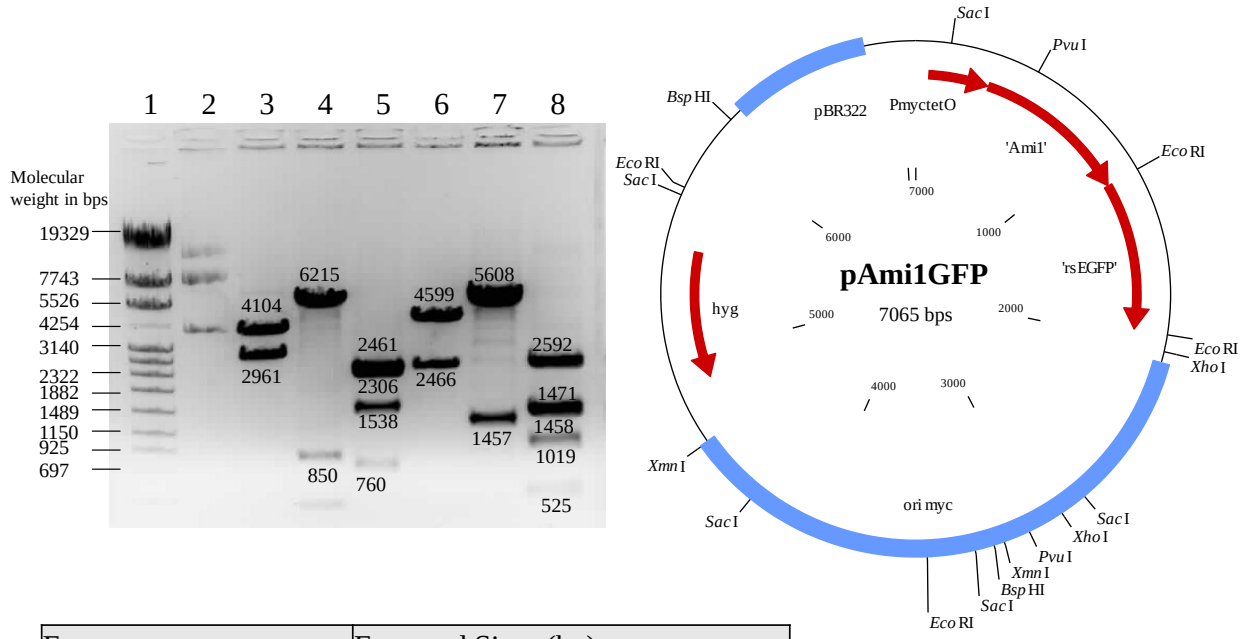

Enzyme	Expected Sizes (bp)
*Bsp*HI	4104, 2961
*Xho*I	6215, 850
*Eco*RI	2461, 2306, 1538, 760
*Pvu*I	4599, 2466
*Xmn*I	5608, 1457
*Sac*I	2592, 1471, 1458, 1019, 525

Figure 3.12: Restriction profile of pAmi1GFP. Shown are the different restriction nucleases used and the expected sizes in a table, which result from restriction digests of the pAmi1GFP vector. The predicted vector map of pAmi1GFP vector and agarose gel depicting the products of restriction digest of pAmi1GFP is also shown. For the agarose gel, Lane 1: Roche Marker IV, Lane 2: Uncut, Lane 3: *Bsp*HI, Lane 4: *Xho*I, Lane 5: *Eco*RI, Lane 6: *Pvu*I, Lane 7: *Xmn*I, Lane 8: *Sac*I.

3.3.5.2 *Construction and screening of the mc^{2}155::pAmi1GFP strain*

The pAmi1GFP vector was electroporated into the mc^{2}155 strain (section 2.4.2); the transformation efficiency obtained from the electro-competent cells was 1.6 × 10^4 CFU/µg vector DNA (determined using the pSE100 control vector). Two clones were selected and screened by PCR using the *ami1*pSELF and the rsEGFPR primers (section 3.2.3) to determine the presence of the *ami1-rsEGFP* fusion DNA fragment (Appendix D, Figure D4).

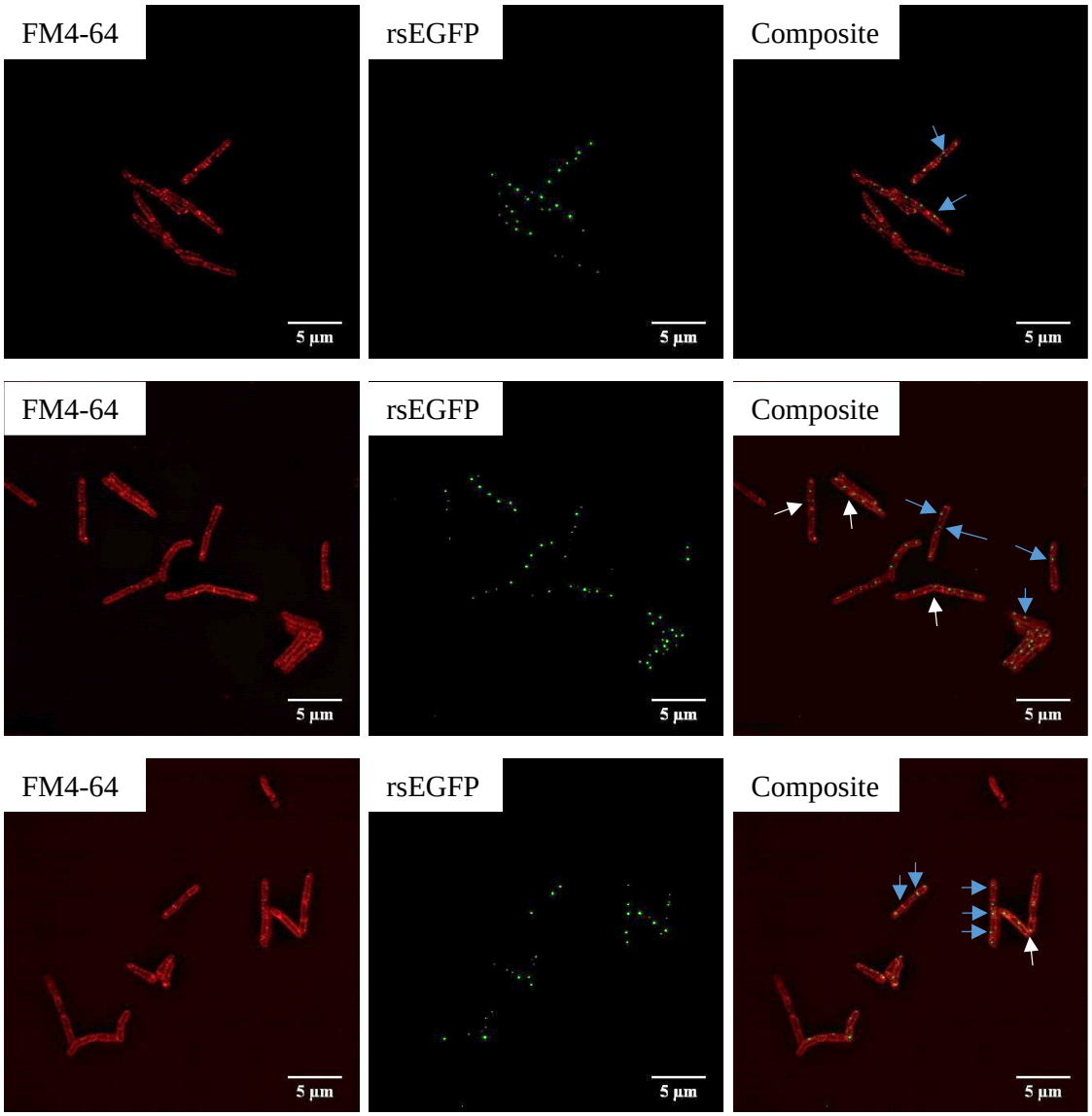

Figure 3.13: Microscopic analysis of fluorescent Ami1-rsEGFP localisation in mc^{2}155 cells. Cells were grown in 7H9S and stained with FM4-64, which stains the plasma membrane, then mounted on agarose pads then images were captured using high resolution TIRF microscopy. Three different fields of view are shown above to provide a visual assessment of the localisation in the most of the cells assessed. White arrows indicate the division septum in cells undergoing cell division while blue arrows indicate individual puncta found across the elongating cell. Scale = 5 µm.

3.3.5.3 *Localisation of mycobacterial Ami1*

Following the construction of the mc^{2}155::pAmi1GFP strain, high resolution TIRF microscopy was conducted to determine the cellular localisation of Ami1-rsEGFP. The cells were stained with the cell membrane strain FM4-64 to identify the membrane in the individual cells, Figure 3.13.

Using TIRF microscopy, the Ami1-rsEGFP displayed punctate localisation throughout the longitudinal axis of the cell. In some instances septal localisation was observed, however, not all

septa displayed the presence of Ami1-rsEGFP. Thus, to further unpack these observations, the three basic localisation patterns observed were quantified, these were: 1, punctate localisation in cells with no septum; 2, non-septal lateral localisation in cells containing a septum and 3; Ami1-rsEGFP septal localisation, Figure 3.14.

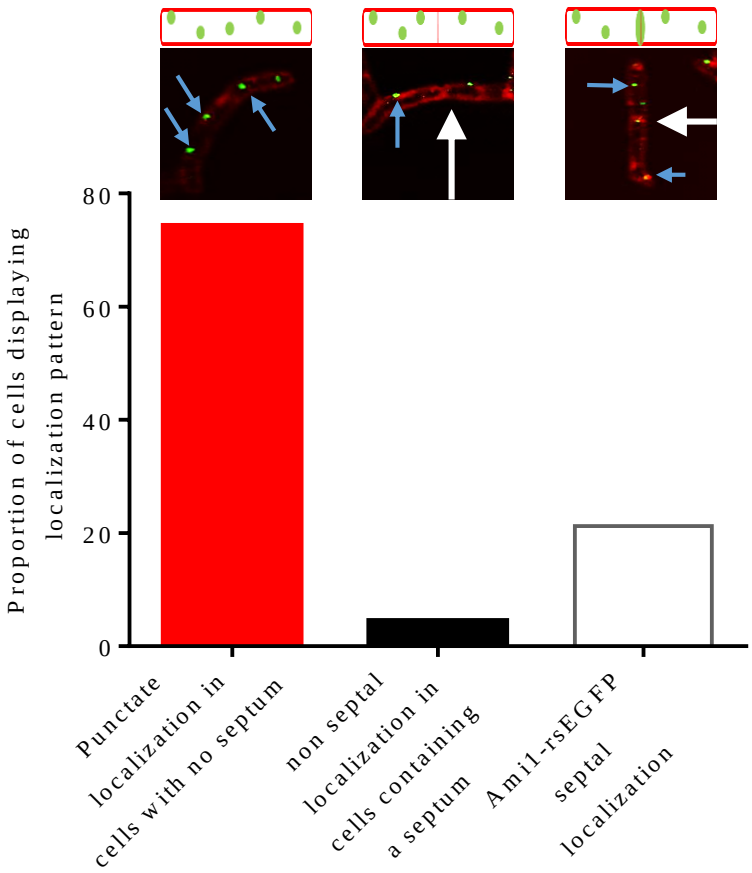

Figure 3.14: Bar graph showing the analysis of Ami1-rsEGFP localisation patterns in the mc^{2}155 strain. Shown is the proportion of the bacterial cells which exhibits various localisation patterns, out of approximately 200 cells, in both strains. White arrows indicate the division septum in cells undergoing cell division and blue arrows indicate individual puncta found across the elongating cell. Bar graph is a representative of two biological replicates.

Quantification of these patterns revealed that 78 % of the population fell in the first localisation class, which was punctate localisation in cells with no-septum. Approximately 2 % of the population displayed non septal localisation in cells containing a septum and 20 % displayed septal Ami1-rsEGFP localisation, suggesting Ami1 could be recruited once the septum has formed. Furthermore, the analysis revealed that 22 % of the cells contained a septum, consistent with mc^{2}155 SEM and BODIPY-vanc data suggesting the wild type strain was not affected by the overexpression of Ami1-rsEGFP.

3.3.5.4 *Complementation of Δami1 with pAmi1GFP*

As the Ami1-rsEGFP localisation data revealed an unexpected pattern, it was prudent to determine whether the localisation was the result of a functional Ami1-rsEGFP derivative and not junk protein. To assess the functionality of the Ami1-rsEGFP, we genetically complemented the Δ*ami1* strain using the *ami1-rsEGFP* containing pAmi1GFP vector.

3.3.5.4.1 Construction and screening of the Δ*ami1*::pAmi1GFP strain

The pAmi1GFP vector was electroporated into the Δ*ami1* strain (section 2.4.2); the transformation efficiency obtained from the electro-competent cells was 5.2×10^3 CFU/µg vector DNA (determined using the pSE100 control vector). Two clones were selected and screened by PCR using the *ami1*pSELF and the rsEGFPR primers (section 3.2.3) to determine the presence of the *ami1-rsEGFP* fusion DNA fragment (Appendix D, Figure D4).

3.3.5.4.2 Analysis of Δ*ami1*::pAmi1GFP strain

High resolution SEM was conducted on the Δ*ami1*::pAmi1GFP strain and same parameters were analysed as previously to determine whether the strain Δ*ami1*::pAmi1GFP reverted to wild type physiological properties. Analysis of the SEM images suggested that the Ami-rsEGFP fusion protein displayed the ability to genetically complement the mutant. From the ~ 400 cells analysed per strain, 1.9 % of the of Δ*ami1*::pAmi1GFP population were in the form of chains, 10.4 % of the population contained septa and 4.4 % possessed abnormal septa, Figure 3.15. Additionally, the cell length of Δ*ami1*::pAmi1GFP ranged from 2 µm to 9 µm with a mean and median of 4.37 µm and 4.16 µm, which was similar to the wild type, thus confirming that the fusion protein was functional, Figure 3.15.

3.3.6 Ectopic branch formation in the Δ*ami1* mutant is mediated by DivIVA

Thus far, we were able to establish that loss of Ami1 resulted in arrested cell division where septa were synthesised but were not degraded to allow for cell separation. Failure to complete cell separation resulted in the ectopic formation of lateral branches that continued to grow. We next sought to understand how this form of growth occurs and how these branches remain viable. To do this, four proteins involved in different parts of cell growth were evaluated. These were FtsZ,

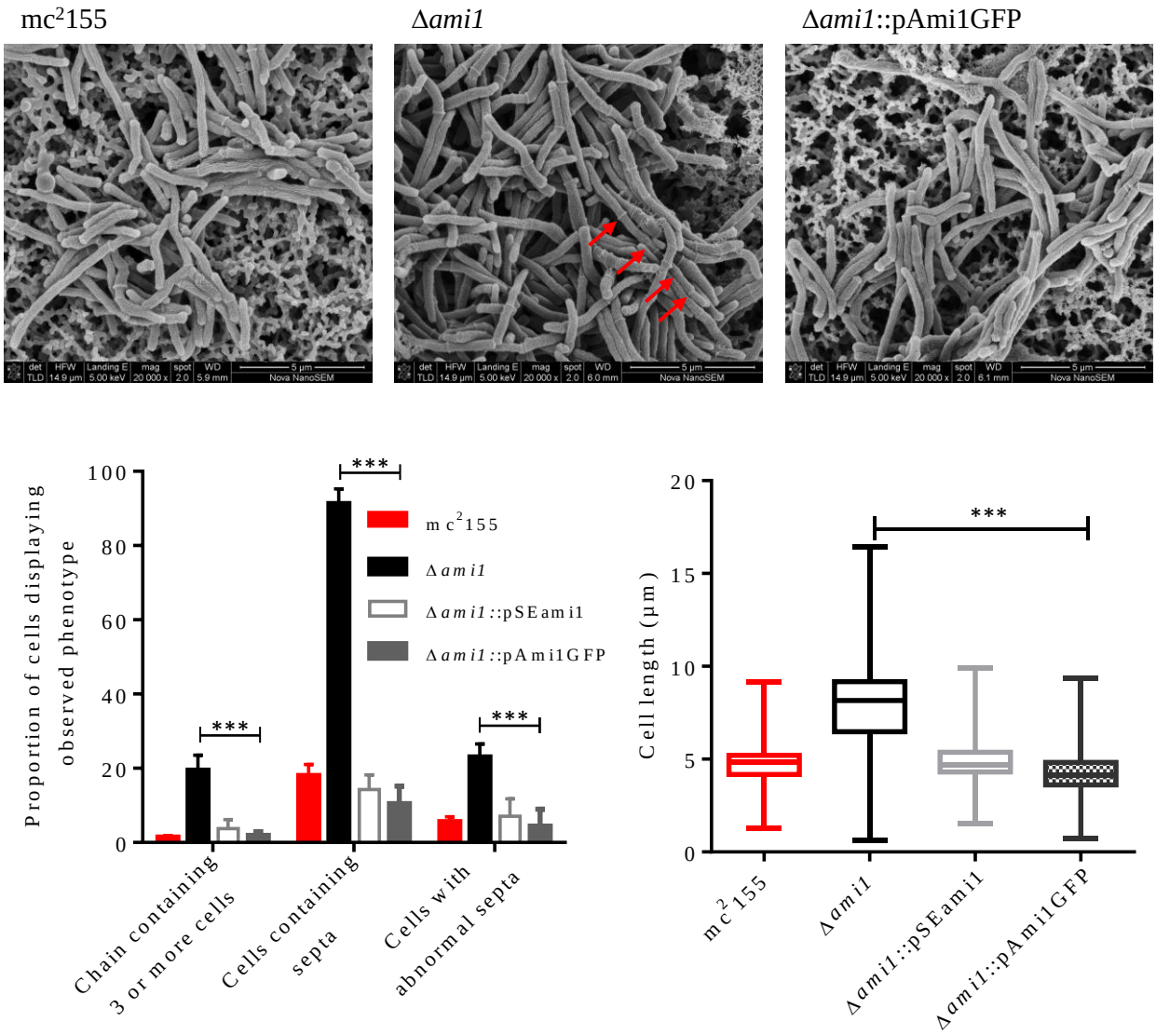

Figure 3.15: Microscopic analysis of the complementation capacity of the Ami1-rsEGFP fusion protein. Shown are SEM images of the mc²155, Δ*ami1* and Δ*ami1*::pAmi1GFP strains and the statistical analysis of the various Δ*ami1* associated phenotypes attained from approximately 400 cells per strains. p-values were attained using the student's *t* – test. ***: $p < 0.001$. Red arrows point to unresolved septa in the *ami1* mutant, a defect that was reverted in the strain complemented with Ami1-rsEGFP. Statistical analysis was conducted using data from three biological replicates.

DivIVA (a marker for cell elongation, which will be discussed further in chapter 4.1), DnaN and ParB, the latter two are both essential components involved in chromosome replication and partitioning during cell division, respectively. These analyses were conducted through the localisation of these various proteins in order to determine how loss of Ami1 affects their tightly controlled subcellular localisation and ultimately their function.

3.3.6.1 *Localisation of mycobacterial FtsZ*

As stated earlier, FtsZ is one of the initial proteins recruited to the site of cell division and plays an important role in the recruitment and anchorage of the bacterial cell division machinery. It also serves as a marker for division sites or future cell division sites (Eskandarian et al., 2017). With this in mind, it was essential to understand whether the mycobacterial cell division site determination mechanisms are affected by the loss of Ami1. To do this, a FtsZ-rsEGFP fusion protein was inserted in mc^{2}155 and Δ*ami1* strains to localise FtsZ. The approach adopted involved cloning of the *ftsZ-rsegfp* fusion product downstream its native promoter, followed by the introduction of the vector into mc^{2}155 and Δ*ami1* and time-lapse fluorescence microscopy.

3.3.6.1.1 Construction of the pFtsZGFP vector

PCR amplification was conducted to amplify the *ftsZ* gene, without the stop codon, containing a 400 bp 5′ region upstream the transcriptional start codon and the *rsEGFP* wild type allele. The fragments were then cloned into pMV306(H) and clones were screened by restriction with *Eco*RI. A single positive clone was then selected and the genetic integrity of the construct was confirmed by extensive restriction profiling, shown in Figure 3.16. In all cases, the fragment sizes observed corresponded to the vector map and expected sizes, confirming the genetic integrity of the vector. The genetic integrity of the vector was then further confirmed by sequencing of the cloned region, which revealed that no mutations had occurred during PCR and cloning processes (data not shown). This vector was then used for construction of the mc^{2}155::pAmi1GFP strain.

3.3.6.1.2 Construction and screening of FtsZ localizing strains

The pAmi1GFP construct was electroporated into the mc^{2}155 strain and Δ*ami1* (section 2.4.2), the transformation efficiency obtained from the electro-competent cells was 1.6×10^4 CFU/µg and 3.9×10^4 CFU/µg vector DNA for mc^{2}155 strain and Δ*ami1*, respectively (determined using the pSE100 control vector). Two clones were selected and screened by PCR using the rsEGFPF and the rsEGFPR primers (section 3.2.3) to determine the presence of the *rsEGFP* DNA fragment as the *ftsZ-rsEGFP* fragment was too large to check by PCR (Appendix D, Figure D5).

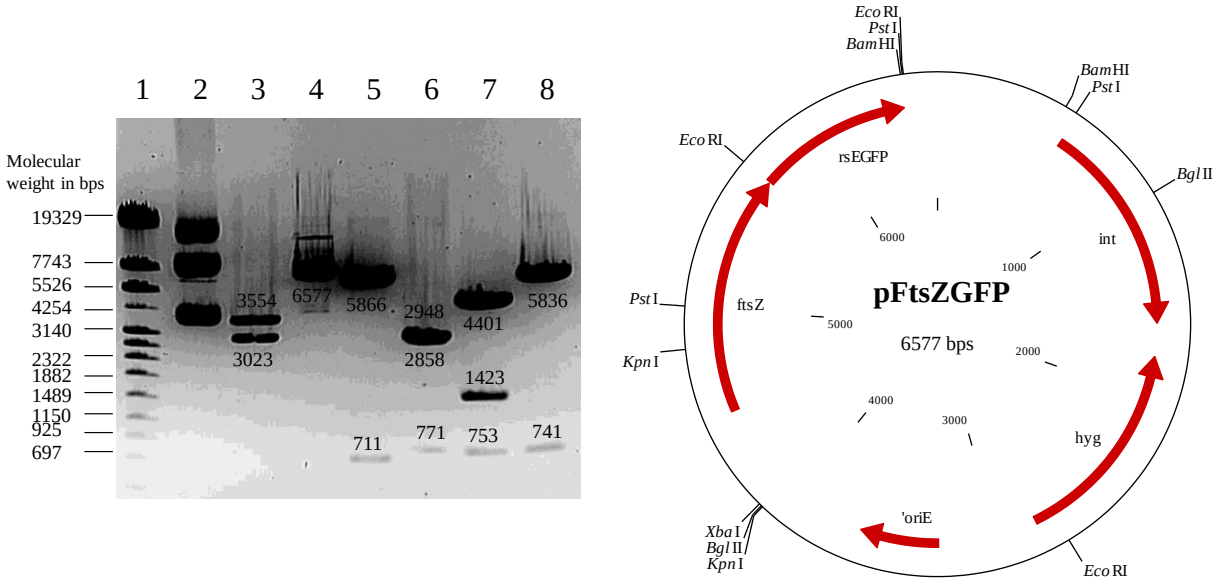

Enzyme	Expected Sizes (bp)
*Bgl*II	3554, 3023
*Xba*I	6577
*Bam*HI	5866, 711
*Eco*RI	2948, 2858, 771
*Pst*I	4401, 1423, 753
*Kpn*I	5836, 741

Figure 3.16: Restriction profile of pFtsZGFP. Shown are the different restriction nucleases used and the expected sizes in a table, which result from restriction digests of the pFtsZGFP vector. The predicted vector map of pFtsZGFP vector and agarose gel depicting the products of restriction digest of pAmi1GFP are also shown. For the agarose gels, Lane 1: Roche Marker IV, Lane 2: Uncut, Lane 3:*Bgl*II, Lane 4: *Xba*I, Lane 5: *Bam*HI, Lane 6: *Eco*RI, Lane 7: *Pst*I, Lane 8: *Kpn*I.

3.3.6.1.3 Localisation of mycobacterial FtsZ

Following the construction of the FtsZ localizing strains, high resolution TIRF microscopy was conducted to determine the cellular localisation of FtsZ-rsEGFP. The cells were stained with the cell membrane stain FM4-64 to identify the membrane, Figure 3.17.

The TIRF microscopic analysis of the mc^{2}155::pFtsZGFP displayed the presence of four basic FtsZ-rsEGFP localisation patterns. These were; 1: no FtsZ-rsEGFP localisation, 2: Preseptal FtsZ-rsEGFP localisation, wherein the FtsZ-ring has assembled but no septum has formed, 3: Septal FtsZ-rsEGFP localisation, wherein both the septum and FtsZ-ring have assembled at the same site and finally, 4: Daughter cell FtsZ-rsEGFP localisation, where the septal FtsZ-ring has

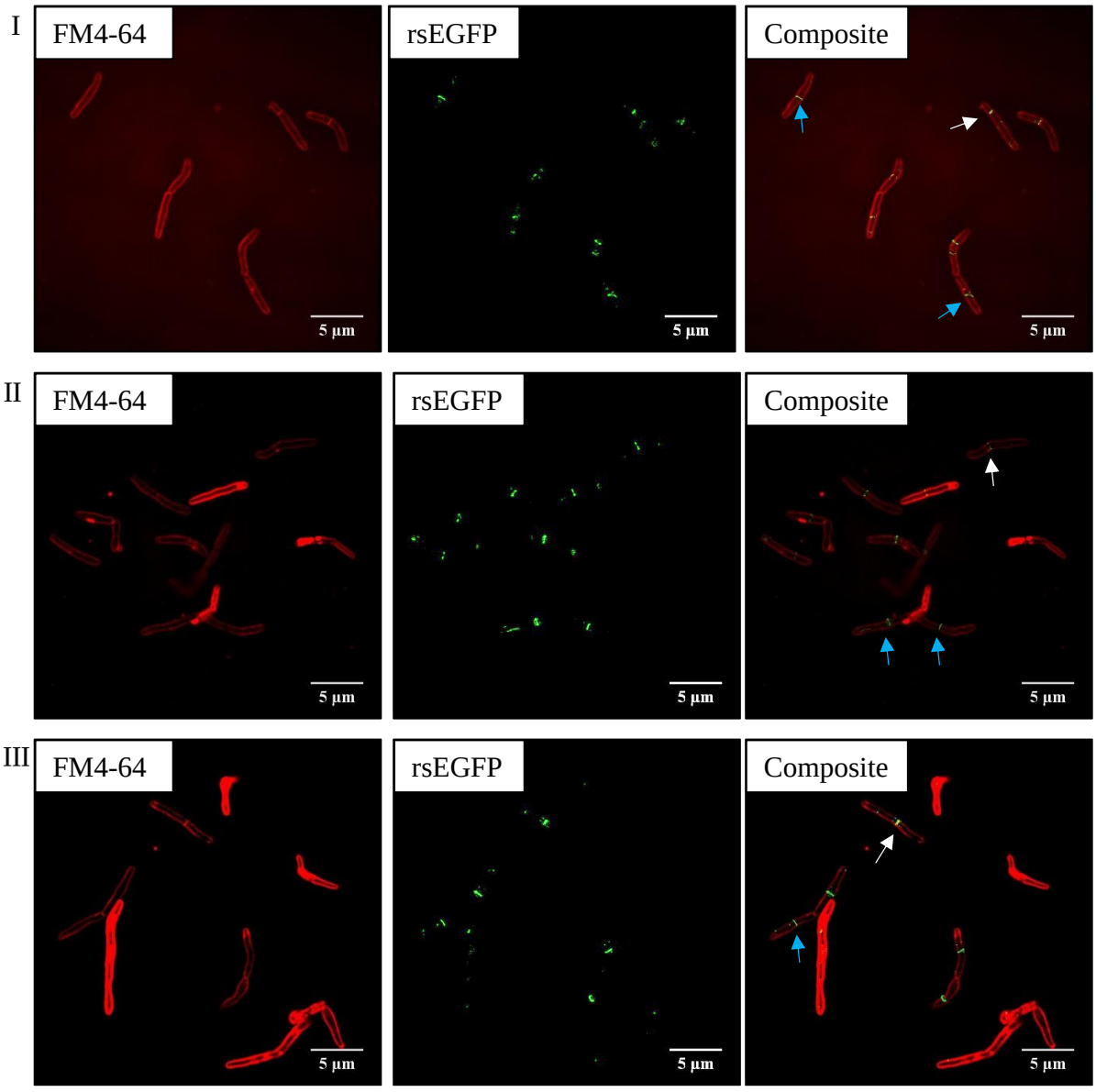
I
FM4-64
rsEGFP
Composite
5 µm
II
FM4-64
rsEGFP
Composite
5 µm
III
FM4-64
rsEGFP
Composite
5 µm

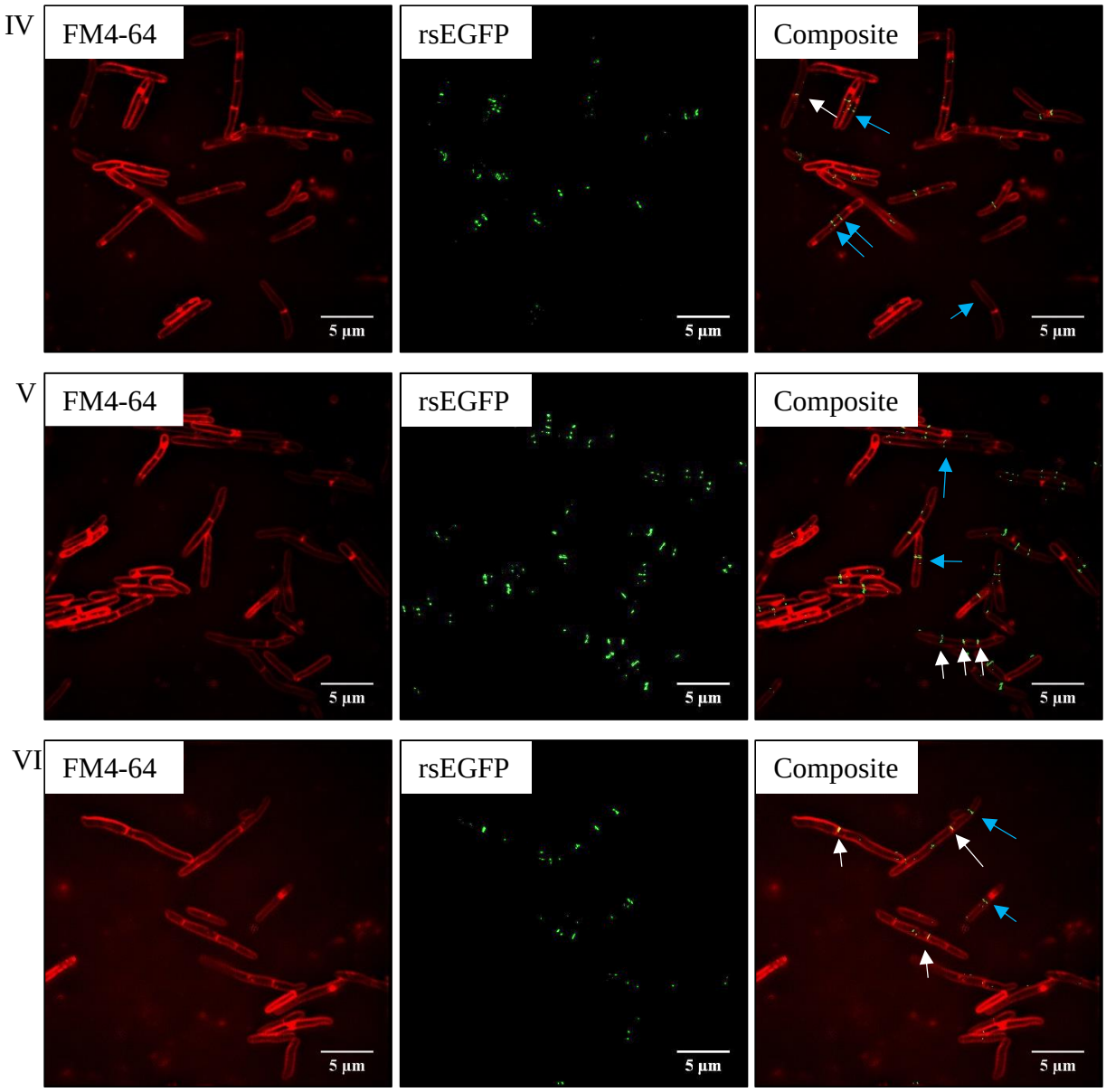

Figure 3.17: Microscopic analysis of fluorescent FtsZ-rsEGFP in mc^{2}155 and Δ*ami1* cells. Bacteria were grown in 7H9 and stained with FM4-64, which stains the plasma membrane, then mounted on agarose pads followed by imaging. I-III depicts FtsZ-rsEGFP localisation in mc^{2}155 and IV-VI represents FtsZ-rsEGFP localisation in the Δ*ami1* strain. White arrows indicate pre-septal FtsZ-rsEGFP localisation and blue arrows indicate septal FtsZ-rsEGFP localisation.

disassembled and has begun to form in the two adjacent daughter cells, Figure 3.18. Analysis of FtsZ localisation in the Ami1 deficient strain revealed the presence of two additional classification patterns, which arose possibly as a result of the Δ*ami1* division defects. These were 1: Daughter cell FtsZ-rsEGFP localisation in a chain, where all the cells in the chain displayed only localisation

with no septal localisation and 2: Multiple FtsZ-rsEGFP rings in a single daughter cell, where three or more FtsZ-rings assemble in a single daughter cell, Figure 3.17.

Quantification of these patterns revealed relatively similar proportions in both populations displayed three localisation patterns which were, no FtsZ-rsEGFP localisation, Preseptal FtsZ-rsEGFP localisation, and Septal FtsZ-rsEGFP localisation, with a high proportion of both populations displaying the Preseptal FtsZ-rsEGFP localisation pattern, 34.6 % for mc^2155 and 29.3 % for Δ*ami1*. The lack of significant differences in this regard suggested that the Z-ring was able to assemble properly in the absence of Ami1. There was, however, a significant difference between the populations displaying daughter cell FtsZ-rsEGFP localisation, in which case 36.7 % of the mc^2155 population displayed this pattern while 21.4 % of the Δ*ami1* population exhibited this pattern, Figure 3.18. Another difference related to the Δ*ami1* associated localisation patterns, which were daughter cell FtsZ-rsEGFP localisation in a chain and multiple FtsZ-rsEGFP rings in a single daughter cell, these were noted in 6.9 % and 14.7 % of cells respectively in the Δ*ami1*::pFtsZGFP strain, while none were found in the mc^2155::pFtsZGFP strain, Figure 3.18. In addition to TIRF microscopy, time-lapse microscopy was conducted to elucidate the effect Ami1 deficiency has on FtsZ placement and assembly, Figure 3.19 and Appendix E, movies 3.10 to 3.18.

Time lapse microscopy of mc^2155::pFtsZGFP revealed that the FtsZ-ring is dynamic and highly mobile, landing at the future cell division site. Also, the FtsZ-ring initially forms as two parallel rings close to the future cell division site these then eventually coalesce at the site of cell division resulting in constriction and cell division (Eskandarian et al., 2017). This two-ring confirmation of FtsZ is dysregulated in the Δ*ami1* strain and instead of the two ring conformation, the FtsZ is predominantly found in the form of highly mobile puncta. These eventually merge to form a single FtsZ-ring. Furthermore, the Z-ring appears to be unstable as in some cases the ring disassembled when cell separation failed, presumably due to the lack of septum degradation, Figure 3.19 VII. This event was usually followed by Z-ring formation at the same site, which either disassembled again or proceeded through cell division. Furthermore, in certain instances (25 of 84 micro-colonies counted) cell separation failure resulted in the death of one daughter cell, predominantly the fast growing cell followed by the emergence of a new daughter cell at the failed septum (Figure 3.19 IV to VI).

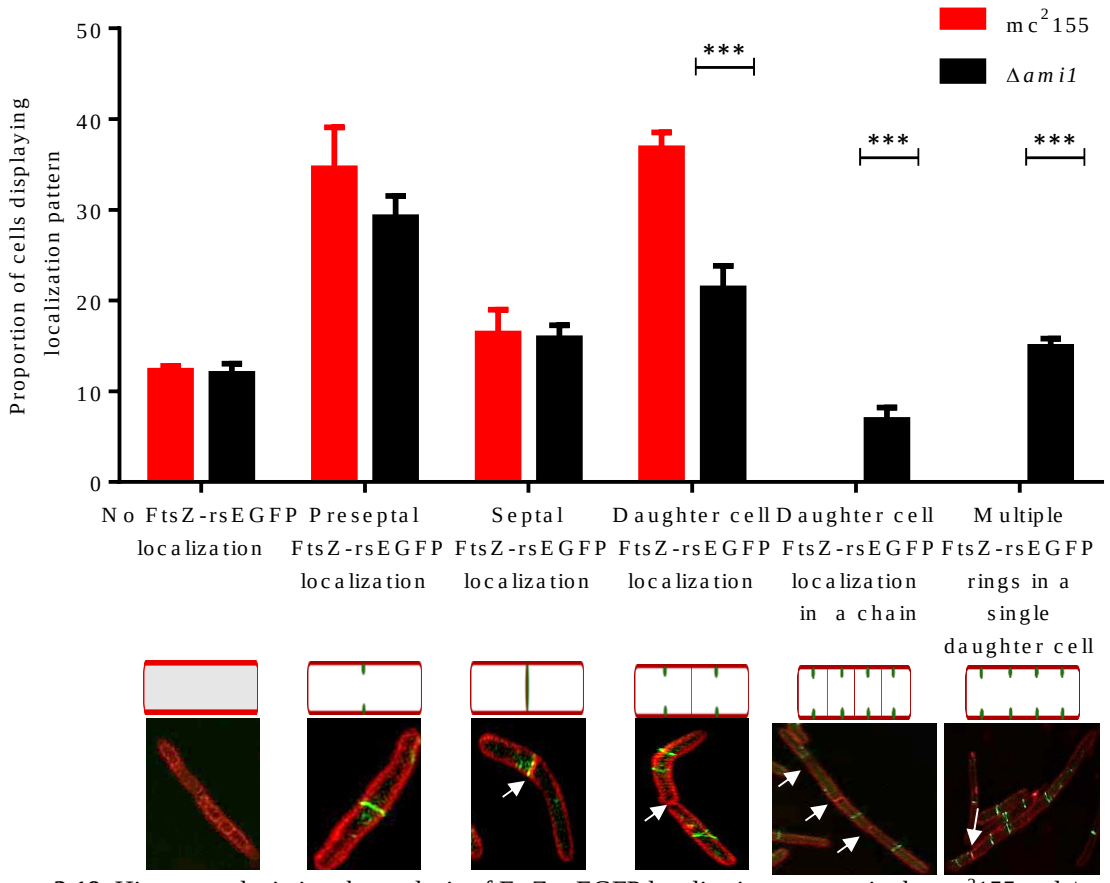

Figure 3.18: Histogram depicting the analysis of FtsZ-rsEGFP localisation patterns in the mc^{2}155 and Δ*ami1* strains. Shown is the proportion of bacterial cells which exhibit various localisation patterns, out of approximately 200 cells, in both strains white arrows show division septa. p-values were obtained using the student's *t* – test. ***: $p < 0.001$. The bar graph is a representative of three biological replicates.

3.3.6.2 *Localisation of mycobacterial DivIVA*

DivIVA is an essential protein that functions as a marker for sites of mycobacterial cell elongation, which generally occurs at the poles (section 4.1). Given that the branching pattern of growth observed for the *ami1* mutant suggested ectopic elongation on the lateral axis, we sought to understand how this protein localises in the Δ*ami1* strain, particularly during branch formation. To do this DivIVA-rsEGFP fusion protein-containing mc^{2}155 and Δ*ami1* strains were created to localise DivIVA. The approach adopted involved the introduction of the plS220 construct, which is a pMV361 derivative containing a DivIVA-GFP fusion regulated by the *hsp60* promoter, into mc^{2}155 and Δ*ami1* followed by time-lapse fluorescence microscopy (Santi et al., 2013).

3.3.6.2.1 Construction and screening of the Δ*ami1*::plS220 strain

The plS220 vector was electroporated into the mc^{2}155 and Δ*ami1* strain (section 2.4.2), the transformation efficiency obtained from the electro-competent cells was 2.6×10^4 CFU/µg and 1.7

× 10^4 CFU/µg vector DNA (determined using the pSE100 control vector) for mc^{2}155 and Δ*ami1* strains, respectively. Five clones were selected and screened by fluorescence microscopy to determine whether the strains exhibited DivIVA-GFP localisation (data not shown). Thereafter, one clone of each strain was used for further characterisation.

3.3.6.2.2 Time-lapse microscopy to localise DivIVA

Following the construction of the Δ*ami1*::plS220 and mc^{2}155::plS220 strains, time-lapse microscopy was conducted to determine the cellular localisation of DivIVA-GFP, Figure 3.20 and Appendix E, movies 3.19 to 3.24. Time lapse microscopy in mc^{2}155 revealed the previously reported DivIVA localisation pattern, where DivIVA localises only to the cell poles and the septum (Santi et al., 2013). In the case of the Δ*ami1* strain, a number of differences, from the normal localisation pattern, were observed. In the ami1 mutant, DivIVA was recruited to the septum as with the wild type strain. However, failure of cells to separate after septum synthesis resulted in these septal DivIVA foci nucleating new cell pole synthesis at the septum, observed in 37 of 52 micro-colonies examined, Figure 3.20 (panels IV-VI). From this, we were able to conclude that failure of cells to separate results in ectopic localisation of the cell elongation apparatus, leading to branch formation.

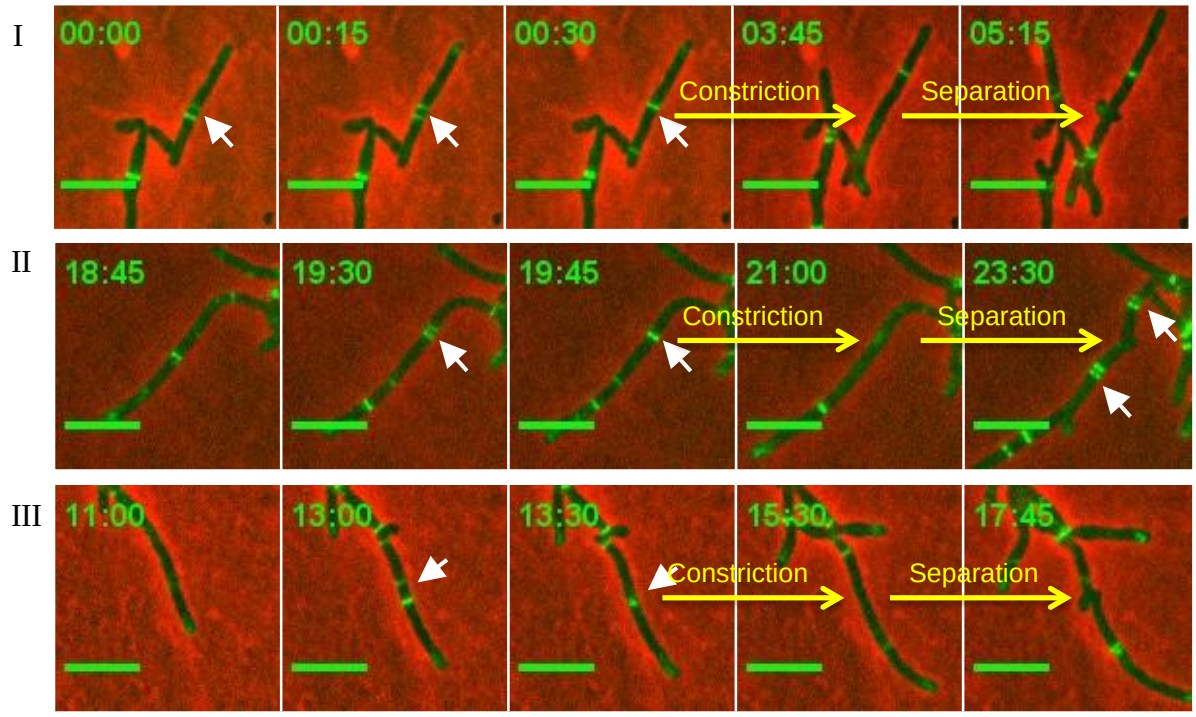

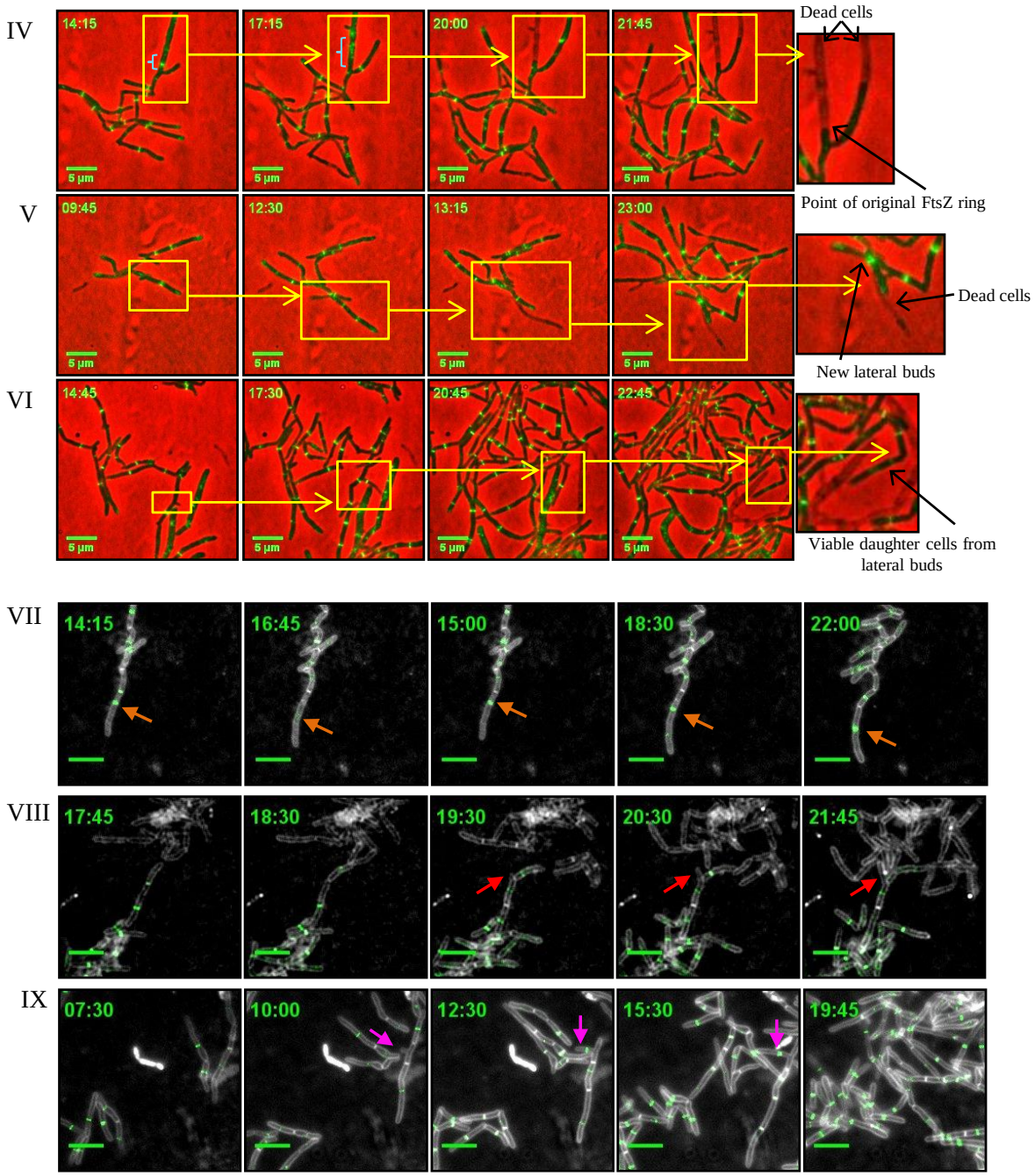

Figure 3.19: Time-lapse microscopic analysis of FtsZ-rsEGFP localisation in the mc^2155 and Δ*ami1* strains. Cells were grown and imaged in 7H9. (I-III) depicts three representative mc^2155 micro-colonies showing the formation and ultimate fusion of two parallel FtsZ-rings to form a final division site followed by cell division. (IV-VI) depicts three representative Δ*ami1* micro-colonies showing the formation and premature disassembly of the FtsZ-ring resulting in ultimate bacterial death and (VII to IX) depicts Δ*ami1* micro-colonies stained with the membrane stain FM4-64 showing the formation and disassembly of multiple FtsZ-rings at a single site (orange arrows), the formation of septal branches as a result of failed cell separation (red arrows) and the formation and growth of an ectopic branch followed by FtsZ-ring assemble within the branch indicating the presence of cell division machinery within ectopic branches (magenta arrows). Movies were generated by N. Dhar and the student. The movies were processed and analysed by the student. The FM4-64 staining experiment was only done with the Δ*ami1* mutant (Senzani et al., 2017).

In some cases DivIVA localised aberrantly at the longitudinal axis during cell elongation in the absence of a septum, resulting in the formation of a new growth pole and ultimate branch formation, observed in 12 of 52 micro-colonies examined, Figure 3.20.

3.3.6.3 *Localisation of mycobacterial DnaN and ParB*

Whilst assessing the spatial pattern of DivIVA localisation in the *ami1* mutant, we noted that many of the ectopic branches, nucleated by DivIVA remained viable and were able to grow into long cells, which sometimes branched also. We next sought to study this further by determining whether chromosome partitioning was maintained in the ectopic branches. Hence, we localised DnaN (as a DnaN-GFP fusion) and ParB (as a ParB-mCherry fusion) in the *ami1* mutant. These proteins play an essential role in chromosome replication and partitioning during cell division. DnaN, the clamp that anchors DNA-polymerases to the replication fork forms part of the chromosome replication machinery and ParB, which binds to *parS* sites on the origin of replication forms part of the chromosome partitioning machinery. Consequently, understanding how these proteins localise during bud formation and branch elongation was important to elucidate how lateral buds retain DNA. To do this, *ami1* was deleted in the mc^{2}155::ParBM-DnaNG background and the resulting strain was studied with time-lapse fluorescence microscopy to track both ParB-mCherry and DnaN-GFP in the knockout strain.

3.3.6.3.1 Construction and screening of the Δ*ami1*::ParBM-DnaNG strain

The p2ΔAmi1G19 knockout vector was electroporated into the mc^{2}155::ParBM-DnaNG strain (section 2.4.2), the transformation efficiency obtained for the electro-competent cells was 4.9 × 10^4 CFU/μg vector DNA determined using the pSE100 control. A single blue clone (SCO strain) was cultured and subjected to sucrose counter selection (section 3.2.4). White colonies were then screened by PCR to identify clones which possess only the deleted allele. Thereafter, Southern blot analysis was conducted to confirm the deletion of the wild type allele without imposing additional unintended chromosome rearrangements, Figure 3.21.

PCR analysis revealed 3 possible deletion strains, clones 3, 4 and 5, indicated by the 327 bp mutant band, Figure 3.21. Genomic DNA from all was extracted and southern blot analysis was conducted to confirm the genotype of the Δ*ami1*::ParBM-DnaNG strain and to confirm correct site-specific integration of the deletion allele. The probe for Southern blotting was constructed by PCR and the primers used to amplify the upstream homologous region (MsmAmi1SF and MsmAmi1SR).

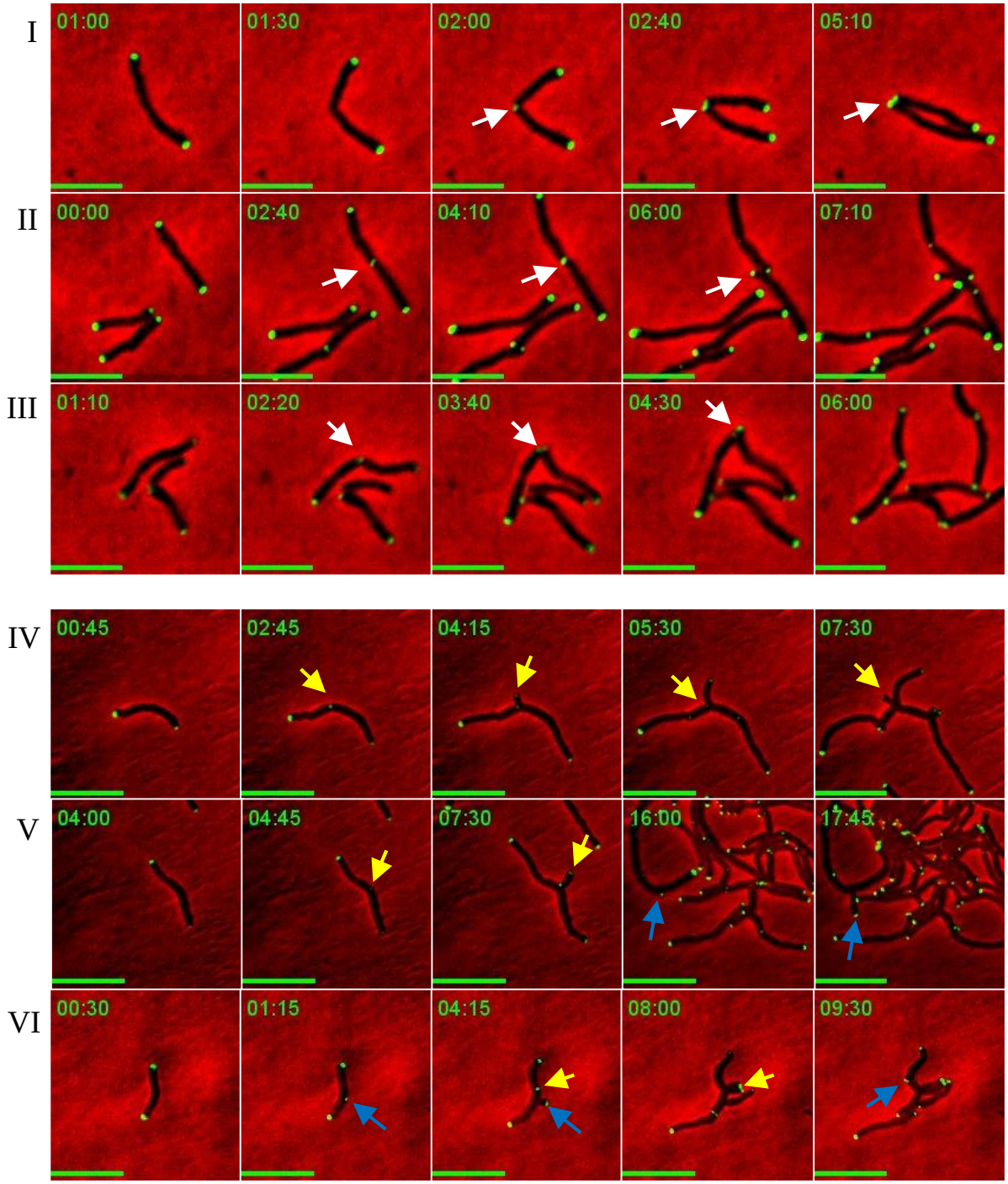

Figure 3.20: Time-lapse microscopic analysis of DivIVA-GFP localisation in the mc^2155 and Δ*ami1* strains. Cells were grown and imaged in 7H9. I-III depicts three representative mc^2155 micro-colonies and IV-VI depicts three representative Δ*ami1* micro-colonies. White arrows indicate the septal localisation of DivIVA, which became two new growth poles following cell separation. Yellow arrows depict septal localisation of DivIVA in the Δ*ami1* strain, which resulted in the formation of two new growth poles leading to lateral budding and branch elongation and blue arrows indicate ectopic localisation of DivIVA in the Δ*ami1* strain, which resulted in the establishment of a single growth pole leading to lateral budding and branch elongation. Scale = 5 µm. Movies were generated, processed and analysed by the student (Senzani et al., 2017).

Southern blot analysis using the restriction enzyme *Bam*HI was conducted on the mc^{2}155 and Δ*ami1* strains, which would yield 7303 bp for mc^{2}155::ParBM-DnaNG and 10185 bp for the Δ*ami1*::ParBM-DnaNG strain. The corresponding expected sizes were observed, confirming successful deletion of ami1 in the Δ*ami1*::ParBM-DnaNG strain, Figure 3.21.

3.3.6.3.2 Time-lapse microscopy of mycobacterial DnaN and ParB in a Δ*ami1* mutant

Following the construction of the Δ*ami1*::ParBM-DnaNG strain, time-lapse microscopy was conducted to determine the cellular localisation of DnaN-GFP and ParB-mCherry, Figure 3.22 and Appendix E, movies 3.25 to 3.27.

Time-lapse microscopy of Δ*ami1*::ParBM-DnaNG revealed a localisation pattern whereby DnaN is extremely dynamic, starting off near mid-cell and then localizing with the ¼ to ¾ region of the cell as the nucleoid replicates. ParB displays a similar pattern, beginning at mid-cell and moving to the ¼ and ¾ regions without disassembling (Santi et al., 2013). This suggests loss of Ami1 does not affect the mechanisms which replicate and partition the bacterial chromosome. This is also evidenced by the fact that this localisation pattern is maintained during ectopic bud and subsequent branch formation, whereby ParB localises at the point of bud formation (during bud formation and elongation) and moves towards the pole of the aberrant branch followed by DnaN. This suggested that chromosome replication occurs during branch formation, followed by ParB driven chromosome partitioning, resulting in the retention of the mycobacterial chromosome within the ectopic branch.

3.3.7 Antibiotic susceptibility of the Δ*ami1* mutant.

Disruption of cell division enzymes in *E. coli* results in increased susceptibility to antibiotics either due to a weakened cell wall or failed division (Heidrich et al., 2001, Korsak et al., 2005). We sought to test whether a similar situation prevailed in mycobacteria with the deletion of *ami1*. To do this, antibiotic susceptibility assays were conducted on the mc^{2}155, Δ*ami1* and Δ*ami1*::pMVami1 strains (Appendix D, Table D1). This initial analysis, however, could not be used as the pMVami1 strain displayed increased resistance towards all antibiotics tested (data not shown). The basis for this was unknown and it was decided that a new complement strain using the episomal pSE100 vector as the backbone was required (section 3.3.1). Following construction

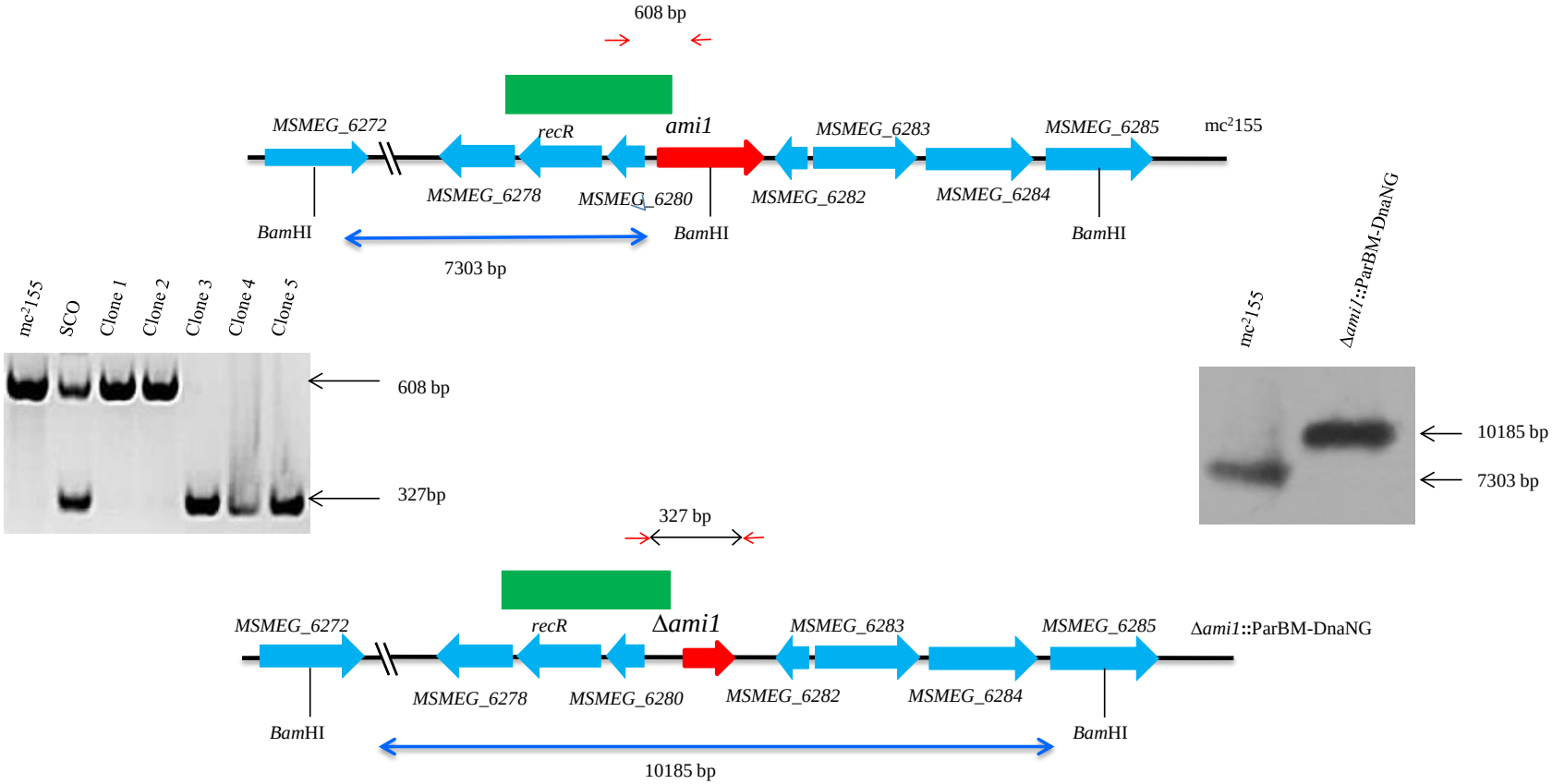

Figure 3.21: Genotypic analysis of the Δ*ami1*::ParBM-DnaNG strain by PCR and Southern blot analysis. The genomic map of the relevant locus is shown for the wild type mc^{2}155 and Δ*ami1*::ParBM-DnaNG strain. Also shown on the left is the PCR screen of possible Δ*ami1*::ParBM-DnaNG strains and southern blotting of a single positive clone is shown on the right. For PCR confirmation, chromosomal DNA was used to amplify the *ami1* alleles from the wild type and mutant strains using the primers listed in Table 3.3 and indicated as red arrows above. The expected sizes of the amplicons are as follows: *ami1*, 608 bp and Δ*ami1*, 327 bp. For the Southern blot analysis chromosomal DNA from the SCO, parental and mutant strain was digested with *BamH*I. The probe used for hybridisation is shown as a solid green box and the expected sizes are indicated by the blue arrows.

of the new complementation strain (which was used in all the assays reported thus far) antibiotic susceptibility assays were repeated using antibiotics which target various cell wall, cytoplasmic and periplasmic components (Table 3.4).

The antibiotic susceptibility assays revealed a reduction in the amount of antibiotic required to inhibit mycobacterial growth in most cases, with the exception of cefamandole, which displayed no change and D-cycloserine, in which case deletion of *ami1* led to increased tolerance. There were cases wherein the reduction in MIC was more significant, these included, cefoxitin, cefotaxime and ceftraxone, which are all cephalosporins. We did not consider a two-fold change in antibiotic susceptibility significant as this falls within the experimental variation of this assay. The somewhat dramatic changes in antibiotic susceptibility to cell wall targeting antibiotics were suggestive of a defective cell wall in the *ami1* mutant.

To further understand this, an ethidium bromide (EtBr) diffusion assay was conducted to determine whether the increase in antibiotic susceptibility was associated with an increase cellular permeability, Figure 3.23.

Analysis of the diffusion rate of EtBr in all three strains revealed elevated cell envelope permeability in the Δ*ami1* strain, suggesting the reduction in antibiotic requirement could be a result of increased antibiotic penetrance.

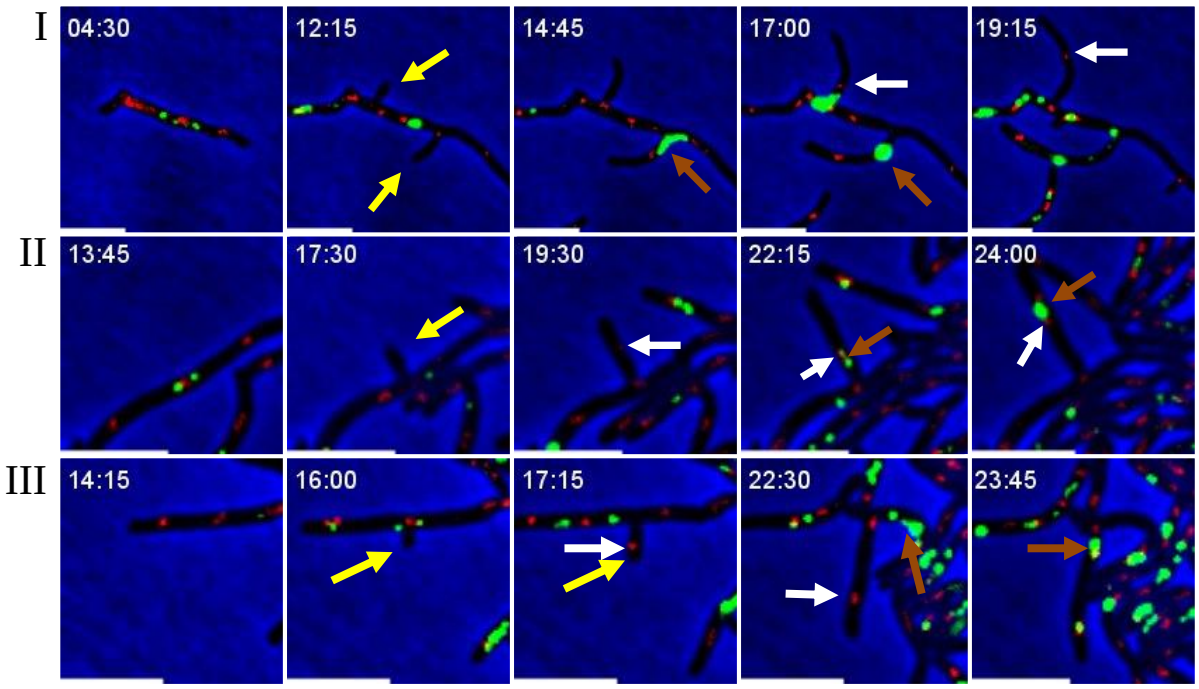

Figure 3.22: Time-lapse microscopic analysis of ParB and DnaN in the *ami1* mutant. Shown is the localisation ParB-mCherry (red) and DnaN-GFP (green) localisation in the Δ*ami1*::ParBM-DnaNG strains. Cells were grown and imaged in 7H9. I-III depicts three representative Δ*ami1*::ParBM-DnaNG micro-colonies. Yellow arrows indicated the initiation of branch formation. White arrows track the movement of ParB-mCherry during branch elongation and Orange arrows track the movement of DnaN-GFP during branch elongation. Scale = 5 µm. Movies were generated by N. Dhar then processed and analysed by the student.

Table 3.4: MIC of the mc^{2}155, Δ*ami1* and Δ*ami1*::pSEami1 strains

Drug	**MIC***		
	mc^{2}155	**Δ*ami1***	**Δ*ami1*::pSEAmi1**
Ampicillin	150	78	150
Erythromycin	6.25	3.1	6.25
Vancomycin	0.78	0.20	0,78125-1,5625
Rifampicin	0.625	0.3125	0.625
Cefamandole	500	500	500
Cefoxitin	40	10	40
Cefotaxime	93.75	23	93,75-187,5
Ceftriaxone	250	62	250
Cefapirin	50	25	50
D-cycloserine	32	62	32

*MIC in µg/ml,

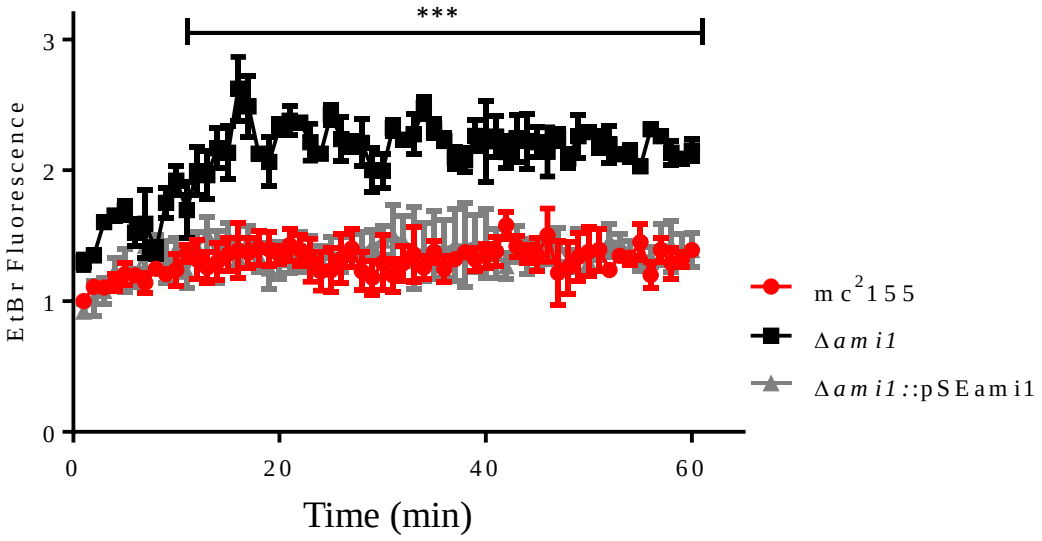

Figure 3.23: EtBr diffusion in the *ami1* mutant. Shown in a line graph depicting EtBr diffusion into the cytoplasmic space of the mc^{2}155, Δ*ami1* and Δ*ami1*::pSEami1 strains, as an indicator of cell envelope permeability. Error bars determined using the standard error of the mean and p-values using the student's *t* – test. ***: $p < 0.001$. The graph represents the average of three independent replicates.

3.4 Discussion

Cell division is an essential component of the bacterial life cycle and understanding this process is important to designing effective inhibitors that target it. Much like a multitude of bacterial processes, the various components involved in cell division are carefully regulated in response to environmental conditions and other aspects of bacterial metabolism, an example of which is coordination of chromosome replication with cell wall growth (Egan and Vollmer, 2013). Many of the components involved in bacterial replication have been the subject of intense study and in this context, various divisome constituents, including Fts proteins, have been well characterised in model organisms. However, growth and division, particularly the role played by PG hydrolysing enzymes, still require further investigation in mycobacteria (Hett and Rubin, 2008).

PG hydrolysing enzymes are important components of bacterial cell division as they play an central role in the coordinated breakdown of septal PG to facilitate daughter cell separation. Work conducted in various bacterial organisms, including *E. coli, Pseudomonas aeruginosa, Neisseria gonorrhoeae* and *Staphylococcus* spp. has highlighted the importance of two classes of PG hydrolysing enzymes in this process, the lytic transglycosylases and the cell wall amidases (Heidrich et al., 2002, Jorgenson et al., 2014, Yakhnina et al., 2015, Cloud and Dillard, 2004, Garcia and Dillard, 2006, Sugai et al., 1995, Stapleton et al., 2007). In *E. coli* deletion of three lytic transglycosylases or cell wall amidases resulted in the formation of chains consisting of 3 to 9 or 6 to 24 cells, respectively, illustrative of cells that were unable to complete the final steps of cell division (Heidrich et al., 2002). Similarly in *P. aeruginosa*, depletion of the essential cell wall amidase, *amiB*, led to the formation of long cell chains, while deletion of lytic transglycosylase *rlpA* resulted in the formation of short chains consisting of 4 cells (Jorgenson et al., 2014, Yakhnina et al., 2015). This function is not only limited to rod shaped bacteria as deletion of either the lytic transglycosylase, *ltgC*, or cell wall amidase, *amiC*, in *Neisseria gonorrhoeae*, led to the formation of cell clusters attached to each other by septa (Cloud and Dillard, 2004, Garcia and Dillard, 2006). In addition, the deletion of lytic transglycosylase, *sceD*, or a cell wall amidase-containing major autolysin, *atl*, in *Staphylococcus aureus*, led to the formation of clusters (Sugai et al., 1995, Stapleton et al., 2007). Collectively, these observations suggest both enzyme classes conduct important and possibly non-redundant roles during cell division, as both are required for cell separation.

In mycobacteria, division mechanisms seem to have diverged somewhat. This is illustrated by the observation that deletion of all the lytic transglycosylases, in this case the resuscitation promoting factors (Rpfs), in *M. smegmatis* did not result in any significant cell division defects (Beukes, 2014). This finding suggested that other PG hydrolysing enzymes such as cell wall amidases may be important in mycobacterial cell division. Thus, herein, we set out to characterise the role of the PG hydrolysing enzyme, Ami1, in the growth and division of *M. smegmatis*, with the intention of advancing the knowledge on the cell division machinery in mycobacteria.

Bioinformatics analysis of the mycobacterial genome led to the identification of four cell wall amidases in Mtb (Senzani, 2014, Machowski et al., 2014). Further analysis of these revealed that two of them, Ami1 and Rv3915 (Ami2) were homologues to the *E. coli* cell division amidases, however, only one, Ami1, retained all the corresponding residues required for catalytic activity (Appendix D, Figure D1) (Machowski et al., 2014, Senzani, 2014). As such, Ami1 was selected for further study to assess the role this enzyme plays during cell division. The approach taken was to delete *ami1* and subsequently characterise the resulting Δ*ami1* strain to identify phenotypic changes that occurred (Appendix D, Figure D2) (Senzani et al., 2017, Senzani, 2014). Preliminary microscopic analysis of the Δ*ami1* strain depicted a possible role for Ami1 during cell division. Much like in *E. coli* and *P. aeruginosa*, deletion of this enzymes resulted in the formation of chains consisting of multiple cells attached to each other by the septum (Senzani, 2014). This defect was further assessed in this PhD where microscopy and statistical analysis was conducted on the Δ*ami1* strain to determine whether the observed cell division defects were significant. This analysis demonstrated that 22 % of the cell population displayed the formation of cellular chains consisting of 3 to 8 cells. This was consistent with data on the *E. coli* Δ*amiC* mutant, which indicated that loss of AmiC led to the formation of chains consisting of 3 to 6 cells in 20 to 30 % of the population (Heidrich et al., 2001). Furthermore, we noted the presence of division septa in 94 % of the Δ*ami1* population, as opposed to 18 % in the mc^2155 population, indicating a temporary yet significant stall during cell division, resulting in a high proportion of the population undergoing cell division at any given point. We hypothesise that this is due to a delay in cell separation rather than an increase in the frequency of cell division events in the *ami1* mutant. This notion is based on the demonstrated role for amidases in the degradation of the septum to facilitate the last steps of cell division. Furthermore, BODIPY-vanc staining confirmed that PG synthesis occurs at the septum, resulting in the formation of mature septa that are not degraded.

Interestingly, this chaining phenotype has been reported previously in *M. smegmatis*, as a result of depletion of an unrelated PG hydrolysing enzyme. Mycobacteria possess a variety of PG hydrolysing enzymes and thus far, an interesting interaction between some of these enzymes, including RpfB, Rpf-interaction proteins A (RipA) and B (RipB), has been shown to be important for cell division (Hett et al., 2007, Martinelli and Pavelka, 2016). RipA and RipB are PG hydrolysing endopeptidases (Böth et al., 2011). These are operonic, redundant, essential proteins, which are individually dispensable for growth. However loss of both results in bacterial growth arrest (Martinelli and Pavelka, 2016). Deletion of either gene does not appear to affect bacterial cell division. However, depletion of both led to the formation of bacterial chains, containing lateral growth appendages (Hett et al., 2008, Martinelli and Pavelka, 2016). In this context, there is a striking similarity between the defects observed for the collective depletion of RipA-RipB and the deletion of *ami1*. This suggests that there might be an interplay between these septal degradation mechanisms, further supported by the fact that they degrade different bonds in the PG. RipA and RipB are endopeptidases that cleave within the stem peptide in PG whilst Ami1 cleaves between the stem peptide and the glycan backbone. The hypothesis that these enzymes have specialist function is further supported by the observations that deletion or depletion of either system is not compensated for by the remaining enzymes as clear cell division defects are manifested in both cases. Further interaction studies and real-time localisation of these different enzymes at the septum may help to unravel this interplay.

As the Ami1 enzyme appeared to conduct an important role in cell separation, we sought to localise it and track the movement of Ami1 during growth to determine when this enzyme was recruited to the division septum. This was not possible as the Ami1GFP signal was unstable and single foci could not be tracked over time. Analysis of the localisation patterns using TIRF microscopy, however, showed that Ami1GFP localised as punctate foci during cell elongation and is recruited to the septum; perhaps late during division once the septum has formed, as indicated by the subpopulation of cells containing a division septum without the localisation of Ami1GFP. This type of localisation has been previously reported in *E. coli* where all three cells division amidases exhibit a diffused localisation pattern during elongation and are then recruited to the septum during cell division (Peters et al., 2011). It is also possible that the punctate localisation suggests a function for Ami1 during cell elongation, which would be the maintenance of bacterial cell shape as loss of *ami1* not only resulted in the formation of thin cells but also the occurrence of cell bulges,

possibly due to the dysregulation of the systems which maintain the shape of the cell. However, this explanation is largely speculative and requires further investigation.

Another striking observation was the influence of Ami1 in FtsZ-ring stability. Loss of Ami1 resulted in some Z-ring defects, the first being the pattern at which the final Z-ring forms. In the presence of Ami1 the Z-ring formed as two concentric rings which oscillated to a final assembly point at the septum – presumably on either side of the septum of a dividing cell. However, in the Δ*ami1* strain this assembly mechanism does not occur, instead a single ring forms at the final site of cell division. FtsZ mobility is maintained in the Δ*ami1* strain but the ring sometimes occurred in the form of disorganised foci rather than rings. Furthermore, in some cases the Z-ring formed and disassembles prior to septum synthesis. This generally led to the reassembly of the Z-ring at the same site, either resulting in septum synthesis or disassembly of the ring. The repeated formation and disassembly of the Z-ring at a single site suggests Ami1 does not influence the mechanism underpinning the site of Z-ring placement but the failure to separate does affect the stability of the Z-ring. How this is achieved is currently unclear, primarily as the localisation data suggested Ami1 is recruited later during cell division and the presence of a signal peptide in the Ami1 polypeptide suggests it resides outside the cytoplasmic space while FtsZ is a cytoplasmic component (Senzani, 2014). There is a possibility that Ami1 stabilises the Z-ring through interactions with an intermediary septum protein, which in turn functions to stabilise the Z-ring.

Unlike the depletion of RipA-RipB, loss of Ami1, and the resulting cell division defects, was not associated with a reduction in bacterial growth in broth culture (Hett et al., 2008). This can be partially attributed to the mycobacterial growth cycle wherein cell elongation and division seems to be uncoupled; as such a halt in cell division does not result in the inhibition of cell elongation (Aldridge et al., 2012, Wachi and Matsuhashi, 1989, Fenton and Gerdes, 2013). This continued bacterial growth, in the absence of effective cell separation, appears to occur in numerous bacteria when cell division hydrolases are deleted/depleted. In this regard, with the exception of the essential cell wall amidase, *amiB*, in *P. aeruginosa*, loss of either a cell wall amidase or a lytic transglycosylase in the organisms listed above did not result in reduced bacterial growth (Heidrich et al., 2002, Jorgenson et al., 2014, Yakhnina et al., 2015, Cloud and Dillard, 2004, Garcia and Dillard, 2006, Sugai et al., 1995, Stapleton et al., 2007). How this growth continues to occur in these chains and clusters is not clear. As such, utilising single cell time lapse microscopy, we

sought to unpack how elongation continues in the presence of stalled cell division in the Δ*ami1* strain.

Single cell analysis of the Δ*ami1* strain revealed 2 key findings, the first being the formation of lateral branches, similar to those observed in the *ripAB* depletion strain and the second is the utilisation of these branches to bypass failed cell separation (Hett et al., 2008). In addition to depletion of *ripAB,* this branched growth form was also observed in the overexpression of the growth pole determining component, DivIVA (Hett et al., 2008, Kang et al., 2008). As such it was hypothesised that the formation of these lateral branches in the Δ*ami1* strain was a result of ectopic DivIVA recruitment, resulting in the formation of a growth pole at the septum. This was confirmed by single cell time-lapse microscopy of DivIVA localizing strains, wherein stalled cell division resulted in the establishment of the elongation machinery driven by DivIVA at the septum, in both daughter cells, resulting in septal cell elongation leading to lateral growth. Lateral growth, however, was also observed at non septal regions, in which case DivIVA was found to localise in an aberrant manner along the longitudinal axis during cell elongation in a similar manner to that seen in the filamentous *Streptomyces coelicolor* (Hempel et al., 2008). This suggested an additional role for Ami1 during elongation wherein it could function to inhibit ectopic DivIVA localisation. This hypothesis was further supported by the Ami1 localisation pattern which presented as ectopic foci during the cell elongation phase of growth. Both septal and ectopic branches resulted in viable cells, which elongated and subsequently underwent cell division. However, there were instances where these branches died, followed by the emergence of a new branch at the site of the previous branch, suggesting these cells could be anucleate and were not able to undergo successive replication cycles. These observations suggested that the DNA segregation machinery in the Δ*ami1* strain was dysregulated leading to the formation of anucleate cells.

To test this hypothesis, DnaN and ParB were localised in the Δ*ami1* strain, these two components involved in chromosome replication/segregation. DnaN forms part of the DNA polymerase III holoenzyme responsible for DNA replication. ParB is the DNA binding component of the ParABS system, which is pulled to the opposite cell poles by ParA polymers, responsible for the segregation of the two newly synthesised genomes into the daughter cells, thus movement ParB would indicate the movement of a single genome (Burgers et al., 1981, Murray and Errington, 2008). Localisation

of both these proteins in the mc^{2}155 background has demonstrated that chromosome replication and segregation begins at the midcell as both the DnaN and ParB foci were recruited to the midcell (Santi et al., 2013, Santi and McKinney, 2015). This is followed by the movement of the ParB foci to the opposite poles while DnaN remains at the midcell indicating that the replication machinery remains somewhat static and DNA is pulled through DNA polymerase III as the newly synthesised genome is pulled to the poles by the ParABS system (Santi and McKinney, 2015). A similar localisation pattern was observed in the Δ*ami1* strain as the movement of ParB into lateral branches was observed indicating the movement of genetic material into these branches. Movement of DnaN into these branches was also observed in the Δ*ami1* strain, suggesting a possible unidirectional ParABS pull in some of these branches which could result in polyploidy or guillotining of genomic material, resulting in irreparable DNA damage and possible cell death (Santi and McKinney, 2015).

In addition to its involvement in cell elongation and division, Ami1 appears to play a role in antibiotic tolerance. This is demonstrated by the reduction in antibiotic tolerance of the Δ*ami1* strain relative to mc^{2}155 to certain classes of antimicrobials. Similar observations have been noted in a number of bacterial organisms including *P. aeruginosa*, *S. enterica* and *E. coli* wherein the loss of various amidases led to antibiotic hypersensitivity, against PG targeting enzymes, partially attributed to the β-lactamase induction pathway in *E. coli*, which is regulated by cell wall amidases, and antimicrobial peptides (Korsak et al., 2005, Weatherspoon-Griffin et al., 2011, Jacobs et al., 1995). This phenotype has been attributed to an increase in cell envelope permeability; however, the link between cell division defects and increased envelope permeability remains unclear. We sought to further investigate this by studying the permeability of the cell wall using EtBr and found enhanced EtBr penetration across the cell envelope in the absence of Ami1. This effect was reduced in both the mc^{2}155 and Δ*ami1*::pMVami1 strains. In this case, the defect could be the possible outcome of a potential reduction in septum stability, confirmed by the extrusion of cell wall material from the septum in some cases. This could result in a weak point in the PG structure thus allowing for penetrance of more antimicrobial molecules.

PG analysis of the Δ*ami1* strain revealed an increase in the proportion of 3-3 stem peptide crosslinks, but more importantly between stem peptides which only possess three amino acids, when compared to the mc^{2}155 strain (Senzani et al., 2017). Though the abundance of 3-3

crosslinks in mycobacterium has been reported, the overwhelming presence of this specific confirmation in the Δ*ami1* strain, suggests that the Δ*ami1* septal PG may exist with 3-3 corsslinks, post synthesis conducted by PBPs removing the terminal D-alanines (Lavollay et al., 2008, Lavollay et al., 2011). Once this has occurred the resulting structure can no longer undergo modifications. One of the more striking observations from this study was the release of cell wall material from the division septum. Though the release of PG in not a new phenomenon, this is usually in the form of small molecules such as muropeptides (Templin et al., 1999, Goodell and Schwarz, 1985). The release of large portions of cell wall material in the Δ*ami1* strain, suggest a breakdown in the interplay between septal cell wall synthesis and degradation, possibly resulting in the overproduction and release of cell wall material.

In conclusion, this section of the PhD dissertation represented the first extensive characterisation of a cell division amidase in the actinomycete family and serves to offer a broader understanding of amidase function in mycobacteria (a proposed model is given in Figure 3.24). Ami1 represents the first reported case of a single mycobacterial PG hydrolase being important for cell division. How this function relates to the biological role of other PG hydrolysing enzymes is an exciting area for future research.

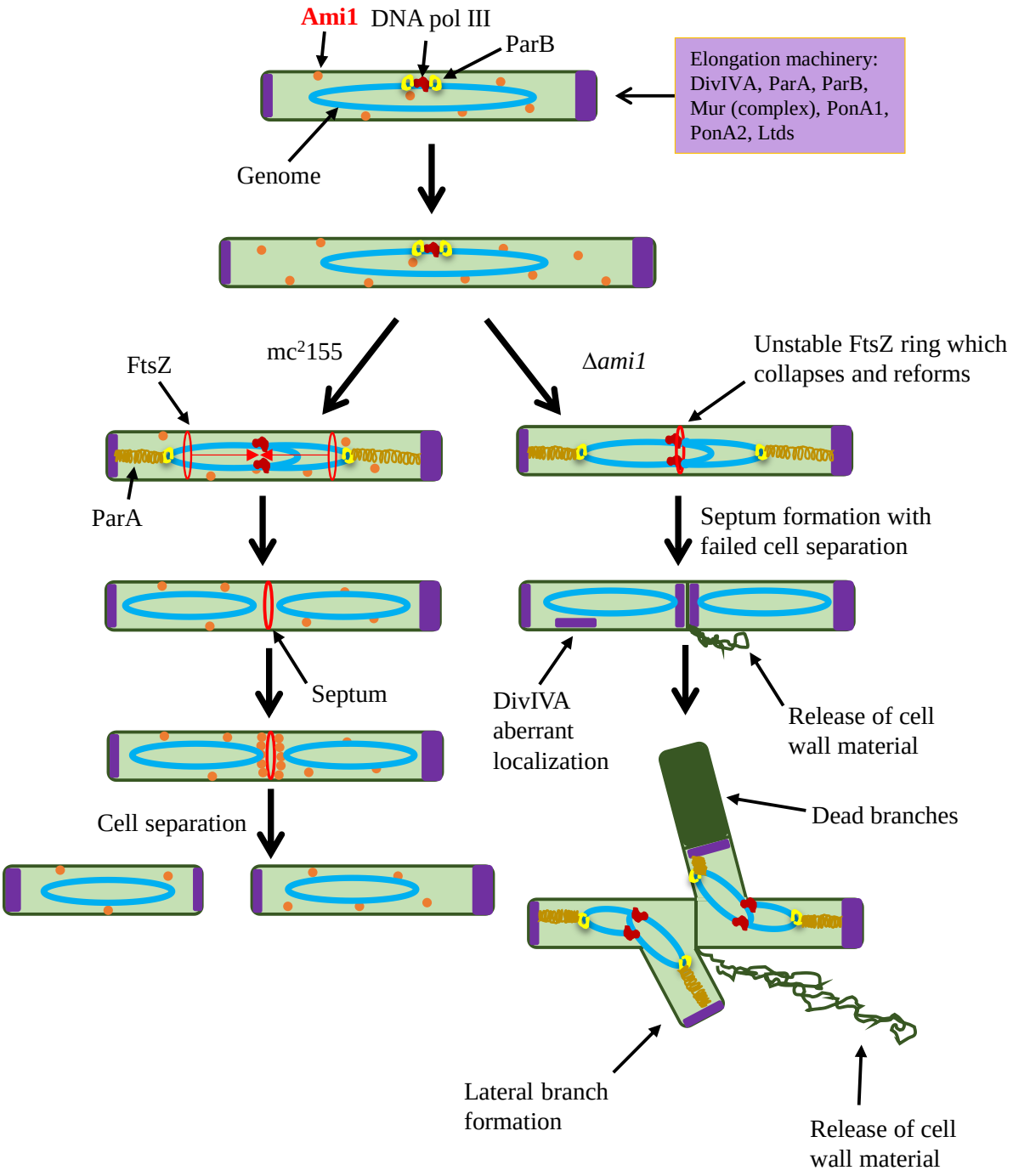

Figure 3.24: Proposed model for Ami1 function in mycobacteria. Shown is the role of Ami1 depicted by the mc²155 branch, depicting the punctate localisation of Ami1 responsible for maintaining bacterial cell shape. Following septal synthesis, Ami1 is recruited to the septum resulting in septal cleavage. Deletion of *ami1* results in the formation of cell chains, which are thinner than wild type bacteria, with aberrant cell growth/division modalities such as lateral budding. Defective division in cell chains also results in destabilisation of the FtsZ-ring, resulting in multiple cycles of FtsZ-ring assembly and collapse during a single division cycle.

Chapter 4

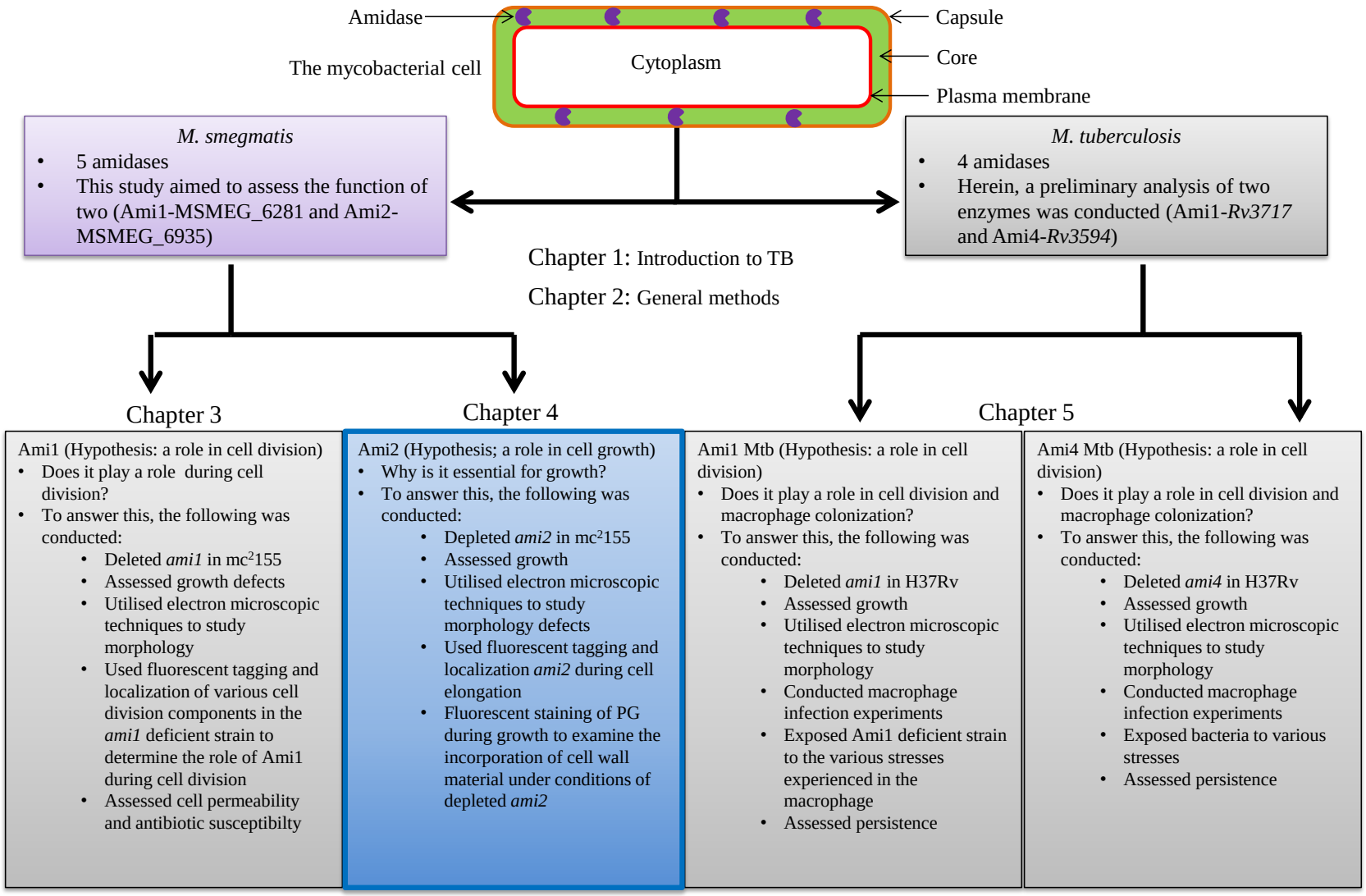

Figure 4.1: Flow chart highlighting the focus of chapter 4. Highlighted is the portion of the study which will be addressed in the following chapter. The figure was drawn by S. Senzani.

4 The role of Ami 2 in cell elongation

4.1 Introduction

4.1.1 Bacterial cell elongation

Much like cell division, elongation is an important part of the bacterial life cycle. With respect to the PG, this process entails the overall expansion of the bacterium, which involves remodelling of the PG sacculus to allow for this growth (Typas et al., 2011). Elongation requires the synthesis of new PG units, which occurs in the cytoplasm, using an extensive complement of biosynthetic genes to create the PG precursor molecule called Lipid II (Typas et al., 2011, Vollmer et al., 2008). Once synthesised, the molecule, which is membrane associated, is flipped into the periplasm where it gets incorporated into the existing PG sacculus by penicillin-binding proteins (PBPs). PBPs integrate the new precursor into the glycan strand and also crosslink the stem peptides to create a mesh-like structure. This entire process is carefully coordinated with a variety of PG synthases and hydrolases.

4.1.1.1 *Lipid II synthesis*

Lipid II is the building block for all bacterial PG. This component consists of a disaccharide backbone made up of GlcNAc and MurNAc linked by β-1,4-glycosidic bonds (Vollmer et al., 2008). Attached to this, via the MurNAc residue is a five amino acid stem peptide consisting of L-alanine, D-glutamic acid, a *meso*-diaminopimelic acid (meso-DAP) moeity or L-lysine (depending on bacterial species) and two terminal D-alanines (Vollmer et al., 2008). The synthesis of this component occurs entirely in the cytoplasm and is conducted by a set of essential enzymes that possess various functions including; transferases, dehydrogenases and amino acid ligases (Barreteau et al., 2008). Metabolically, PG synthesis is dependent, to some extent on glycolysis, which yields the production of pyruvate and other intermediate metabolites such as fructose – 6 – phosphate (Barreteau et al., 2008). For PG biosynthesis, the resulting fructose – 6 – phosphate is processed by three proteins, the amidotransferase GlmS, the aminotransferase GlmM and the bi-functional protein GlmU, yielding the production of UDP-GlcNAc (Barreteau et al., 2008). This is followed by the first committed step towards Lipid II synthesis, which is carried out by MurA, involving the attachment of enol-pyruvate to UDP-GlcNAc (Barreteau et al., 2008). Following this, is the reduction of the GlcNAc residue by MurB, converting it to UDP-MurNAc (McCoy et al., 2003, Brown et al., 1995, Benson et al., 1993, Typas et al., 2011). The amino acid stem peptide

is then attached to the MurNAc residue in a step wise manner by various amino acid ligases, beginning with MurC, which attaches the L-alanine (Typas et al., 2011, Barreteau et al., 2008). After this, a D-glutamic acid residue is added to the L-alanine and this is facilitated by MurD. Thereafter, the meso-DAP residue is added to D-glutamic acid by MurE (Typas et al., 2011, Akira et al., 2001). The final two residues are added to the stem peptide by MurF as a pair (Barreteau et al., 2008, Typas et al., 2011). This is a pair of D-alanines, obtained from the activity of two essential enzymes, the alanine racemase (Alr), which is responsible for the conversion of L-alanine to D-alanine and D-alanine-D-alanine ligase (Ddl), which ligates two D-alanines resulting in the production of the D-alanine pair (Typas et al., 2011, Barreteau et al., 2008). The resulting UDP-MurNAc-pentapeptide molecule is then translocated to the cell membrane where the remainder of the process occurs (Barreteau et al., 2008, Typas et al., 2011). First, the PG monomer is linked to membrane-associated undecaprenol phosphate, a step catalysed by MraY, resulting in the formation of Lipid I (Barreteau et al., 2008, Typas et al., 2011). This is then finally processed by MurG, responsible for the addition of UDP-GlcNAc to Lipid I, leading to the production of membrane bound GlcNAc-MurNAc-pentapeptide also known as Lipid II, which is then translocated to the periplasm by RodA or FtsW where the rest of the PG synthetic steps can occur (Typas et al., 2011, Barreteau et al., 2008). A diagrammatic representation of this process is given in Figure 4.2.

4.1.1.2 *The periplasmic steps of PG biosynthesis*

Once in the periplasmic space, Lipid II is utilised by a group of enzymes collectively known as PBPs, initially named for their affinity to bind penicillin (Vollmer et al., 2008). There are three main proteins that utilise Lipid II to ultimately integrate this precursor into PG. These are class A, class B and low molecular weight (LMW) PBPs (Vollmer et al., 2008, Typas et al., 2011). Class A PBPs are high molecular weight PBPs, which contain both glycosyl transferase and transpeptidase activity (Bertsche et al., 2005, Born et al., 2006). These enzymes play a crucial role in the integration of Lipid II into pre-existing PG, by incorporating Lipid II into the sugar backbone and also by driving the formation of stem peptide crosslinks between newly incorporated PG units and pre-existing PG (Bertsche et al., 2005, Born et al., 2006). Deletion or reduction of these enzymes in *B. subtilis* results in the formation of thin long cells indicating a further role in determining bacterial cell shape (Popham and Setlow, 1995, Murray et al., 1996, McPherson and Popham, 2003). Similar to class A, class B PBPs are also high molecular weight penicillin-binding

proteins, however these only possess transpeptidase activity (Wei et al., 2003). In many organisms, there appears to be a redundancy of these proteins but their activity is essential for cell elongation, specifically in rod-shaped bacteria as evident by the formation of spherical cells in the absence of these enzymes (Wei et al., 2003). The final class of PBPs are the LMW PBPs, which possess carboxypeptidase activity (Nelson and Young, 2000). The main function for these enzymes is the removal of one terminal D-alanine from the pentapeptide stem (Pollock et al., 1974). Though the importance of this activity is currently unclear, the prevailing hypothesis is that the removal of the terminal alanine abrogates the ability to use that particular stem peptide to form a crosslink. Consequently, these PBPs are expected to regulate the level of PG crosslinking. Additionally, this function appears to have an important role in maintaining cell shape also as deletion of LMW PBPs in *E. coli* results in the formation of deformed bacterial cells (Nelson et al., 2002, Nelson and Young, 2001, Nelson and Young, 2000).

An important aspect of PG biosynthesis is the spatial coordination of the process - it is important that PG synthesis is directed to the correct site of cell elongation. The composition of the elongation machinery, referred to as the elongasome, varies between different bacteria primarily because elongation occurs differently in various bacteria, thus the mechanisms controlling the process are not the same (Daniel and Errington, 2003). The most widely understood mechanisms utilised for directing the synthesis of PG is the MreB system. This functions much like the Fts system as it involves the recruitment of a polymerised anchor (MreB) to the inner membrane, which then recruits other components required for the association of PBPs and lytic enzymes essential for PG synthesis (Errington, 2015). MreB is an actin like protein that forms filaments in the presence of ATP or GTP and plays an important role during elongation, as depletion of MreB results in a halt in cell elongation, and an increase in cell width, which ultimately leads to cell lysis in *E. coli* (Maeda et al., 2012, Kruse et al., 2005).

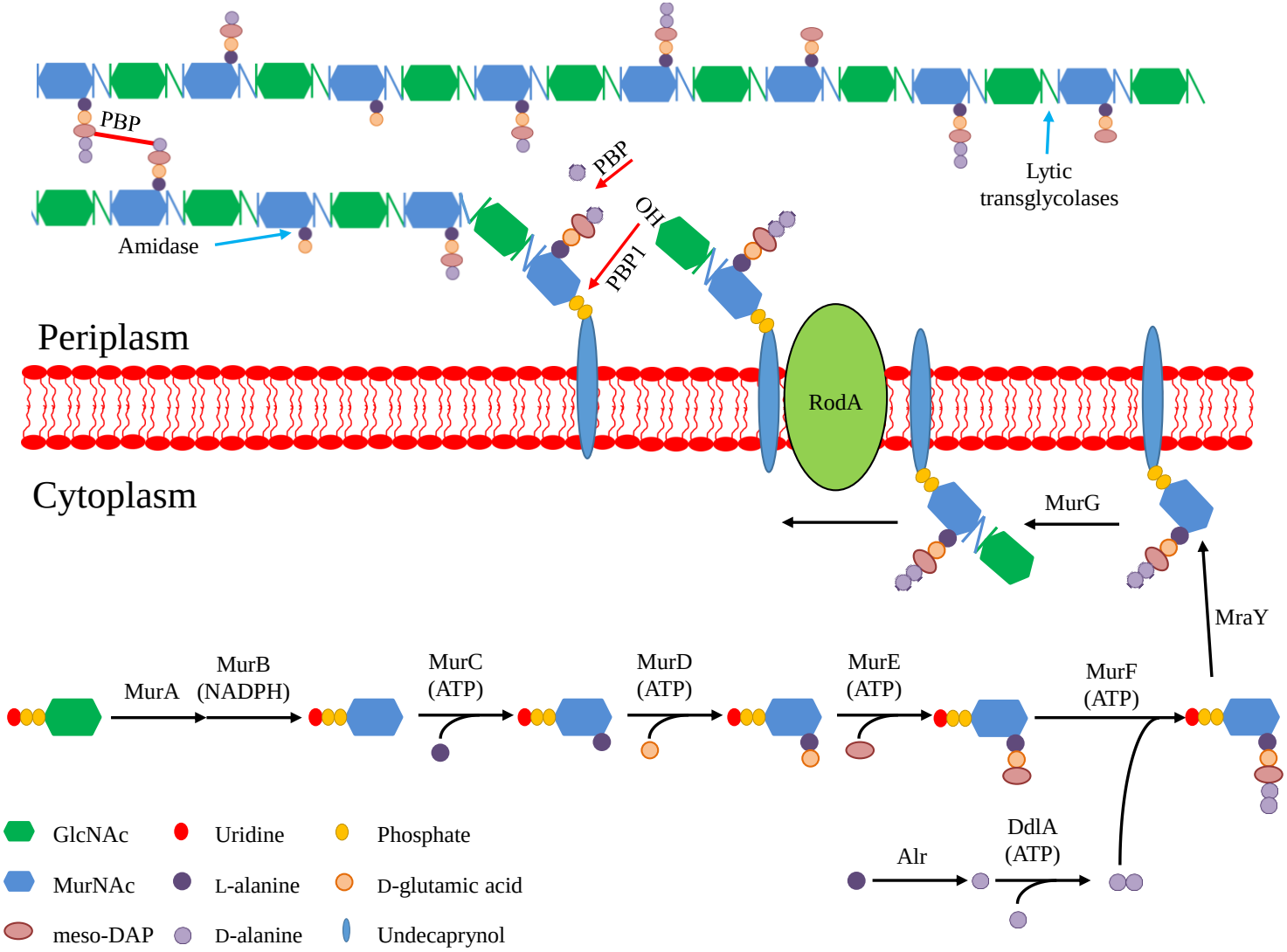

Figure 4.2: Diagrammatic representation of PG biosynthesis, depicting the various cytoplasmic and periplasmic steps. Shown are the different enzymes and the reactions that they catalyse, as well as the various periplasmic reactions catalysed by PBPs (Red arrows and lines). Also indicated are the various PG hydrolases shown to be essential for PG synthesis in different organisms (blue arrows) (adapted from Typas et al, 2012). Figure drawn by S. Senzani.

MreB was initially thought to direct PG synthesis through the formation of long helical filaments along the longitudinal axis of the bacterium thus directing synthesis in a helical manner. However, subsequent studies have demonstrated that MreB filaments localise as patches, which then move in a somewhat helical manner synthesizing PG as they move (Garner et al., 2011, Dominguez-Escobar et al., 2011, van Teeffelen et al., 2011). MreB attachment to the inner membrane and rotation appears to be directed by one of the MreB interacting partners, the cell shape determinant, RodZ (Morgenstein et al., 2015). This motion is not only essential for elongation but also plays an important role in maintaining the integrity of the rod shape, as the loss of RodZ leads to the formation of ovococcoid cells (Alyahya et al., 2009, Morgenstein et al., 2015). These defects could be partially complemented with specific mutations in the *mreB* gene, indicating a potential to bypass the need for RodZ (Shiomi et al., 2013). The impact of these mutations in MreB localisation and movement has yet to be described. MreB forms a complex with two other components, MreC and MreD (Kruse et al., 2005, Leaver and Errington, 2005). These are both membrane-associated proteins that play an essential role in the recruitment of PBPs and lytic transglycosylases, required to hydrolyse the PG backbone allowing for the insertion of new PG material (Leaver and Errington, 2005). Additionally, the Mre complex interacts with a number of the components that comprise the cytoplasmic PG synthesis machinery including MurB, MurC, MurE, MurF and MraY, suggesting this complex serves as a central hub for all steps in PG synthesis (White et al., 2010).

The Mre complex is essential in all rod-shaped bacteria that possess the gene coding for MreB (Daniel and Errington, 2003). However, there are rod-shaped bacteria which do not possess the Mre system, primarily the actinomycetes (Singh et al., 2010). In these organisms, a different approach is adopted due to the absence of this canonical system and also because of the differences in the modalities of cell growth. Bacteria which use the Mre system to grow do so by the insertion of new PG material along the longitudinal axis of the cell. However, actinomycetes such as streptomyces and mycobacteria grow by inserting PG material at the poles, more specifically in a ring-like conformation in sub-polar space (Meniche et al., 2014). This polar growth is driven by the tropomyosin-like protein DivIVA, which localises to the bacterial subpolar region, due to its affinity to bind areas of negative curvature (Meniche et al., 2014). The biological function of DivIVA is a subject of much ongoing research. Depletion and/or over-expression studies conducted in mycobacteria and various other organisms has demonstrated the importance of this protein during cell elongation, as depletion lead to the formation of short, wide cells while

overexpression resulted in long, branched cells indicating elevated activity of the elongation machinery (Kang et al., 2008). Furthermore, recent studies have shown interaction between DivIVA and RodA, implicating the latter protein in the regulation of cell elongation in actinobacteria (Sieger and Bramkamp, 2015).

In addition to DivIVA, another enzyme has been shown to play an important role in cell elongation, which is the high molecular weight PBP, PonA1 (Kieser et al., 2015). The mycobacterial PonA1 is a bi-functional PG synthase which contains both transglycosylation and transpeptidation activity as such, it possesses the capability to insert new PG precursors into the cell wall. Work conducted by Keiser et al, 2015, has shown PonA1 is essential for growth in *M. smegmatis* (Kieser et al., 2015). The essential nature of PonA1 was primarily linked to the transglycosylation activity, as deletion of this transglycosylase domain could not yield viable bacteria, while deletion of the transpeptidase domain resulted in shorter but viable cells (Kieser et al., 2015). Though PonA1 is not essential for growth in Mtb, this enzyme has been shown to play an important role in bacterial survival during infection as deletion of PonA1 in Mtb led to a reduction in the CFUs found in the lungs and spleen of infected mice (Kieser et al., 2015). Much like DivIVA, PonA1 localises at the bacterial poles and septum suggesting a possible interaction between the two, which is plausible considering overexpression of PonA1 results in phenotypes similar to those observed when overexpressing DivIVA, this interaction however remains to be confirmed (Kieser et al., 2015, Kang et al., 2008).

During elongation, PG hydrolysing enzymes are expected to be important for the insertion of new PG subunits as the cell elongates. As such, a recent study conducted in mycobacteria has shown an essential cell wall amidase (MSMEG_6935) (herein referred to as Ami2, also referred to CwlM) plays an important role in the synthesis of PG at the poles. The importance of Ami2 in cell elongation does not appear to be PG hydrolysis, allowing for insertion of new PG, but rather the activation of PG synthesising components. Work conducted by Boutte et al., 2016, has demonstrated that depletion of Ami2 resulted in the formation of short cells, suggesting a possible role during cell elongation (Boutte et al., 2016). Furthermore, it was shown that Ami2 interacts with PknB. This interaction results in the phosphorylation of the Ami2 C terminal tail, which in-turn phosphorylates MurA (Boutte et al., 2016). This phosphorylation results in the activation of MurA, and consequently the initiation of Lipid II synthesis thus promoting bacterial growth. Therefore, Ami2 serves as an important intermediate between PknB signalling and bacterial

elongation (Boutte et al., 2016). Cytoplasmic signal transduction is not new to cell wall amidases, as it occurs in *E. coli*; however, the direct phosphorylation of downstream elements has never been shown. Unlike mycobacteria, *E. coli* conduct this function indirectly through the activity of AmpD. AmpD much like Ami2 is a cytoplasmic cell wall amidase which plays an important role in PG recycling and the regulation of β-lactamase (*ampC*) expression (Jacobs et al., 1995). AmpD conducts this function through the hydrolysis and deactivation of muropeptides, by-products of PG remodelling, which possess the ability to induce a signal cascade resulting in the expression of *ampC* (Jacobs et al., 1995). Consistent with these findings, preliminary work conducted at our lab demonstrated that depletion of Ami2 results in the formation of short cells (Senzani, 2014). In this section of the PhD research, we aimed to expand on these findings.

Hypothesis: Ami2 is important for polar elongation of cells and, therefore, localises to the cell poles during growth. Depletion of Ami2 will be lethal for mycobacterial cells, an effect resulting from stalled cell elongation and defective PG turnover.

Preliminary work prior to this PhD. As part of an MSc study (Senzani, 2014) an Ami2 depletion strain was generated and a preliminary phenotypic characterisation was carried out.

Aims and objectives: The main aim of this section of the PhD was to carefully characterise the existing Ami2 depletion strain to establish a biological function for this enzyme. Given the demonstrated role for Ami2 in cell elongation, we also aimed to study the cellular localisation of this protein. As such, the specific objectives included:

1. Characterisation of the *ami2* depletion strain using growth assays, microscopy and single-cell time-lapse microscopy.
2. Confirmation that Ami2 is essential for growth in *M. smegmatis* through the deletion of the native *ami2* allele in the presence of a second copy of *ami2* integrated at the *attB* site.
3. Construction of the Ami2 localisation strain, mc^2155::pAmi2GFP and cellular localisation of Ami2GFP.
4. Confirming Ami2GFP functionality through the deletion of the native *ami2* allele in a strain carrying *ami2-rsEGFP* integrated at the *attB* site.
5. Construction of the Ami2-N and C- terminally FLAG tagged strains, mc^2155::pFAmi2N and mc^2155::pFAmi2C, followed by cell fractionation and localisation of the Ami2-FLAG variants.

4.2 Methods

4.2.1 Demonstrating the essentiality of *ami2*

The method adopted to prove *ami2* is essential, is a modified version of the method used by Gomez and Bishai, 2000, which involved the creation of a merodiploid strain. This entailed the construction of an *ami2* SCO strain followed by insertion of an additional *ami2* gene at a secondary site, driven off the native promoter, resulting in a strain containing two full-length *ami2* alleles and a truncated version (Appendix D, Figure D6) (Gomez and Bishai, 2000). This was then followed by the resolution of the SCO to a DCO resulting in either the deletion of the *ami2* gene located at the native allele or the removal of the truncated version resulting in a strain possessing two full length *ami2* genes (Gomez and Bishai, 2000).

4.2.1.1 *Construction of the mc²155::pMVami2 strain*

Primers were designed; *ami2*pMVCF and *ami2*pMVCR listed in Table 4.3, to amplify the *ami2* gene as well as 400 bp upstream the transcriptional start codon. PCR amplification of the respective fragments was carried out using Phusion polymerase, using an annealing temperature of 60 °C for *ami2* and an elongation time of 1 min to allow for complete amplification of the *ami2* fragment, which is 1619 bp. The PCR products were purified using the Nucleospin PCR purification Kit. Thereafter, 3 µg of pMV306 (H) was digested with *Hind*III and *Pvu*II and the PCR product was restricted with *Hind*III. The pMV306 (H) restriction product was then treated with FastAP phosphatase for 30 min. The restriction products were separated on a 0.8 % agarose gel and the respective bands [4258 bp for pMV306 (H) and 1598 bp for *ami2*] were excised from the gel and purified using the Nucleospin gel purification kit. These were then quantified using the NanoDrop spectrophotometer and ligations were set up containing 50 ng of pMV306 (H) and varying molar ratios of *ami2*. The fragments were ligated using Fermentas T4 ligase for 1 h, transformed into DH5α cells and plated on LA_{Hyg200}. Thereafter, 10 possible clones were selected and screened by restriction digest with *Bam*HI, which would yield two fragments, a 3560 bp and a 2304 bp band. A single positive clone was grown in 50 ml LB_{Hyg200} overnight then bulk vector extraction was carried out using the Nucleobond bulk vector extraction kit. Extracted vector DNA was quantified and restricted with a variety of enzymes to profile the *ami2* complementation construct (pMVami2), then the vector was sent for sequencing to check for the presence of mutations within the amplicon (data not shown). After confirmation, 1 µg of pMVami2 was electroporated into

electrocompetent mc^{2}155 cells, plated on 7H10$_{Hyg50}$ and incubated at 37 ºC for 5 days to create the mc^{2}155**::**pMVami2. A single clone was then selected and used for the construction of the Δ*ami2***::**pMVami2

Table 4.1: Bacterial strains created/used in this study

Strain	**Genotype**	**Reference**
mc^{2}155	High frequency transformation mutant of *M. smegmatis* ATCC 607	(Snapper et al., 1990)
Δ*ami1*	Derivative of mc^{2}155 carrying an unmarked, out-of-frame deletion in *ami1*	(Senzani, 2014)
mc^{2}155::pMVami2	Derivative of mc^{2}155 carrying pMVami2 integrated at the bacterial *attB* phage attachment site, Hyg^R	This study
Δ*ami2***::**pMVami2	Derivative of mc^{2}155::pMVami2 carrying an unmarked, out-of frame deletion of *ami2*	This study
*ami2*KDP	Derivative of SRS carrying pSEAmi2P integrated in the upstream promoter region of *ami2* to allow for ATc-regulation, Kan^R, Hyg^R	(Senzani, 2014)
mc^{2}155::pAmi2GFP	Derivative of mc^{2}155 carrying an episomal pSAmi2GFP vector, Hyg^R	This study
mc^{2}155::pMAmi2GFP	Derivative of mc^{2}155 carrying pMAmi2GFP integrated at the *attB* bacterial phage attachment site, Hyg^R	This study
Δ*ami1::*pAmi2GFP	Derivative of Δ*ami1* carrying episomal pAmi2GFP, Hyg^R	This study
mc^{2}155:: pAmi2NFLAG	Derivative of mc^{2}155 carrying an episomal pAmi2NFLAG vector, Hyg^R	This study
mc^{2}155:: pAmi2NFLAG	Derivative of mc^{2}155 carrying an episomal pAmi2NFLAG vector, Hyg^R	This study
mc^{2}155::pFAmi2N	Derivative of mc^{2}155 carrying an episomal pFAmi2N vector, Hyg^R	This study
mc^{2}155::pFAmi2C	Derivative of mc^{2}155 carrying an episomal pFAmi2C vector, Hyg^R	This study

Kan^R: Kanamycin Resistance, Hyg^R: Hygromycin Resistance

4.2.1.2 *Construction of the Δami2::pMVami2 strain*

To construct the p2ΔAmi2G17 vector used to make the Δ*ami2***::**pMVami2 strain, the p2ΔAmi2G19 vector and pGOAL17 were restricted with *Pac*I. The p2ΔAmi2G19 restriction product was then phosphatased using FastAP phosphatase for 30 min. The restriction products were separated on 0.8 % agarose and the respective bands (6754 bp for p2ΔAmi2G19 and 6359 bp for pGOAL17) were excised from the gel and purified using the Nucleospin gel purification kit. These were then quantified using the NanoDrop spectrophotometer and ligations were set up

containing 50 ng of p2ΔAmi2G19 and varying molar ratios of pGOAL17. The fragments were ligated using

Table 4.2: Vectors created and/or used in this study

Vectors	Genotype	Reference
p2NILΔAmi2	Derivative of p2NIL carrying the Δ*ami2* deletion allele, with a 1021 bp internal deletion; Kan^R	This study
p2ΔAmi2G17	Derivative of p2NILΔAmi2 carrying the *lacZ*, *sacB* and *hyg* genes from pGOAL17, Kan^R	This study
pMVAmi2	Derivative of pMV306(H) carrying a functional *ami2* gene and the upstream native promoter region Hyg^R	This study
pAmi2GFP	Derivative of pSE100 carrying the *ami2-rsEGFP* fusion gene downstream the P_{myc}-tet Hyg^R	This study
pAmi2GFPN	Derivative of pMV306(H) carrying a functional *ami2-rsEGFP* gene and the upstream native promoter region Hyg^R	This study
pAmi2NFLAG	Derivative of pFLAGEM carrying a functional *ami2* gene and the upstream native promoter region Hyg^R	This study
pAmi2CFLAG	Derivative of pFLAGEM carrying a functional *ami2* gene and the downstream native promoter region Hyg^R	This study
pFAmi2C	Derivative of pMV306(H) carrying a functional *ami2* gene, upstream the FLAG tag Hyg^R	This study
pSEAmi2P	Derivative of pSE100 carrying the first 350 bp region of the *ami2* gene and the *panC* ribosomal binding site Hyg^R	This study
p2ΔAmi2G19	Derivative of p2NIL carrying the *lacZ*, *sacB* and *hyg* genes from pGOAL19, Kan^R	This study

Kan^R: Kanamycin Resistance, Hyg^R: Hygromycin Resistance, Amp^R: Ampicillin Resistance

Fermentas T4 ligase for 10 min, transformed into DH5α cells and plated LA_{Kan50}. Thereafter, 10 possible clones were selected and screen by restriction with *Eco*RI, which would yield five fragments, a 4988 bp, 3594 bp, 2747 bp, 1863 bp and a 766 bp band. A single positive clone was grown in 50 ml LB_{Kan50} overnight then bulk vector extraction was carried out using the Nucleobond bulk vector extraction kit. Extracted vector DNA was quantified and restricted with a variety of enzymes to profile the *ami2* deletion construct (p2ΔAmi2G17).

Using the p2ΔAmi2G17 vector generated previously, 1, 3 and 5 µg of DNA was electroporated into electrocompetent mc^2155**::**pMVami2 cells and plated on 7H10 containing Kan, Hyg and 0.004 % X-gal, then incubated at 37 ˚C for 7 days to create SCOs. A single blue colony was then

cultured in 2×TY supplemented with Kan and Hyg at 37 ºC; this was then sub-cultured in 2 × TY without antibiotic. The resulting cells were subjected to sucrose counter

Table 4.3: List of primers used in the *M. smegmatis*, *ami2* study

Gene	**primers**	**Amplicon**
*ami2*pMVCF	GCGCGCGCCAGCTGGCCGGTGCTGGTCGATTT	1619 bp *ami2* amplicon including 400 bp upstream the *ami2* start codon
*ami2*pMVCR	GCCGCCGCAAGCTTTCAGGCGCCGCGGCCGGC	
*ami2*KOSCF	CAGGACGCGCTTGGCGTT	*ami2* screening primers which produce either a 429 bp wild type amplicon or a 231 bp Δ*ami2* amplicon
*ami2*KOSCR1	TGCCTGTGAATTCAGGTCAG	
*ami2*KOSCR2	TGTAGAAGCCGAGGTCCTG	
*ami2*RTF	GCTGTACTTCCTCGGCTCAC	qPCR which amply a 112 bp region within the *ami2* ORF
*ami2*RTR	ATCGATGATGACCCGCTTAC	
*ami2*RTR2	AGGATGTCGGCCTCACTGAT	RT-PCR conversion primer
SigARTF	GGGCGTGATGTCCATCTCCT	qPCR which amply a 122 bp region within the *sigA* ORF
SigARTR	GTATCCCGGTGCATGGTC	
*ami2*pFLNF	GCGCGCGGTACCATGTCGAGTCTGCGTCGC	1215 bp *ami2* amplicon excluding the transcriptional stop codon
*ami2*pFLNR	GCCGCCAAGCTTAAAGGTTGCGGTTCAGGG	
*ami2*pFLCF	GCGCGCGGATCCATGTCGAGTCTGCGTCGC	1212 bp *ami2* amplicon excluding the transcriptional stop codon
*ami2*pFLCR	GCCGCCTGTACAGGCGCCGCGGCCGGCCTG	
*ami2*pSELF	GCGCCGCCGCATGCCTGGAGGGGCCCCGTATG	1219 bp *ami2* amplicon excluding the transcriptional stop codon
*ami2*pSELR	GCGCGCGCGAATTCGGCGCCGCGGCCGGCCTG	
*ami2*pSELNF	CGCGCGTCTAGAGCCGGTGCTGGTCGATTT	1616 bp *ami2* amplicon including 400 bp upstream the *ami2* start codon
*ami2*pSELNR	GCGCGCGCGAATTCGGCGCCGCGGCCGGCCTG	
rsEGFPF	CGCGCGGAATTCATGGTGAGCAAGGGCGAGGA	720 bp *rsEGFP* amplicon
rsEGFPR1	GCGCGCCTGCAGAGGAGTCCAAGCTCAGCTAA	
rsEGFPR2	GCGCGCAAGCTTAGGAGTCCAAGCTCAGCTAA	When used in conjunction with rsEGFPF, produces a 720 bp *rsEGFP* amplicon used for cloning in pMV306(H)

*red: restriction endonuclease site

selection by plating 100 µl of a 10-fold serial dilution series onto media containing sucrose, Hyg and X-gal.

The plates were incubated for 3 - 5 days until blue and white colonies emerged. White colonies represent strains, which have undergone the second cross over event at the *ami2* locus to yield either a reversion to wild type or a mutant strain and blue colonies represent strains, which have

incurred a mutation in *sacB* to render them resistant to the toxic effects of sucrose. Subsequently 10 white colonies were selected and PCR screens were conducted on these using the *ami2*KOSCF, *ami2*KOSCR1 and *ami2*KOSCR2 primers, which would yield a 429 bp band in the case of wild type and a 231 bp band for the Δ*ami2***::**pMVami2 strain.

4.2.2 Construction of the Ami2 localisation strains

Localisation of Ami2 was conducted using the rsEGFP fluorescent tag. The approach involved PCR amplification of the rsEGFP tag and the *ami2* gene, with and without the native promoter region. The amplification would be followed by three way cloning of the *ami2* and rsEGFP fragment into pSE100 downstream the Tet operator resulting in a construct wherein the P_{myc}-tet regulates the expression of an amidase gene which contains a C-terminal rsEGFP tag or pMV306(H) in which case expression of the *ami2-rsEGFP* product is regulated by the mycobacterial *ami2* promoter.

Primers were designed, *ami2*pSELF and *ami2*pSELR for *ami2*, *ami2*pSELNF and *ami2*pSELNR for *ami2* containing the native promoter, and rsEGFPF and rsEGFPR1 for the *rsEGFP* tag used cloning into pSE100 and rsEGFPR and rsEGFPR2 for the *rsEGFP* tag used for cloning into pMV306(H) listed in Table 4.3. In the case of the amidase primers, these were designed to amplify a product which does not contain the transcriptional stop codon allowing for the transcription of the C-terminal *rsEGFP* tag. PCR amplification of the respective fragments was carried out using Phusion polymerase, using an annealing temperature of 60 ºC and an elongation time of 1 min to allow for complete amplification of the *ami2* fragment. The PCR products were purified using the Nucleospin PCR purification Kit. Thereafter, pSE100 and the PCR products were then restricted. To create the P_{myc}-tet regulated construct, pSE100 was restricted with *Sph*I and *Pst*I, the *ami2* fragment, without the native promoter, was restricted with *Sph*I and *Eco*RI and the rsEGFP fragment was restricted with *Eco*RI and *Pst*I. The pSE100 was then phosphatased using FastAP phosphatase for 10 min. The restriction products were separated on a 0.8 % agarose gel and the respective bands (5498 bp for pSE100, 1194 bp for *ami2* and 698 bp for *rsEGFP*) were then cut from the gel and purified using the Nucleospin gel purification kit. Thereafter, these were quantified using the NanoDrop spectrophotometer and ligations were set up containing 50 ng of pSE100 and varying molar ratios of *ami2* and *rsEGFP* fragment. The fragments were ligated using

Fermentas T4 ligase for 10 min, transformed into DH5α cells and plated on LA_{Hyg200}. Ten possible clones were selected and screened by restriction with *Eco*RI, which would yield four fragments, a 2857 bp, 2306 bp, 1538 bp and a 760 bp band. A single positive clone (pAmi2GFP) was grown in 50 ml LB_{Hyg200} overnight then bulk vector extraction was carried out using the Nucleobond bulk vector extraction kit. Extracted DNA was quantified and restricted with a variety of enzymes to profile the rsEGFP tagged amidase construct. The second construct, which contains a *ami2-rsEGFP* fusion regulated by the mycobacterial *ami2* promoter, was created using pMV306(H). For this, pMV306(H) was restricted with *Xba*I and *Hind*III, the *ami2* fragment, containing the native promoter, was restricted with *Xba*I and *Eco*RI and the rsEGFP fragment was restricted with *Hind*III and *Eco*RI. The restricted pMV306(H) vector was then phosphatased using FastAP phosphatase for 10 min. The restriction products were separated on a 0.8 % agarose gel and the respective bands (4238 bp for pMV306(H), 1611 bp for *ami2* and 673 bp for *rsEGFP*) were then cut from the gel and purified using the Nucleospin gel purification kit. Thereafter, these were quantified using the NanoDrop spectrophotometer and ligations were set up containing 50 ng of pMV306(H) and varying molar ratios of *ami2* and rsEGFP fragment. The fragments were ligated using Fermentas T4 ligase for 10 min, transformed into DH5α cells and plates on LA_{Hyg200}. Ten possible clones were selected and screened by restriction with *Eco*RI, which would yield two fragments, a 3577 bp, and a 2981 bp band. A single positive clone (pAmi2GFPN) was grown in 50 ml LB_{Hyg200} overnight then bulk vector extraction was carried out using the Nucleobond bulk vector extraction kit. Extracted vector DNA was quantified and restricted with a variety of enzymes to profile the rsEGFP tagged amidase construct. The vectors were also sent for sequencing to check for mutations which might have occurred during PCR amplification process (data not shown). Finally, 1 µg of the pAmi2GFP construct was then electroporated into electrocompetent mc^2155 and Δ*ami1* cells, plated on $7H10_{Hyg50}$ and incubated at 37 ºC for five days to create the mc^2155::pAmi2GFP and Δ*ami1*::pAmi2GFP. Clones were selected; colony boil was conducted followed by PCR screening using the *ami2*pSELF and the rsEGFPR primers to determine whether clones possessed the full length *ami2-rsEGFP* fusion fragment. PCR products were separated on a 0.8 % agarose gel. The pAmi2GFPN construct was electroporated into electrocompetent mc^2155, screened as stated above then the native *ami2* allele was deleted as in section 4.2.1.2.

4.2.3 Construction of Ami2-FLAG tagged strains

Primers were designed, *ami2*pFLNF, *ami2*pFLNR, *ami2*pFLCF and *ami2*pFLCR listed in Table 4.3, to amplify the *ami2* gene. PCR amplification of the respective fragments was carried out using Phusion polymerase, using an annealing temperature of 60 °C for *ami2* and an elongation time of 1 min to allow for complete amplification of the *ami2* fragments, which were 1215 bp and 1212 bp. The PCR products were purified using the Nucleospin PCR purification Kit. Following this, 3 µg of pFLAGEM was restricted with *Hind*III and *Kpn*I for the Ami2 *N*-terminal FLAG tagged construct and *Bam*HI and *Bsr*GI for the Ami2 C-terminal FLAG-tagged construct. The PCR products were then restricted with *Hind*III and *Kpn*I for the, *ami2*pFLNF and *ami2*pFLNR product and *Bam*HI and *Bsr*GI for the *ami2*pFLCF and *ami2*pFLCR product respectively. The pFLAGEM restriction products were then phosphatased using FastAP phosphatase for 30 min. The restriction products were separated on a 0.8 % agarose gel and the respective bands (5602 bp and 5591 bp pFLAGEM fragments for N and C terminal tagging, respectively and 1197 bp and 1194 bp *ami2* fragments for N and C terminal tagging, respectively) were excised from the gel and purified using the Nucleospin gel purification kit. These were then quantified using the NanoDrop and ligations were set up containing 50 ng of pFLAGEM and varying molar ratios of *ami2*. The fragments were ligated using Fermentas T4 ligase for 1 h, transformed into DH5α cells and plated on LA_{Hyg200}. Thereafter, possible clones were selected and screened by restriction with *Eco*RI, which would yield two fragments, a 4523 bp and a 2306 bp for the N-terminal tag construct and 4479 bp and 2306 bp for the C-terminal tag construct. A single positive clone, per vector, was grown in 50 ml LB_{Hyg200} overnight then bulk vector extraction was carried out using the Nucleobond bulk vector extraction kit. Extracted vector DNA was quantified and restricted with a variety of enzymes to profile the *ami2* FLAG tagged constructs (pAmi2NFLAG and pAmi2CFLAG) and the vector was sent for sequencing to check for the presence of mutations within the amplicon. After sequence confirmation, 1 µg of the pAmi2NFLAG and pAmi2CFLAG constructs were electroporated into electrocompetent mc^2155 cells, plated on $7H10_{Hyg50}$ and incubated at 37 ºC for five days to create the mc^2155:: pAmi2NFLAG and mc^2155:: pAmi2CFLAG. A single hyg resistant colony per strain was selected and used for cell wall fractionation studies.

4.2.4 Mycobacterial cell fractionation

The mycobacterial cell was fractionated into the cell wall, cell membrane and cytoplasmic fraction using a protocol by Rezwan et al., 2007. Mycobacterial cultures were grown to OD_{600nm} = 0.8 in a 50 ml volume. Cultures were centrifuged at 3500 × g for 10 min. The supernatant was discarded and pellet was resuspended in lysis buffer (0.05 M potassium phosphate, 0.022 % mercaptoethanol, pH 6.5). The cells were sonicated three times for 20 min then centrifuged at 1000 × g for 10 min to remove unbroken cells. The lysate was then centrifuged at 27000 × g, 5 times for 40 min. The supernatant and pellet were separated and the supernatant was stored at 4 °C for future use. The pellet was sonicated once and centrifuged at 27000 × g for 40 min, and then the resulting supernatant was pooled with the stored supernatant. The pellet, which is the PG fraction, was stored at 4 °C. The supernatant was centrifuged at 100 000 × g for 1 h and the pellet (cell membrane) and supernatant (cytoplasm) were separated and stored at 4 °C (Rezwan et al., 2007).

4.2.5 Acrylamide gel electrophoresis

Acrylamide gel electrophoresis was conducted using acrylamide gels made using the TGX stain free fastcast acrylamide Kit (Bio-Rad laboratories) as per the manufacture's instruction. Various proteins samples were prepared by mixing with equal volume 2 × loading buffer (0.1 M Tris-HCl pH 6.8, 4 % SDS, 20 % glycerol [v/v], 25 % β-mercaptoethanol [v/v] and 0.05 % bromophenol blue) and incubated at 95 ˚C for 2 min prior to loading. Electrophoresis was carried out in resolving buffer (Appendix B) at 80 – 100 V for 2 h in Mini protean tetra cell tanks (Bio-Rab laboratories). PageRuler Plus prestained protein ladder (Thermo fisher) was separated on the same gel to indicate the molecular weight of the samples examined. To visualise proteins, gels were stained with Coomasie blue overnight, shaking at room temperature subsequently destained until protein bands became visible.

4.2.6 Western blot analysis

Proteins samples were separated on an acrylamide gel at 80 V for 2 to 4 h. The gel was then washed in transfer buffer (Appendix B). This was then overlaid with polyvinylidene fluoride (PVDF) membrane, sandwiched between four Whatman filter papers and six sponges, then pre-soaked in transfer buffer. The sandwich was carefully placed in a gel cassette (Bio-Rad Laboratories) and transferred to an SB10 tank (Bio-Rad Laboratories) containing transfer buffer. Samples were transferred to the PVDF membrane at 400 mA for 2 h. The membrane was incubated in blocking

solution containing 2 % skim milk for 30 min at room temperature. Thereafter, the membrane was incubated in 20 ml of primary antibody solution (20 ml 1 × blocking solution and 10 µg/ml ANTI-FLAG M2 monoclonal antibody [Sigma]) for 30 min with gentle agitation at room temperature, followed by rinsing three times for 5 min in TBST (Appendix B). The membrane was incubated in 20 ml of secondary antibody solution (1:25 000 dilution of Rabbit Anti-Mouse IgG, Peroxidase Conjugate [Sigma] in 20 blocking solution) for 1 h with gentle agitation at room temperature, followed by five washes for 5 min in TBST (Appendix B). The membrane was placed in a hybridisation bag and 1 ml chemiluminescent peroxidase substrate (CPS) was aliquoted onto the membrane and incubated at room temperature for 10 min, the excess CPS was then removed, the hybridisation bag was sealed. The membrane was exposed to X-ray film (Kodak Biomax Light or CL-Xposure™ Film-Thermo Scientific) for 30 seconds to 5 min, to attain the desired band intensity and the film was developed using an automated Axim developer.

Figure 4.3 illustrates the basic outline of the research undertaken in this chapter, with reference to the specific methods.

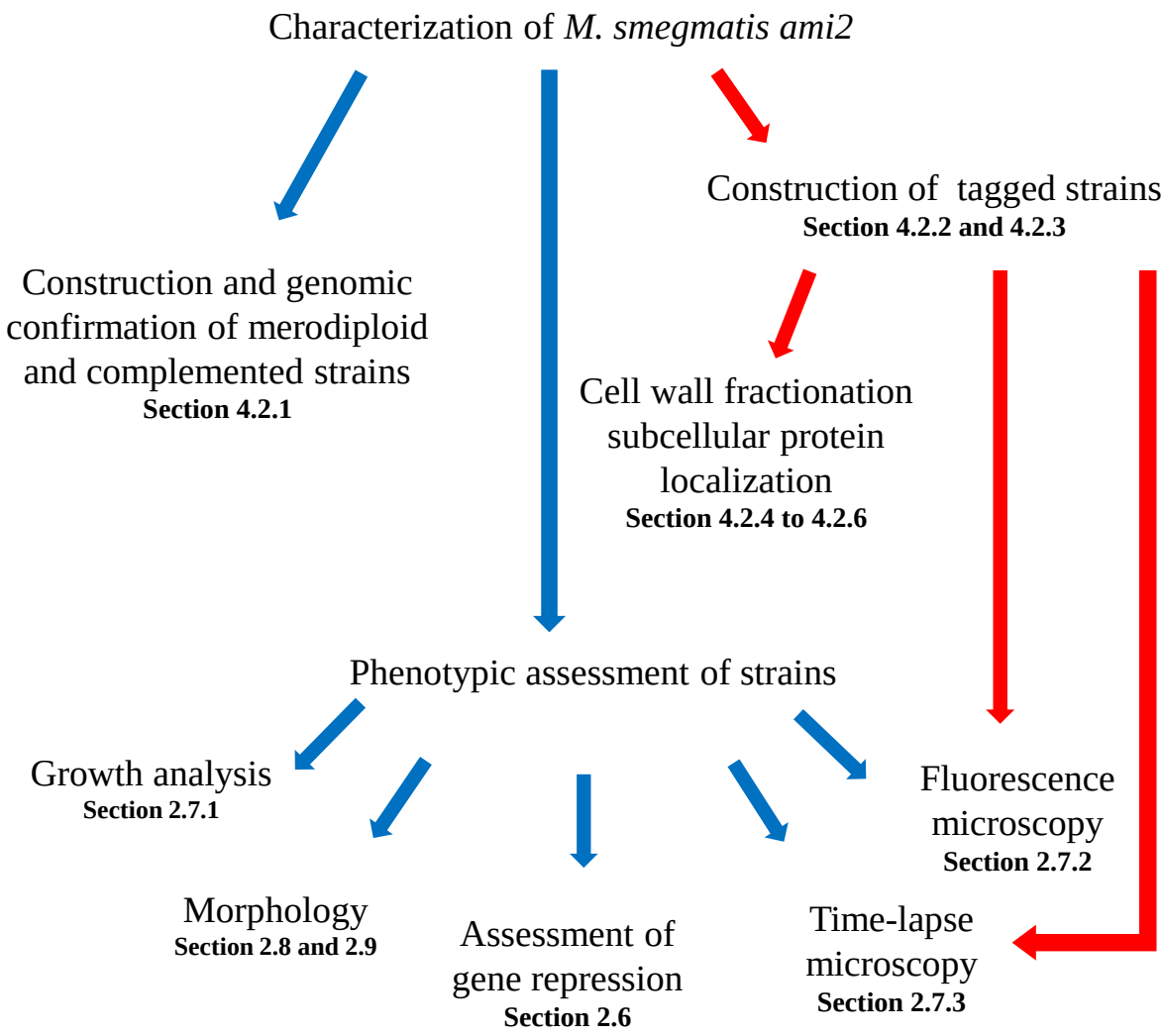

Figure 4.3: Flow chart depicting the experimental layout for the *M. smegmatis ami2* research.

4.3 Results

4.3.1 Demonstrating the essentiality of *ami2*

Numerous attempts to delete *ami2* proved unsuccessful (data not shown, Senzani, 2014) and considering this, we hypothesised that it was essential for *M. smegmatis* growth. Consistent with this, was the prediction that the Mtb counterpart was predicted to be essential by saturating transposon mutagenesis (Griffin et al., 2011, Sassetti and Rubin, 2003). To demonstrate this, a merodiploid strain was constructed, that carried two copies of *ami2* and we attempted to delete the gene in this background. This involved the construction of an SCO in a strain containing two copies of Ami2 followed by the subsequent deletion of the native allele (Appendix D, Figure D6).

4.3.1.1 *Construction of the mc^{2}155::pMVami2 strain*

PCR amplification was conducted to amplify the *ami2* gene and 400 bp upstream the transcriptional start codon. The fragments were then cloned into pMV306 (H) and clones were screened by restriction digest with *Bam*HI. A single positive clone was then selected and the genetic integrity of the construct was confirmed by extensive restriction profiling, shown in Figure 4.4. In all cases, the fragment sizes observed corresponded to the vector map and expected sizes, confirming the genetic integrity of the vector. The genetic integrity of the vector was then further confirmed by sequencing of the cloned region, which revealed that no mutations had occurred during PCR and cloning processes (data not shown). This vector was then used for construction of the mc^{2}155**::**pMVami2 strain. For this, the vector was electroporated into the mc^{2}155 strain (section 2.4.2); the transformation efficiency obtained from the electro-competent cells was 7.2×10^3 CFU/µg vector DNA (determined using the pSE100 control vector). A single hyg resistant clone was then selected and used for the construction of the Δ*ami2***::**pMVami2 strain.

4.3.1.2 *Construction and screening of the* Δ*ami2::*pMVami2 *strain*

The pGOAL17 cassette and *ami2* p2NIL deletion fragments were excised from pGOAL17 and p2ΔAmi2G19 vectors respectively, then cloned together to create the p2ΔAmi2G17 vector. The smaller *Pac*I cassette, without the hyg gene, was required so that *hyg* could be used as a selectable marker for the merodiploid copy. The resulting clones were screened using *Eco*RI and a single positive clone was then selected and the genetic integrity was confirmed by extensive restriction profiling, shown in Figure 4.5.

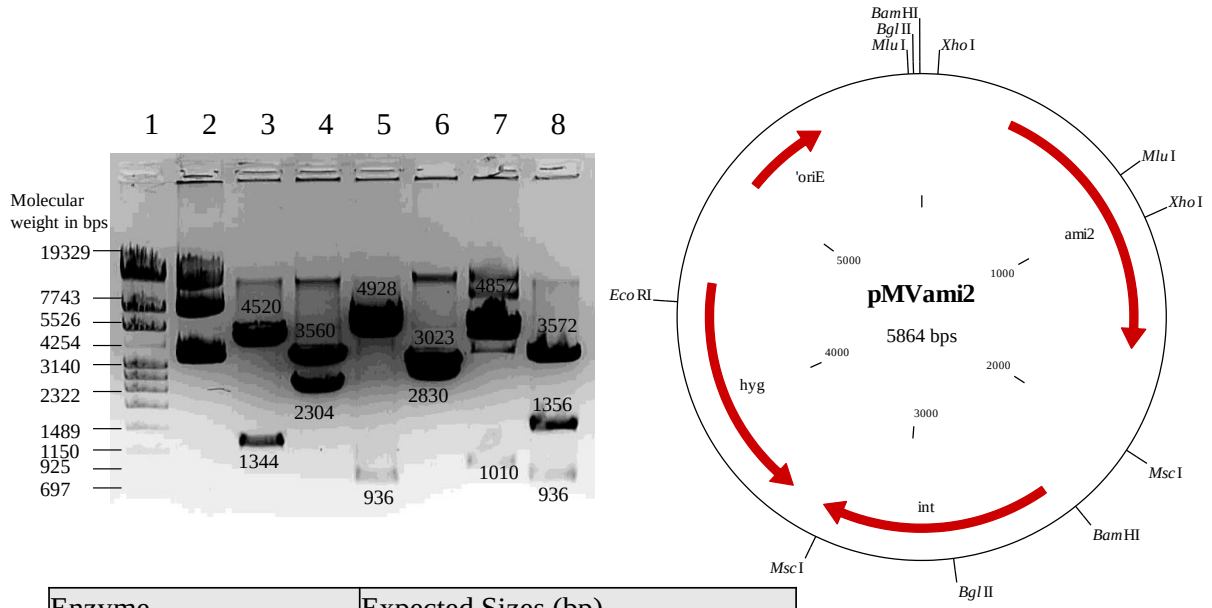

Enzyme	Expected Sizes (bp)
*Msc*I	4520, 1344
*Bam*HI	3560, 2304
*Mlu*I	4928, 936
*Bgl*II	3023, 2841
*Xho*I	4854, 1010
*Mlu*I and *Eco*RI	3572, 1356, 936

Figure 4.4: Restriction profile of pMVami2. Shown are the different restriction nucleases used and the expected sizes in a table, which result from restriction digests of the pMVami2 vector. The predicted vector map of the pMVami2 vector and agarose gel depicting the products of restriction digest of pMVami2 are also shown. Lane 1: Roche Marker IV, Lane 2: Uncut, Lane 3: *Msc*I, Lane 4: *Bam*HI, Lane 5: *Mlu*I, Lane 6: *Bgl*II, Lane 7: *Xho*I, Lane 8: *Mlu*I and *Eco*RI.

All the observed sizes were as expected with the exception of the *Eco*RI, 766 bp band which was smaller than expected. As the homologous regions were sequenced, with no mutations detected (data not shown), we expect that this difference was related to a restriction site in the vector. The p2ΔAmi2G17 knockout vector was electroporated into the mc^{2}155::pMVami2 strain (section 2.4.2); the transformation efficiency obtained for the electro-competent cells was 9.2×10^4 CFU/µg vector DNA determined using the pSE100 control. A single blue clone (SCO strain) was cultured and subjected to sucrose counter selection (section 4.2.3). White colonies were then screened by PCR to identify clones which possess only the deleted allele, and then southern blot analysis was conducted to confirm the second homologous event removed the wild type allele without imposing additional unintended chromosome rearrangements, Figure 4.6.

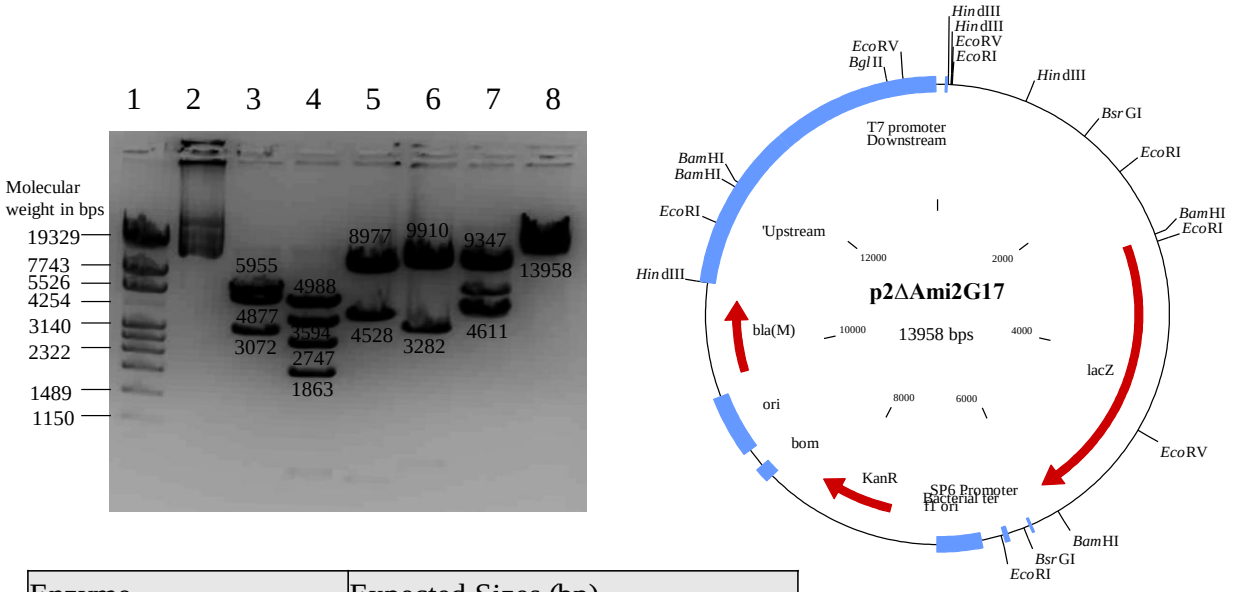

Enzyme	Expected Sizes (bp)
*Bam*HI	5955, 4877, 3072, 54
*Eco*RI	4988, 3594, 2747, 1863, 766
*Eco*RV	8977, 4528, 453
*Hind*III	9910, 3282, 739, 27
*Bsr*GI	9347, 4611
*Bgl*II	13958

Figure 4.5: Restriction profile of p2ΔAmi2G17. Shown are the different restriction nucleases used and the expected sizes in a table, which result from restriction digests of the p2ΔAmi2G17 vector. The predicted vector map of the p2ΔAmi2G17 vector and agarose gel depicting the products of restriction digest of p2ΔAmi2G17 are also given. Lane 1: Roche Marker IV, Lane 2: Uncut, Lane 3: *Bam*HI, Lane 4: *Eco*RI, Lane 5: *Eco*RV, Lane 6: *Hind*III, Lane 7: *Bsr*GI, Lane 8: *Bgl*II. Fragments below 1000 bp were difficult to visualise.

Southern blot analysis using the restriction enzyme *Pvu*II was conducted on the mc^{2}155, the SCO strain and the Δ*ami2*::pMVami2 strains, which would yield 4386 bp for mc^{2}155::pMVami2 and 3364 bp for the Δ*ami2*::pMVami2 strain. All the expected sizes were observed, confirming the genetic integrity of the merodiploid knockout. These results confirmed that *ami2* is essential as a mutant was only obtained in the presence of a second copy of the gene.

4.3.2 Ami2 is essential for bacterial cell elongation

Preliminary work conducted in *M. smegmatis* pointed to a possible role for Ami2 in cell elongation, as shown by the presence of short cells and cells with polar bulges when Ami2 was depleted (Appendix D, Figure D7) (Senzani, 2014). Additionally, defects in sliding motility and colony morphology were observed further indicating a possible role during cell growth (Appendix D, Figure D8).

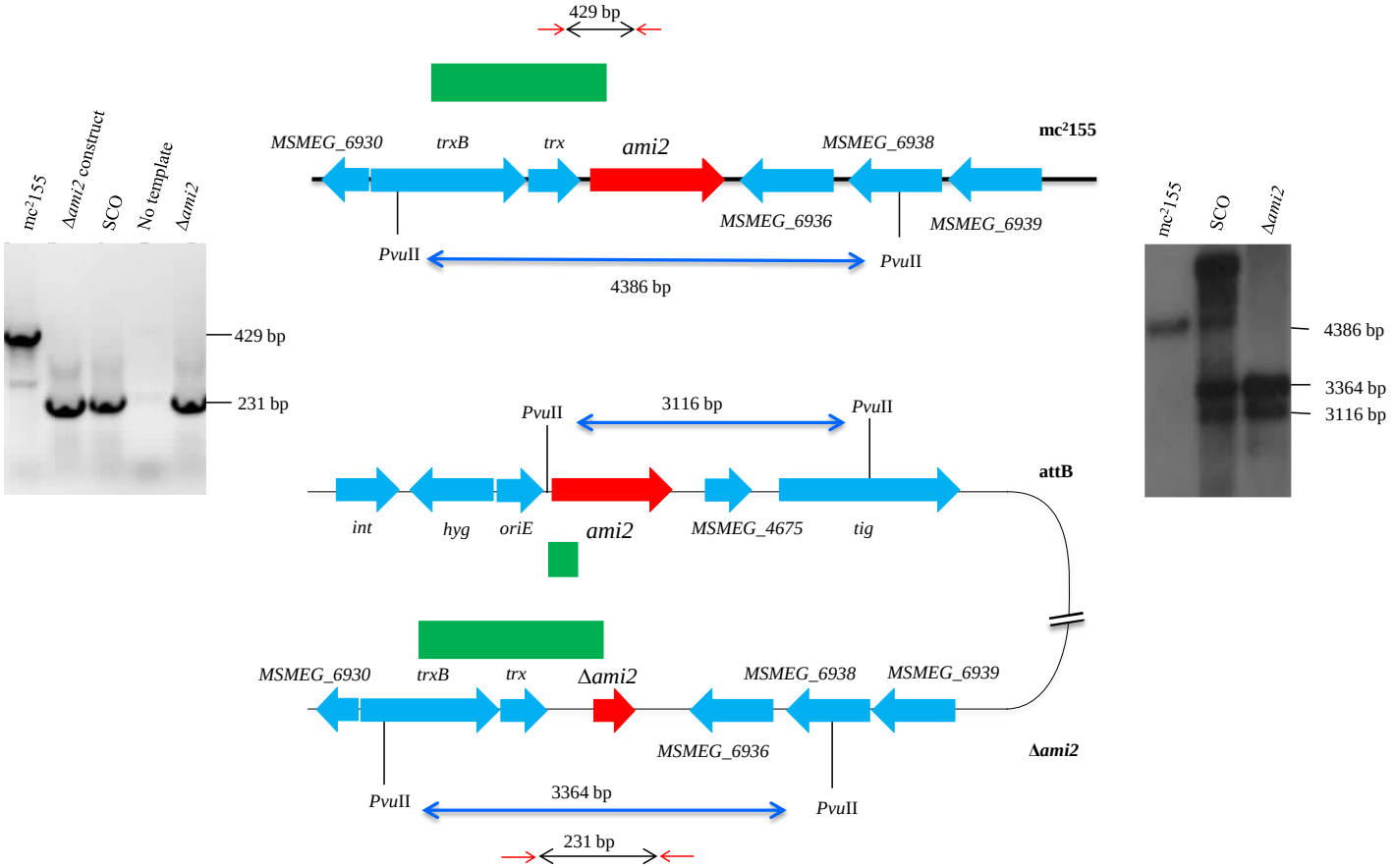

Figure 4.6: Genotypic analysis of the Δ*ami2*::pMVami2 strain by PCR and Southern blot analysis. The genomic map of the relevant locus is shown for the wild type mc^{2}155 and Δ*ami2*::pMVami2 strain which also depict the integration of a functional *ami2* gene at the attB site. Also shown on the left is the PCR confirmation of the genotype and southern blotting is shown on the right. For PCR confirmation, chromosomal DNA was used to amplify the *ami2* alleles from the wild type and mutant strains using the primer pairs described in Table 3 and indicated as red arrows above. The expected sizes of the amplicons are as follows: *ami1*, 429 bp and Δ*ami1*, 231 bp. For the Southern blot analysis, chromosomal DNA from the SCO, parental and mutant strain was digested with *Pvu*II. The probe used for hybridisation is shown as a solid green box and the expected sizes are indicated by the blue arrows. The figures are not drawn to scale.

To confirm this, an in-depth analysis was conducted to assess the effects of *ami2* depletion. The *ami2* depletion strain (ami2KDP), previously created by promoter replacement of the native *ami2* promoter with the P_{myc}-tet operator, Figure 4.7, was used to assess the essentiality of *ami2*. In this case, *ami2* gene expression is under the control of the P_{myc}-tet operator such that addition of the inducer, anhydrotetracycline (ATc), allows for gene expression. In the absence of ATc, the *ami2* gene expression is repressed. Using this system, we tested the essentiality of *ami2* by growing the *ami2*KDP strain in the presence of various concentrations of the inducer, Figure 4.7. This analysis demonstrated a retarded growth rate in cultures containing no or low ATc concentrations (0 ng/ml and 0.001 ng/ml). Bacterial growth rates increased in the presence of higher concentrations of ATc. However, early growth rates never reached the level of mc^2155 and all strains eventually plateaued at the same density in stationary phase.

To determine whether the changes in growth rate corresponded to the expression levels of *ami2,* transcriptional analysis was conducted 6, 12 and 18 h post initiation of the growth curve, Figure 4.7. In the absence of inducer, we were able to achieve a 40 % reduction in *ami2* transcript levels when compared to wild type, Figure 4.7B. This expression increased moderately in the presence of 0.001 ng/ml of ATc and was restored to levels similar to that of the wild type in the presence of 0.05 ng/ml ATc. Addition of higher levels of ATc, at 1 ng/ml and 50 ng/ml, resulted in moderate overexpression with *ami2* mRNA peaking at levels 3-fold higher than that of mc^2155. Analysis of *ami2* expression levels 18 h post induction revealed an overall reduction in the expression of *ami2*, with the higher ATc concentrations displaying expression levels similar to that of mc^2155, suggesting possible ATc degradation over time.

Thus far, we were able to demonstrate that in the *ami2*KDP strain, repression of *ami2* led to a ca. 40 % reduction in gene expression, which was associated with retardation of growth. To further assess the impact of *ami2* depletion in bacterial physiology, high resolution SEM was conducted on samples taken 12 h post induction, as the greatest difference with regards to bacterial growth was noted at this time point. SEM was conducted on mc^2155, the *ami2*KDP strain grown with 0 ng/ml and 0.05 ng/ml ATc. Bacterial length was also measured to determine whether *ami2* depletion affected the overall bacterial size, Figure 4.8 and Figure 4.9. From the ~ 400 cells analysed per sample, 13 % of the *ami2*-depleted population were shorter than 3 µm, while only

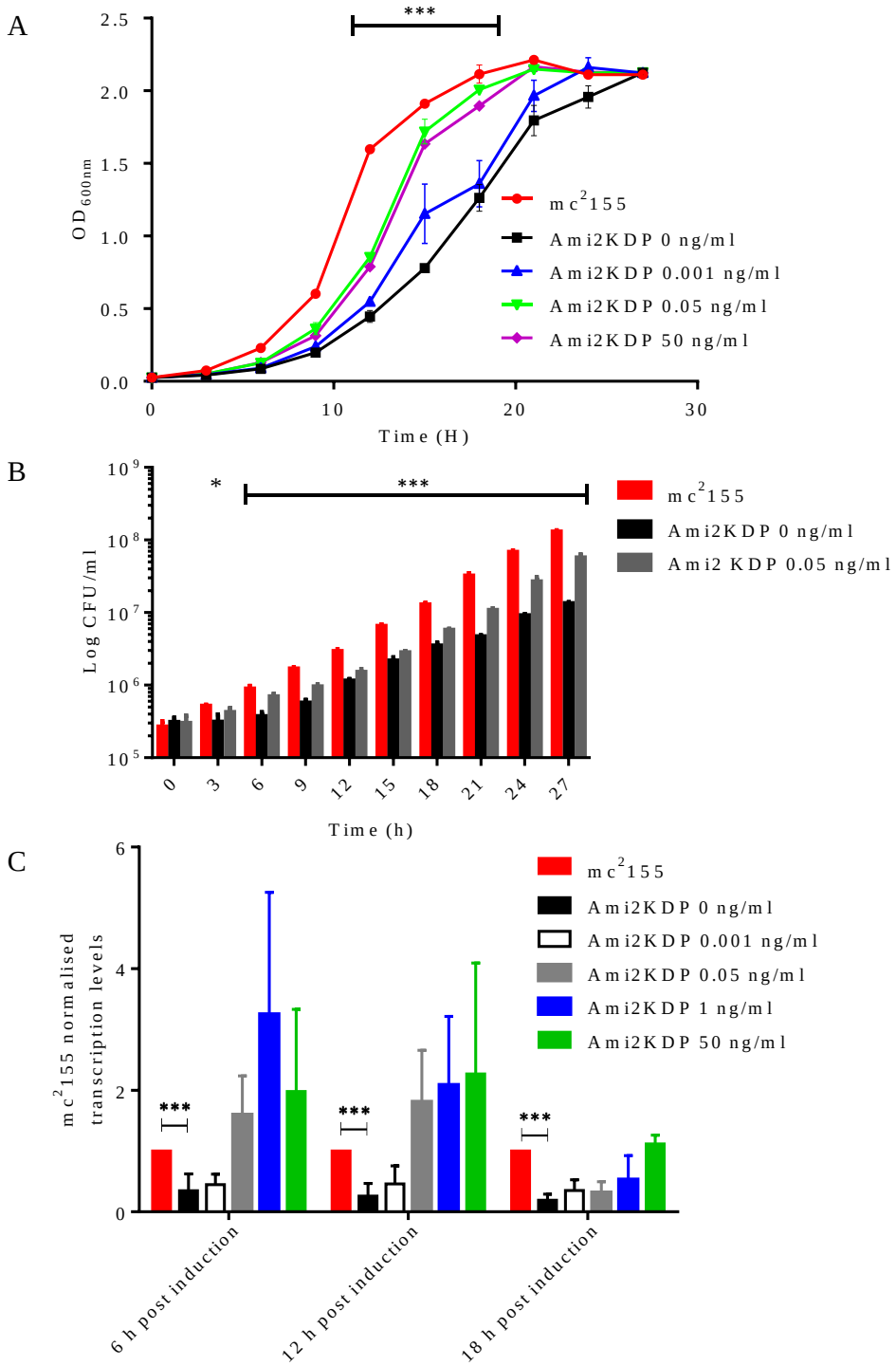

Figure 4.7: Growth analysis of mc²155 and *ami2*KDP strains. (A) Growth kinetics analysis of mc²155 and *ami2*KDP strains at different ATc concentrations establish varying levels of *ami2* expression. (B) shows the CFU/ml counts from the mc²155 and the Ami2KDP cultures containing 0 ng/ml and 0.05 ng/ml ATc. (C) shows the transcriptional analysis of samples taken at different time points from the growth kinetics analysis depicting the impact of different ATc concentrations on *ami2* transcript abundance. Shown are the *ami2* transcript levels first normalised to *sigA* (to account for differences in RNA between reactions) and subsequently normalised to levels found in the wild type strain. The data represents three biological replicates Statistical analysis was conducted using the student's *t*-test, ***: $p < 0.001$

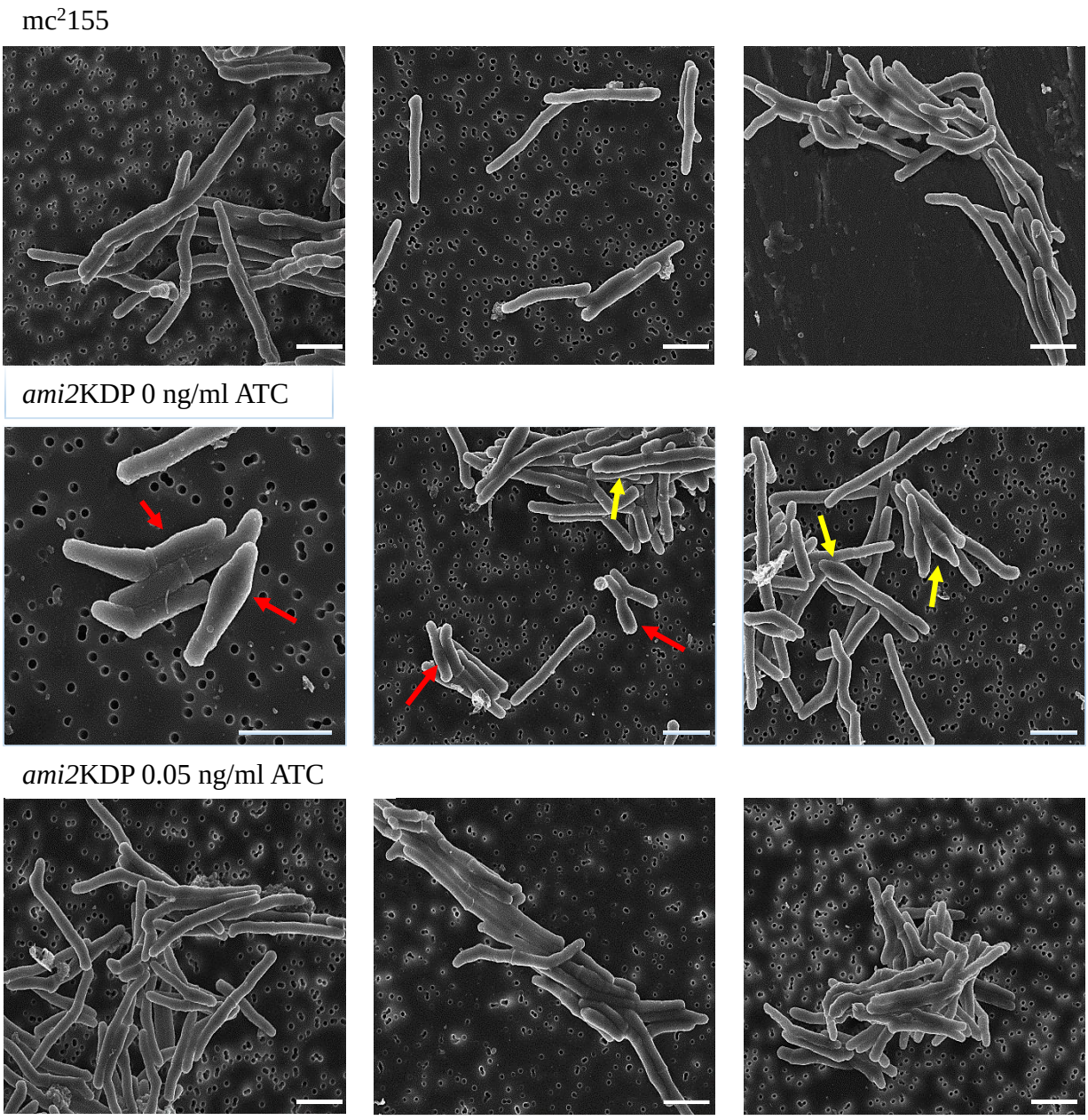

Figure 4.8: Microscopic analysis of the mc²155 and *ami2*KDP strains. Shown are SEM images of the mc²155, *ami2*KDP strain grown in the presence of 0 ng/ml and 0.05 ng/ml ATc. Samples were taken from the growth kinetics analysis at time point 12 h, then fixed, dehydrated, carbon coated and imaged using high resolution SEM. Red arrow depict cells shorter than 3 µm and yellow arrows indicated polar cell bulges. Data are representative pictures from three independent experiments.

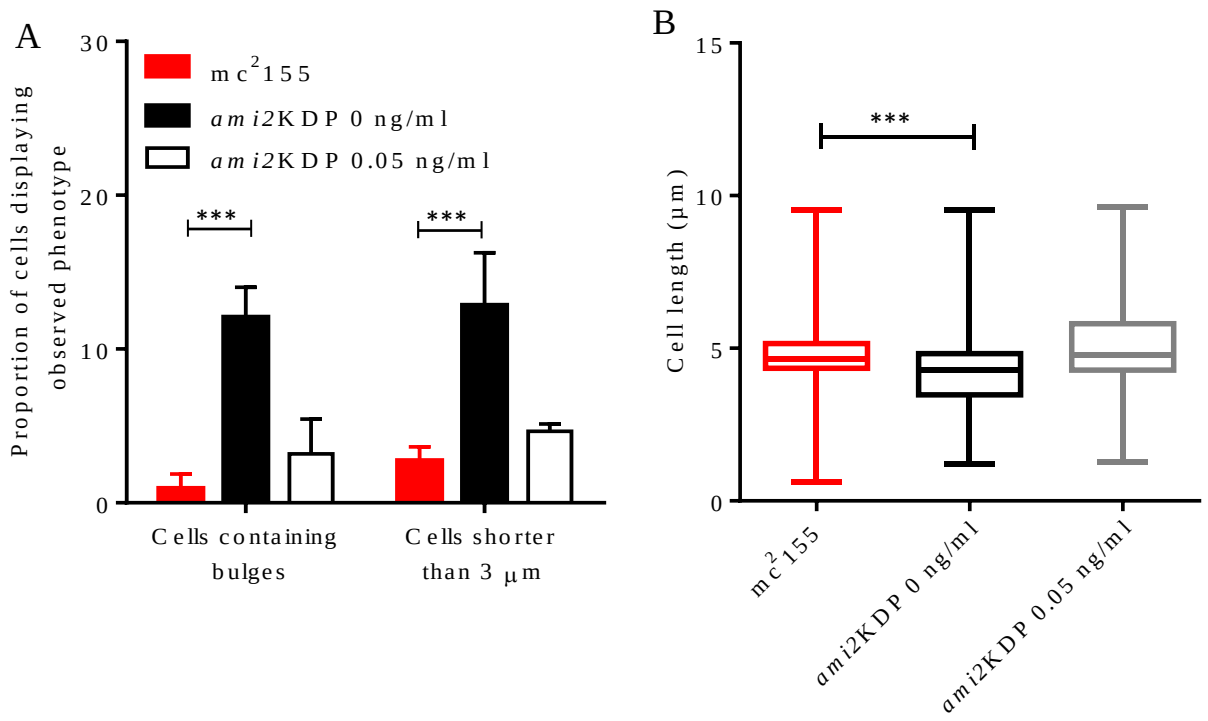

Figure 4.9: Statistical analysis of the defects associated with repression of *ami2*. (A) Bar graph showing the quantification of the various Ami2-associated phenotypic defects. Displayed are the two distinctive phenotypes which emerged as a result of *ami2* depletion and the proportions in which they were observed in the mc^{2}155, *ami2*KDP strains growth with 0 ng/ml and 0.05 ng/ml ATc. (B) Box-and-whisker analysis of the mc^{2}155, *ami2*KDP strains grown with 0 ng/ml and 0.05 ng/ml ATc, comparing the variation in cell length. The analysis demonstrated a change in the distribution of cell length in the in the presence of diminished Ami2. Graphs were generated using 3 biological replicates, counting a total of approximately 400 cells per strain, p-values were attained using the student's *t* – test. ***: $p < 0.001$.

2.7 % and 4.6 % of the mc^{2}155 and *ami2*KDP, grown with 0.05 ng/ml ATc, populations displayed this phenotype, respectively. Additionally, repression of *ami2* gave rise to cells with a bulge at a single pole, 12 % of the *ami2* depleted population contained a bulge at a single pole, while only 0.9 % and 3.1 % of the mc^{2}155 and *ami2*KDP, grown with 0.05 ng/ml ATc, populations displayed this phenotype, respectively. Further analysis of bacterial cell length revealed the *ami2* depleted strain was shorter than the mc^{2}155 and *ami2*KDP, grown with 0.05 ng/ml ATc, counterparts. The *ami2* depleted population displayed cells lengths of between 1.2 µm to 9.5 µm with a mean and median of 4.22 µm and 4.31 µm respectively. The mc^{2}155 and *ami2*KDP, grown with 0.05 ng/ml ATc, populations both fell within a cell length range of 2.1 µm to 9.5 µm with a mean and median of 5.01 µm and 4.66 µm for the mc^{2}155 population and 5.12 µm and 4.77 µm for the Δ*ami1*::pSEami1 population, Figure 4.9.

As Ami2 has been shown to initiate PG synthesis through the activation of MurA (Boutte et al., 2017), samples were taken from log phase *ami2*KDP log phase cultures containing no ATc and BODIPY-vanc staining was conducted to determine whether PG synthesis continued to occur primarily at the poles when *ami2* was depleted (Figure 4.10).

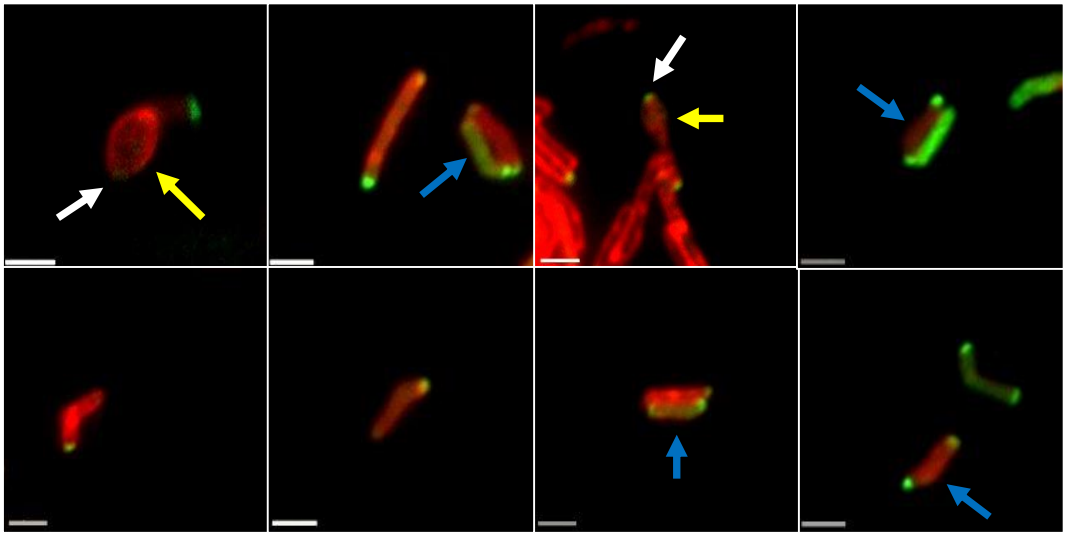

Figure 4.10: Microscopic analysis of the fluorescent BODIPY-Vanc (green) and FM4-64 (red) stained depleted *ami2*KDP cells depicting polar staining of both bulged and miniature cells. White arrows indicate polar BODIPY-Vanc staining, yellow arrows indicate polar bulges and blue arrows indicate miniature cells. The images are representatives of biological replicates. Scale = 2 µm.

As Shown by figure 4.10 both miniature and bulged cells retained polar vancomycin staining, indicating PG synthesis, under conditions of depleted *ami2*, continued to occur at the cell poles.

4.3.3 Single-cell analysis of the effects of *ami2* gene depletion.

Though growth was retarded when *ami2* was repressed, the bacterial culture was able to grow to a significant biomass in stationary phase. This suggested that mutants that escaped ATc regulation may have arisen during growth. To further assess the effects of *ami2* gene repression, we conducted single-cell time-lapse microscopy to assess individual micro-colonies. The individual bacteria imaged, was incubated in the presence of ATc resulting in growth. However, removal of the inducer, ATc, resulted in stalled growth and apperant death, depicted by the loss of membrane staining, Figure 4.11, Appendix E, movies 4.1 to 4.3. These observations illustrated that repression of *ami2* led to cessation of growth and most likely, death of cells. We observed this effect in 37/59 micro- colonies assessed. In 22/59 micro-colonies, we noted that bacteria continued to grow, suggesting that these cells represented escape mutants.

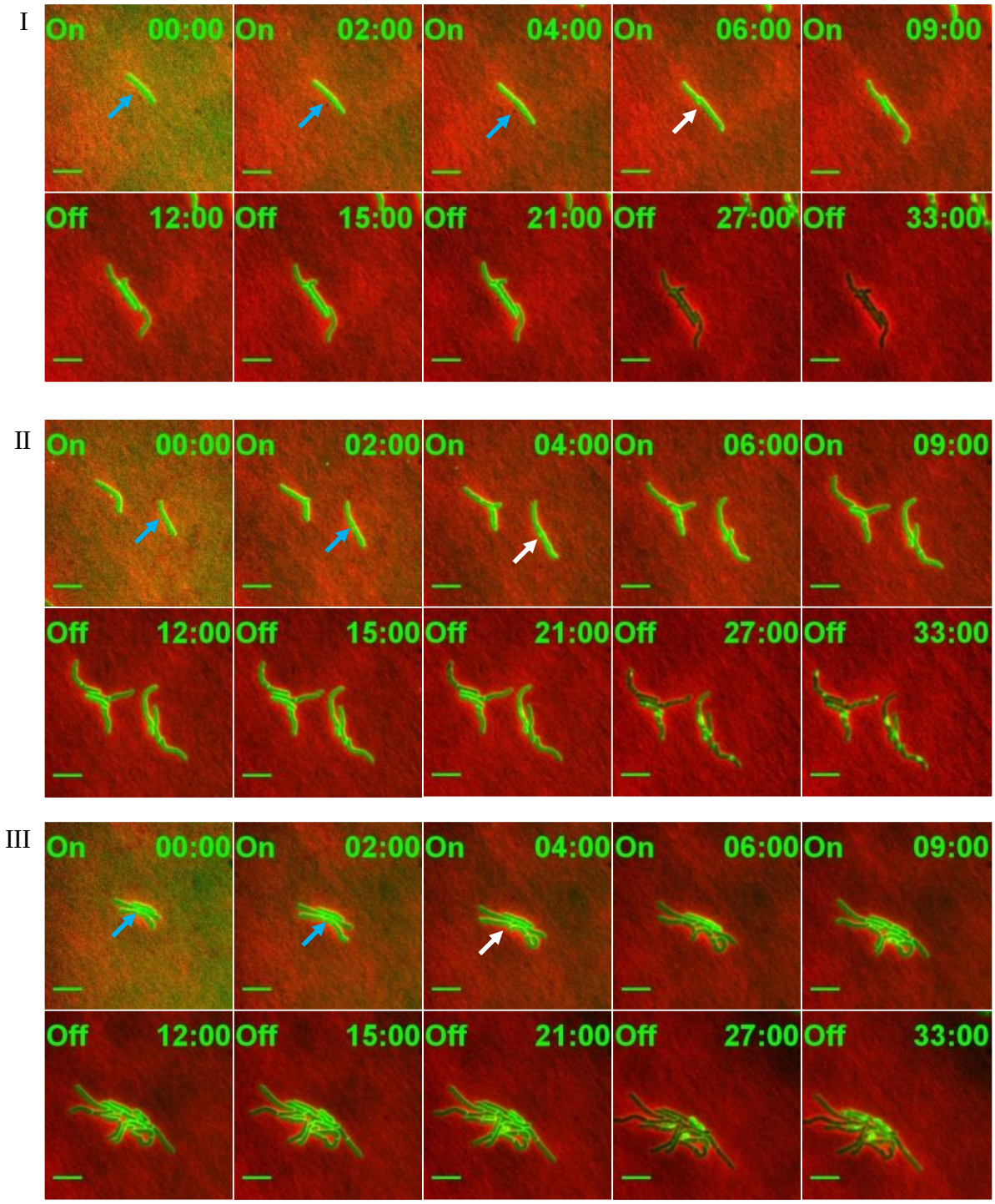

Figure 4.11: Time lapse microscopic analysis showing the effects of *ami2* depletion in *M. smegmatis*. Shown in panel I to III are Cells initially grown on the presence of ATc (On) for 12 h resulting in bacterial growth and cell division depicted by the blue and white arrows, respectively (slides 1-5), followed by removal of the inducer (Off) resulting in an immediate stall in bacterial growth and loss of membrane stain in the *M. smegmatis ami2*KDP strain (slide 6 – 10). Green stain is FM4-64 which stain the bacterial cell membrane (green bar = 5 µm)

To further test this, growth curve analysis was conducted on mc^{2}155 and the *ami2*KDP strain in the absence of ATc, where cells were allowed to reach stationary phase then a sample of the stationary phase culture, that was repressed from initation of growth, was used to start a secondary growth curve. This analysis showed similar retarded growth patterns upon a second round of *ami2* gene repression, suggesting that escape, whilst a notable phenomenon, did not distort the readout of *ami2* essentiality in broth culture, Figure 4.12. The lower growth rate observed with the *ami2*KDP strain in the absence of inducer, instead of complete cessation of growth, may have been due to the ability to repress *ami2* further at a transcriptional level.

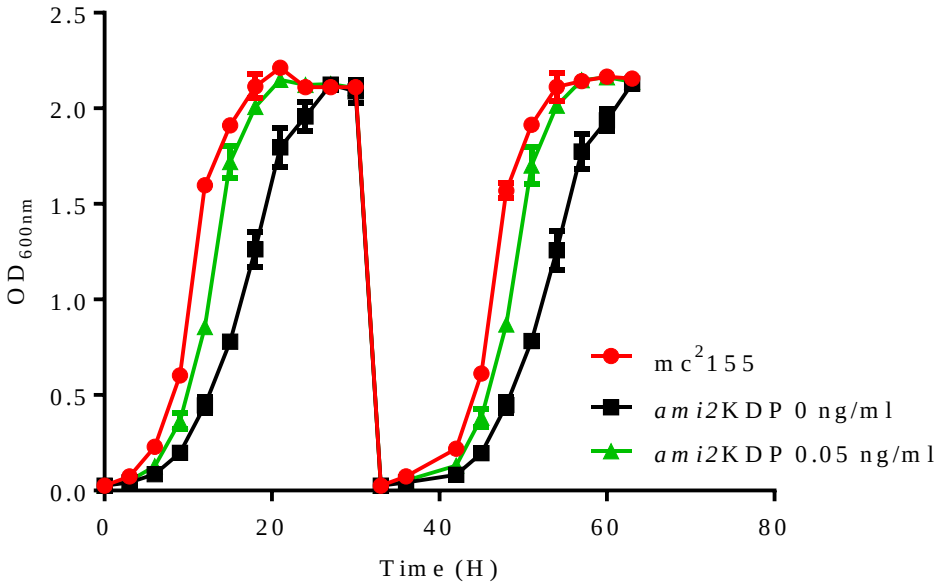

Figure 4.12: Growth analysis of mc^{2}155 and *ami2*KDP strains. Shown is the growth kinetics analysis of mc^{2}155 and *ami2*KDP growth with 0 ng/ml and 0.05 ng/ml ATc. The first phase was conducted as per the previous growth curve then a sample from the 0 ng/ml ATc *ami2*KDP population was used as a pre-culture to inoculate the 0 ng/ml and 0.05 ng/ml cultures in the second phase. Both growth phases displayed a similar growth pattern suggesting the growth of the ami2KDP strain was a result of residual *ami2* expression, rather than the emergence of large numbers of escape mutants. The graphs are a representation of three biological replicates.

4.3.4 Localisation of mycobacterial Ami2

As the *ami2* strain displayed the formation of bulges at the pole we sought to determine whether this protein is associated with the cell pole. A recent report on Ami2 (CwlM) function in *M. smegmatis* confirmed a role for this amidase in activating PG biogenesis at the cell pole. However, localisation of Ami2 was not assessed. Therefore, an Ami2-rsEGFP fusion protein-containing mc^{2}155 and Δ*ami1* strain was created in this study to localise Ami2. The approach involved

cloning of the *ami2-rsegfp* fusion product downstream the P_{myc}-tet promoter (for constitutive expression of fusion product), followed by the introduction of the construct into *M. smegmatis*.

4.3.4.1 *Construction of the pAmi2GFP vector*

PCR amplification was conducted to amplify the *ami2* gene without the stop codon and the *rsEGFP* gene. The fragment was then cloned into pSE100 and clones were screened by restriction with *Eco*RI. A single positive clone was then selected and the genetic integrity of the construct was confirmed by extensive restriction profiling, Figure 4.13.

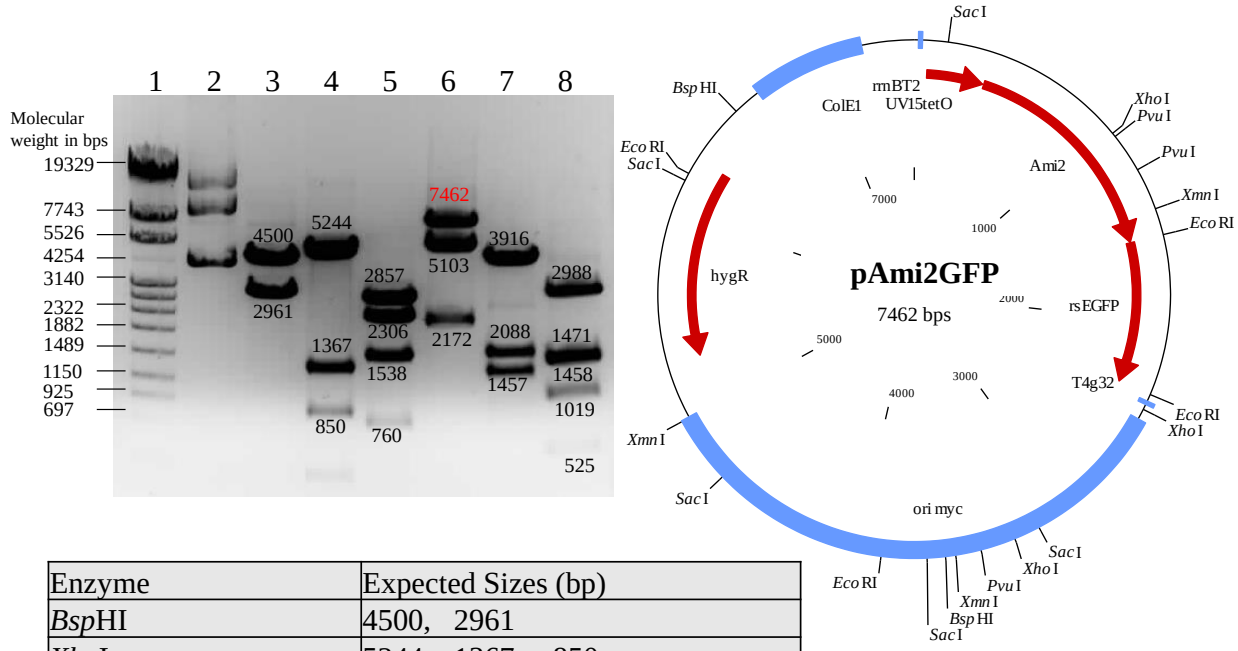

Enzyme	Expected Sizes (bp)
*Bsp*HI	4500, 2961
*Xho*I	5244, 1367, 850
*Eco*RI	2857, 2306, 1538, 760
*Pvu*I	5103, 2172, 186
*Xmn*I	3916, 2088, 1457
*Sac*I	2988, 1471, 1458, 1019, 525

Figure 4.13: Restriction profile of pAmi2GFP. Shown are the different restriction nucleases used and the expected sizes in a table, which result from restriction digests of the pAmi2GFP vector. The predicted vector map of pAmi2GFP vector and agarose gel depicting the products of restriction digest of pAmi2GFP are also shown. Lane 1: Roche Marker IV, Lane 2: Uncut, Lane 3: *Bsp*HI, Lane 4: *Xho*I, Lane 5: *Eco*RI, Lane 6: *Pvu*I, Lane 7: *Xmn*I, Lane 8: *Sac*I.

In all cases, all the fragment sizes observed corresponded to the vector map and expected sizes, confirming the genetic integrity of the vector, with the exception of *Pvu*I which displayed a 7462 bp band, which was a result of incomplete restriction endonuclease digestion. Also, there was an unexpected small band in the *Xho*I digest, the result of an unmapped vector site. The genetic

integrity of the vector was then further confirmed by sequencing of the cloned region, which revealed that no mutations had occurred during PCR and cloning processes (data not shown). This vector was then used for construction of the mc^{2}155::pAmi2GFP and Δ*ami1*::pAmi2GFP strain.

4.3.4.2 *Construction of the pAmi2GFPN vector*

PCR amplification was conducted to amplify a fragment containing the 400 bp region upstream the *ami2* transcriptional start codon and the *ami2* gene without the stop codon. The fragments were then cloned into pPV306(H) and the resulting clones were screened by restriction with *Bam*HI. A single positive clone was then selected and the genetic integrity of the construct was confirmed by extensive restriction profiling, Figure 4.14.

All the sizes observed on the agarose gel were as expected which the exception of *Bam*HI and *Pst*I digests, which displayed additional bands that can be attributed to partial vector digestion by the enzymes and *Hind*III, possibly as a result of star activity.

4.3.4.3 *Construction and screening of the mc^{2}155::pAmi2GFP and Δami1::pAmi2GFP strain*

The pAmi2GFP construct was electroporated into the mc^{2}155 and the Δ*ami1* strains (section 2.4.2), the transformation efficiency obtained from the electro-competent cells was 7.2×10^4 CFU/µg and 1.9×10^3 CFU/µg vector DNA, respectively (determined using the pSE100 control vector). Given that the *ami1* mutant displayed severe cell division defects, we sought to assess how Ami2 would localise under these conditions. Two clones were selected and screened by PCR using the *ami2*pSELF and the rsEGFPR primers (section 4.2.4) to determine the presence of the *ami2-rsEGFP* fusion DNA fragment (Appendix D, Figure D9).

4.3.4.4 *Construction of the Δami2::pAmi2GFPN strain*

To determine whether the Ami2-rsEGFP fusion protein is functional, a merodiploid strain was constructed containing the *ami2-rsEGFP* fusion, integrated at the *attB* site, regulated by the native promoter. To do this, the pAmi2GFPN construct was electroporated into the mc^{2}155 strain to create the mc^{2}155::pAmi2GFPN strain (section 2.4.2). The transformation efficiency obtained

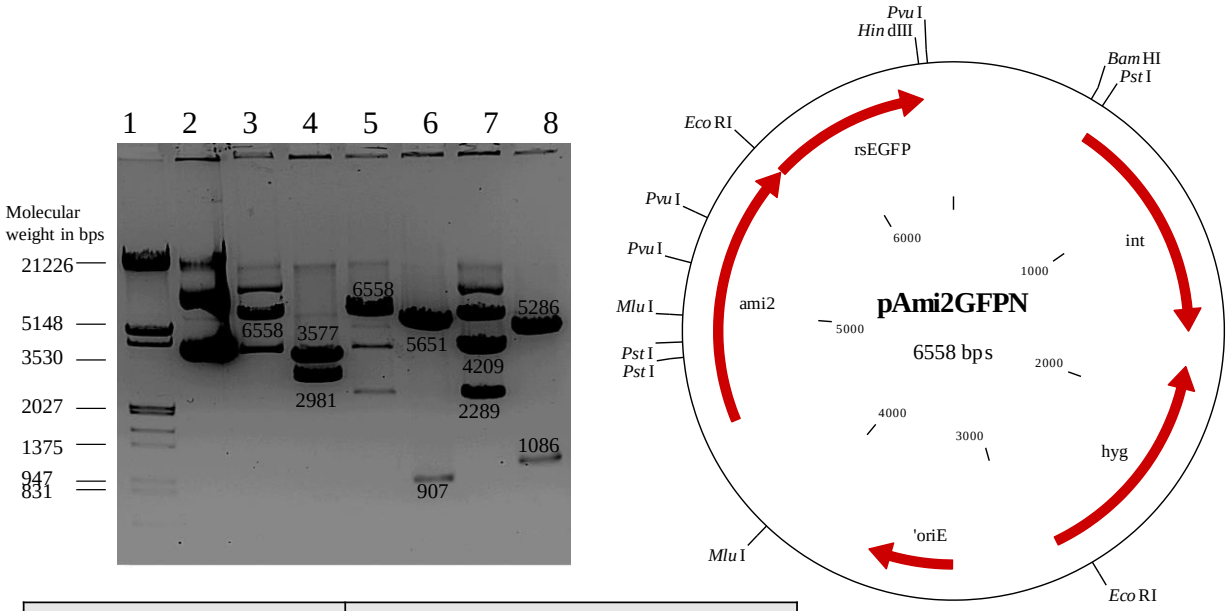

Enzyme	Expected Sizes (bp)
*Bam*HI	6558
*Eco*RI	3577, 2981
*Hin*DIII	6558
*Mlu*I	5651, 907
*Pst*I	4209, 2289, 60
*Pvu*I	5286, 1086, 186

Figure 4.14: Restriction profile of the pAmi2GFPN vector. Shown are the different restriction nucleases used and the expected sizes in a table, which result from restriction digests of the pAmi2GFPN vector. The predicted vector map of pAmi2GFPN vector and an agarose gel depicting the products of restriction digest of pAmi2GFPN are also shown. Lane 1: Roche Marker III, Lane 2: Uncut, Lane 3: *Bam*HI, Lane 4: *Eco*RI, Lane 5: *Hind*III, Lane 6: *Mlu*I, Lane 7: *Pst*I, Lane 8: *Pvu*I.

from the electrocompetent mc^2155 cells was 5.3×10^4. A single clone was selected then the p2ΔAmi2G17 knockout vector was electroporated into mc^2155::pAmi2GFPN strain (section 2.4.2), the transformation efficiency obtained for the electrocompetent cells was 3.1×10^4 CFU/μg vector DNA determined using the pSE100 control. A single blue clone (SCO strain) was cultured and subjected to sucrose counter selection (section 4.2.3). White colonies were then screened by PCR to identify clones which possess only the deleted allele, and then southern blot analysis was conducted to confirm the second homologous event removed the wild type allele without imposing additional unintended chromosome rearrangements, Figure 4.15.

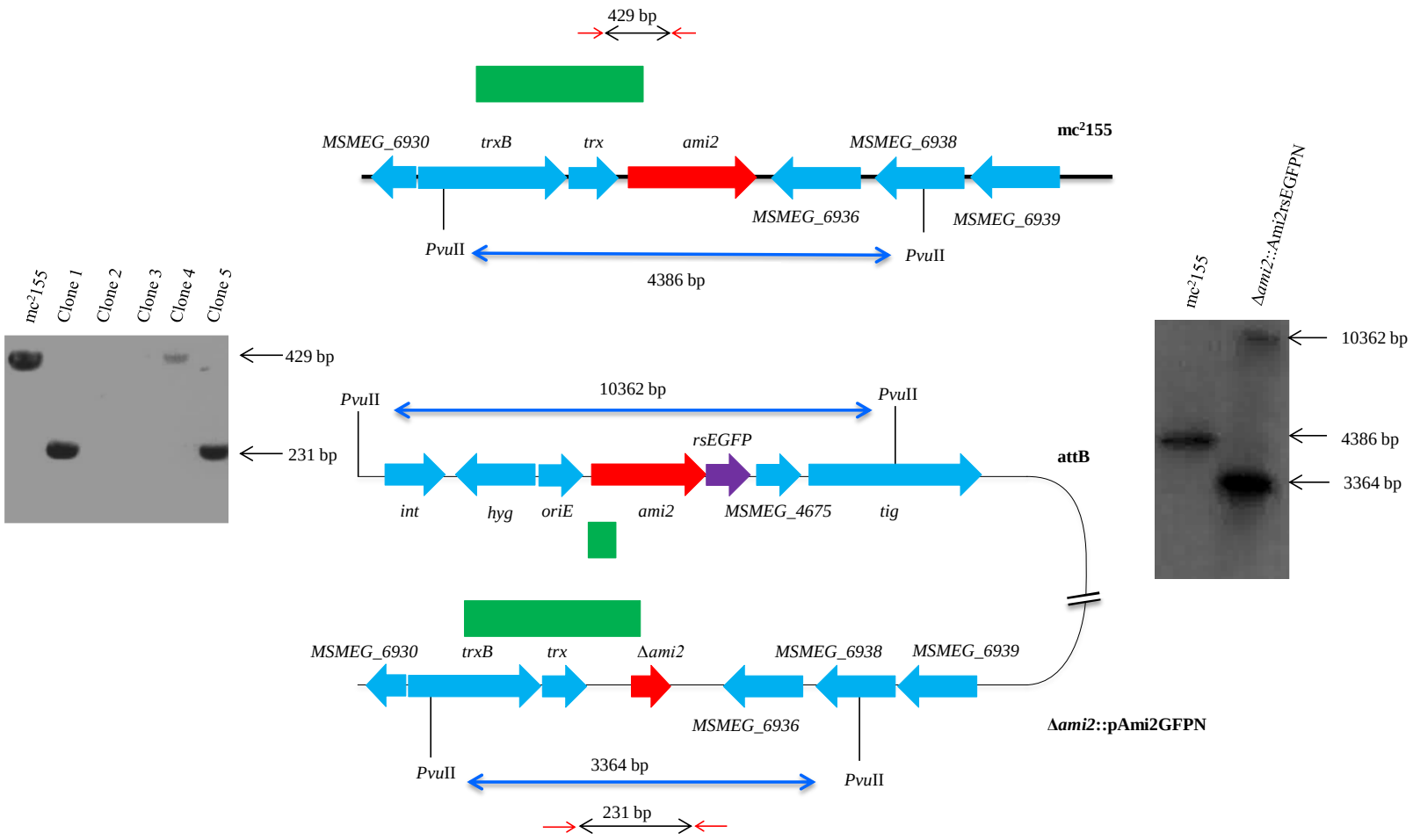

Figure 4.15: Genotypic analysis of the Δ*ami2*::pAmi2GFPN strain by PCR and Southern blot analysis. The genomic map of the relevant locus is shown for the wild type mc^{2}155 and Δ*ami2*::pAmi2GFPN strain which also depict the integration of a functional *ami2rsEGFP* fusion at the attB site. Also shown on the left is the PCR confirmation of the genotype and southern blotting is shown on the right. For PCR confirmation, chromosomal DNA was used to amplify the *ami2* alleles from the wild type and mutant strains using the primer pairs described in Table 4.3 and indicated as red arrows above. The expected sizes of the amplicons are as follows: *ami1*, 429 bp and Δ*ami1*, 231 bp. For the Southern blot analysis, chromosomal DNA from the SCO, parental and mutant strain was digested with *Pvu*II. The probe used for hybridisation is shown as a solid green box and the expected sizes are indicated by the blue arrows. The figures are not drawn to scale.

4.3.4.5 *Localisation of mycobacterial Ami2*

Following the construction of the Ami2 localisation strains, high resolution TIRF microscopy was conducted to determine the cellular localisation of Ami1-rsEGFP. The cells were stained with the cell membrane strain FM4-64 to identify the membrane, Figure 4.16.

The TIRF microscopy revealed a polar localisation pattern for Ami2-rsEGFP, with the majority of cells displayed distinct polar focus. Furthermore, this pattern was maintained in the Δ*ami1*::pAmi2GFP strain where the Ami2-rsEGFP fusion protein maintained the polar localisation pattern with no septal localisation observed, confirming that Ami2 plays an important role in the polar elongation of mycobacterial cells. To further analyse these observations, the 6 basic localisation patterns observed were quantified, these were: 1, No Ami2-rsEGFP localisation, 2, Ami2-rsEGFP localisation in the larger daughter cell 3, Ami2GFP localisation in the smaller daughter cell, 4, Ami2-rsEGFP localisation on single pole in a chain, 5, Ami2-rsEGFP localisation on both poles and 6, Ami2-rsEGFP localisation on a single pole.

Quantification of these patterns revealed relatively a high proportion, 60.15 %, of the mc^2155 population displayed the single pole localisation pattern of Ami2, Figure 4.17. As the majority of the population is not undergoing cell division, these were not classified under the daughter cell classification groups which depict dividing cells, Figure 4.17. In the Δ*ami1* mutant, the majority of this population, 48.67 %, displayed the Ami2-rsEGFP localisation in the larger daughter cell.

This was expected as a majority of this population is undergoing cell division as a result of the previously reported division arrest. A small proportion of both populations displayed localisation at the smaller of the two daughter cells suggesting that Ami2 preferentially localises at the old pole. Furthermore, in 14 % of the Δ*ami1* population, polar Ami2 localisation in a chain was observed. At this point, it is unclear how this localisation pattern in the *ami1* mutant is mediated and further work is required to resolve this.

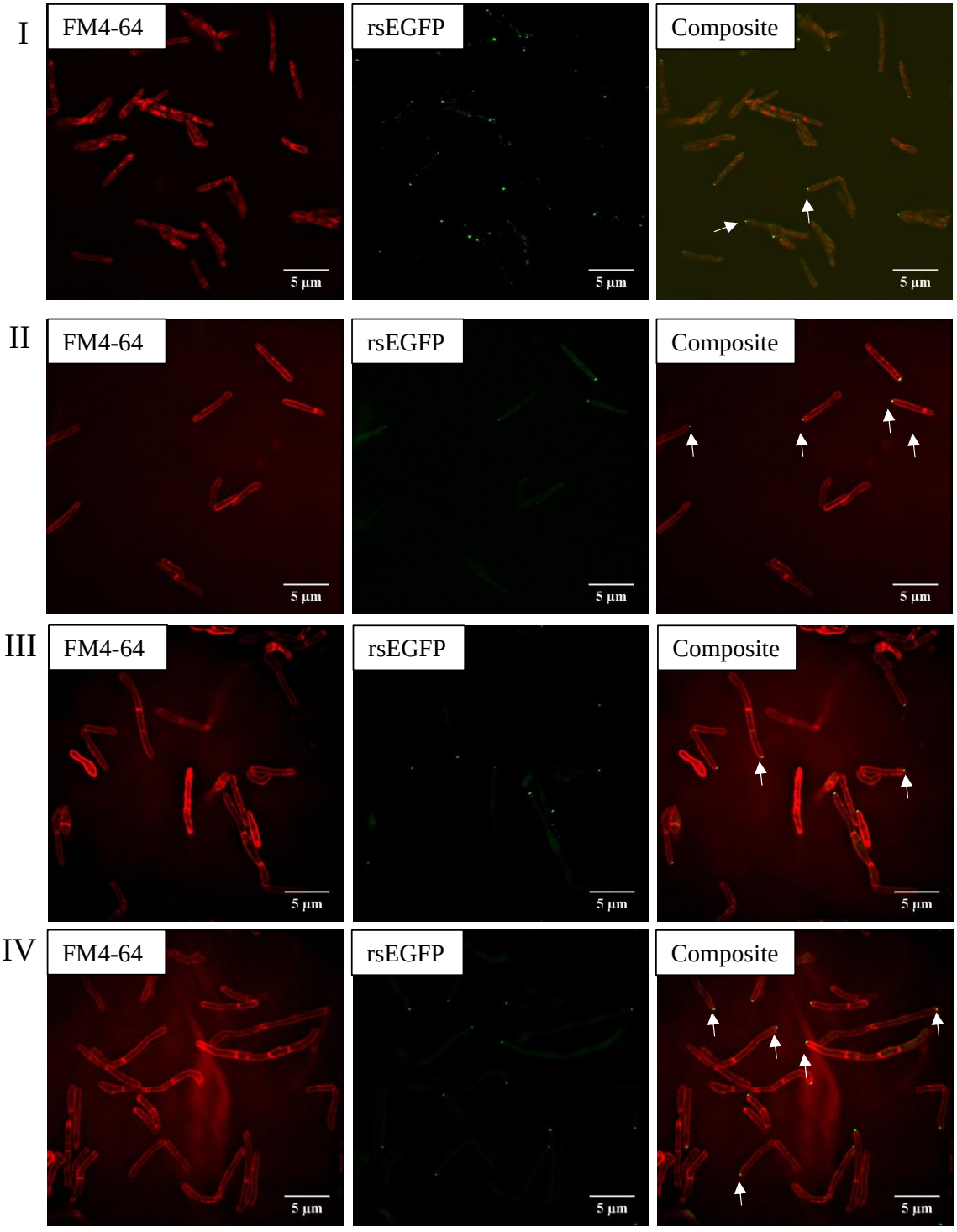

Figure 4.16: Cellular localisation of Ami2-rsEGFP in mc^{2}155 and Δ*ami1* cells. Bacteria were grown in 7H9 and stained with FM4-64 which stains the plasma membrane then mounted on agarose pads followed by imaging. I-II depicts Ami2-rsEGFP localisation in mc^{2}155 and III-IV represents Ami2-rsEGFP localisation in the Δ*ami1* strain showing the localisation of a single Ami2-rsEGFP foci in individual cells and in Δ*ami1* chains. White arrows indicate polar Ami2-rsEGFP localisation.

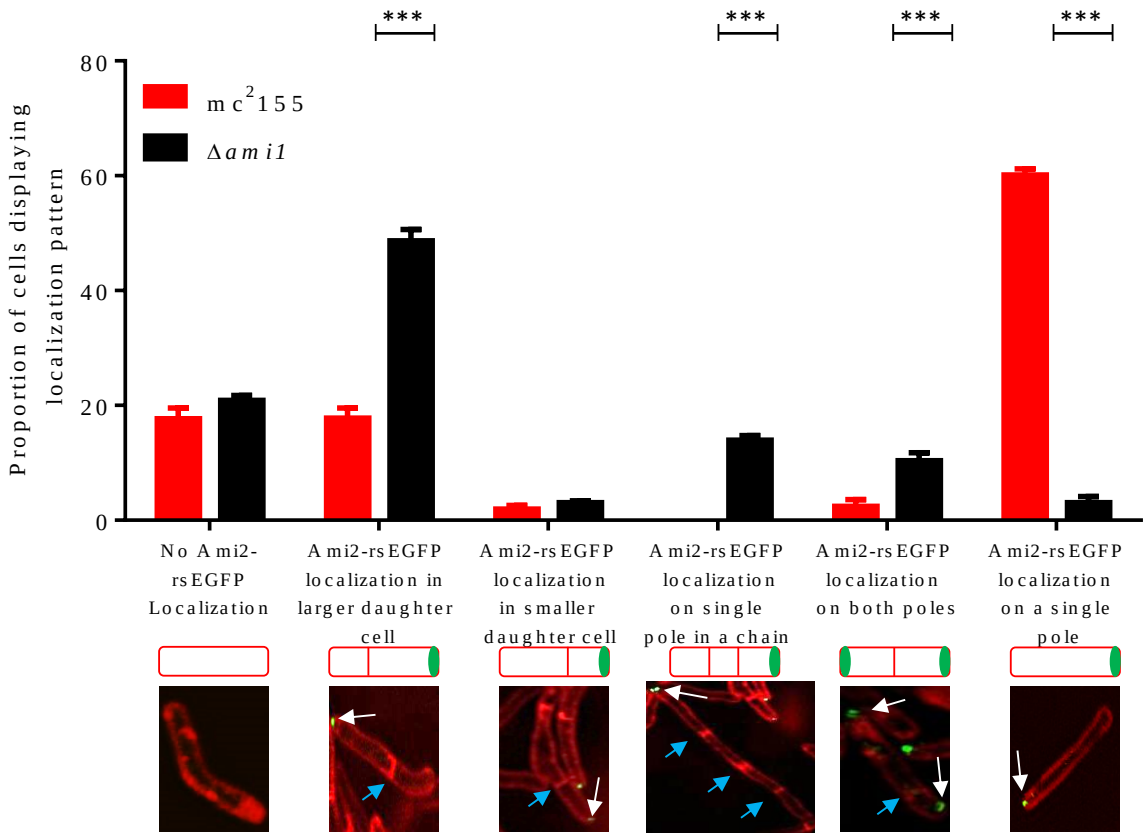

Figure 4.17: Histogram depicting the analysis of the Ami2-rsEGFP localisation patterns in the mc^{2}155 and Δ*ami1* strains. Shown is the proportion of bacterial cells which exhibit various localisation patterns in both strains white arrows show polar Ami2-rsEGFP localisation and blue arrow indicate division septa, The bar graph was generated using data from 3 biological replicate counting a total of approximately 350 cells. P-values were attained using the student *t* – test. ***: $p < 0.001$.

To further investigate Ami2 localisation in wild type, time-lapse microscopy was conducted on the mc^{2}155::pAmi2GFP strain. Time-lapse microscopy of the mc^{2}155::pAmi2GFP strain confirmed Ami2 polar localisation, Figure 4.18, Appendix E, movies 4.4 to 4.6, which seemed to occur after the cells had initiated polar elongation. The cells retained the single pole localisation pattern until the conclusion of cell division at which point the daughter cell possessing Ami2 continued to grow from that pole. Ami2 was then only recruited to the new pole after the establishment of growth at the pole, Figure 4.18.

4.3.5 Association of Ami2 with the cell membrane

Unlike Ami1, Ami2 does not possess a signal peptide for translocation to the periplasm. However, as Ami2 is predicted to be a PG hydrolysing enzyme, we sought to determine whether it was translocated to the periplasm or remains in the cytoplasm to conduct its function. For this, *N*- and

C- terminally FLAG-tagged variants of Ami2 were constructed and introduced into mc^2155 followed by cell fractionation and western blot analysis to determine the location of Ami2.

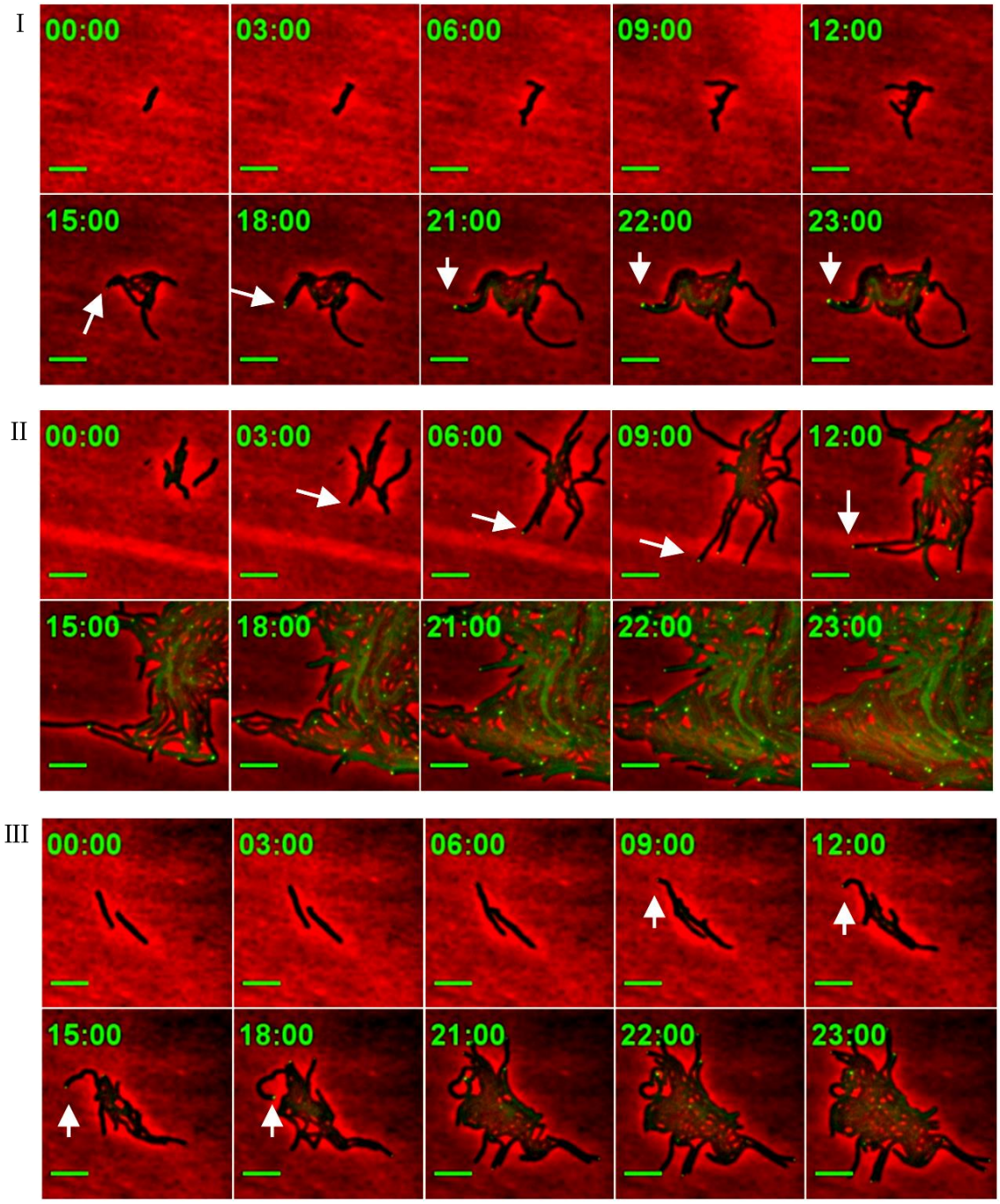

Figure 4.18: Time lapse microscopic analysis of Ami2-rsEGFP localisation in the mc^2155 strain. Cells were grown and imaged in 7H9S. I-III depicts three representative mc^2155 micro-colonies. White arrows indicate the polar localisation of Ami2, which emerge on a single as the cell begins to elongate and remains at the same pole throughout multiple division cycles. Scale = 5 µm

4.3.5.1 *Construction of the pAmi2NFLAG and pAmi2CFLAG vectors*

PCR amplification was conducted to amplify two variants of the *ami2* gene, one full length gene for *N*-terminal tagging and one without the stop codon for C-terminal tagging. The fragments were then cloned into pFLAGEM and clones were screened by restriction with *Eco*RI. A single positive clone was then selected and the genetic integrity of the vector was confirmed by extensive restriction profiling, Figure 4.19 and Figure 4.20.

In all cases, all the fragment sizes observed corresponded to the vector map and expected sizes, confirming the genetic integrity of the vector (Fig 4.19 and Fig 4.20). The genetic integrity of the vector was then further confirmed by sequencing of the cloned region, which revealed that no mutations had occurred during PCR and cloning processes (data not shown). This vector was then used for construction of the mc^2155::pAmi2NFLAG and mc^2155::pAmi2CFLAG strains.

4.3.5.2 *Determining the subcellular localisation of Ami2*

The pAmi2NFLAG and pAmi2CFLAG vectors were electroporated into the mc^2155 strain (section 2.4.2); the transformation efficiency obtained from the electro-competent cells was 5.6×10^4 CFU/µg (determined using the pSE100 control vector). A single clone per strain was selected. This was cultured, fractionated and western blot analysis was conducted to determine the possible export of Ami2 through cellular fraction association, section 4.2.4 and 4.2.5.

As shown in Figure 4.21, both *N*- and C- terminally tagged Ami2 products associated with the cell wall fraction. Furthermore the detection of both variants of the same size, in the same type of fraction, in two distinct strains suggests that the protein is not cleaved during localisation. This was unexpected,

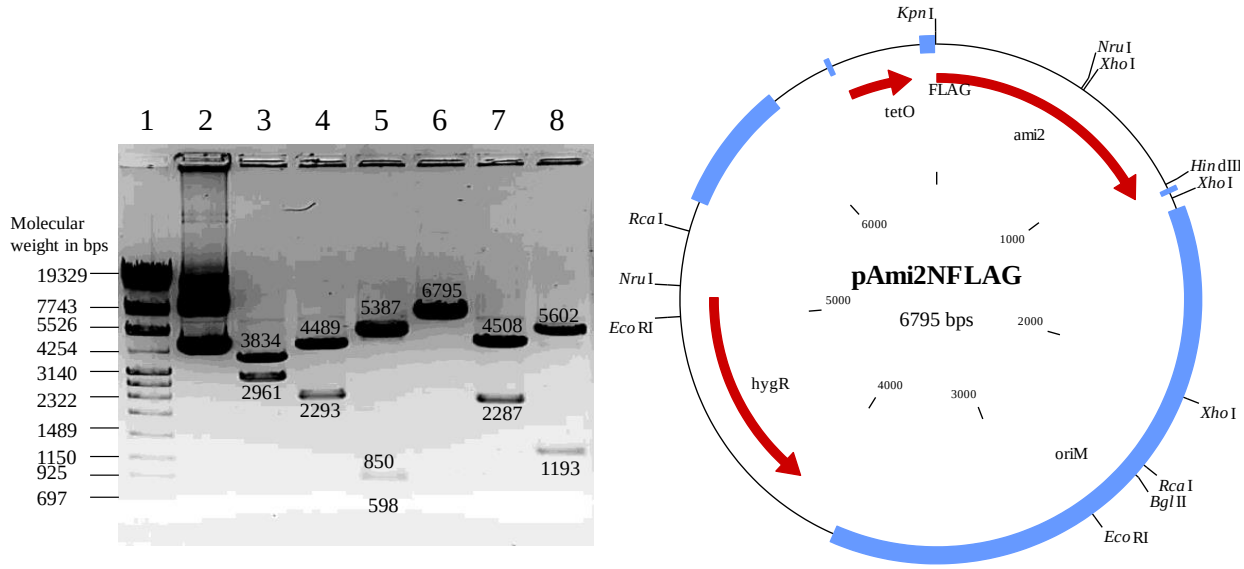

Enzyme	Expected Sizes (bp)
*Rca*I	3834, 2961
*Eco*RI	4489, 2306
*Xho*I	5387, 850, 598
*Bgl*II	6795
*Nru*I	4508, 2287
*Hind*III and *Kpn*I	5602, 1193

Figure 4.19: Restriction profile of pAmi2NFLAG, Shown are the different restriction nucleases used and the expected sizes in a table, which result from restriction digests of the pAmi2NFLAG vector. Predicted vector map of pAmi2NFLAG vector and agarose gel depicting the products of restriction digest of pAmi2NFLAG. Lane 1: Roche Marker IV, Lane 2: Uncut, Lane 3: *Rca*I, Lane 4: *Eco*RI, Lane 5: *Xho*I, Lane 6: *Bgl*II, Lane 7: *Nru*I, Lane 8: *Hind*III and *Kpn*I.

as *ami2* does not possess a signal peptide and was shown to be a cytoplasmic protein (Boutte et al., 2016). The co-localisation of Ami2FLAG could be a result of protein PG interactions during sample preparation. Furthermore, the lack of relevant control antibodies for each fraction makes it difficult to confirm that each fraction contained only cell wall, cell membrane or cytoplasmic material.

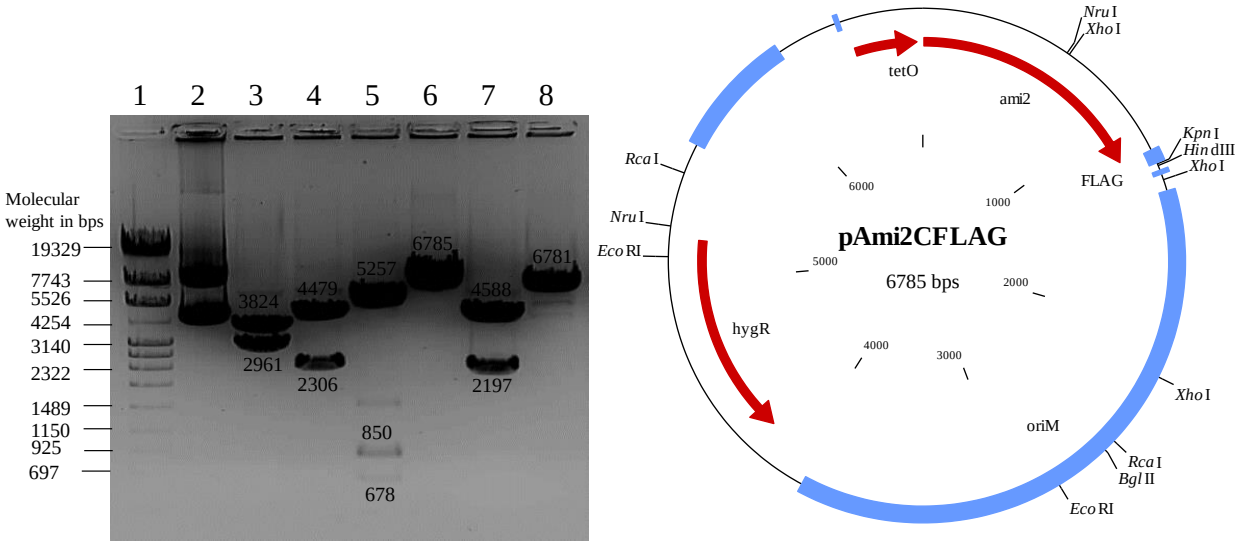

Enzyme	Expected Sizes (bp)
*Rca*I	3824, 2961
*Eco*RI	4479, 2306
*Xho*I	5257, 850, 678
*Bgl*II	6785
*Nru*I	4588, 2197
*Hind*III and *Kpn*I	6781, 4

Figure 4.20: Restriction profile of pAmi2CFLAG. Shown are the different restriction nucleases used and the expected sizes in a table, which result from restriction digests of the pAmi2CFLAG vector. The predicted vector map of pAmi2CFLAG vector and agarose gel depicting the products of restriction digest of pAmi2CFLAG are also shown. Lane 1: Roche Marker IV, Lane 2: Uncut, Lane 3: *Rca*I, Lane 4: *Eco*RI, Lane 5: *Xho*I, Lane 6: *Bgl*II, Lane 7: *Nru*I, Lane 8: *Hind*III and *Kpn*I.

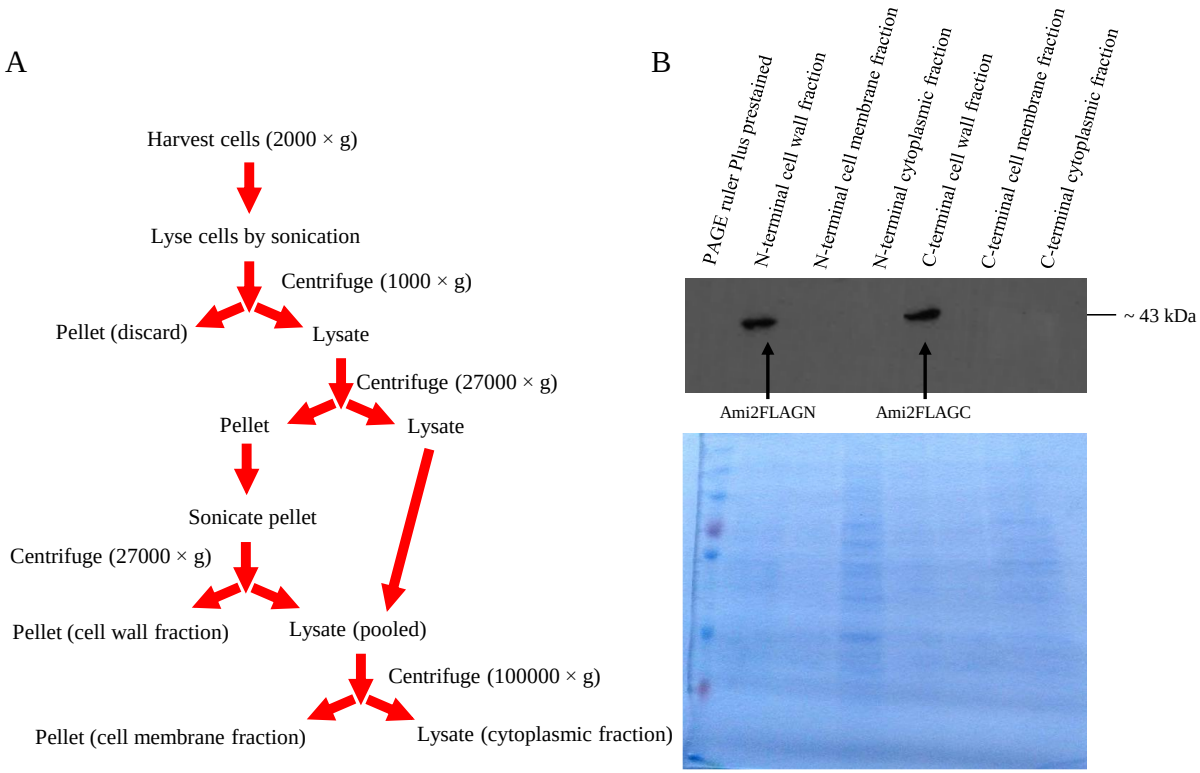

Figure 4.21: Western blot analysis of N- and C- terminally Flag-tagged Ami2. (A) Shown is a flow chart representing the protocol used to fraction the cell into three fractions; the cell wall, cell membrane and cytoplasmic content. (B) Shows western blot analysis conducted on the three cell fractions to detect Flag tagged Ami2 in the three fractions.

4.4 Discussion

In the previous chapter, we demonstrated that Ami1 plays an important role in cell division, more specifically, in daughter cell separation. Our initial bioinformatics analysis identified Ami2 as the second amidase_3-domain-containing PG hydrolase in mycobacteria. Whilst the amidase_2 domain was generally conserved, some of the conventional catalytic residues were replaced with non-canonical amino acids, suggesting a possible divergence in function or substrate specificity, Appendix D, Figure D1. Consistent with this, our analysis of this enzyme confirmed a role in cell elongation. Elongation in mycobacterial cells occurs through polymerisation of new PG at the cell poles (Botella et al., 2017). Little is known about the role of PG hydrolases in cell elongation; however, one class of enzymes which has been well characterised in this context are the PBPs. This is a class of enzymes consisting of various sub-groups conducting different enzymatic reactions, including transglycosylases (which polymerise the glycan strand), transpeptidases (which crosslink the stem peptides) and two groups of hydrolases, which are, the endopeptidases and carboxypeptidases, both responsible for cleaving various peptide bonds within the stem peptide (Hett and Rubin, 2008). The role of carboxypeptidases in cell growth has remained enigmatic, work conducted in *E. coli* has suggested a possible role in cell shape maintenance, as deletion of multiple DD-caboxypepetidases resulted in the formation of long, fat cells containing lateral and polar branches (Nelson and Young, 2001). With regards to endopeptidases. however, it is clear these enzymes are important for cell elongation. Several reports in *E. coli* and *B. subtilis* has demonstrated that deletion of multiple PG endopeptidases results in the formation of short cells which ultimately lyse resulting in bacterial death (Singh et al., 2012, Hashimoto et al., 2012, Meisner et al., 2013). In *M. smegmatis*, depletion of the bi-functional, essential, PBP (ponA1), which conducts both transpeptidase and transglycosylase activity, results in a phenotype similar to that observed in the *M. smegmatis ami1* deletion strain (Kieser et al., 2015, Senzani et al., 2017), indicating this enzyme is essential for cell division (Kieser et al., 2015).

Similar to PonA1, Ami2 was also predicted to be essential for growth of Mtb and we sought to determine whether this essentiality was linked to any role in cellular growth or division (Sassetti and Rubin, 2003, Griffin et al., 2011). This initial prediction of essentiality in Mtb was proven using TraSH (Sassetti and Rubin, 2003, Griffin et al., 2011). This technique possesses certain limitations including secondary effects on downstream genes resulting in false annotations of essentiality and it also relies on negative screening whereby the lack of growth is viewed as

essentiality (Sassetti and Rubin, 2003, Nisa et al., 2010, Ginda et al., 2013). These limitations may give rise to an incorrect assumption of essentiality, as demonstrated for the MoaA1-MoaD1 operon in Mtb, which was initially predicted to be essential by TraSH but later proven to be dispensable (Williams et al., 2011). To address these limitations, a merodiploid technique was adopted to try and prove essentiality (Appendix D, Figure D6). The *ami2* knockout vector was constructed and the ability to knockout *ami2* in mc^2155 was tested, this yielded only wild-type and SCOs, the latter carrying a loss of function mutation in the *sacB* and *lacZ* genes (Senzani, 2014). These data were consistent with the predicted essentiality of Ami2 (Sassetti and Rubin, 2003, Griffin et al., 2011). To further explore this, a second copy of the *ami2* gene, driven off the native promoter was inserted at the *attB* site, and the two-step allelic exchange mutagenesis was attempted again. This yielded two amidase knockout strains, out of 10 possible clones, demonstrating that an additional copy the gene was required for mutagenesis. While we were conducting our analysis, another group also demonstrated the essentiality of *ami2* by adopting a merodiploid approach (Boutte et al., 2016).

The depletion of *ami2* led to a reduction in bacterial growth when compared to mc^2155. In broth culture, this did not result in complete cessation of growth in the absence of the inducer. Our data in this regard are in contrast to that reported by Boutte et al, 2016, who demonstrated complete cessation of growth upon depletion of Ami2 (Boutte et al., 2016). We expect that this is due to the leaky nature of the *tetO* regulated system, which in our case only allowed for a 40% reduction in gene expression under conditions of gene depletion (Ehrt et al., 2005a, Blokpoel et al., 2005). This reduced expression was sufficient to facilitate low level bacterial growth and provided the opportunity to study the effects of *ami2* depletion. Microscopic analysis demonstrated that a reduction in *ami2* levels led to the formation of short cells containing bulges at the polar region, confirming that Ami2 is crucial for cell elongation. This was consistent with findings that Ami2 played an important role during cell elongation through the activation of MurA and the initiation of lipid II biosynthesis (Boutte et al., 2016). Therefore, the depletion of Ami2 would lead to the inhibition of lipid II biosynthesis and retarded cellular growth (Figure 4.22).

We also considered the possibility that escape mutants emerged during growth to bypass the lethal effects of *ami2* repression. Consistent with this, Boutte et al 2016 also demonstrated the occurrence of escape mutant strains in the phospho-ablative Ami2 strains, in which case Ami2 does not possess the ability to activate MurA (Boutte et al., 2016). In these strains, point mutations found

in *murA* resulted in a seemingly constitutively active form of the enzyme rendering, the MurA activation function of Ami2, non-essential for growth (Boutte et al., 2016). To address this issue in our experiments, a sample from the culture, wherein gene depletion was carried out, was used to start a secondary growth kinetics analysis. The hypothesis here was that if the emerging organisms were escape mutants, growth of the secondary culture would resemble the mc^2155 culture, and would not be responsive to ATc depletion. This was not the case as retarded growth was observed again, in a manner similar to the initial growth curve, confirming the ability to regulate growth using ATc. This indicated that in our experiments, the reduced growth seen upon *ami2* gene depletion was due to leaky expression rather than loss of P_{myc}-tet regulation.

As Ami2 appears to be essential for the initiation of PG biosynthesis, BODIPY-vanc staining was conducted on *ami2*KDP to evaluate whether PG synthesis continues to occur at the poles when Ami2 is depleted. In this regard, it was demonstrated that Ami2 plays an important role in regulating the activity of MurA during starvation and stationary phase (Boutte et al., 2016). Furthermore, it has been suggested that a reduction in PG biosynthesis, as a result of stationary phase or starvation, led to the delocalisation of the elongasome and in this context, we expected that depletion of Ami2 would lead to diffused BODIPY-vanc staining (Hayashi et al., 2018). This was not the cases as the *ami2*KDP strain retained polar BODIPY-vanc staining when *ami2* was depleted, this suggests the elongasome remained at the poles and low level *ami2* expression is sufficient as to allow for the synthesis of lipid II.

As PG biosynthesis seemed to be occurring at the cell poles in the *ami2*KDP strain, single cell microscopy was conducted to evaluate how these strains were growing. This revealed that depletion of *ami2* did in-fact result in substantive growth inhibition, an effect that was noted in a substantive number of micro-colonies analysed. Given the dramatic loss of FM4-64 staining observed in cells where *ami2* was depleted, we assumed that depletion resulted in death but this would need to be further confirmed with live/dead staining techniques or by re-introduction of ATc to the system. Despite these limitations, our data seem consistent with previous reports of *ami2* essentiality (Boutte et al., 2016).

Depletion of *ami2* also resulted in the formation of polar bulges. This phenotype has been reported with a number of essential *M. smegmatis* cell elongation components including a *divIVA* depletion strain, where depletion resulted in short cells which contain bulges and *ponA1*, where deletion of

the transpeptidase domain results in short cells containing polar bulges (Kang et al., 2008, Kieser et al., 2015). However, unlike the *ami2* depletion strain the bulges in both the Δ*ponA1* mutant and *divIVA* depletion strains, originate from the septum, during cell division (Kang et al., 2008, Kieser et al., 2015, Hett et al., 2010). This does not appear to be the case in the *ami2*KDP strain as only 2 of the 64 bulges observed were septal in nature and in both instances the septum seemed to be misplaced and was adjacent to the pole.

A comparable phenotype was also noted with the overexpression of *pknB* (Kang et al., 2005). Elevated levels of *pknB* resulted in the formation of short, wider cells, which contained bulges identical to those observed in the *ami2*KDP strain (Kang et al., 2005). This could be the result of altered Ami2 activity, a hypothesis that is supported by the demonstrated interaction between Ami2 and PknB, which results in Ami2 phosphorylation and PknB dephosphorylation (Boutte et al., 2016). However, it is unusual that *pknB* overexpression would result in the formation of long cells (Kang et al., 2008). One possible reason for this is the broad substrate specificity of PknB, which phosphorylates a multitude of proteins including RshA (Prisic et al., 2010, Park et al., 2008). RshA is an anti-sigma factor which regulates the activity of SigH by binding and inhibiting the expression of stress responsive genes (Song et al., 2003). This interaction is regulated by PknB, as it was demonstrated that phosphorylation of RshA by PknB hinders the interaction between SigH and RshA, leading to transition to a stress tolerant form, possibly similar to that observed in the PknB overexpression strain (Song et al., 2003, Park et al., 2008, Kang et al., 2005, Shleeva et al., 2010). This would suggest Ami2 and PknB regulate each other, thus a reduction in Ami2 would not only result in a decrease in active MurA, but also an increase in active PknB resulting in the formation of short cells with polar bulges (Figure 4.22).

As localisation of both DivIVA and PonA1 was shown to be both polar and septal in nature, we sought to determine whether Ami2 localises in a similar manner (Hett et al., 2010, Kang et al., 2008). Our localisation data indicated that Ami2 localises exclusively to the pole, furthermore it appears to be recruited once the leading pole is established as shown by the late arrival of Ami2 to the growing pole. Although, it is difficult time Ami2 localisation accurately in the absence of other markers of cell division. This pattern of Ami2GFP localisation was observed in approximately half the cells examined using live cell microscopy, however images acquired with TIRF microscopy indicated approximately 80 % of the population contained localisation foci at the poles. This

discrepancy in the proportion of cells localizing Ami2GFP could be due to the higher sensitivity of TIRF microscopy enabling it to detect fluorescent signals with lower intensity (Mattheyses et al., 2010). Furthermore, analysis of the TIRF acquired Δ*ami1*::pAmi2GFP data revealed a similar localisation pattern in a Δ*ami1* chain, consisting of three or more cells indicating that failure to separate did not affect the localisation pattern. How Ami2 is directed to the cell pole is still unclear.

Cell fractionation analysis of the C- and *N*-terminally FLAG-tagged Ami2 suggested the association of Ami2 with the cell wall fraction. This was unexpected as the polypeptide does not contain a translocation signal sequence; furthermore, it has been demonstrated that Ami2 is cytoplasmic in nature (Boutte et al., 2016). One possible answer to this is the presence of a mycobacterial fraction which consists of a tightly associated plasma and cell membrane (PM-CW) fraction (Hayashi et al., 2016, Morita et al., 2005). Work conducted by Hayashi et al., 2016, indicated the association of Ami2 which the PM-CW fraction (Hayashi et al., 2016). This association is perhaps stronger with the CW component of this fraction, as Ami2 possesses two cell wall binding domains and no plasma membrane binding domain (Hayashi et al., 2016, Machowski et al., 2014). This study and observations by Hayashi et al, 2016 suggest the possible translocation of Ami2 to the cell wall; however, the mechanism involved is unknown. This is plausible as a number of mycobacterial proteins without a signal sequence have been shown to be secreted (De Souza et al., 2011). That said, caution should be used when intepreting these experiments and as a result, we sought an alternate explanation. There is the possibility where due to the presence of the cell wall binding domains, Ami2 possesses the ability to bind PG, as such this interaction could have occurred during fraction preparation resulting in the co-precipitation of the Ami2-FLAG protein with the PG fraction (Machowski et al., 2014). Furthermore the lack of specific antibodies to differentiate the three fractions, using enzymes demonstrated to precipitate with each fraction, makes it difficult to confirm the validity of the fractionation approach. We are actively seeking alternatives to determine cellular localisation of this protein.

Collectively, herein we confirm the essentiality of Ami2 for polar elongation of mycobacterial cells. We demonstrated that depletion of this enzyme results in a dramatic reduction in growth at a single-cell levels and substantive morphological defects including short cells and the presence of bulges. We also show that Ami2 localises the cell pole, the mechanism that supports this has yet to be unravelled.

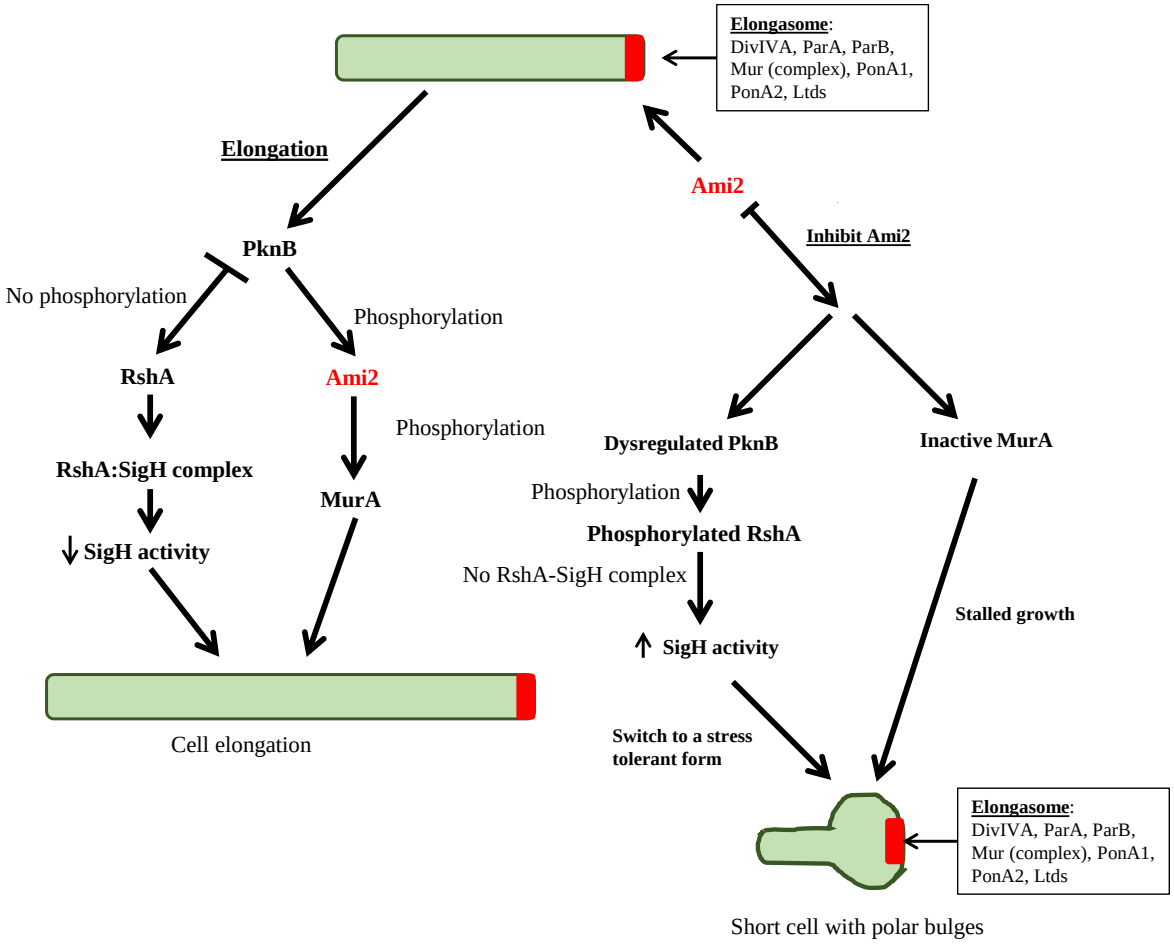

Figure 4.22: Proposed model for the role of Ami2 during cell growth in mycobacteria. PknB phosphorylates Ami2, which in turn phosphorylates MurA, resulting in the activation of MurA, followed by PG synthesis and cell elongation. Ami2 phosporylation also regulates the level of active PknB thus indirectly regulating the activity of SigH. When Ami2 is depleted this results in an increase in active PknB, which then phosphorylates RshA, leading to increased SigH activity causing a bacterial switch to a stress tolerant form. The reduction of Ami2 results in a reduced levels of active MurA in the cell leading to retarded growth and the formation of short cell with bulges at the poles (figure drawn by S. Senzani).

Chapter 5

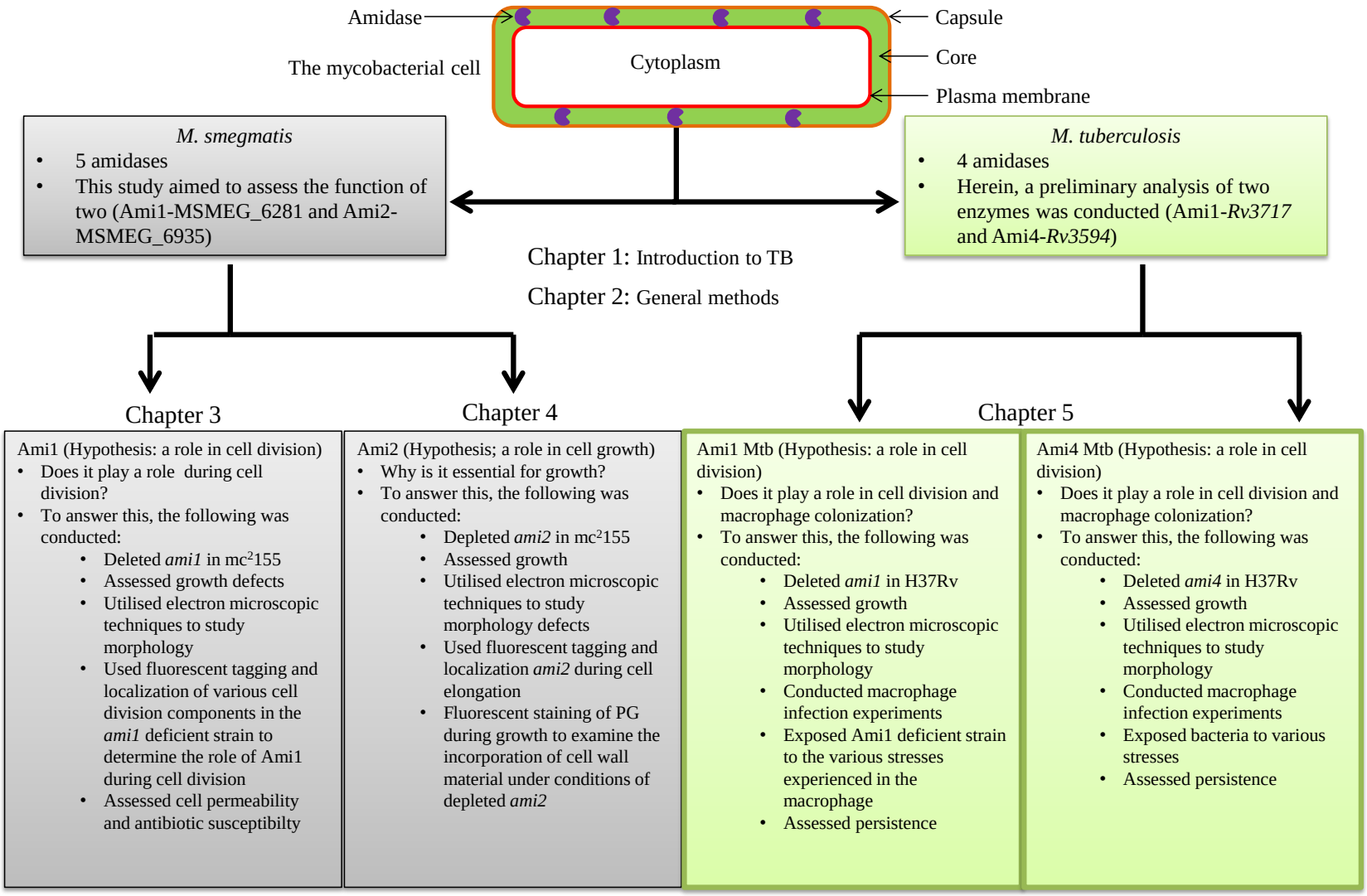

Figure 5.1: Flow chart highlighting the focus of chapter 5. Highlighted is the portion of the study which will be addressed in the following chapter. (figure drawn by S. Senzani)

5 Mtb amidases in bacterial growth and survival

5.1 Introduction

As bacteria constantly find themselves under stressful conditions, survival is critically reliant on the ability to sense the environment and respond to changes (Justice et al., 2008). In addition to playing a vital structural role, bacteria are able to use their cell walls to sense environmental changes and respond appropriately. Within the cell wall, the PG layer is a dynamic and fluid structure, continuously undergoing remodelling for various purposes and as has been discussed, many of these related to cell growth and division (Horcajo et al., 2012, Alvarez et al., 2014). Some PG modifications, however, are important for responding to stress. In many cases, deletion of PG remodelling enzymes generally results in elongation or division defects, which are generally severe and obfuscate any role these enzymes play in responding to stress (Heidrich et al., 2001, Korsak et al., 2005). One example of how PG remodelling is critical for responding to stress is illustrated in *Bacillus subtilis* during spore formation.

5.1.1 The role of amidases in *B. subtilis*

B. subtilis possesses 10 cell wall amidases, five of these are amidase_2 domain containing enzymes designated as CwlH, CwlA, XlyA, XlyB and BlyA (Smith et al., 2000). From an evolutionary perspective, some of the amidase_2 domain containing enzymes are predicted to be of viral origin, as their expression is regulated by viral elements (Nugroho et al., 1999, Longchamp et al., 1994, Mizuno et al., 1996, Regamey and Karamata, 1998). The biological role of the entire bacillus amidases_2 domain containing enzymes and how they are related to each other is unknown; however, the catalytic activity has been demonstrated (Nugroho et al., 1999, Longchamp et al., 1994, Mizuno et al., 1996, Regamey and Karamata, 1998). *B. subtilis* also contains five amidase_3 domain containing amidases designated CwlD, YqiI, LytC, CwlC and CwlB, which seem to be required for sporulation, protection against high osmolarity and cell division. These will be discussed further in detail below.

Sporulation is an adaptive process carried out by members of the *bacillus* species under conditions of stress such as nutrient starvation (Errington, 1993). This process entails the formation and release of an endospore, which remains dormant until conditions become favorable for growth. Sporulation begins with the formation of asymmetric division septa (Piggot and Hilbert, 2004).

This is followed by phagocytosis of the miniature cell by the adjacent mother cell (Piggot and Hilbert, 2004). The engulfed cell is then coated with an additional PG layer, termed the spore cortex, finally followed by lysis of the mother cell resulting in spore release (Piggot and Hilbert, 2004). Cell wall amidases play a role at various stages along the sporulation process, beginning with spore cortex maturation. Formation of this polymer is facilitated by CwlD (Sekiguchi et al., 1995). Analysis of strains lacking this amidase revealed the formation of spores which were unable germinate under nutrient rich conditions (Sekiguchi et al., 1995). The authors hypothesise that CwlD plays an important role in the hydrolysis of the spore cortex resulting in the release of the endospore leading to bacterial growth. CwlD expression analysis, however, showed that this gene is only expressed during spore formation, suggesting that an alternate mechanism must prevail (Sekiguchi et al., 1995). Analysis of spore cortex PG from Δ*cwlD* spores revealed the absence of a δ-lactam structure on the NAM residues (Smith et al., 2000, Popham et al., 1996, Atrih et al., 1996). This NAM - δ-lactam structure is found in approximately 50 % of the spore cortex PG and plays an important role in spore germination, as spore lacking this structure fail to germinate (Popham, 2002, Popham et al., 1996). Thus, CwlD most likely modifies the peptide stem in the spore cortex, which subsequently allows the formation of the δ-lactam structure.

Three cell wall amidases LytC, CwlC and CwlB are also involved in mother cell lysis (Smith and Foster, 1995). In this case, deletion of each amidase individually has no impact on mother cell lysis; however, deletion of two or more resulted in abrogation of mother cell lysis (Smith et al., 2000). Furthermore, double mutants containing a *cwlC* knockout displayed a higher proportion of unlysed mother cells, indicating CwlC plays the major role during mother cell lysis, possibly in synergy with LytC and CwlB (Smith and Foster, 1995).

B. subtilis amidases also play a role in maintaining bacterial osmolarity (Fischer and Bremer, 2012). Deletion of any amidase_3 domain-containing amidase resulted in retarded growth in media containing high salt concentration (Fischer and Bremer, 2012). The exact mechanism for osmotic tolerance is unknown. However it is predicted that amidases play a role in remodeling the cell wall to yield a conformation that allows for minimal water loss (Fischer and Bremer, 2012). As deletion of multiple cell wall amidases did not exacerbate the phenotype, the authors predict the presence of an osmolarity pathway involving all the *B. subtilis* amidase_3 amidases, each possessing a

specific role, where deletion of a single amidase would result in the collapse of the pathway (Fischer and Bremer, 2012).

Unlike in *E. coli*, the amidases do not appear to play a major role in cell division in *B. subtilis*. LytC is the only amidase demonstrated to play a role during cell division (Blackman et al., 1998). This function is conducted in synergy with the glucosaminidase LytD, as deletion of LytC individually does not induce any septation defects. However, the *lytC lytD* double mutant is characterised by the formation of abnormally long chains (Blackman et al., 1998).

5.1.2 Amidases in other organisms

Cyanobacterium Anabaena PCC 7120 a filamentous, photosynthetic prokaryotic organism, which forms specialised cells, called heterocysts from vegetative cells (Berendt et al., 2012). Heterocysts are nitrogenase containing cells, which are responsible for filamentous nitrogen assimilation (Berendt *et al*., 2012). These cells are morphologically different from vegetative cells, as they possess a thick PG layer to allow for protection of oxygen sensitive nitrogenases from the O_2 produced by vegetative photosynthetic cells (Berendt *et al*., 2012). Heterocyst formation is tightly regulated to ensure the formation of a single heterocyst for every 10 to 20 vegetative cells (Berendt et al., 2012, Golden and Yoon, 2003). Deletion of amidases in these organisms resulted in a reduction in the amount of heterocyst cells formed (Berendt et al., 2012). This led to the hypothesis that amidases are required to actively remodel the PG layer resulting in the formation of the thick-walled conformation. Further research, however, uncovered another role for the *C. anabaena* amidase, wherein it was demonstrated that this amidase plays an important role in the formation and maturation of septal pores, which allow for exchange between adjacent cells (Zheng et al., 2017). Deletion of this amidase resulted in the formation of pores which are smaller in diameter possibly limiting the movement specific elements (Zheng et al., 2017). This exchange could include intercellular markers, which target specific cells for heterocyst formation and reduction in the movement of these markers could reduce the amount of heterocysts formed. This hypothesis requires further investigation.

5.1.3 Amidase response to host immune associated stress

The constant remodelling associated with PG results in the release PG breakdown products, which can be used by neighbouring cells for various purposes including metabolism and as signalling

molecules (Shah et al., 2008, Goodell, 1985). With regards to signalling, PG is important in inducing certain immune responses during infection (Takeda and Akira, 2005). This is discussed in further detail below.

5.1.3.1 *Why bacteria release PG fragments?*

Muropeptides are strong inducers of the immune system. However, these molecules also have an important role in bacterial signalling (Shah et al., 2008, Nikitushkin et al., 2013). The release of muropeptides can occurs as a by-product of active bacterial growth. As such, these molecules can be used by non-replicating organisms as cues to signal the presence of growth permissive conditions (Shah et al., 2008, Nikitushkin et al., 2013). In *B. subtilis* it has been shown that muropeptides have the capacity to induce the germination of dormant spores (Shah et al., 2008). This capacity was only present when the muropeptide possessed a three or more amino acid stem peptide, with the *meso*-DAP being the third amino acid (Shah et al., 2008). Treatment of these muropeptides with cell wall amidases eliminated the ability to induce germination, indicating that amidase activity, as is the case with the host immune system, is important for modulating the stimulatory properties of muropeptides (Shah et al., 2008). The mechanism, in this case, involves signalling through serine threonine protein kinases. It is also possible that a similar phenomenon occurs through the function of lytic transglycosylase like proteins, resuscitation promoting factors (Rpfs), which are required for muropeptide formation, in combination with an endopeptidase RipA (Mukamolova et al., 2006, Cohen Gonsaud et al., 2005, Nikitushkin et al., 2013). Though mycobacteria do not form dormant spores, they have been shown to possess the capacity to enter a state of non-culturability (Parrish et al., 1998, Wayne, 1994). It is widely thought this ability may contribute to the establishment of latent TB infection, thus helping the organism persist under hostile conditions (Parrish et al., 1998, Wayne, 1994, Barry et al., 2009). However, it is emerging that latent TB infection is characterised by a dynamic immune response, suggestive of a similarly dynamic underlying bacterial population (Barry et al., 2009, Russell et al., 2009). Various studies have demonstrated that Rpfs play an important role in the growth stimulation of viable but non-culturable bacteria (Nikitushkin et al., 2013, Kana et al., 2008, Russell-Goldman et al., 2008, Downing et al., 2005, Tufariello et al., 2006). The ability of muropeptides to stimulate the growth of non-replicating mycobacteria has been tested, with equivocal results, suggesting that an alternate mechanism may prevail in these organisms (Nikitushkin et al., 2013, Mir et al., 2011).

5.1.3.2 *Host responses to PG*

As PG is unique to bacteria, eukaryotic hosts have developed various mechanisms to identify organisms possessing this structure in order to detect possible invasion by bacteria (Palaniyar et al., 2010). Two main pathways are important for this, including the TLR and nucleotide-binding oligomerisation domain (Nod) system. Both are constituents of the innate immune response (Takeda and Akira, 2005). The TLR system consists of various cytoplasmic and cell membrane bound receptors tasked with the responsibility of identifying various foreign components, ranging from cellular organelles to RNA (Takeda and Akira, 2005). This comprises 11 receptors containing two domains an external TLR domain and an Internal Toll/IL-1 receptor (TIR) domain (Takeda and Akira, 2005). The TLR domain is the primary ligand binding component, which associates with different elements including PG, this leads to the activation of the TIR domain, resulting in a signalling cascade that induces a response (Takeda and Akira, 2005, Takeuchi et al., 2000). In the case of PG, it has been shown TLR2 is an important receptor for binding. Binding of PG to TLR2 leads to TIR domain activation, resulting in the recruitment TIR domain-containing adaptor protein (TIRAP), which in-turn recruits MyD88 (Yamamoto et al., 2002). MyD88 then binds interleukin-1 receptor-associated kinase - 4 (IRAK-4) (Takeda and Akira, 2005). IRAK–4 phosphorylates IRAK – 1, which associates with tumor necrosis factor receptor-associated factor 6 (TRAF6), resulting in the activation of two distinct signalling pathways. The first involves activation of AP-1 transcription factors through the activation of MAP Kinases and second involves activation of the TAK1/TAB complex (Takeda and Akira, 2005, Gray et al., 2006). Activation of TAK1/TAB complex leads to enhanced IκB Kinase (IKK) complex activity, which phosphorylates IκB, leading to subsequent degradation (Takeda and Akira, 2005, Gray et al., 2006). This results in the release and nuclear translocation of NF-κB transcription factors and subsequent transcription of pro-inflammatory cytokines such as TNF-α and IL-12 (Gray et al., 2006). This mechanism is illustrated in Figure 5.2. In Drosophila, some of the TLR2 activated NF-κB factors include Dif and Dorsal, which induce the expression of antimicrobial peptides that target fungal and bacterial organisms (Lemaitre et al., 1997).

The second system that utilises the identification of PG derivatives as indicators of bacterial invasion is the Nod system. Nod recognizes the presence of cytoplasmic muropeptides as an indicator of bacterial invasion. It consists of two essential elements Nod1 and Nod2, which recognize different muropeptide structures (Inohara et al., 2003, Girardin et al., 2003b, Girardin et

al., 2003a, Chamaillard et al., 2003). Nod1 recognizes muropeptides containing a minimum of three peptides on the stem peptide with the third peptide being a Meso-Dap subunit while Nod2 recognizes a stem peptide containing 2 peptides (Inohara et al., 2003, Girardin et al., 2003a, Chamaillard et al., 2003, Coulombe et al., 2009, Girardin et al., 2003b).

Muropeptides binding to either Nod1/Nod2 induce oligomerisation of Nod proteins resulting in the recruitment of the serine/threonine kinase RICK (Kanneganti et al., 2007, Inohara and Nunez, 2003). This in turn results in the recruitment of the IKK complex, which subsequently phosphorylates IκB leading to subsequent degradation (Kanneganti et al., 2007). IκB degradation results NF-κB translocation and subsequent gene expression (Takeda and Akira, 2005, Deshpande et al., 1997, Gerondakis et al., 1999). In this case, NF-κB Relish is activated and leads to the transcription of antimicrobial agents such a diptericin (Lemaitre et al., 1997). The overall mechanism is shown in Figure 5.2.

Both the Toll and Nod systems are central to induce an immune response and as with all immune responses, these systems require careful regulation (Fukata et al., 2009). In light of this, eukaryotic organisms have developed mechanisms to regulate the level of PG mediated immune induction through the modification of the PG ligands. This is achieved by a class of eukaryotic proteins called PG recognition proteins (PGRPs) (Palaniyar et al., 2010, Dziarski, 2004). PGRPs are a group of proteins that have the ability to bind to bacterial PG (Dziarski, 2004, Palaniyar et al., 2010). These are essential for various cellular processes including phagocytosis, activation of Toll-mediated immune response, antimicrobial activity and reduction of PG mediated pro-inflammatory response (Dziarski, 2004, Palaniyar et al., 2010). The regulatory capacity of these proteins is due to the function of eukaryotic PG amidases, found in both vertebrate and invertebrate organisms (Palaniyar et al., 2010, Dziarski, 2004). Similar to the counterparts found in bacteria, these enzymes act by cleaving the stem peptides from PG, thus rendering the ligand inept, inactivating PG mediated pro-inflammatory responses (Palaniyar et al., 2010, Dziarski, 2004).

With the evolution of muropeptide directed immune responses, pathogenic bacterial have developed countermeasures to evade these systems. These mainly include the modification of the glycan backbone of PG such as, glycolylation and deacetylation of the sugars and modification of the stem peptide, primarily the substitution of specific amino acids (Humann and Lenz, 2009). The

role that amidases play in this process is not clear though they have been found to be essential for pathogenesis in various species such as *Neisseria gonorrhoeae* and *Helicobacter pylori*, where deletion of these enzymes resulted in reduced pathogenicity (Chaput et al., 2006, Garcia and Dillard, 2008, Melly et al., 1984). Furthermore, transposon mutagenesis of Ami1 in Mtb resulted in a dissemination defect, localizing the infection to the lungs (Sassetti and Rubin, 2003).

The role of mycobacterial PG associated enzymes in the ability to adapt to changes in the environment is currently limited with anecdotal evidence provided by the ability of Rpfs to respond to stressful conditions during reactivation of infection in mice (Tufariello et al., 2006). The role of Mtb amidases in any of these processes is also currently unknown. Here, we assess the role of the Mtb amidases, Ami1and Ami4, in growth, cell division and bacterial responses to environmental stress. We chose Ami1 as it was the direct counterpart of Ami1 in *M. smegmatis* and was demonstrated to be important in cell division. Attempts to generate an ami2 knockdown in Mtb were fraught with challenges and due to time limitations, this was not pursued further. Upon surveying the literature Ami4 emerged as an enzyme that would potentially be important in responding to stress conditions, as it was identified through transposon mutagenesis as 1 of 18 proteins important for tolerance to reactive oxygen species (Mestre et al., 2013). Hence, we selected this enzyme for further study.

Hypothesis: As with *M. smegmatis*, Ami1 in Mtb plays and important role in cell division and deletion thereof will result in growth and morphological defects. Deletion of *ami4* will result in reduce the ability of the tubercle bacillus to respond to stress.

Preliminary work prior to this PhD. Vectors for deleting *ami1* and *ami4* in Mtb were constructed and confirmed by M. Chengalroyen.

Aims and objectives: The main aim of this section was to construct and characterise mutants of Mtb that were defective for Ami1 and Ami4. Given limited time, what follows herein is a prelimenary characterisation of these enzymes in Mtb. The specific objective included:

1. Confirmation of existing knockout vectors.
2. Construction and confirmation of *ami1* and *ami4* deficient strains, H37Δ*ami1*S and H37Δ*ami4*S.
3. Construction and confirmation of *ami1* and *ami4* complementation vectors, pAmi1TB and pAmi4TB.
4. Genetic complementation of H37Δ*ami1*S and H37Δ*ami4*S using pAmi1TB and pAmi4TB vectors, respectively.
5. Characterisation of growth of amidase deficient strains in rich and minimal media. Growth was also conducted under stress conditions.
6. Elucidating antibiotic susceptibility the H37Δ*ami1*S and H37Δ*ami4*S strains.
7. Elucidating the survival of H37Δ*ami1*S and H37Δ*ami4*S strains in macrophages.

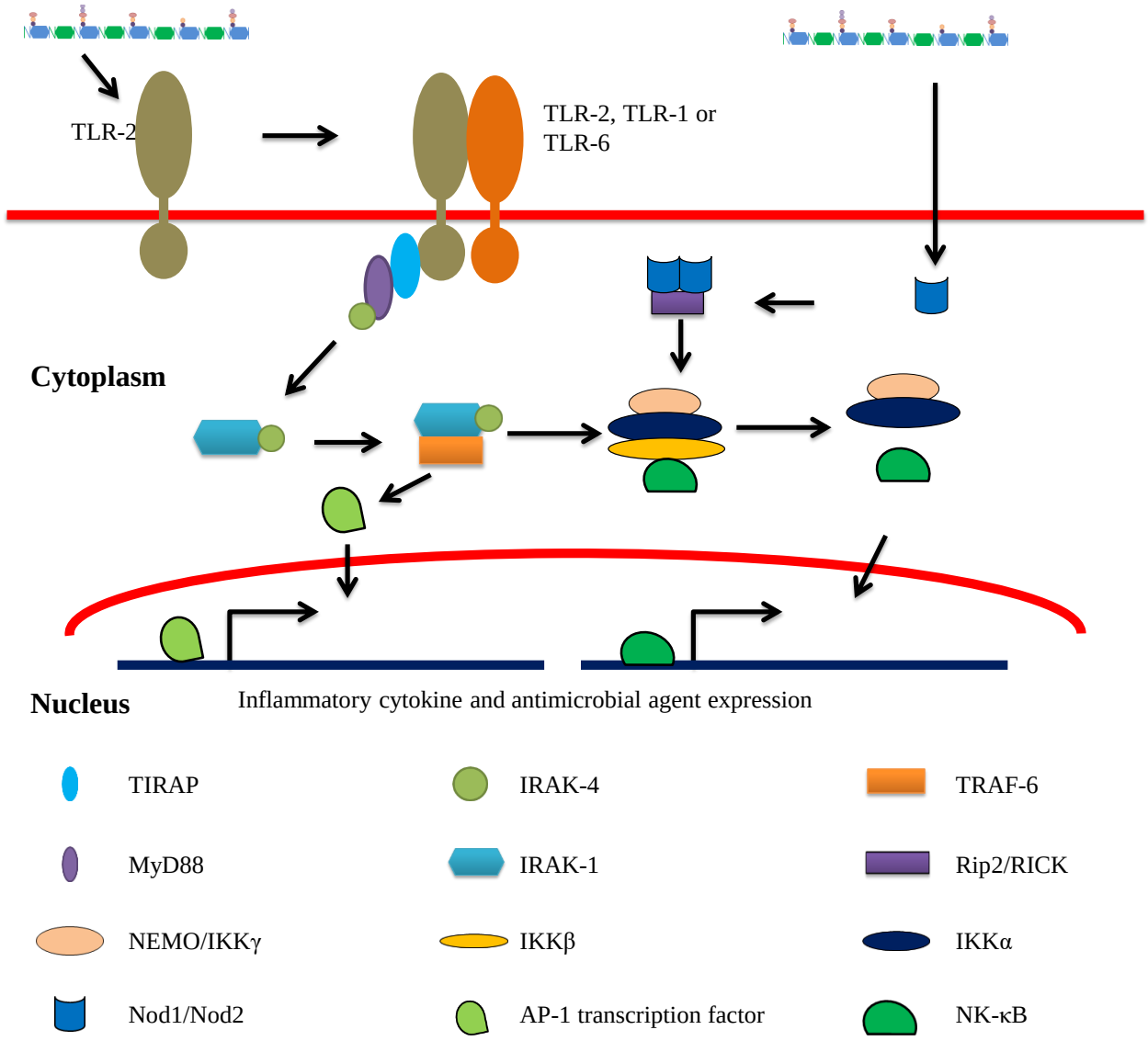

Figure 5.2: Diagrammatic representation of both the Toll and Nod PG-mediated immune responses. Shown is the stepwise progression of the cascade from ligand binding to cytokine expression (adapted from Inohara and Nunez, 2003, Takeda and Akira, 2005). Figure drawn by S. Senzani.

5.2 Methods

5.2.1 Bacterial Strains, vectors and primers

All the bacterial strains, vectors and primers used and/created in this study are listed on Table 5.1, Table 5.2 and Table 5.3, respectively.

Table 5.1: Bacterial strains created/used in this study

Strain	Genotype	Reference
Escherichia coli DH5α	*SupE44 ΔlacU169 hsdR17 recA1 endA1 gyrA96 thi-1 relA1*	Promega, Madison, WI
H37RvS	Virulent laboratory isolate ATCC 25618	Laboratory Stock
H37Δ*ami1*S	Derivative of H37RvS carrying an unmarked, in-frame deletion in *ami1,* containing 96 bp of the 5′ and 78 bp 3′ regions, lacking 551 bp of the *ami1* gene	This Study
H37Δ*ami1*S::pAmi1TB	Derivative of H37Δ*ami1* carrying pAmi1TB integrated at the bacterial *attB* phage attachment site, Hyg^R	This Study
H37Δ*ami4*S	Derivative of H37RvS carrying an unmarked, in-frame deletion in *ami4,* containing 39 bp of the 5′ and 82 3′ regions, lacking 707 bp of the *ami4* gene	This Study
H37Δ*ami4*S::pAmi4TB	Derivative of H37Δ*ami4* carrying pAmi4TB integrated at the bacterial *attB* phage attachment site, Hyg^R	This Study

Kan^R: Kanamycin Resistance, Hyg^R: Hygromycin Resistance

Table 5.2: Vectors created and/or used in this study

Vectors	Genotype	Reference
p2H37ΔAmi1G17	Derivative of p2NIL carrying a truncated derivative of the H37RvS *ami1* gene and the *lacZ* and *sacB* genes from pGOAL17, Kan^R	M. Chengalroyen
pAmi1TB	Derivative of pMV306(H) carrying a functional H37RvS *ami1* gene and the upstream native promoter region Hyg^R	This study
p2H37ΔAmi4G17	Derivative of p2NIL carrying a truncated derivative of the H37RvS *ami4* gene and the *lacZ* and *sacB* genes from pGOAL17, Kan^R	M. Chengalroyen
pAmi4TB	Derivative of pMV306(H) carrying a functional H37RvS *ami4* gene and the upstream native promoter region Hyg^R	This study

Kan^R: Kanamycin Resistance, Hyg^R: Hygromycin Resistance, Amp^R: Ampicillin Resistance

Table 5.3: List of primers used in the Mtb, *ami1* study

Gene	primers	Amplicon
H37*ami1*pMVF	GCGCGCGCAAGCTTGCCATCTTCGTCACCTGC	1126 bp *ami1* amplicon including 400 bp upstream the *ami1* start codon
H37*ami1*pMVR	GCCGCCGCGTTAACCTAACGCGCCTGGCCCTG	
H37*ami4*pMVF	GCGCGCGCAAGCTTCGGCCTCGCCCGTCCGAC	1311 bp *ami4* amplicon including 400 bp upstream the *ami4* start codon
H37*ami4*pMVR	GCCGCCGCGTTAACCCGGTTGACATCGTTGCA	
H37*ami1*KOUSF	GTGAAGCTTGCCGCATTACCAGCTATGAC	1577 bp amplicon the 5′ region of the *ami1* gene and 96 bp of the *ami1* gene
H37*ami1*KOUSR	GTGTCTAGAGTCGATGAAGACGACCATGC	
H37*ami1*KODSF	GTGTCTAGACGAGGGCAGGCAAAAATAC	1579 bp amplicon the 3′ region of the *ami1* gene including 78 bp of the *ami1* gene
H37*ami1*KODSR	GTGGGTACCGCCATCAACCTCCAGTAGACA	
H37*ami4*KOUSF	GTGAAGCTTACCGGCAAGACTGCATAAC	1557 bp amplicon the 5′ region of the *ami4* gene and 39 bp of the *ami4* gene
H37*ami4*KOUSR	GTGTCTAGACACCTCCTCGAGCCAAATC	
H37*ami4*KODSF	GTGTCTAGACGAGCTCGGCAATAAGGTC	1530 bp amplicon the 3′ region of the *ami1* gene including 82 bp of the *ami1* gene
H37*ami4*KODSR	GTGGGTACCCGATCCGCTGTGACAATAGA	

*red: restriction endonuclease site

5.2.2 Construction of the H37Δ*ami1*S and H37Δ*ami4* strains

To construct the H37Δ*ami1*S and H37Δ*ami4* strains, the native *ami1* and *ami4* genes were deleted using homologues recombination. Using the p2H37ΔAmi1G17 and p2H37ΔAmi4G17 vectors generated previously, 1, 3 and 5 µg of DNA was electroporated into electrocompetent H37RvS cells and plated on 7H11 containing Kan and 0.004 % X-gal, then incubated at 37 ˚C for 6 weeks to create SCOs. A single blue colony per gene was then cultured in 7H9 supplemented with Kan at 37 ºC then sub-cultured in 7H9 without antibiotic. The resulting cells were subjected to sucrose counter selection by plating 100 µl of a 10-fold serial dilution series onto media containing sucrose and X-gal. The plates were incubated for 5 - 6 weeks until blue and white colonies emerged. White colonies represent strains that have undergone the second cross over event to yield either a reversion to wild type or a mutant strains and blue colonies represent strains, which have incurred a mutation in *sacB* to render them resistant to the toxic effects of sucrose. Subsequently, 10 white colonies were selected and colony boils and PCR were conducted on these using the H37*ami1*pMVF and H37*ami1*pMVR primers for *ami1* which would yield a 1126 bp band in the H37RvS strain and a 580 bp band in the H37Δ*ami1*S strain and H37*ami4*pMVF and

H37*ami4*pMVR primers for *ami4* which would yield a 1311 bp band in the H37RvS strain and a 580 bp band in the H37Δ*ami4*S strain.

5.2.3 Construction of the H37Δ*ami1*S::pAmi1TB and H37Δ*ami4*S::pAmi4TB strains

Primers were designed, H37*ami1*pMVF and H37*ami1*pMVR for *ami1* and H37*ami4*pMVF and H37*ami4*pMVR for *ami4*, listed in Table 5.3, to amplify the TB *ami1* and *ami4* genes respectively, as well as 400 bp upstream the transcriptional start codon. PCR amplification of the respective fragments was carried out using Phusion DNA polymerase, using an annealing temperature of 60 °C for *ami1* and an elongation time of 1 min to allow for complete amplification of both the *ami1*and *ami4* fragments. The PCR products were purified using the Nucleospin PCR purification Kit. Thereafter, 3 µg of pMV306 (H) and PCR product was then restricted with *Hind*III and *Hpa*I. The pMV306 (H) restriction product was then phosphatased using FastAP phosphatase for 30 min. The restriction products were separated on a 0.8 % agarose gel, the respective bands (4248 bp for pMV306 (H), 1102 bp for *ami1* and 1293 bp for *ami4*) were excised from the gel and purified using the Nucleospin gel purification kit. These were then quantified using the NanoDrop spectrophotometer and ligations were set up containing 50 ng of pMV306 (H) and varying molar ratios of the amidase fragments. The fragments were ligated using Fermentas T4 ligase for 1 h, transformed into DH5α cells and plated on LA_{Hyg200}. Following this, five possible clones per gene were selected and screen by restriction digest with *Bam*HI, which would yield two fragments, a 3560 bp and a 1822 bp band for pAmi1TB and a 3560 bp and a 1822 bp band for pAmi4TB. A single positive clone was selected, grown in 50 ml LB_{Hyg200} overnight and bulk vector extraction was carried out using the Nucleobond bulk vector extraction kit. Vector DNA was quantified and digested with a variety of enzymes to profile the amidase complementation constructs, then the vectors were sent for sequencing to check for the presence of mutations within the amplicon. The pAmi1TB and pAmi4TB vectors were electroporated in the H37Δ*ami1*S and H37Δ*ami4*S strains respectively, 10 colonies were selected and PCR was conducted on these using the H37*ami1*pMVF and H37*ami1*pMVR primers which would yield a 1126 bp band representing the presence of a full length *ami1* gene and the H37*ami4*pMVF and H37*ami4*pMVR primers which would yield a 1311 bp band representing the presence of a full length *ami4* gene.

5.2.4 Bacterial survival in macrophages

5.2.4.1 *Culturing of J774 Mouse macrophage cells*

A single 1 ml frozen stock of J774 cells was thawed at room temperature and inoculated in 20 ml macrophage media consisting of 10 % Fetal Bovine Serum (FBS) in Dulbecco's Modified Eagle's Medium (DMEM). The cells were then harvested through centrifugation at 200 × g for 10 min. Thereafter, they were gently resuspended in 500 µl fresh media and inoculated into 10 ml of fresh media in a 50 ml cell culture flask and incubated at 37 ˚C in 5 % CO_2 for 4 h. The media was then discarded and replaced with 10 ml fresh media and incubated overnight. The attached macrophage population was assessed daily using an inverted microscope and the media was replaced until the macrophage cell completely covered the bottom of the cell culture flask.

Once the culture was ready, the media was discarded and the attached cells were washed with 10 ml cold PBS. A 2 ml aliquot of accutase was added to the cells and this was incubated at 37 ˚C for 5 min to allow the cells to detach. The cells were then dislodged by vigorously snapping the flask onto the palm of the hand four to five times. The suspension was then transferred into a fresh falcon tube, 10 ml of fresh DMEM was added to the flask, swirled and transferred into the cell suspension to remove remaining cells. The suspension was adjusted to 25 ml using fresh DMEM and the cells were harvested by centrifugation at 200 × g for 10 min. The cells were resuspended in 500 µl fresh DMEM, the volume was adjusted to 50 ml using and transferred into a 550 ml cell culture flask and incubated at the 37 ˚C for 4 h to allow for cell attachment. Thereafter, the media was discarded and replaced with 50 ml fresh media and incubated overnight. The attached macrophage population was assessed daily using an inverted microscope and the media was replaced daily until the macrophage cell completely covered the bottom of the cell culture flask.

5.2.4.2 *Preparing plates for infections*

Once the macrophage culture was ready the media was discarded and the cells were washed with 20 ml cold PBS, harvested as before and the 500 µl final cell suspension was then placed on ice. A 2 µl aliquot of the cell suspension was inoculated into 98 µl of 0.4 % trypan blue solution. A 10 µl aliquot of this solution was then spotted on a hemocytometer and unstained cells were counted, these represented viable macrophage cells. The concentration of viable cells was calculated using the following equation:

$$\text{Number of cells/ml} = \text{Number of viable cells} \times 5 \times 10^5$$

The cell suspension concentration was then adjusted to make a 1×10^5 cells/ml suspension using fresh DMEM and 1 ml of this was inoculated into 24 well tissue culture plates and incubated at 37 ˚C overnight.

5.2.4.3 *Macrophage infections*

Bacterial cells were grown to an OD_{600} of 0.5, which approximates to a concentration 5×10^8 CFU/ml. using this as a framework, bacterial cells were adjusted to 5×10^5 CFU/ml using fresh DMEM media and stored at room temperature. The 24 well plates were checked for macrophage attachment using an inverted microscope and if confluent, a 1 ml aliquot of the DMEM bacterial suspension was inoculated into the 24 well plates, in duplicate, per strain for each time point. Two samples per time point were inoculated with DMEM media to serve as the uninfected controls. These were incubated at 37 ˚C for 4 hours to allow for bacterial phagocytosis. The supernatant was then discarded, the cells were washed twice in PBS then, 1 ml fresh macrophage media was aliquoted into each well and incubated at 37 ˚C, sacrificing two wells per time point to determine bacterial survival.

5.2.4.4 *Determining bacterial survival through CFU calculation*

The macrophage supernatant was filtered in 0.2 µm filters and stored at – 80 ˚C for future analysis. The wells containing infected macrophages where then washed twice with PBS and lysed with 0.1 % SDS in PBS. A serial dilution of the lysate was conducted from 10^{-1} to 10^{-4} and plated on 7H11 media. This was incubated at 37 ˚C for four to five weeks. The same was conducted for the uninfected control to ensure macrophages were not contaminated.

5.2.5 Growth assays

A bacterial culture was grown to an OD_{600nm} of 0.5. This was then washed and re-suspended in 1 ml 7H9 containing ADS as a substitute for Middlebrook OADC. The cells were then diluted to a final OD_{600nm} of 0.005 in media and incubated at 37 ˚C. CFU analysis was then conducted 0 and 24 h post incubation.

Figure 5.3 illustrates the basic outline of the research undertaken in this chapter, with reference to the specific methods.

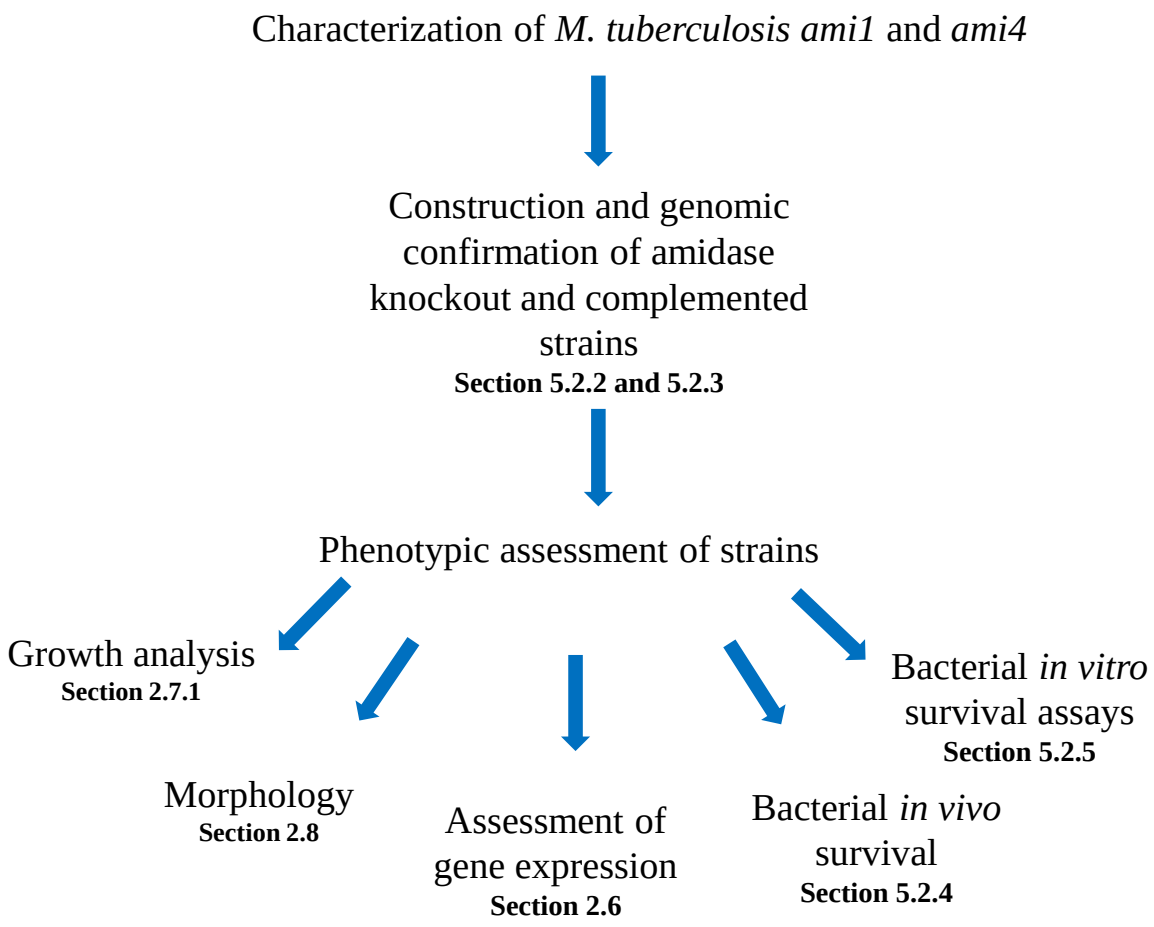

Figure 5.3: Flow chart depicting the experimental layout for the Mtb *ami1*and *ami4* research.

5.3 Results

5.3.1 Construction of the H37Δ*ami1*S strain

The p2H37ΔAmi1G17 and p2H37ΔAmi4G17 vectors obtained from Dr. M. Chengalroyen and extensive restriction profiling was conducted to ensure genetic integrity, Figure 5.4 and Figure 5.5.

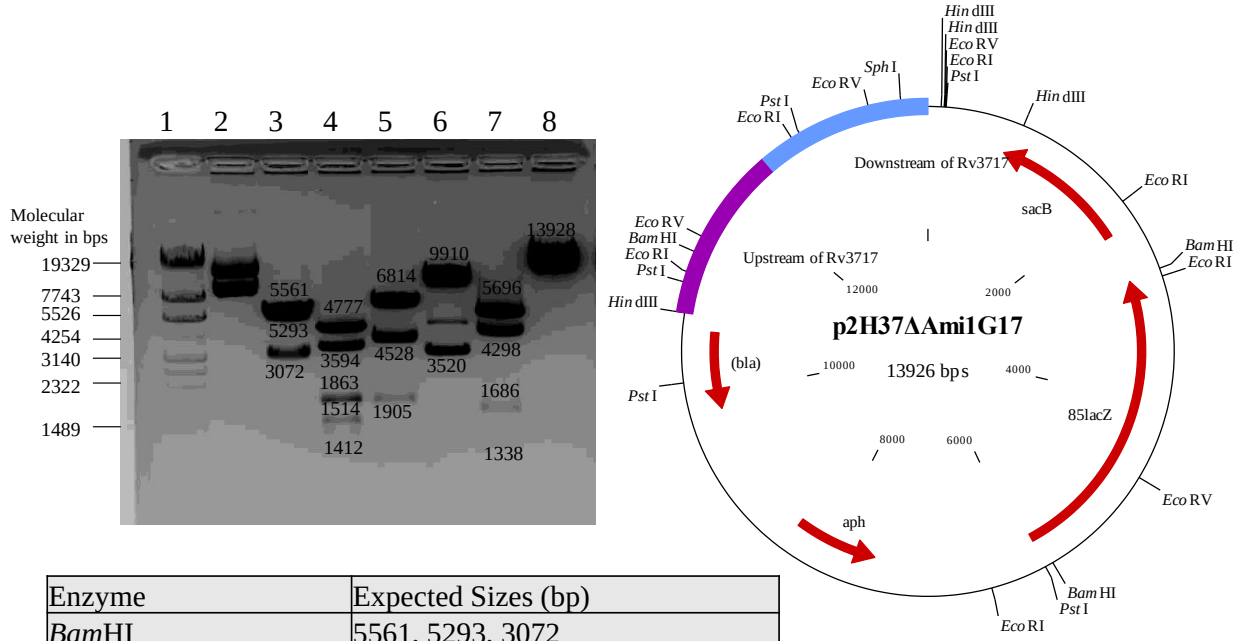

Enzyme	Expected Sizes (bp)
*Bam*HI	5561, 5293, 3072
*Eco*RI	4777, 3594, 1863, 1514, 1412, 766
*Eco*RV	6814, 4528, 1905, 679
*Hind*III	9910, 3250, 739, 27
*Pst*I	5696, 4298, 1686, 1338, 905
*Sph*I	13926

Figure 5.4: Restriction profile of p2H37ΔAmi1G17. Shown are the different restriction nucleases used and the expected sizes in a table, which result from restriction digests of the p2H37ΔAmi1G17 vector. The predicted vector map of p2H37ΔAmi1G17 vector and agarose gel depicting the products of restriction digest of p2H37ΔAmi1G17 are also shown. Lane 1: Roche Marker IV, Lane 2: Uncut, Lane 3: *Bam*HI, Lane 4: *Eco*RI, Lane 5: *Eco*RV, Lane 6: *Hind*III, Lane 7: *Pst*I, Lane 8: *Sph*I. Fragments below 1000 bp were difficult to visualise.

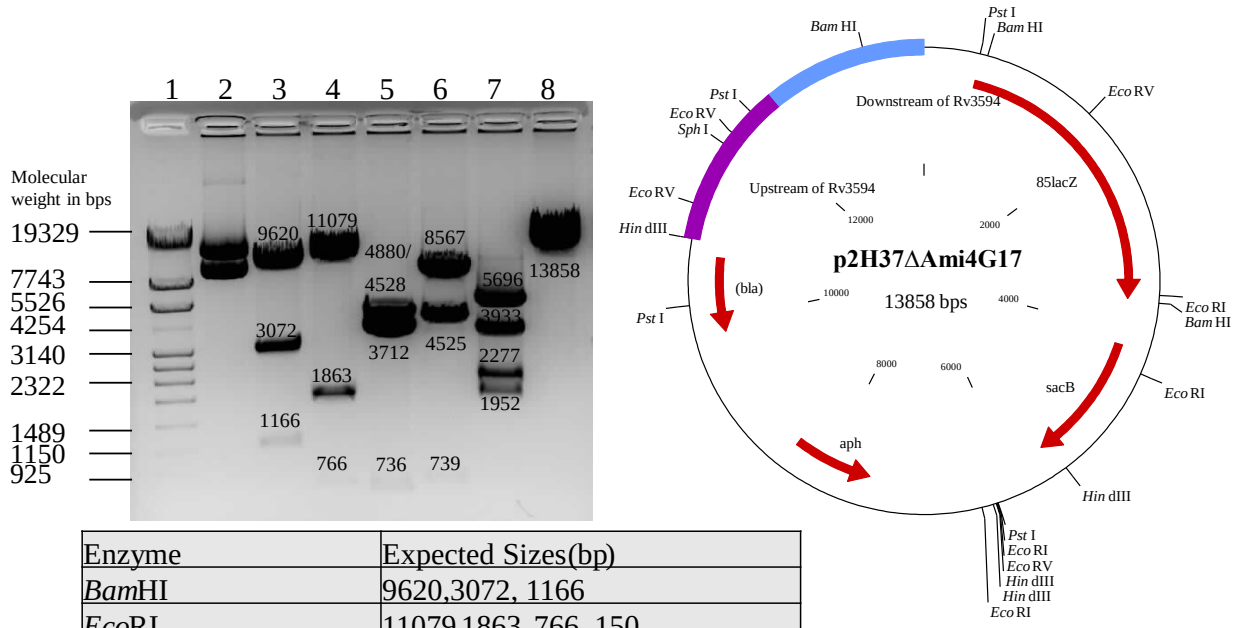

Enzyme	Expected Sizes(bp)
*Bam*HI	9620,3072, 1166
*Eco*RI	11079,1863, 766, 150
*Eco*RV	4880, 4528, 3712, 738
*Hind*III	8567, 4525,739, 27
*Pst*I	5696, 3933, 2277, 1952
*Sph*I	13858

Figure 5.5: Restriction profile of p2H37ΔAmi4G17. Shown are the different restriction nucleases used and the expected sizes in a table, which result from restriction digests of the p2H37ΔAmi4G17 vector. The predicted vector map of p2H37ΔAmi4G17 vector and agarose gel depicting the products of restriction digest of p2H37ΔAmi4G17 are also shown. Lane 1: Roche Marker IV, Lane 2: Uncut, Lane 3: *Bam*HI, Lane 4: *Eco*RI, Lane 5: *Eco*RV, Lane 6: *Hind*III, Lane 7: *Pst*I, Lane 8: *Sph*I. Fragments below 1000 bp were difficult to visualise.

In both cases, with p2H37ΔAmi1G17 and p2H37ΔAmi4G17 knockout vectors, all the expected sizes were observed upon restriction profiling. Hence, these vectors were electroporated into the H37RvS strain (section 2.4.2); the transformation efficiency obtained for the electro-competent cells was 4.9×10^5 CFU/µg vector DNA determined using the pSE100 control. A single blue clone (SCO strain) was cultured and subjected to sucrose counter selection (section 5.2.2). White colonies were then screened by PCR to identify clones which possess only the deleted allele, and then Southern blot analysis was conducted to confirm the second homologous event removed the wild type allele without imposing additional unintended chromosome rearrangements, Figure 5.6 and Figure 5.7).

5.3.2 Complementation of the H37Δ*ami1S* and H37Δ*ami4S* strains

The complementation of the H37Δ*ami1S* and H37Δ*ami4S* strains was conducted to serve as a control. These strains were used to show all phenotypic variations which arose in the

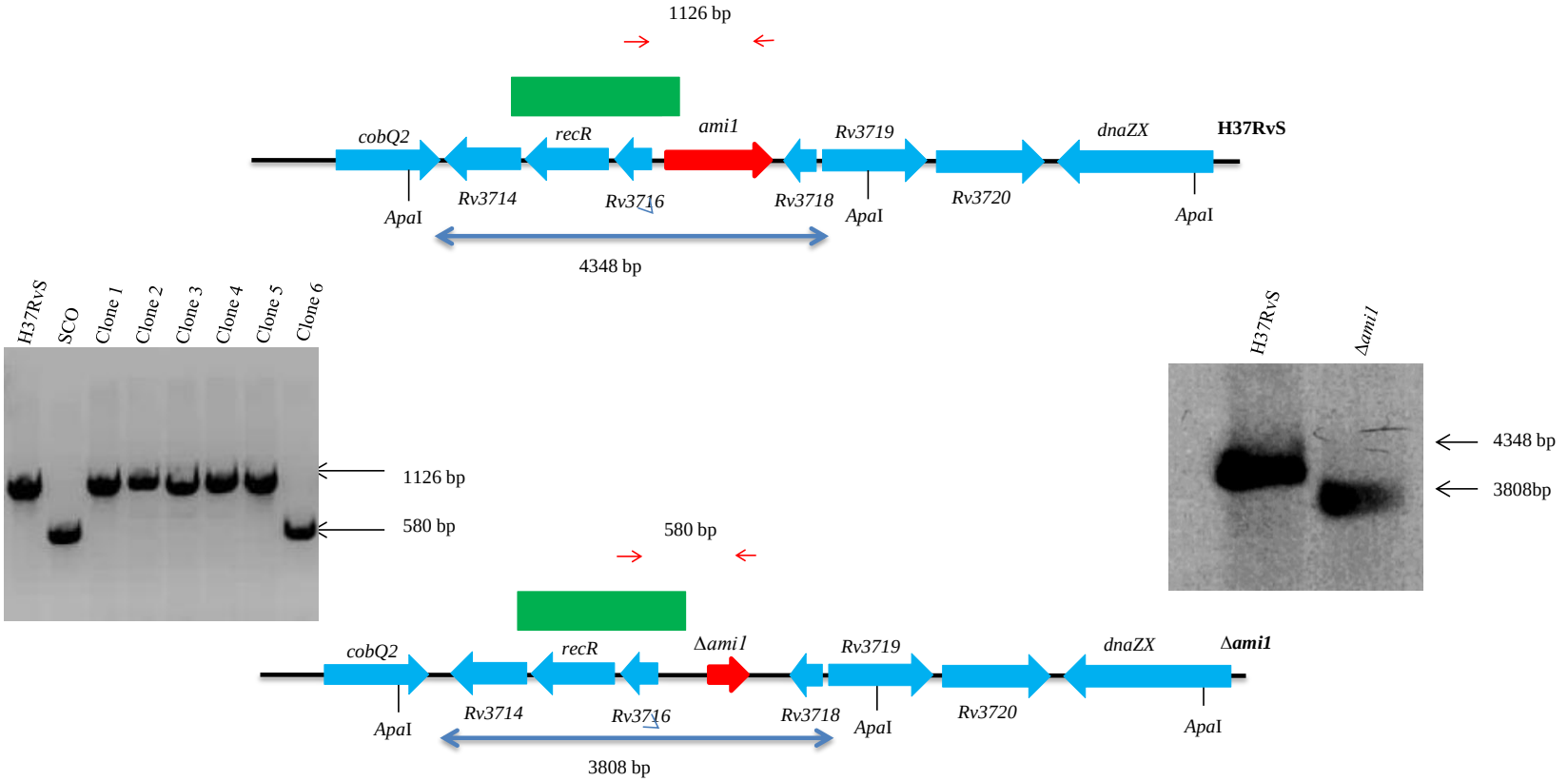

Figure 5.6: Genotypic analysis of the H37Δ*ami1*S strain by PCR and Southern blot analysis. The genomic map of the relevant locus is shown for the wild type mc^{2}155 and H37Δ*ami1*S strain. Also shown on the left is the PCR confirmation of the genotype and Southern blotting is shown on the right. For PCR confirmation, chromosomal DNA was used to amplify the *ami1* alleles from the wild type and mutant strains using the primers H37*ami1*pMVF and H37*ami1*pMVR described in Table 5.3 and indicated as red arrows above. The expected sizes of the amplicons are as follows: *ami1*, 1126 bp and Δ*ami1*, 580 bp. For the Southern blot analysis chromosomal DNA from the parental and mutant strain was digested with *Apa*I. The probe used for hybridisation is shown as a solid green box and the expected sizes are indicated by the blue arrows. The figures are not drawn to scale.

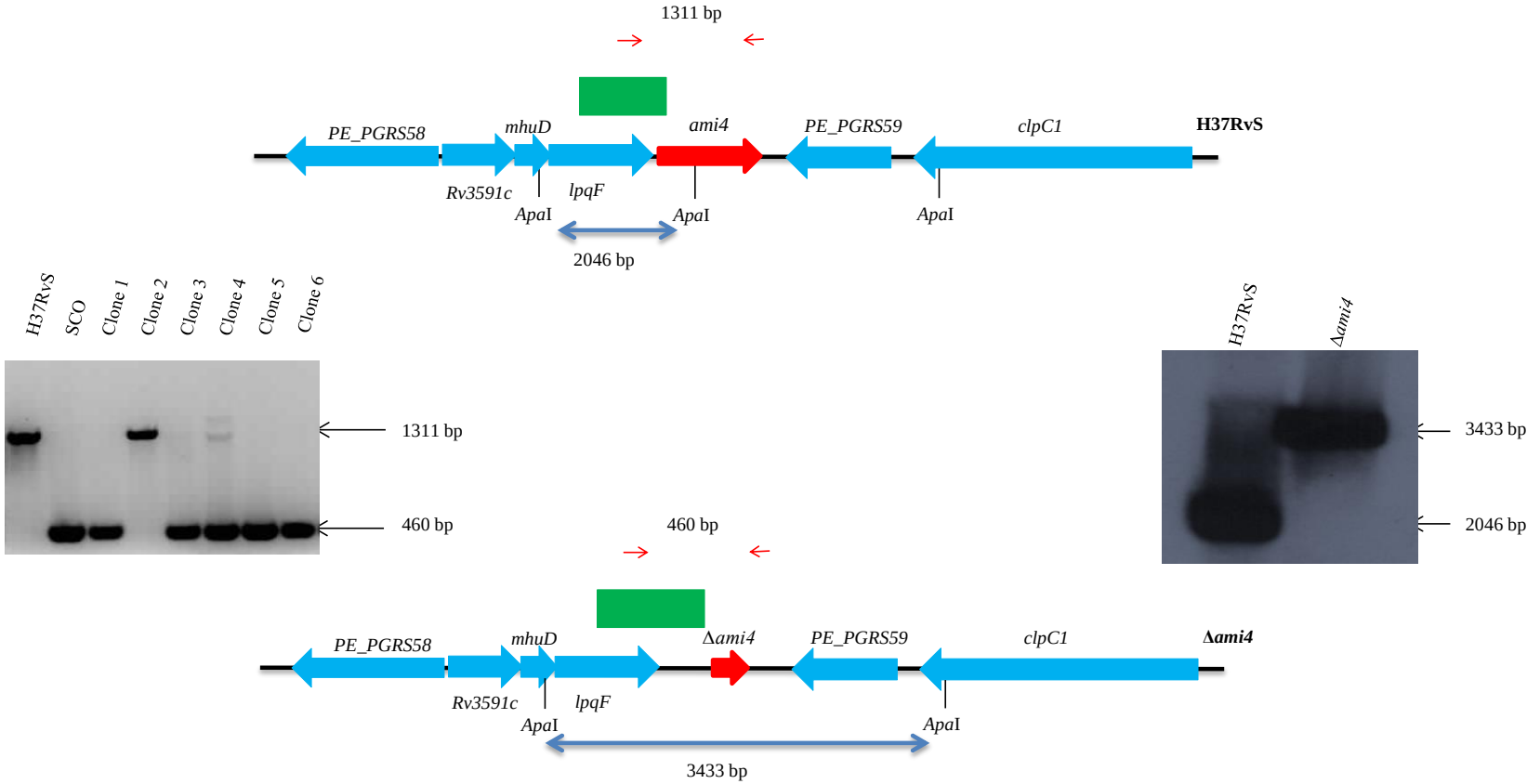

Figure 5.7: Genotypic analysis of the H37Δ*ami4*S strain by PCR and Southern blot analysis. The genomic map of the relevant locus is shown for the wild type mc^{2}155 and H37Δ*ami4*S strain. Also shown on the left is the PCR confirmation of the genotype and Southern blotting is shown on the right. For PCR confirmation, chromosomal DNA was used to amplify the *ami4* alleles from the wild type and mutant strains using the primers H37*ami4*pMVF and H37*ami4*pMVR described in Table 6.3 and indicated as red arrows above. The expected sizes of the amplicons are as follows: *ami4*, 1311 bp and Δ*ami4*, 460 bp. For the Southern blot analysis chromosomal DNA from the parental and mutant strain was digested with *Apa*I. The probe used for hybridisation is shown as a solid green box and the expected sizes are indicated by the blue arrows. The figures are not drawn to scale.

H37Δ*ami1S* and H37Δ*ami4S* strains can be reversed through the re-introduction of the full length amidase

5.3.2.1 *Construction of the pAmi1TB and pAmi4TB vectors*

PCR amplification was conducted to amplify the amidase genes and 400 bp upstream the transcriptional start codon. The fragments were then cloned into pMV306 (H) and clones were screened by restriction with *Bam*HI. A single positive clone was then selected and the genetic integrity of the vector was confirmed by extensive restriction profiling (Fig 5.8 and Fig 5.9).

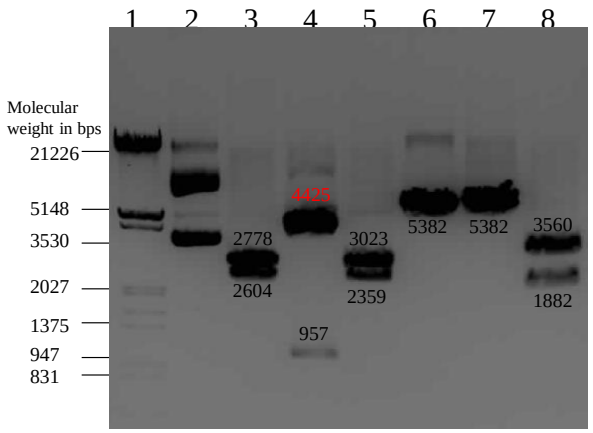

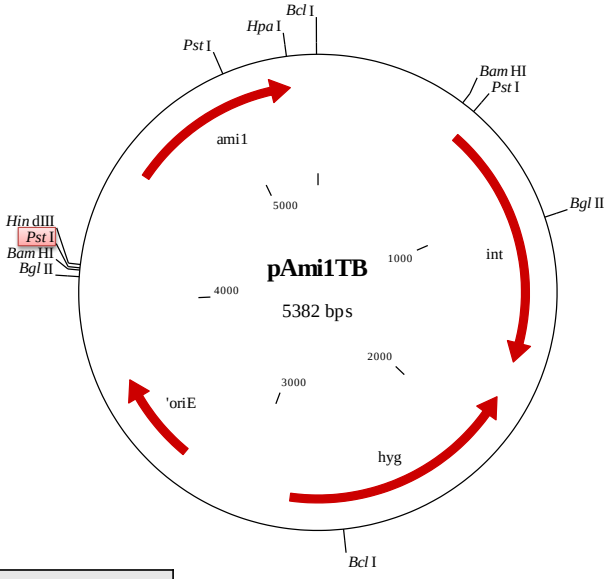

Enzyme	Expected Sizes (bp)
*Bcl*I	2778, 2604
*Pst*I	3518, 957, 907
*Bgl*I	3023, 2359
*Hind*III	5382
*Hpa*I	5382
*Bam*HI	3560, 1882

Figure 5.8: Restriction profile of pAmi1TB. Shown are the different restriction nucleases used and the expected sizes in a table, which result from restriction digests of the pAmi1TB vector. The predicted vector map of pAmi1TB vector and agarose gel depicting the products of restriction digest of pAmi1TB are shown. Lane 1: Roche Marker III, Lane 2: Uncut, Lane 3: *Bcl*I, Lane 4: *Pst*I, Lane 5: *Bgl*II, Lane 6: *Hind*III, Lane 7: *Hpa*I, Lane 8: *Bam*HI.

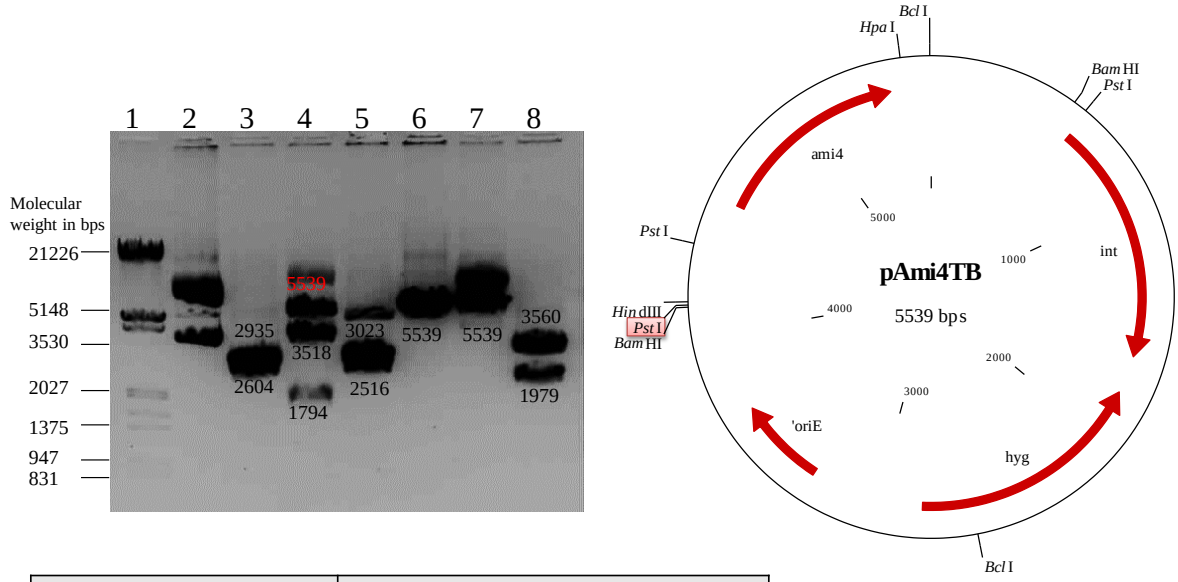

Enzyme	Expected Sizes (bp)
*Bcl*I	2935, 2604
*Pst*I	3518, 1794, 227
*Bgl*I	3023, 2516
*Hind*III	5539
*Hpa*I	5539
*Bam*HI	3560, 1979

Figure 5.9: Restriction profile of pAmi4TB. Shown are the different restriction nucleases used and the expected sizes in a table, which result from restriction digests of the pAmi4TB vector. The predicted vector map of pAmi4TB vector and agarose gel depicting the products of restriction digest of pAmi4TB are also shown. Lane 1: Roche Marker III, Lane 2: Uncut, Lane 3: *Bcl*I, Lane 4: *Pst*I, Lane 5: *Bgl*II, Lane 6: *Hind*III, Lane 7: *Hpa*I, Lane 8: *Bam*HI.

In all cases, the fragment sizes observed corresponded to the vector map and expected sizes, with the exception of the *Pst*I in which case the 905 bp band in pAmi1TB was missing while the 3518 bp band in both the pAmi1TB and pAmi4TB vectors was bigger. This was mapped back to a mutation in the *Pst*I next to the *oriE* resulting in a loss of the restriction (Fig 5.8 and Fig 5.9). The genetic integrity of the vector was then further confirmed by sequencing of the cloned region, which revealed that no mutations had occurred during PCR and cloning processes (data not shown). This vector was then used for construction of the H37Δ*ami1*S::pAmi1TB and H37Δ*ami4*S::pAmi4TB strains as previously described.

5.3.3 Deletion of Ami1 or Ami4 does not affect bacterial growth in nutrient rich media

To assess the role of Ami3 and Ami4 on bacterial growth, growth kinetics analysis was conducted on the H37RvS, H37Δ*ami1*S, H37Δ*ami1*S::pAmi1TB, H37Δ*ami4*S and H37Δ*ami4*S::pAmi4TB strains in Middlebrook 7H9, Figure 5.10. No Significant difference

was observed in the growth kinetics of the amidase deficient strains, when compared to the parental strain, similar to observations in broth culture upon deletion of *ami1* in *M. smegmatis*.

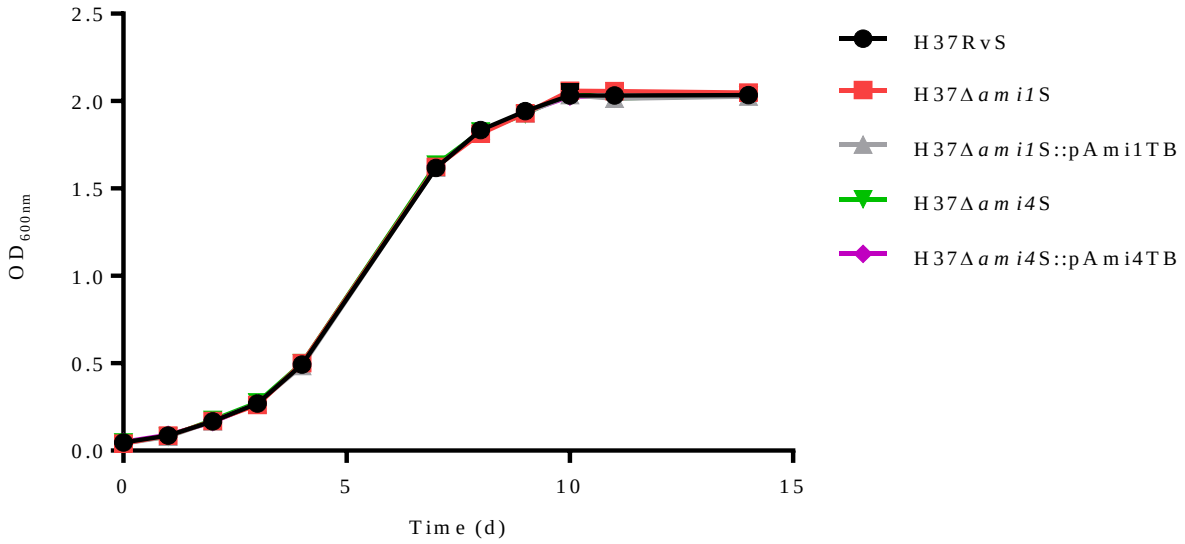

Figure 5.10: Growth analysis of H37RvS, H37Δ*ami1*S, H37Δ*ami1*S::pAmi1TB, H37Δ*ami4*S and H37Δ*ami4*S::pAmi4TB strains. Shown is the growth kinetics analysis of H37RvS, H37Δ*ami1*S, H37Δ*ami1*S::pAmi1TB, H37Δ*ami4*S and H37Δ*ami4*S::pAmi4TB in Middlebrook 7H9 containing Middlebrook OADC at 37 ˚C, assessed over 15 days. The data represent an average of three independent experiments.

Deletion of the *M. smegmatis ami1* gene resulted in a robust, detrimental impact on bacterial cell division. Thus, to determine whether the same occurs upon deletion of the Mtb homologs, SEM was conducted on the H37RvS, H37Δ*ami1*S, H37Δ*ami1*S::pAmi1TB, H37Δ*ami4*S and H37Δ*ami4*S::pAmi4TB strains, to elucidate whether deletion of *ami1* or *ami4* in Mtb resulted in similar defects to that observed in *M. smegmatis*, Figure 5.11A and Figure 5.11B.

SEM revealed no significant changes in bacterial cell division in the absence of either amidase, suggesting that these enzymes do not play a role in this process. Analysis of bacterial cell length revealed a general reduction in Mtb size when compared to *M. smegmatis*, observed in all the strains examined, with sizes ranging from 0.43 µm to 10.05 µm and a mean of ~ 3.5 µm, Figure 5.11B. No difference was observed between the sizes of the amidase deficient stains and wild type.

A

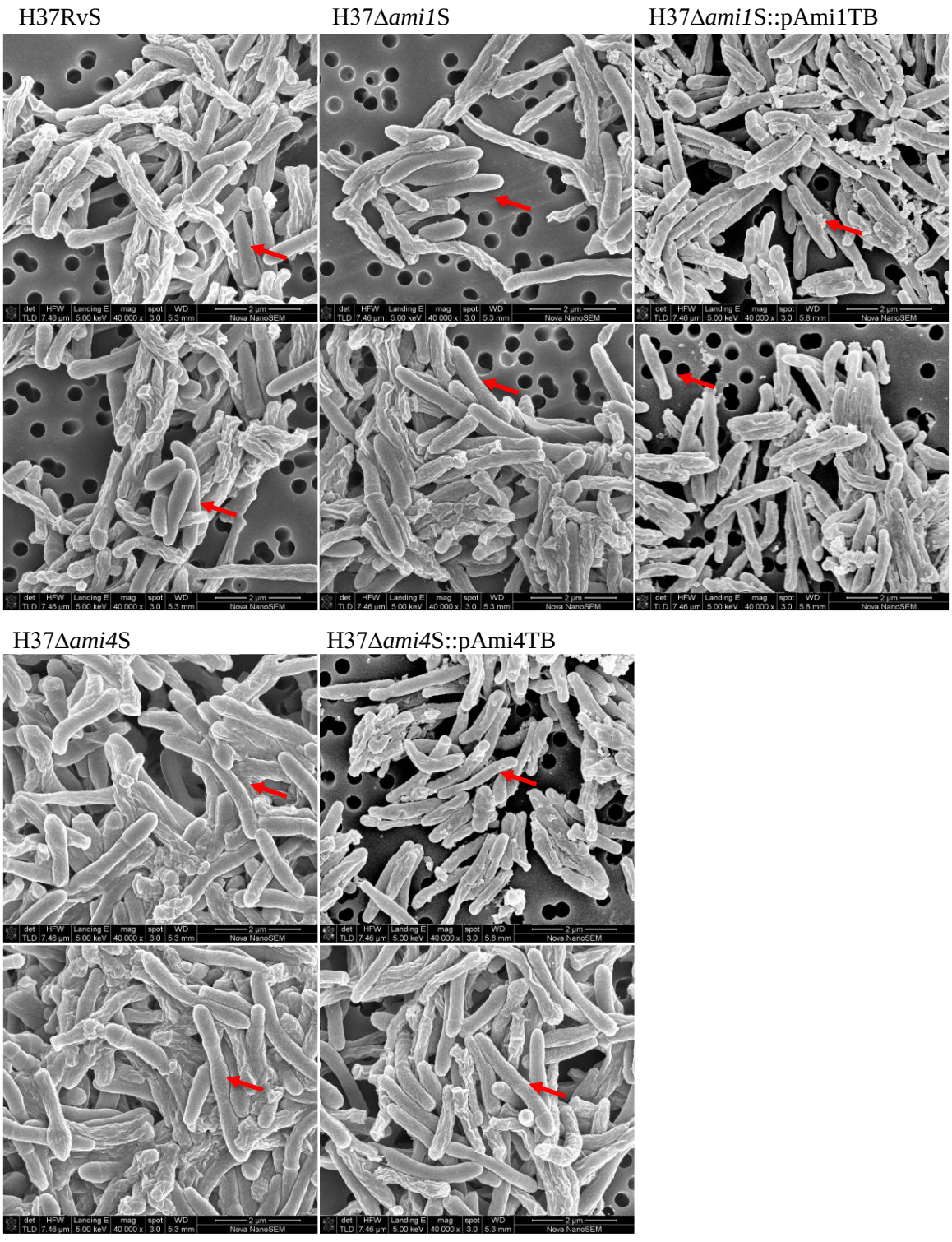
H37RvS
H37Δami1S
H37Δami1S::pAmi1TB
H37Δami4S
H37Δami4S::pAmi4TB

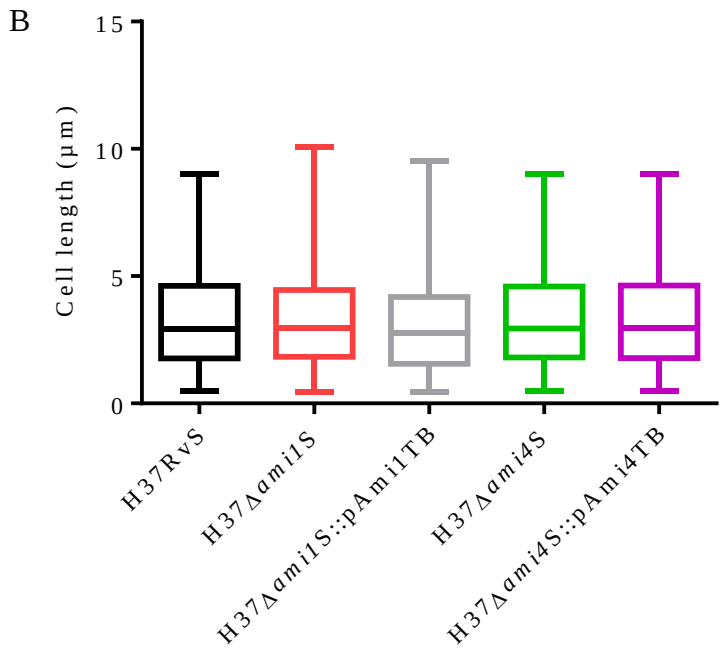

Figure 5.11: Microscopic analysis of the H37RvS, H37Δ*ami1*S, H37Δ*ami1*S::pAmi1TB, H37Δ*ami4*S and H37Δ*ami4*S::pAmi4TB strains. (A) Shown are SEM images of the H37RvS, H37Δ*ami1*S, H37Δ*ami1*S::pAmi1TB, H37Δ*ami4*S and H37Δ*ami4*S::pAmi4TB strains. Strains were grown in 7H9 to log phase then fixed, dehydrated, carbon coated and imaged using high resolution SEM, shown are normal Mtb cells depicted by the red arrows.. (B) Box-and-whisker analysis of the H37RvS, H37Δ*ami1*S, H37Δ*ami1*S::pAmi1TB, H37Δ*ami4*S and H37Δ*ami4*S::pAmi4TB strains, showing the various cell lengths of the respective strains generated approximately 300 cells per strain.

5.3.4 Ami1 plays a role in bacterial growth under nutrient starved conditions

As both Ami1 and Ami4 did not appear to play a significant role in cell division in Mtb, the role of these enzymes on bacterial growth under nutrient limited conditions was assessed. This was assessed through growth kinetic analysis in Sauton's and Modified *M. phlei* (MPL) media, which both utilise glycerol as the sole carbon source and ammonium and sodium nitrate as the sole nitrogen source, respectively (Fig 5.12).

In both cases, the H37Δ*ami1*S strain displayed retarded growth rate as well as a reduction in biomass in stationary phase. This phenotype was more severe in the MPL media. In the case of the H37Δ*ami4*S strain, however, no significant difference was observed in the growth kinetics of the H37Δ*ami4*S strain when compared to the parental strain in all conditions tested, suggesting Ami4 plays no role during bacterial growth, Figure 5.12. To further assess the defect in the *ami1* defective mutant, SEM was conducted to evaluate physiological changes which arise in the H37RvS, H37Δ*ami1*S, and H37Δ*ami1*S::pAmi1TB, Figure 5.13. The *ami4* defective strains were also included, Figure 5.13.

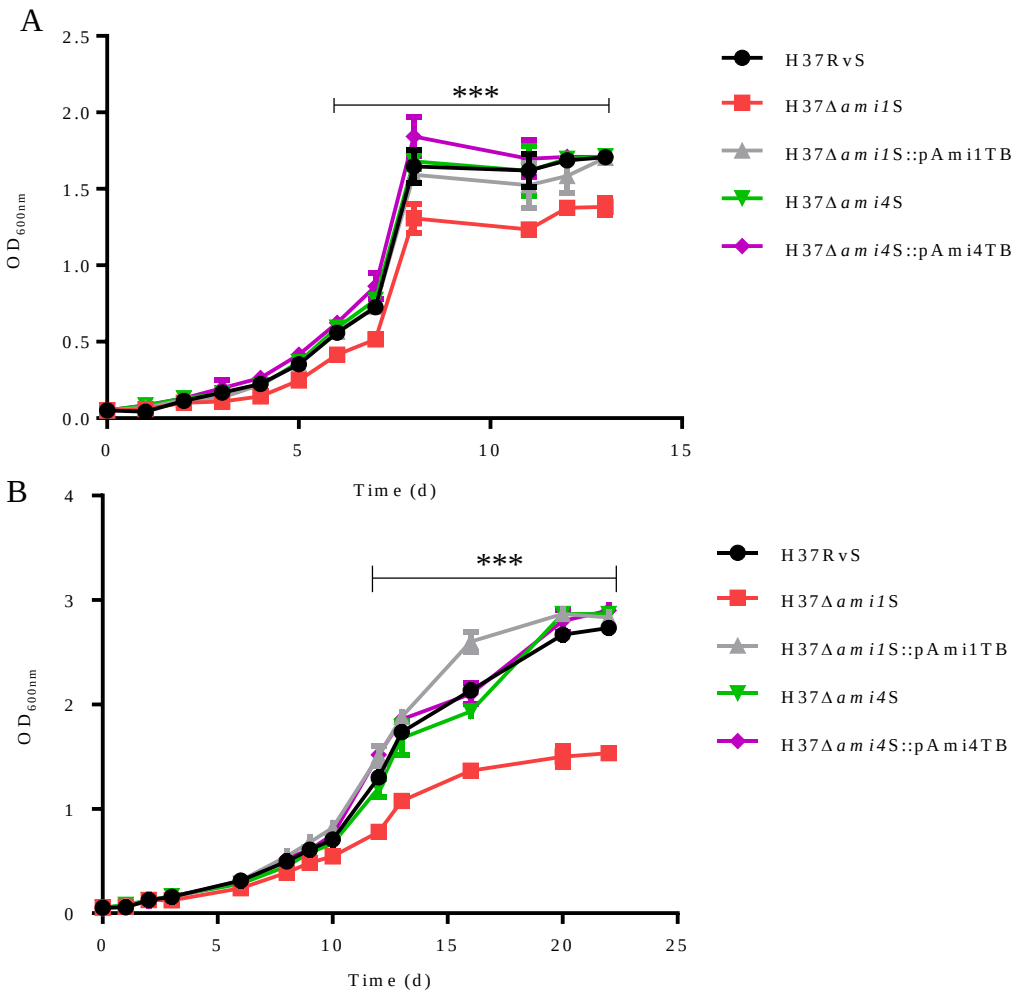

Figure 5.12: Growth analysis of H37RvS, H37Δ*ami1*S, H37Δ*ami1*S::pAmi1TB, H37Δ*ami4*S and H37Δ*ami4*S::pAmi4TB strains in Sauton's minimal media and MPL media. Shown is the growth kinetics analysis of H37RvS, H37Δ*ami1*S, H37Δ*ami1*S::pAmi1TB, H37Δ*ami4*S and H37Δ*ami4*S::pAmi4TB strains in Sauton's minimal media at 37 ˚C, assessed over 13 days (A) and MPL media over 23 days (B). Graphs represent 3 biological replicates. Statistical analysis was conducted comparing H37RvS and the H37Δ*ami1*S strains using the student *t*-test, ***: $p < 0.001$.

In the case of the H37Δ*ami1*S strain grown in MPL media, the formation of lateral branches similar to those observed in the *M. smegmatis* Δ*ami1* strain were observed, with 16.8 % of the population displaying this phenotype, Figure 5.13A and C. Analysis of bacterial cell length revealed a general increase in size when compared to strains grown in 7H9T, observed in all the strains examined, with sizes ranging from 2.01 µm to 10.69 µm and a mean of ~ 6 µm, similar to the size of *M. smegmatis* grown in 7H9T, Figure 5.13B. However, no differences in cell size were observed between the mutant strains and the wild type.

5.3.5 Ami1 and Ami4 play a role in bacterial tolerance to external stress

The role of Ami1 and Ami4 on bacterial tolerance to stress was analysed using two forms of stress, nitrosative and oxidative stress, using survival assays (Section 5.2.5). In the case of

A

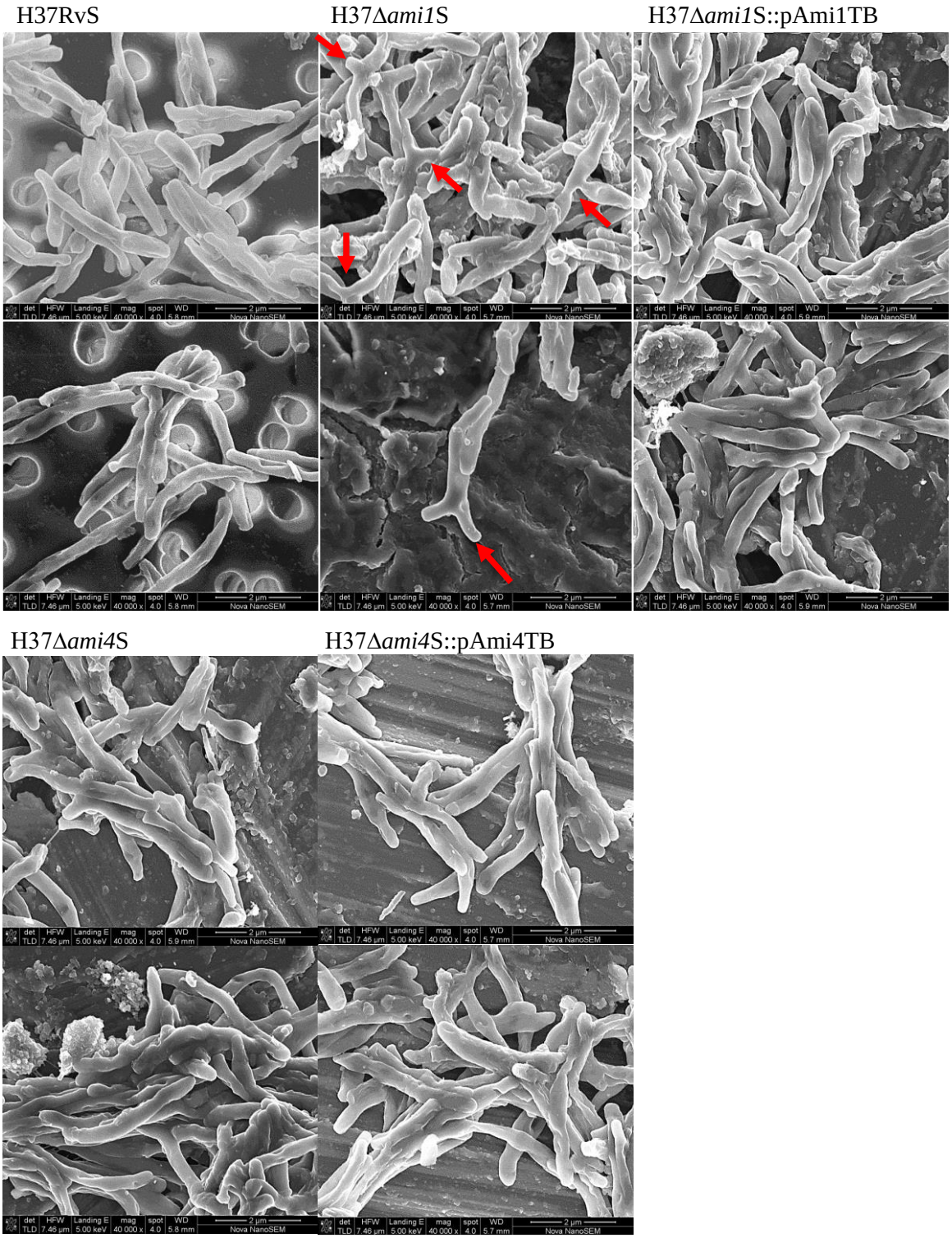
H37RvS
H37Δami1S
H37Δami1S::pAmi1TB
H37Δami4S
H37Δami4S::pAmi4TB

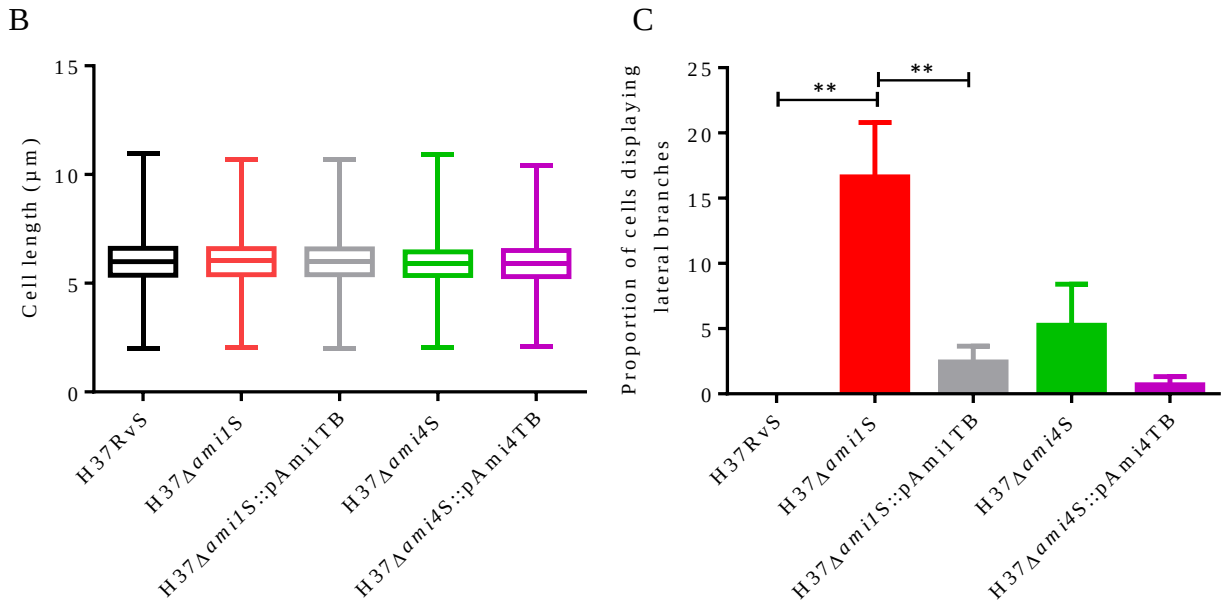

Figure 5.13: Microscopic analysis of MPL grown H37RvS, H37Δ*ami1*S, H37Δ*ami1*S::pAmi1TB, H37Δ*ami4*S and H37Δ*ami4*S::pAmi4TB strains. (A) Shown are SEM images of the H37RvS, H37Δ*ami1*S, H37Δ*ami1*S::pAmi1TB, H37Δ*ami4*S and H37Δ*ami4*S::pAmi4TB strains. Strains were grown in MPL, sampled at day 15 (log phase) then fixed, dehydrated, carbon coated and imaged using high resolution SEM. (B) Box-and-whisker analysis of the H37RvS, H37Δ*ami1*S, H37Δ*ami1*S::pAmi1TB, H37Δ*ami4*S and H37Δ*ami4*S::pAmi4TB strains, showing the various cell lengths of the respective strains. (C) Bar graph showing the proportion Mtb containing lateral branches. Data is representative of 3 biological replicates and graphs were generated by counting a total of approximately 200 cells per strain. Statistical analysis was conducted using the student's *t*-test **: $p < 0.01$

nitrosative, stress the H37RvS, H37Δ*ami1*S, H37Δ*ami1*S::pAmi1TB, H37Δ*ami4*S and H37Δ*ami4*S::pAmi4TB strains were incubated in 7H9, pH 5.3 containing various concentration of sodium nitrite, ranging between 0 to 96 mM creating various levels of nitrosative stress 24 h, Figure 5.14. While in the case of oxidative stress, the strains were incubated in 7H9 containing 5 mM hydrogen peroxide for 48 h, Figure 5.15.

In the case of both sodium nitrite and hydrogen peroxide the H37Δ*ami1*S strain displayed higher susceptibility to both stresses. With regards to oxidative stress, the H37Δ*ami1*S strain exhibited faster death, when compared to both the parental and complemented strains. In terms of the nitrosative stress, the H37Δami1S strain required less sodium nitrite to induce death, indicating and increased susceptibility to nitrosative stress. This was not the case with regards to the H37Δ*ami4*S strain as it was not affected by nitrosative stress. The H37Δ*ami4*S strain, however, displayed resistance to oxidative stress, which was partially complemented in the H37Δ*ami4*S::pAmi4TB strain.

5.3.6 Ami1 is important for survival under immune assault

Following the observation that Ami1 has an impact on the ability to tolerate both oxidative and nitrosative stress, we sought to assess survival of the amidase defective mutants in macrophages, where these stresses are thought to prevail. To do this, resting and activated J774

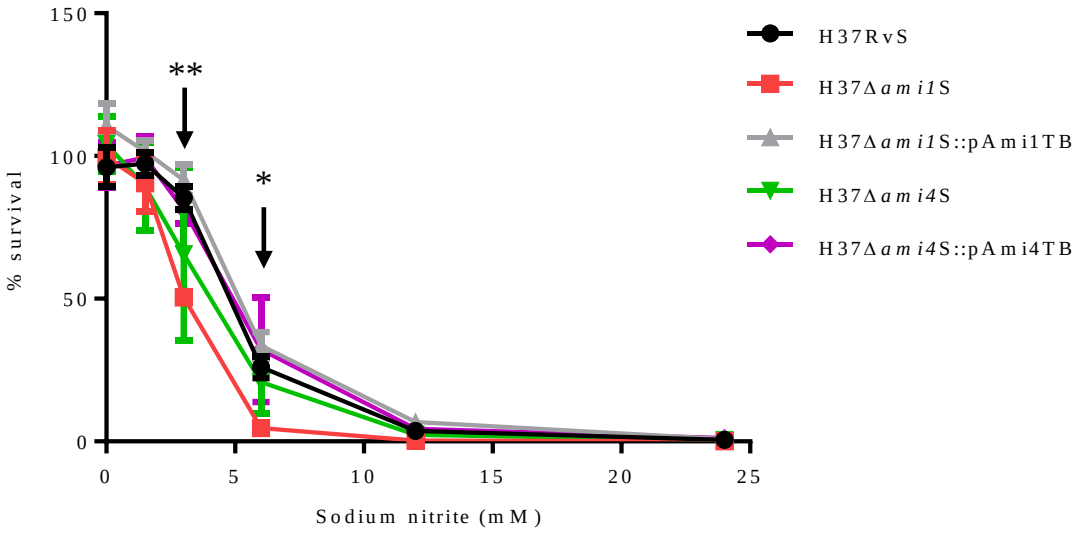

Figure 5.14: Line graph showing survival of H37RvS, H37Δ*ami1*S, H37Δ*ami1*S::pAmi1TB, H37Δ*ami4*S and H37Δ*ami4*S::pAmi4TB strains exposed to nitrosative stress. Depicted is the percentage survival of the various bacterial strains, calculated using CFU/ml count determined at 0 and 24 hours post inoculation into media, pH 5.3, containing 0, 1.5, 3, 6, 12 and 24 mM sodium nitrite, the graph is a representative of 3 biological replicates. Statistical analysis was conducted comparing H37RvS and the H37Δ*ami1*S strains using the student's *t*-test *: $p < 0.1$ and **: $p < 0.01$

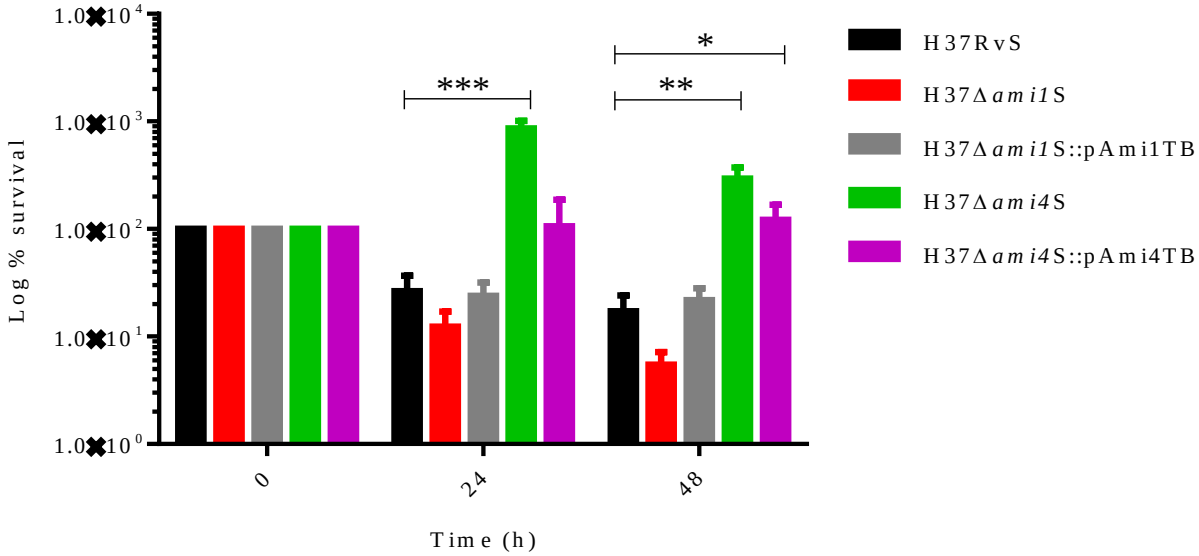

Figure 5.15: Bar graph showing survival of H37RvS, H37Δ*ami1*S, H37Δ*ami1*S::pAmi1TB, H37Δ*ami4*S and H37Δ*ami4*S::pAmi4TB strains exposed to oxidative stress. Depicted is the Log percentage survival of the various bacterial strains, calculated using CFU/ml count determined 0, 24 and 48 hours post inoculation into media containing 5 mM hydrogen peroxide, the graph is a representative of three biological replicates. Statistical analysis was conducted using the student's *t*-test *: $p < 0.1$, *: $p < 0.01$ and ***: $p < 0.001$

macrophages were infected with the H37RvS, H37Δ*ami1*S and H37Δ*ami1*S::pAmi1TB strains, these were incubated at 37 ˚C and macrophage samples were sacrificed at various time intervals to record bacterial load, Figure 5.16.

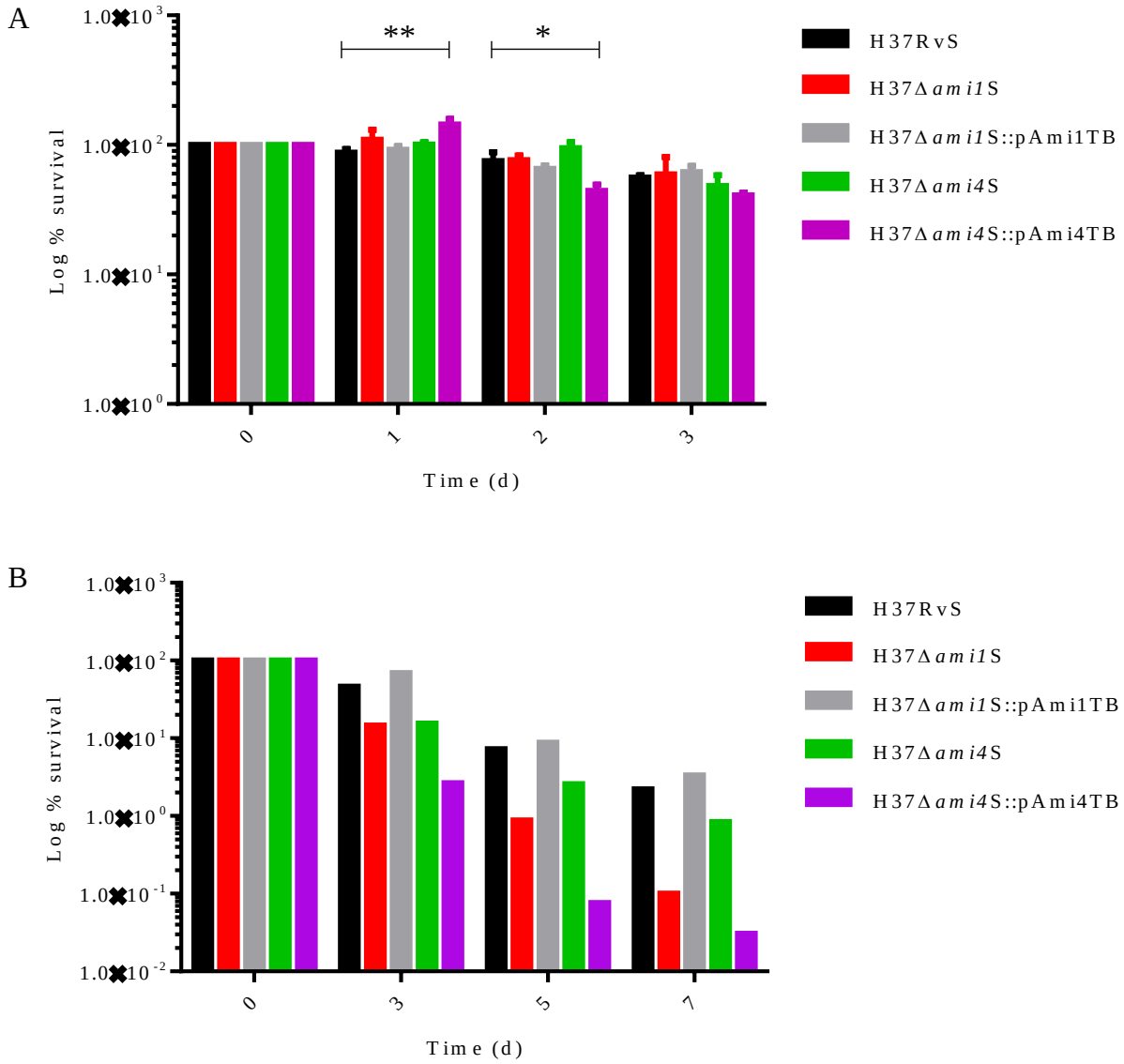

Figure 5.16: Bar graph showing survival of H37RvS, H37Δ*ami1*S, H37Δ*ami1*S::pAmi1TB, H37Δ*ami4*S and H37Δ*ami4*S::pAmi4TB strains in J774 macrophages. Depicted is the log percentage survival of the various bacterial strains, calculated using CFU/ml count determined at various time point throughout the macrophage infection. (A) Resting macrophages were infected with the various bacterial strains for 4 hours, macrophages were washed and sacrificed at day 0, 1, 2 and 3 then supernatant was plated to determine the amount of viable intracellular bacteria, the bar graph is a representative of three biological replicates. (B) Amidase deficient strains grown in activated macrophages, which were activated through treatment with LPS and INF-γ for 16 hours followed by infection for 4 fours. Macrophages were washed and sacrificed at day 0, 3, 5 and 7 then supernatant was plated to determine the amount of viable intracellular bacteria, the bar graph is a representative of a single experiment. Statistical analysis was conducted on resting macrophage samples using the student's *t*-test *: $p < 0.1$ and **: $p < 0.01$.

Loss of Ami1 did not affect bacterial ability to persist in the naive macrophage environment, as the bacterial population did not decline over time. However, rapid killing of the H37Δ*ami1*S strain was observed when macrophages were activated with LPS and IFN-γ, suggesting that Ami1 plays an important role in colonisation of macrophages (Fig 5.16B). This defect was reversed in the genetically complemented derivative. Due to time limitations, this experiment was only conducted once; further repetitions are required to make definitive conclusions.

Similarly, loss of Ami4 does not significantly affect bacterial ability to persist in the resting macrophage environment, as the bacterial population did not decline at a significantly higher rate over time when compared to the parental strain. A minor increase in bacterial killing of the H37Δ*ami4*S strain was observed when macrophages were activated with LPS and IFN-γ, which was less severe than that observed in the *ami1* deficient strain. An unexpected observation that was noted in both the naïve and activated macrophage infection was that the genetically complemented strain was rapidly cleared in activated macrophages, suggesting that ectopic expression of *ami4* is detrimental to the cell.

5.3.7 Ami4 regulation in the complemented strain

As the macrophage and oxidative damage data suggested aberrant survival/growth of the *ami4* complemented, RT-qPCR was conducted to check the expression of *ami4* in both the H37RvS and H37Δ*ami4*S::pAmi4TB strains to check for differences in gene expression, the H37Δ*ami4*S strain was included to serve as a negative control (Fig 5.17).

As shown by figure 5.17, there was no difference in the expression of *ami4* in both the H37RvS and H37Δ*ami4*S::pAmi4TB strains, suggesting the phenotypic variations observed were not due to the mis-regulation of *ami4* in the H37Δ*ami4*S::pAmi4TB strain.

5.3.8 Antibiotic susceptibility of H37Δ*ami1*S and H37Δ*ami4*S

We next assessed antibiotic susceptibility to determine whether deletion of *ami1* or *ami4* led to a change in tolerance towards antibiotic treatment. To do this, antibiotic susceptibility assays were conducted on the H37RvS, H37Δ*ami1*S, H37Δ*ami1*S::pAmi1TB, H37Δ*ami4*S and H37Δ*ami4*S::pAmi4TB strains, using antibiotics that target the cell wall, Table 5.4.

The antibiotic susceptibility assay revealed a reduction in the amount of antibiotic required to inhibit mycobacterial growth of the H37Δ*ami1*S for some antibiotics tested. We did not consider a two-fold reduction significant. Hence, treatment with cefoxitin and vancomycin, which target various components of the cell, resulted in significant increases in drug

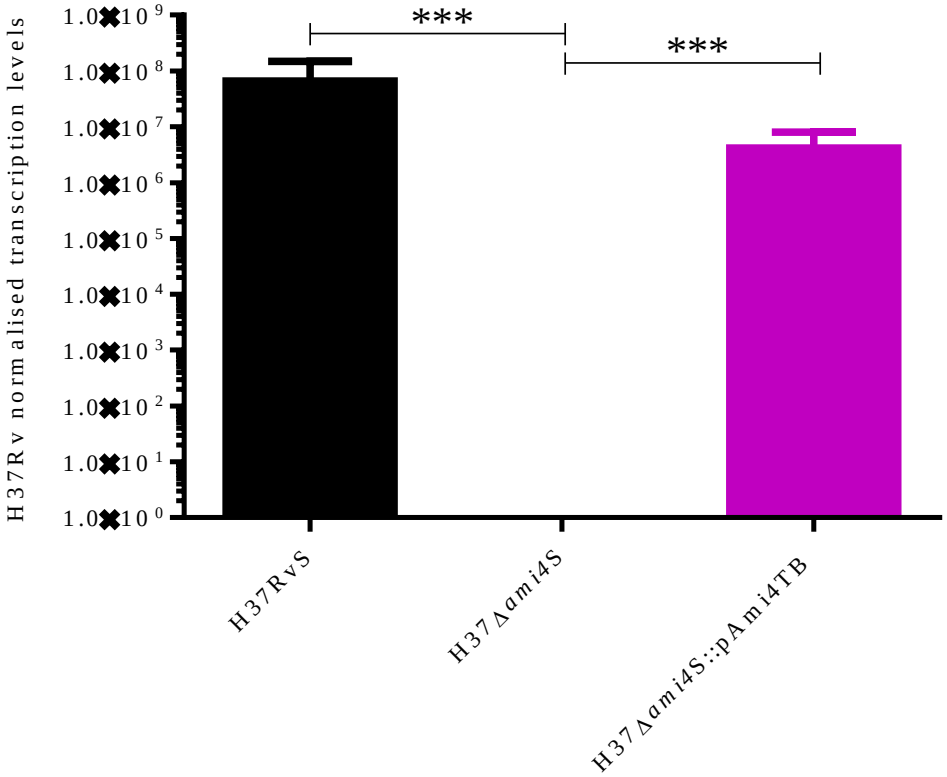

Figure 5.17: Bar graph showing the ami4 expression levels in the H37RvS, H37Δ*ami4*S and H37Δ*ami4*S::pAmi4TB strains. Cultures were grown to an OD_{600nm} of between 0.7 - 0.8, mRNA was extracted and qPCR was conducted to determine the level of *ami4* transcript in all three strains. The constitutively expressed *sigA* gene was used to normalise the various samples the graph is a representative of three biological replicates. Statistical analysis was conducted using the student's *t*-test ***: $p < 0.001$

susceptibility. We also noted increased susceptibility to RIF and erythromycin, indicating the reduction in bacterial tolerance to antibiotics was not limited to cell wall antibiotics. This was not the case with the H37Δ*ami4*S strain, there was no significant change observed.

As loss of *ami1* resulted in elevated bacterial sensitivity to a number of external stress factors tested. Kill curves were conducted to determine whether this increases sensitivity was a result of the inability to form persiters. To do this, survival assays were conducted as per section 5.2.5 with a few exceptions; 1. Cells were resuspended in 7H9T containing 32 µg/ml isoniazid, 2. Cells were incubated at 37 ˚C shaking at 100 rpm. CFUs were then taken daily to track bacterial survival as per de Steenwinkel et al, 2010 (Fig 5.18) (de Steenwinkel et al., 2010). Isoniazid was used instead of the enzymes listed on Table 5.4, as the study by de Steenwinkel et al., 2010, showed treatment with this antibiotic consistently resulted in persister formation whilst other antibiotics tested in the study resulted in bacterial death (de Steenwinkel et al., 2010).

The kill curve revealed a lack in the ability to form a persister population in the strain lacking *ami1* suggesting Ami1 plays an important role in the ability to form a persister population, while no significant difference in persister formation was observed in the population lacking *ami4*, indicating Ami4 plays no role in this phenomenon.

Table 5.4: MIC of the H37RvS, H37Δ*ami1*S, H37Δ*ami1*S::pAmi1TB, H37Δ*ami4*S and H37Δ*ami4*S::pAmi4TB strains

Drug	MIC*				
	H37RvS	**H37Δ*ami1*S**	**H37Δ*ami1*S:: pAmi1TB**	**H37Δ*ami4*S**	**H37Δ*ami4*S:: pAmi4TB**
Ethambutol	3.13	1.6	1.6-3.13	3.13	3.13
Erythromycin	250	15.6-31.3	125-250	125	250
Vancomycin	6.25-12.5	0.78-1.56	12.5	6.25-12.5	6.25-12.5
Rifampicin	0.003	0.0008	0.003-0.006	0.003	0.003
Streptomycin	0.39	0.1-0.2	0.1-0.2	0.05-0.1	0.05-0.2
Cefoxitin	80-160	10-20	80-160	80-160	80-160
D-cycloserine	6.25-12.5	3.125-6.25	6.25-12.5	6.25	6.25-12.5

MIC in µg/ml,

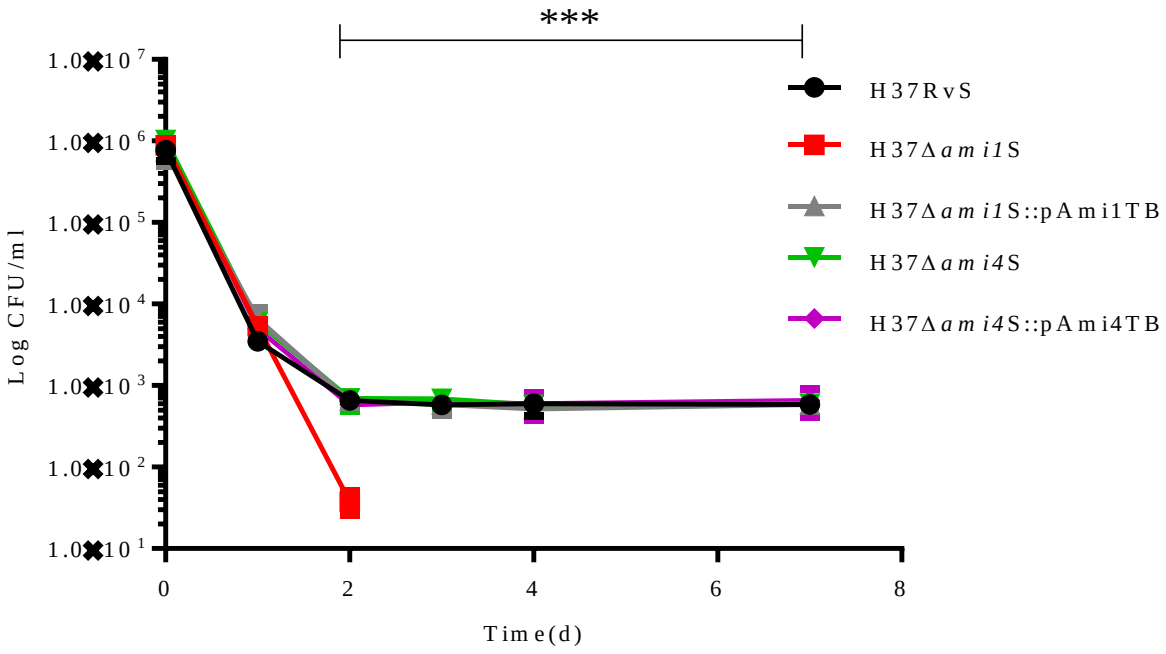

Figure 5.18: Line graph showing survival of H37RvS, H37Δ*ami1*S, H37Δ*ami1*S::pAmi1TB, H37Δ*ami4*S and H37Δ*ami4*S::pAmi4TB strains exposed to isoniazid. Depicted is bacterial survival, over seven days in media containing antibiotics, calculated using CFU/ml count determined at 0 and 1, 2, 3, 4 and 7 days post inoculation into media, containing 32 µg/ml isoniazid. The graph is a representative of three biological replicates. Statistical analysis was conducted comparing H37RvS and the H37Δ*ami1*S strains using the student's *t*-test, ***: $p < 0.001$.

5.4 Discussion

One of the key contributing factors to the survival of any living species is the ability to adapt and persist in a changing environment. There are two main ways in which this can be achieved; the first being random genetic mutations followed by the selection and propagation of fit mutants which confer a survival benefit in the prevailing environment and the second being phenotypic plasticity, which entails the ability to adopt a different phenotype in response to a change in the environment (Justice et al., 2008, Cava and de Pedro, 2014). Both these systems are prevalent in the bacterial world and are used constantly as survival tools leading to the formation of drug tolerant strains (Justice et al., 2008, Cava and de Pedro, 2014, Levin et al., 2000). Drug tolerance has been well documented in Mtb; however, the mechanisms driving this plasticity remain a mystery (Morris et al., 1995). Understanding how these organisms navigate harsh conditions is a key component in identifying essential elements required for survival in the host under constant bombardment by the immune system. Herein, we set out to characterise the role of mycobacterial amidases in cell division in Mtb but instead, noted an interesting role for these enzymes in modulating tolerance. We present a very preliminary analysis of the biological function of amidases in Mtb, due to the primary focus on *M. smegmatis* for this PhD and appending time constraints.

Unlike in *M. smegmatis*, both Ami1 and Ami4 in Mtb do not appear to participate in cell division and bacterial growth under nutrient rich conditions, as deletion of either did not result in the formation of notable cell division defects such as the formation of chains or an increase in the formation of cell division septa. This suggests that the function of these amidases is not conserved between these closely related species. Cell wall amidases have been shown to be important for processes that are distinct from cell division in other organisms including *B. subtilis* and *C. anabaena*, where in both instances they appear to play an essential role in the formation of stress tolerant cells through cell wall modification (Blackman et al., 1998, Smith et al., 2000, Piggot and Hilbert, 2004, Berendt et al., 2012).

In Mtb, loss of *ami1* resulted in reduced growth under nutrient limited conditions as depicted by the retarded growth in both Sautons and MPL media. This phenotype was exaggerated in MPL media possibly because MPL contains less glycerol than Sautons, thus exerting a higher starvation pressure. SEM analysis of cells cultured in MPL revealed a general increase in bacterial cell size from an average of ~3.5 µm seen in 7H9T to ~ 6 µm. This was unexpected as the OD doubling time in 7H9T was ~ 22 h and 48 h in MPL. The longer doubling time would

predict a slower growth rate of individual cells, possibly leading to the presence of smaller cells in MPL, as the mycobacterial cell cycle is time dependent where cells divide at constant time intervals, regardless of cell size (Aldridge et al., 2012). Under these conditions, we also noted the occurrence of lateral growth appendages in the H37Δ*ami1*S strain, similar to those found in the *M. smegmatis* Δ*ami1*strain but these were not associated with notable division defects. In *M. smegmatis*, lateral growth in the Δ*ami1*strain occurred under nutrient rich conditions but in Mtb, we noted this defect during nutrient starvation. None of these lateral buds where found near the septum suggesting their formation was primarily a result of DivIVA mis-localisation rather than cell division arrest. The fact that these branches only occurred in the MPL media and not in 7H9T, suggests that Ami1 becomes important during conditions of stress or that Mtb alters the composition of its cell division machinery under these conditions. This is supported by the data indicating loss of *ami1* resulted in increased susceptibility to nitrosative stress and the inability to replicate proficiently in activated macrophages. Furthermore, loss of *ami1* led to a reduction in the ability to form persisters in the presence on isoniazid, affirming the importance of *ami1* for this process. We chose isoniazid for this analysis as persistence studies in Mtb routinely use this antibiotic. Hence, these observations require further investigation using various antibiotics including those that displayed increase potency against the H37Δ*ami1*S strain.

In Mtb, Ami4 seems to be important for oxidative stress. Loss of *ami4* did not affect the ability of Mtb to survive under starvation, nitrosative and antibiotic stress; however, we noted an increase in bacterial tolerance to oxidative stress. This was unexpected as it contradicted a finding by Mestre et al (2013), who reported that transposon-mediated disruption of *ami4* resulted in hypersensitivity to oxidative stress (Mestre et al., 2013). In our study, this phenotype persisted in the complemented strain suggesting that it may be due poor expression from the vector used for complementation. However, expression analysis demonstrated similar expression levels of *ami4* in both the H37RvS and H37Δ*ami4*S::pAmi4TB, suggesting that failure to complement the oxidative stress phenotype was most likely due to second site effects that may not be related to Ami4 function. Hence, no definitive conclusions can be made regards Ami4 function in Mtb.

In summary, this preliminary characterisation of amidases in Mtb suggests a possible role for these enzymes in tolerance to stress and growth under specialist conditions. It is possible that Ami1 in Mtb functions similarly to the *B. subtilis cwlD*, which plays an important role in the

formation of special structures in the PG and that Ami4 functions like the *C. anabaena amiC2*, which is important for the formation of specifically oxygen tolerant bacterial heterocysts (Berendt et al., 2012, Sekiguchi et al., 1995). However, these explanations are largely speculative and require more research.

6 Concluding remarks

In model organisms such as *E. coli*, amidases predominantly appear to be hydrolytic enzymes that are important for cell division through mediating coordinated degradation of the division septum (Korsak et al., 2005, Heidrich et al., 2001, Smith et al., 2000). Until recently, amidase function in mycobacteria has remained unresolved. We set out to address this knowledge gap through a characterisation of amidase_3 domain containing enzymes in *M. smegmatis*. This revealed that Ami1 is required for cell division in *M. smegmatis* but is most likely not the only septal degradation system, as deletion thereof was not lethal. In *E. coli*, deletion of multiple amidases is required to manifest a severe division defect; however, this does not seem to be the case in mycobacteria. Deletion of *ami1* was also accompanied by ectopic DivIVA localisation that resulted in the formation of lateral branches, which were able to segregate the chromosome. Loss of *ami1* also led to defective septal cell wall turnover and increased permeability of the cell wall. In contrast, depletion of *ami2* resulted in cessation of bacterial growth and the formation of morphologically aberrant cells. Cellular localisation studies place Ami2 at the cell pole, possibly with a role in coordinating PG growth. Preliminary characterisation of the Mtb Ami1 and Ami4 suggest a role in growth and survival under specialist conditions.

7 Future studies

In *E. coli*, amidases are produced in an inactive form and require post-translational activation by M23-domain-containing peptidases. It will be important to assess whether a similar situation prevails in mycobacteria and similarly, if the mycobacterial amidases require interaction with other divisome proteins to exert their function. In Mtb, a more detailed characterisation of Ami1 function is required as our preliminary analysis suggests a divergence of function between Mtb and *M. smegmatis*. This would involve transcriptional analysis of the *ami1* defective mutant under various conditions and the use of division reporters to characterise cell division in this mutant.

8 Appendix

8.1 Appendix A: Culture Media

Lysogeny Agar (LA)

10 g Tryptone, 10 g NaCl, 5 g Yeast extract, 30 g Agar and sdH_2O up to 1 l

Lysogeny Broth (LB)

10 g Tryptone, 10 g NaCl, 5 g Yeast extract and sdH_2O up to 1 l

2 × TY Broth

16 g Tryptone, 5 g NaCl, 10 g Yeast extract and sdH_2O up to 1 l

Middlebrook 7H9 media

4.7 g Difco Middlebrook 7H9 powder, 2 ml glycerol, 10 ml 100 × glucose-salt (*M. smegmatis*) or 100 ml Middlebrook OADC (Mtb), 2 ml Tween80 and sdH_2O up to 1 l

Middlebrook 7H10 media

19 g Difco Middlebrook 7H9 powder, 2 ml glycerol, 10 ml 100 × glucose-salt (M. smegmatis) or 100 ml Middlebrook OADC (Mtb) and sdH_2O up to 1 l

Sautons minimal media (pH 7.2)

0.05 g Ammonium ferric citrate, 4 g Asparagine, 2 g Citric acid, 0.5 g Magnesium sulphate, 0.5 g Potassium dihydrogenorthophosphate, 48 ml glycerol and sdH2O up to 1 l pH with Ammonium hydroxide

Modified *M. phlei* media

20 ml glycerol, 0.6 g Magnesium sulphate, 5 g Potassium dihydrogenorthophosphate, 2 g Sodium citrate, 0.85 g Sodium nitrate, 5 ml Tyloxapol, pH 6.6 (with 10 M NaOH) and sdH_2O up to 1 l (filter sterilised)

100 × Glucose-salt

10 g Glucose, 4.25 g NaCl and sdH_2O up to 500 ml

Tween80 (25 %)

10 ml Tween80 dissolved in 40 ml dH_2O then sterilised by filtration

X-gal (2 %)

1 g X-gal in 50 ml deionised DMF

Media was sterilised by autoclaving at 121 °C for 20 min

8.2 Appendix B – solutions

DNA manipulation solutions

1 M Tris-HCl	: 60.56 g Tris, pH 8.0 with HCl and sdH_2O up to 500 ml
0.5 M EDTA	: 18.6 g powder, pH 8.0 with NaOH and sdH_2O up to 500 ml
1 M Glucose	: 90 g Glucose and sdH_2O up to 500 ml
10 % SDS	: 50 g Sodium Dodecyl Sulfate and sdH_2O up to 500 ml
5 M NaOH	: 20 g Sodium hydroxide and sdH_2O up to 100 ml
Soln I	: 50 mM glucose, 25 mM Tris-HCl, 10 mM EDTA, pH 8.0
Soln II	: 0.2 M NaOH, 1.0 % SDS
Soln III	: 49 g potassium acetate, 11.5 ml glacial acetic acid, and sdH_2O up to 100 ml
TE buffer	: 1 ml 1 M Tris-HCl, 2 ml 0.5 M EDTA
TAE buffer	: 242 g Tris base, 100 ml 0.5 M EDTA, 57.1 ml glacial acetic acid, pH 8.0, 1000 ml final volume dH_2O
Chloroform: Isoamyl	: 24 ml Chloroform, 1 ml Isoamyl alcohol
Phenol: chloroform	: 1 ml Phenol, 1 ml Chloroform
3M Sodium acetate	: 24.6 g Sodium acetate and sdH_2O up to 100 ml
CTAB/NaCl	: 4.1 % NaCl, 10 % Cetyltrimethylammonium bromide dissolved in dH_2O (filter sterilised)

Southern blotting solutions

Denaturation solution	: 0.5 M NaOH, 1.5 M NaCl in dH_2O
Depurination solution	: 0.25 M HCl in dH_2O
TBE (5 ×)	: 500 ml 10 × Tris-Borate-EDTA solution (Sigma) and 500 ml dH_2O
5 M Sodium citrate	: 129.03 g sodium citrate and sdH_2O up to 100 ml
SSC (20 ×)	: 3 M NaCl, 0.3 M sodium citrate in dH_2O
Soln I	: 10 ml 20X SSC, 1 ml 10 % SDS, and sdH_2O up to 100 ml
Soln II	: 2.5 ml 20X SSC, 1 ml 10 % SDS, and sdH_2O up to 100 ml
Maleic acid buffer	: 116.1 g maleic acid powder, 87. 66 g NaCl, pH 7.5 with NaOH pellets and sdH_2O up to 1 l
Wash buffer	: 0.1M Maleic acid buffer, 0.3 % Tween20
Blocking solution (Roche)	: 1 × blocking solution in maleic acid buffer

Detection buffer : 0.1M Tris-HCl, 0.1M NaCl in dH_2O (pH 9.5)

Antibody solution (Roche) : Dilute 1 in 10 000 in blocking solution

CSPD (Roche) : Disodium 2-chloro-5-(4-methoxyspiro (2-dioxetane-3,2 (2-dioxetane-3,2′-(5′-chloro)-tricyclo[3.3.1.1. 3, 7.]decan)-. 4-yl)-1-phenyl phosphate

SDS Gel Electrophoresis and Western blotting solutions

Running buffer : 303 g Tris, 144 g glycine, 10 g SDS and sdH_2O up to 1 l

Coomasie blue : 2 g Coomasie, 400 ml EtOH and 100 ml acetic acid and sdH_2O up to 1 l

De-stain : 400 ml EtOH, 100 ml acetic acid and sdH_2O up to 1 l

Transfer buffer : 3 g Tris, 14.4 g glycine, 1 g SDS, 200 ml methanol and sdH_2O up to 1 l

TBS (10×) : 24.2 g Tris Base, 80 g NaCl in and sdH_2O up to 1 l

TBST : 100 ml 10 × TBS, 1 ml Tween20 and sdH_2O up to 1 l

Blocking solution : 5 g Nonfat dry milk (CellSignal) and TBST up to 100 ml

CPS Reagent (Sigma) : Chemiluminescent Peroxidase Substrate

8.3 Appendix C – Molecular weight markers

DNA Molecular weight marker III

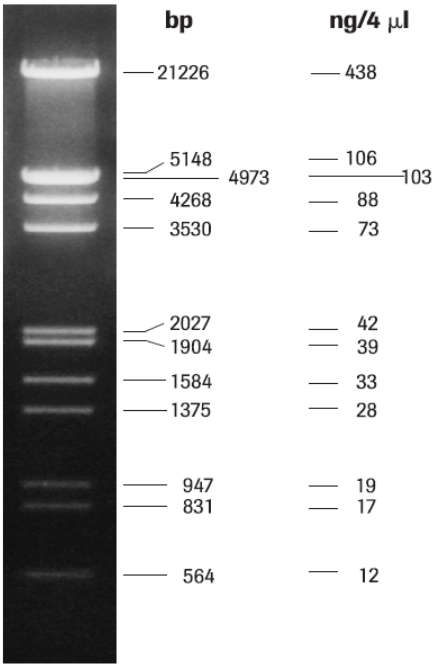

DNA Molecular weight marker III

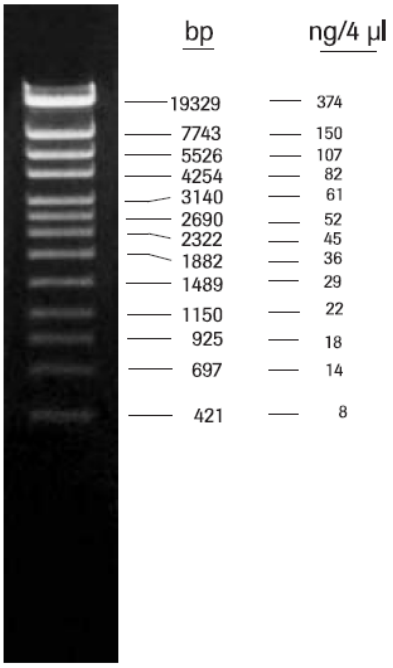

DNA Molecular weight marker III

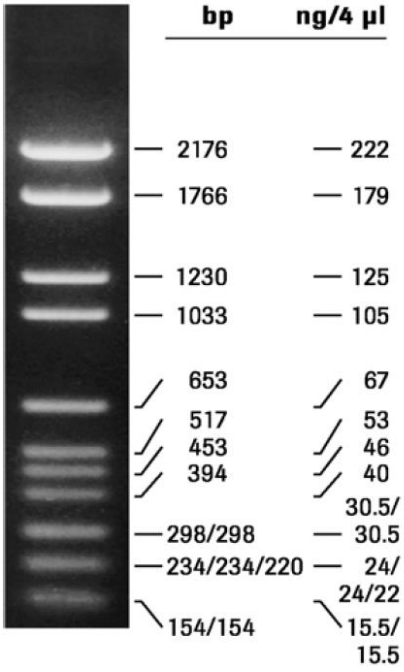

PageRuler Plus prestained, protein ladder

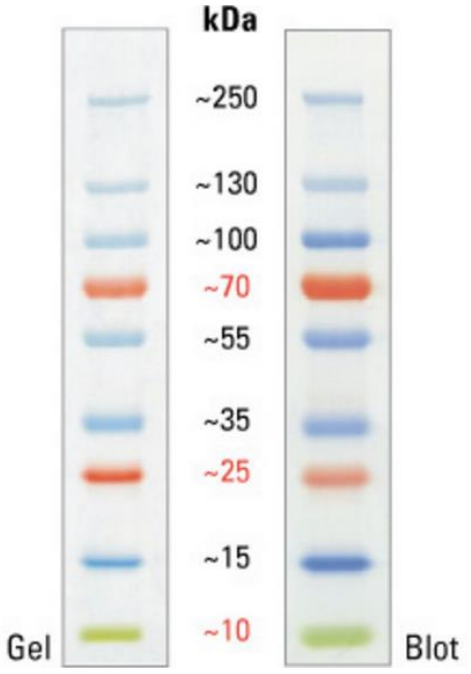

8.4 Appendix D – Additional Figures

A

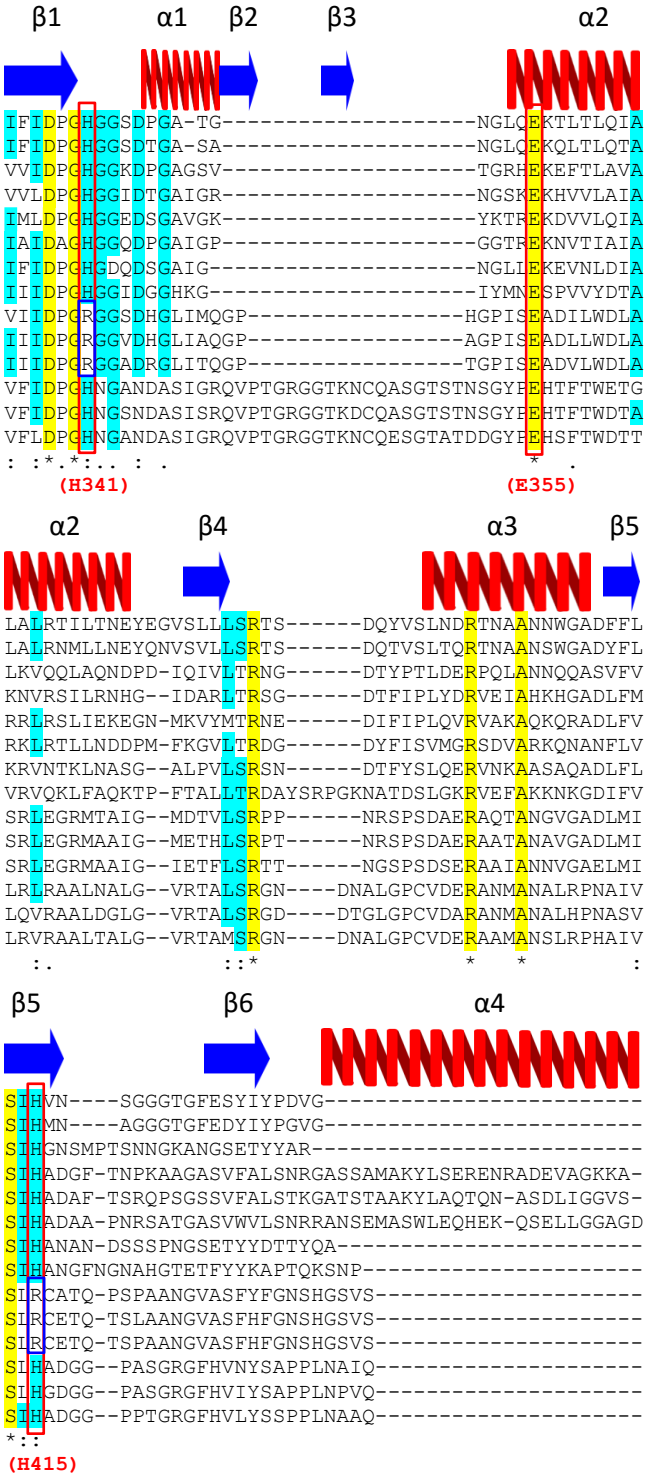

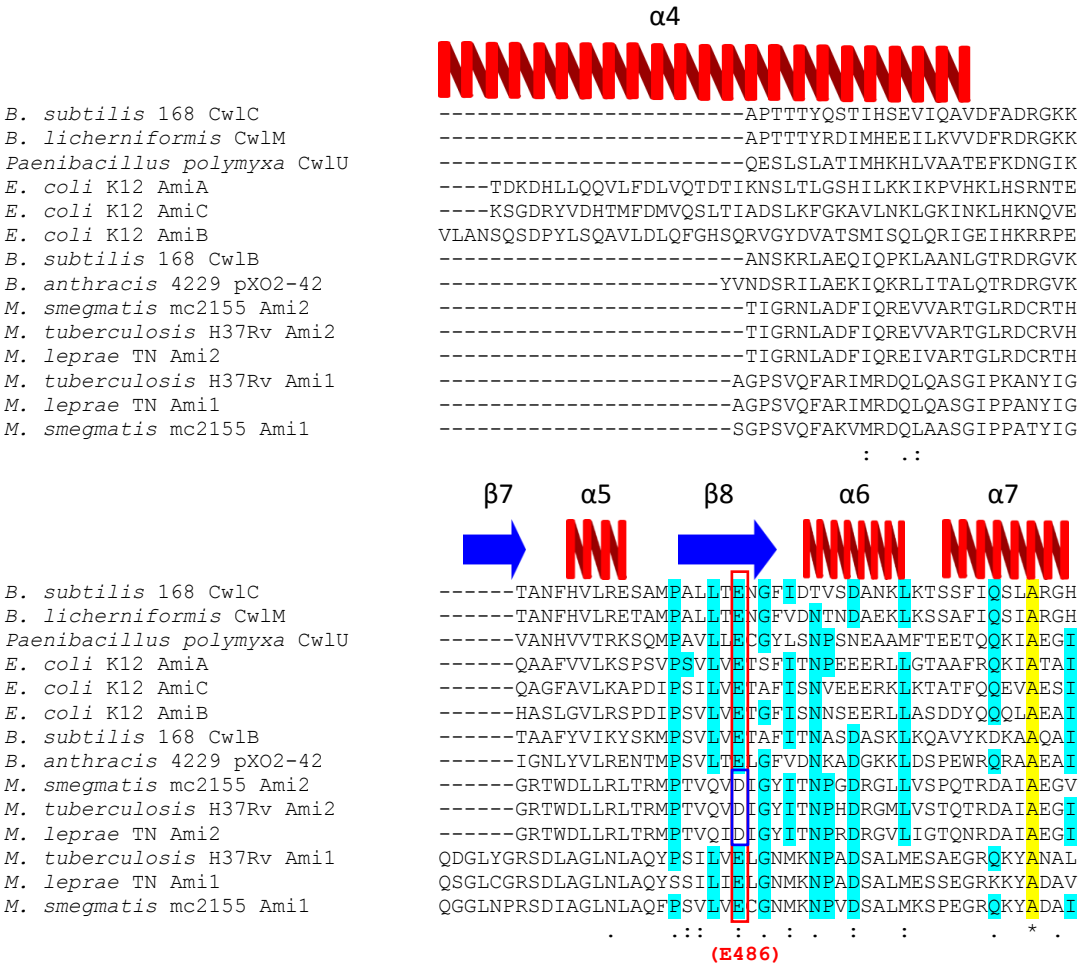
α4
B. subtilis 168 CwlC ----------APTTTYQSTIHSEVIQAVDFADRGKK
B. licherniformis CwlM ----------APTTTYRDIMHEEILKVVDFRDRGKK
Paenibacillus polymyxa CwlU ----------QESLSLATIMHKHLVAATEFKDNGIK
E. coli K12 AmiA ----TDKDHLLQQVLFDLVQTDTIKNSLTLGSHILKKIKPVHKLHSRNTE
E. coli K12 AmiC ----KSGDRYVDHTMFDMVQSLTIADSLKFGKAVLNKLGKINKLHKNQVE
E. coli K12 AmiB VLANSQSDPYLSQAVLDLQFGHSQRVGYDVATSMISQLQRIGEIHKRRPE
B. subtilis 168 CwlB ----------ANSKRLAEQIQPKLAANLGTRDRGVK
B. anthracis 4229 pXO2-42 ----------YVNDSRILAEKIQKRLITALQTRDRGVK
M. smegmatis mc2155 Ami2 ----------TIGRNLADFIQREVVARTGLRDCRTH
M. tuberculosis H37Rv Ami2 ----------TIGRNLADFIQREVVARTGLRDCRVH
M. leprae TN Ami2 ----------TIGRNLADFIQREIVARTGLRDCRTH
M. tuberculosis H37Rv Ami1 ----------AGPSVQFARIMRDQLQASGIPKANYIG
M. leprae TN Ami1 ----------AGPSVQFARIMRDQLQASGIPPANYIG
M. smegmatis mc2155 Ami1 ----------SGPSVQFAKVMRDQLAASGIPPATYIG
β7
α5
β8
α6
α7
B. subtilis 168 CwlC ------TANFHVLRESAMPALLTENGFIDTVSDANKLKTSSFIQSLARGH
B. licherniformis CwlM ------TANFHVLRETAMPALLTENGFVDNTNDAEKLKSSAFIQSIARGH
Paenibacillus polymyxa CwlU ------VANHVVTRKSQMPAVLLECGYLSNPSNEAAMFTEETQQKIAEGI
E. coli K12 AmiA ------QAAFVVLKSPSVPSVLVETSFITNPEEERLLGTAAFRQKIATAI
E. coli K12 AmiC ------QAGFAVLKAPDIPSILVETAFISNVEEERKLKTATFQQEVAESI
E. coli K12 AmiB ------HASLGVLRSPDIPSVLVETGFISNNSEERLLASDDYQQQLAEAI
B. subtilis 168 CwlB ------TAAFYVIKYSKMPSVLVETAFITNASDASKLKQAVYKDKAAQAI
B. anthracis 4229 pXO2-42 ------IGNLYVLRENTMPSVLTELGFVDNKADGKKLDSPEWRQRAAEAI
M. smegmatis mc2155 Ami2 ------GRTWDLLRLTRMPTVQVDIGYITNPGDRGLLVSPQTRDAIAEGV
M. tuberculosis H37Rv Ami2 ------GRTWDLLRLTRMPTVQVDIGYITNPHDRGMLVSTQTRDAIAEGI
M. leprae TN Ami2 ------GRTWDLLRLTRMPTVQIDIGYITNPRDRGVLIGTQNRDAIAEGI
M. tuberculosis H37Rv Ami1 QDGLYGRSDLAGLNLAQYPSILVELGNMKNPADSALMESAEGRQKYANAL
M. leprae TN Ami1 QSGLCGRSDLAGLNLAQYSSILIELGNMKNPADSALMESSEGRKKYADAV
M. smegmatis mc2155 Ami1 QGGLNPRSDIAGLNLAQFPSVLVECGNMKNPVDSALMKSPEGRQKYADAI
(E486)
α7
B. subtilis 168 CwlC ANGLE
B. licherniformis CwlM ANGLA
Paenibacillus polymyxa CwlU VDGLK
E. coli K12 AmiA AEGVI
E. coli K12 AmiC LAGIK
E. coli K12 AmiB YKGLR
B. subtilis 168 CwlB HDGT-
B. anthracis 4229 pXO2-42 YAGIL
M. smegmatis mc2155 Ami2 LAAVK
M. tuberculosis H37Rv Ami2 LAAVK
M. leprae TN Ami2 LAAVK
M. tuberculosis H37Rv Ami1 VRGVA
M. leprae TN Ami1 VRGVE
M. smegmatis mc2155 Ami1 VRGIA

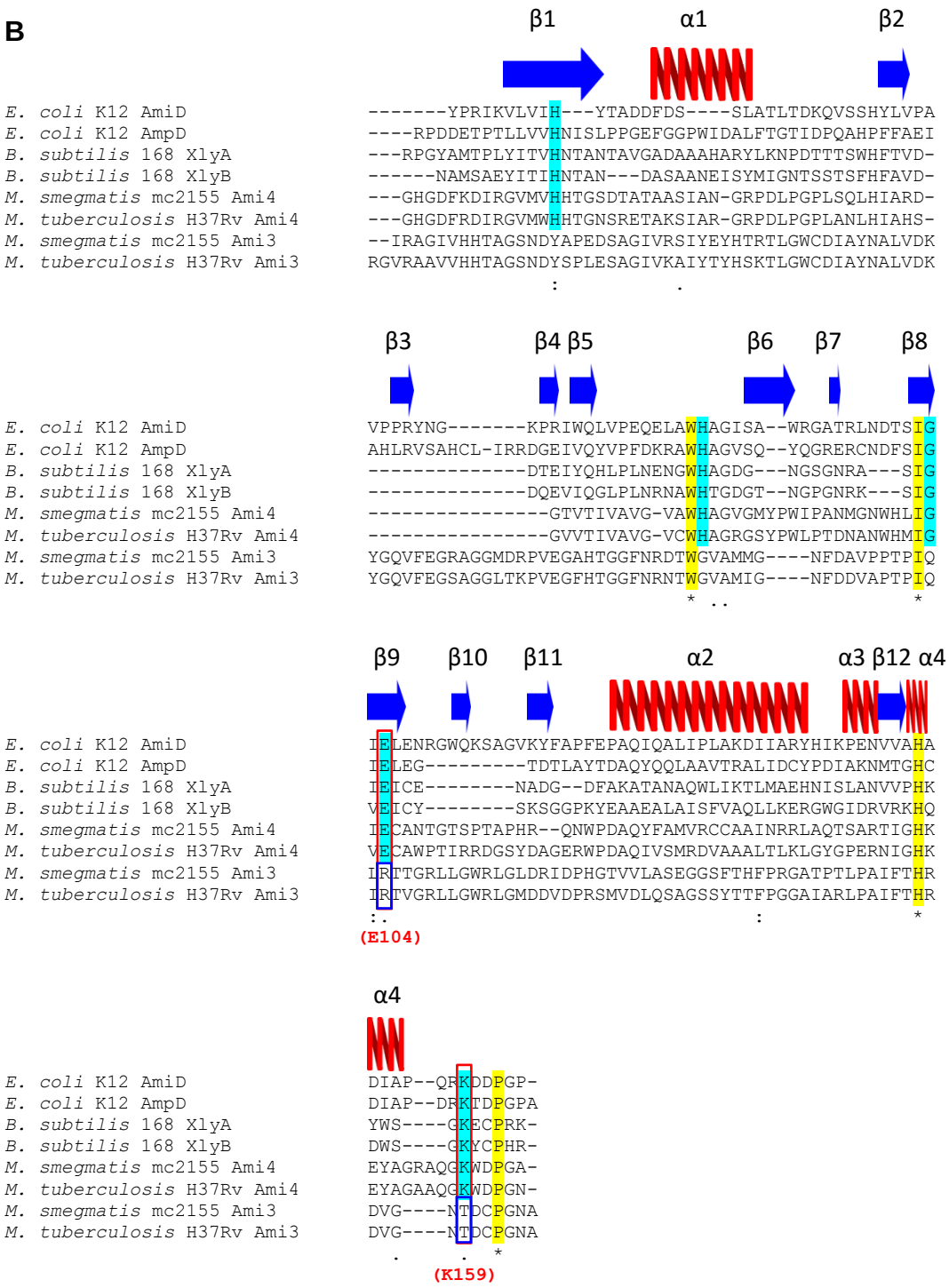

Figure D1: Clustal alignment of the amino acid sequences of amidases from various organisms. Alignments were carried out using Clustal Omega (http://www.ebi.ac.uk/Tools/msa/clustalO/). The conserved domains are highlighted in yellow (100% homologous) and turquoise (≥ 70% homologous). **A.** Alignment of amidase_3 domains, red boxes and red bold text indicate conserved catalytic H341, E355, H415 and E486 residues as well as the mycobacterial H341R, H415R and E486D substitutions in Ami2 (blue boxes). **B.** Alignment of amidase_2 domains conserved catalytic residues (red boxes, red bold text). Shown are the conserved E104 and K159 catalytic residues in *ami4* as well as the E104P and K159T substitutions in *ami3* (blue boxes).

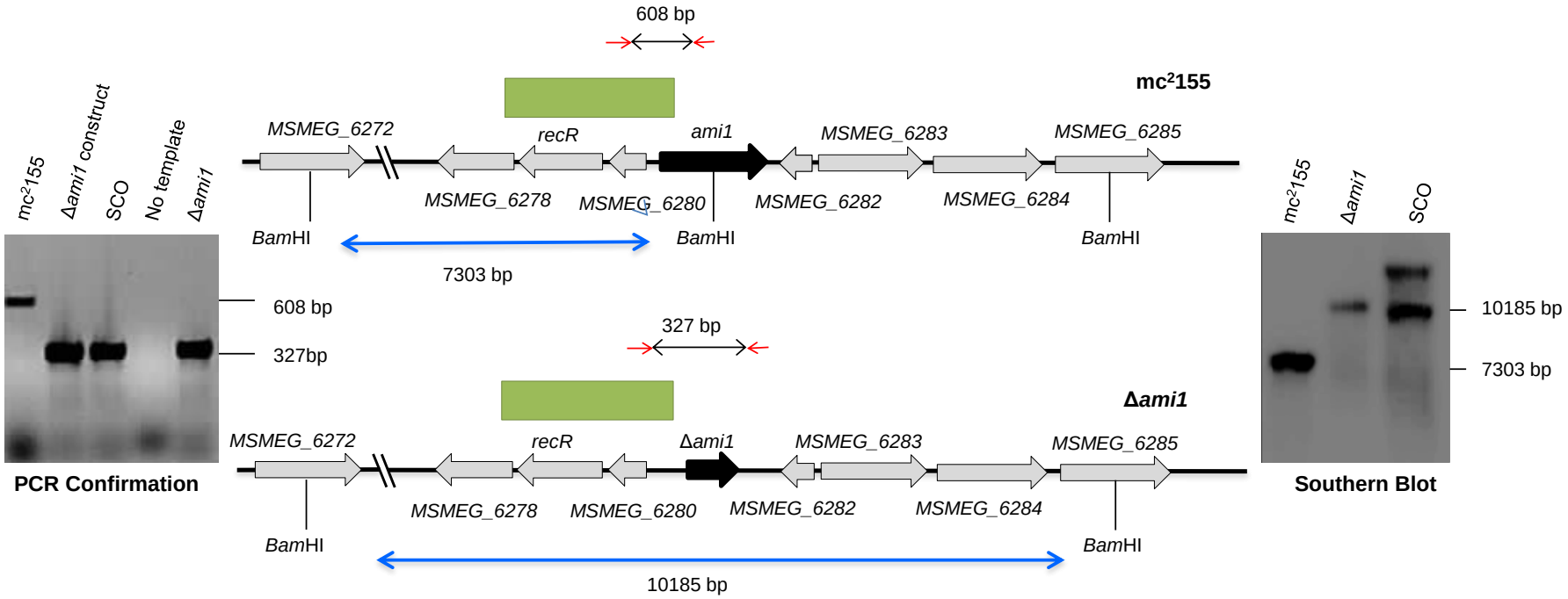

Figure D2. Genotypic analysis of the Δ*ami1* deletion strain by PCR and Southern blot analysis. The genomic map of the relevant locus is shown for the wild type mc^{2}155 and Δ*ami1* strains. Also shown on the left is the PCR confirmation of the genotype and Southern blotting is shown on the right. For PCR confirmation, chromosomal DNA was used to amplify the *ami1* alleles from the wild type and mutant strains using the primer pairs described in Table S3 and indicated by red arrows above. The expected sizes of the amplicons are as follows: *ami1* - 608 bp and Δ*ami1* - 327 bp. For Southern blot analysis, chromosomal DNA from the Single crossover (SCO), parental and mutant strain was digested with *Bam*HI. The probe used for hybridisation is shown as a solid green box and the expected sizes are indicated by the blue arrows. Maps are not drawn to scale. This analysis was conducted in a previous MSc study (Senzani, 2014).

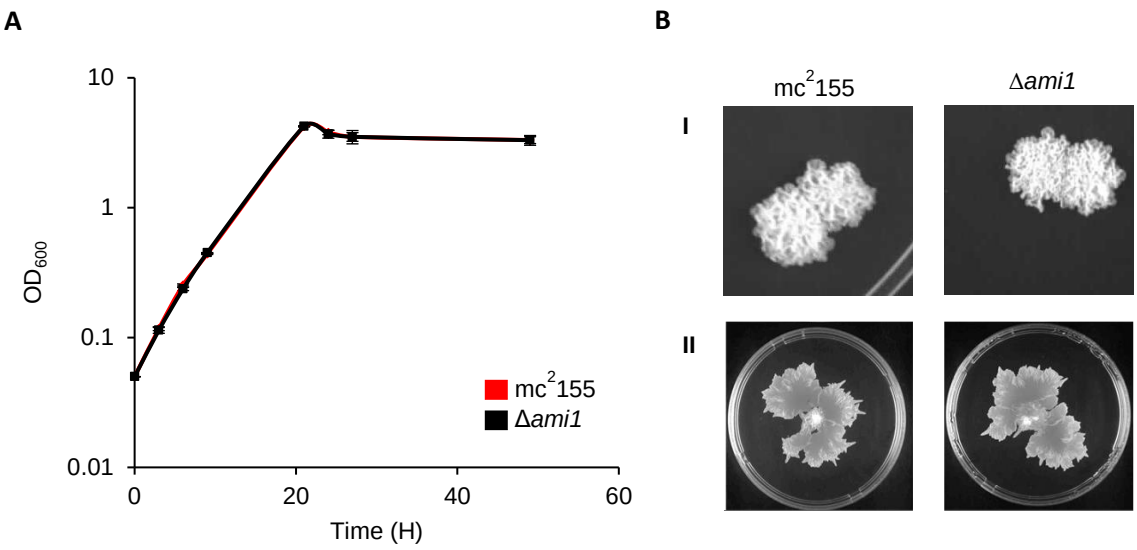

Figure D3. Deletion of *ami1* does not affect growth kinetics, colony morphology and sliding motility. (A) Growth curve depicting the growth kinetics of the mc^{2}155 and Δ*ami1* strains. Error bars represent the standard deviation of three experiments. (B) I. Colony morphology of mc^{2}155 and Δ*ami1* on 7H10 agar. II. Sliding motility assays with the mc^{2}155 and Δ*ami1* strains. Shown is the sliding motility on M63 media containing 0.3 % agar. This analysis was conducted in a previous MSc study (Senzani, 2014).

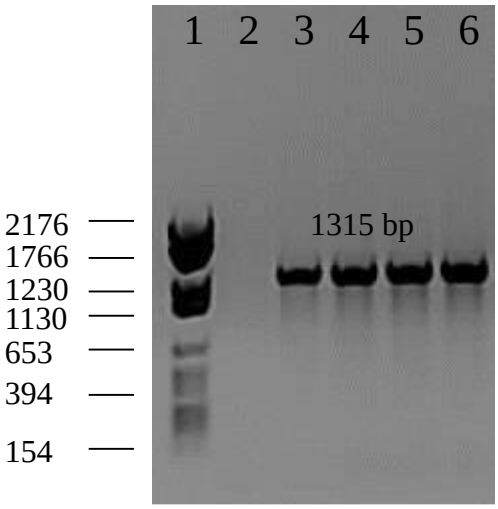

Figure D4: PCR Screen of the mc^{2}155::pAmi1GFP and Δ*ami1*::pAmi1GFP strain. PCR screen for the 2 possible Δ*ami1*::pAmi1GFP clones showing the expected PCR product size (1315 bp); Lane 1: Roche Marker VI, Lane 2: no template control and Lanes 3 and 4: mc^{2}155::pAmi1GFP clone 1 and 2 and Lanes 5 and 6 : Δ*ami1*::pAmi1GFP clone 1 and 2.

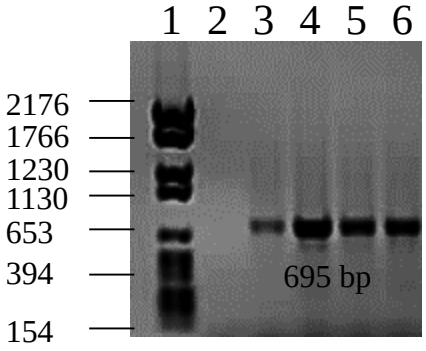

Figure D5: PCR Screen of the mc^{2}155::pFtsZGFP and Δ*ami1*::pFtsZGFP strains. PCR screen for the 2 possible mc^{2}155::pFtsZGFP and Δ*ami1*:: pFtsZGFP clones showing the expected PCR product size (695 bp); Lane 1: Roche Marker IV, Lane 2: no template control and Lanes 3 and 4: clone 1 and 2 for mc^{2}155::pFtsZGFP and Lanes 5 and 6: clone 1 and 2 for Δ*ami1*::pFtsZGFP.

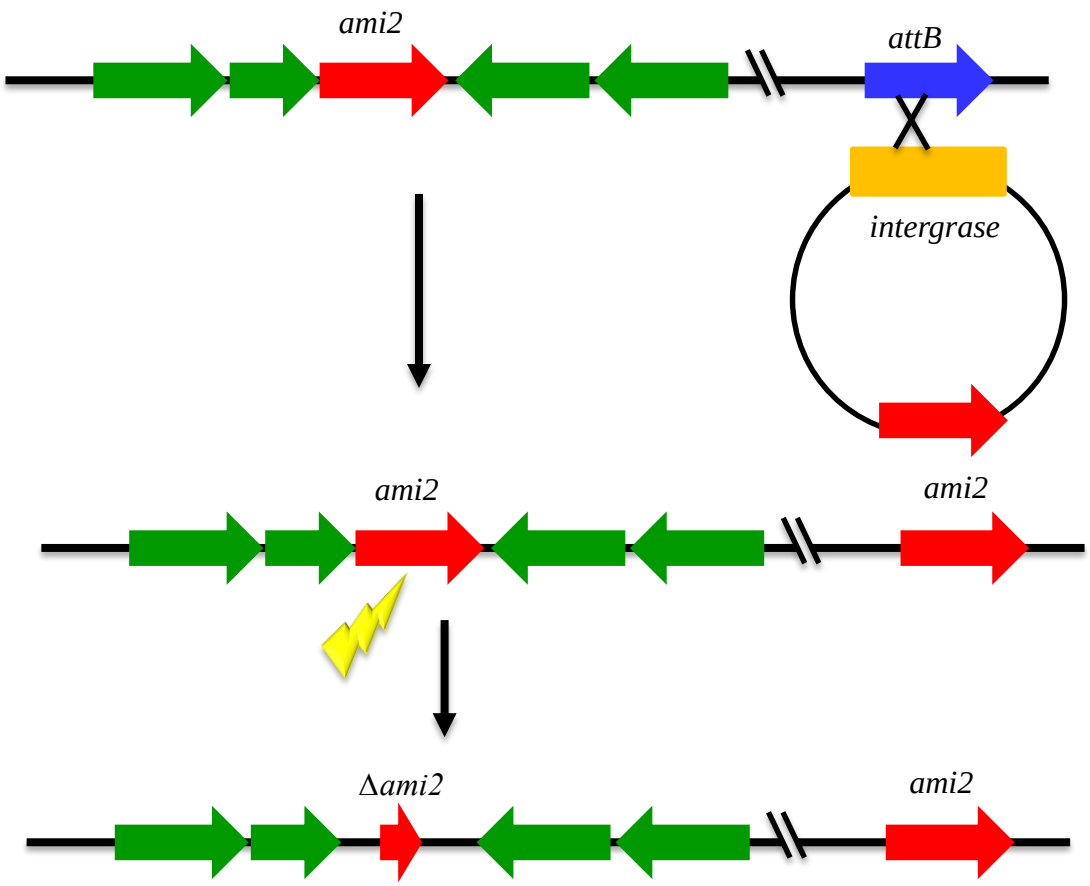

Figure D6: diagrammatic representation of the merodiploid deletion protocol showing the steps involved in deleting the native ami2 allele beginning with the introduction of a functional ami2 gene at the attB site followed by the deletion of the native allele using homologues recombination (figure drawn by S. Senzani)

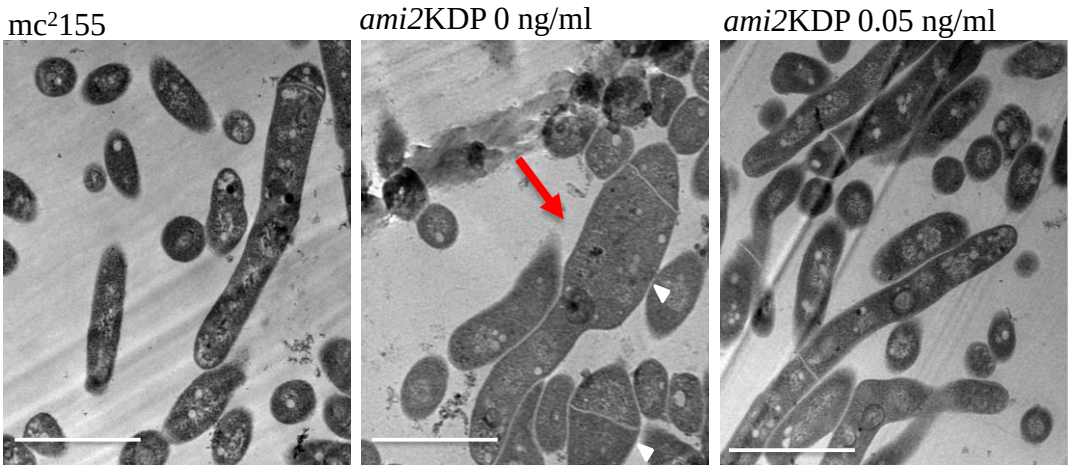

Figure D7: Transmission electron microscopy (TEM) of the mc²155 and ami2KDP strains. Shown is TEM depicting the formation of polar bulges in the ami2KDP strain grown in the absence of ATc (taken from MSc dissertation, Senzani, 2014).

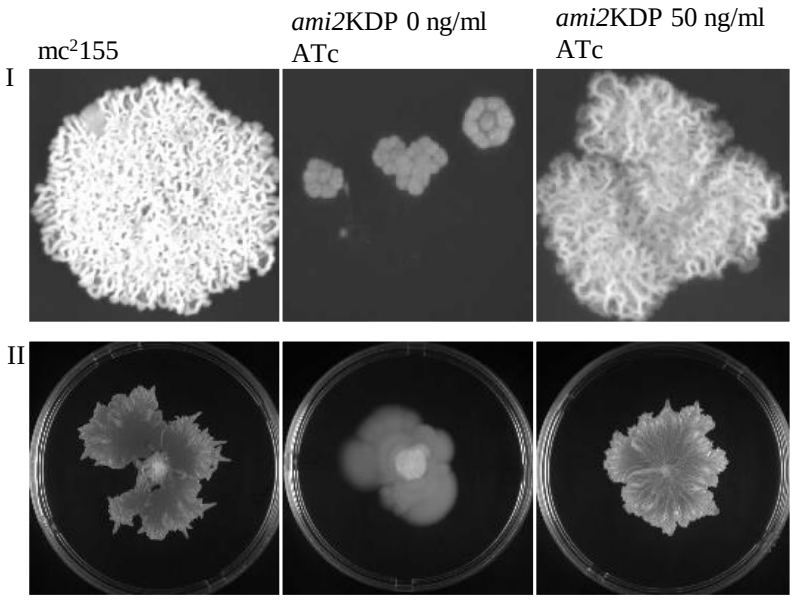

Figure D8: solid media growth morphology of the *ami2*KDP strain. (I) Shown is the colony formation phenotype of the *ami2*KDP strain grown on 7H10S containing 0 ng/ml ATc, displaying the formation of miniature malformed colonies and (II) the sliding morphology phenotype on media containing 0.3 % agar without ATc, resulting in the diffusion of bacterial cells into the media as oppose to growing on the surface as seen in the mc²155 and am2KDP 50 ng/ml ATc plates (taken from MSc dissertation, Senzani, 2014).

Table D1: MIC of the mc^{2}155, Δ*ami1* and Δ*ami1*::pMVami1 strains

Drug	WT	Δ*ami1*	Δ*ami1*::pMVami1
Ampicillin	150	78	>1250
Erythromycin	6.25	3.1	100 - 200
Vancomycin	0.78	0.20	>50
Rifampicin	0.625	0.3125	1.25 - 2.5
Cefamandole	500	500	2000
Cefoxitin	40	10	≥80
Cefotaxime	93.75	23	>750
Ceftriaxone	250	62	>1000
Cefapirin	50	25	800 - 1600
D-cycloserine	32	62	32

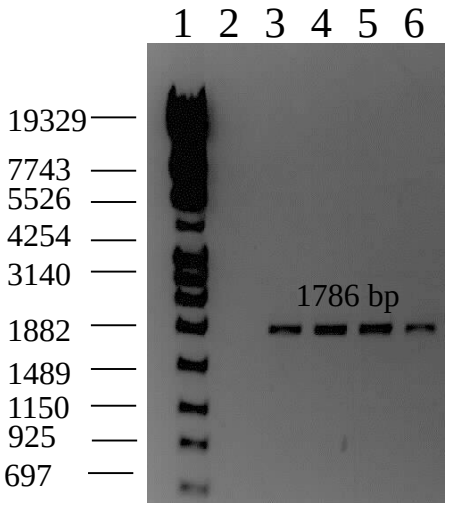

Figure D9: PCR Screen of the mc^{2}155::pAmi2GFP and Δ*ami1*::pAmi2GFP strains. PCR screen for the 2 possible mc^{2}155::pAmi2GFP and Δ*ami1*::pAmi2GFP clones showing the expected PCR product size (1786 bp); Lane 1: Roche Marker IV, Lane 2: no template control and Lanes 3 and 4: clone 1 and 2 for mc^{2}155::pAmi2GFP and Lanes 5 and 6: clone 1 and 2 for Δ*ami1*:: pAmi2GFP.

8.5 Appendix E – Movies

All movies in this study can be found in the attached envelope, or downloaded from: https://mega.nz/#F!q3phHaKL!-ZRwWOp6YIE31_yYqYHIhA

9 References

AARON, L., SAADOUN, D., CALATRONI, I., LAUNAY, O., MEMAIN, N., VINCENT, V., MARCHAL, G., DUPONT, B., BOUCHAUD, O. & VALEYRE, D. 2004. Tuberculosis in HIV-infected patients: a comprehensive review. *Clinical Microbiology and Infection,* 10**,** 388-398.

ADDINALL, S. G. & LUTKENHAUS, J. 1996. FtsA is localised to the septum in an FtsZ-dependent manner. *Journal of Bacteriology,* 178**,** 7167-7172.

AKIRA, S., TAKEDA, K. & KAISHO, T. 2001. Toll-like receptors: critical proteins linking innate and acquired immunity. *Nat Immunol,* 2**,** 675-680.

ALDRIDGE, B. B., FERNANDEZ-SUAREZ, M., HELLER, D., AMBRAVANESWARAN, V., IRIMIA, D., TONER, M. & FORTUNE, S. M. 2012. Asymmetry and aging of mycobacterial cells lead to variable growth and antibiotic susceptibility. *Science,* 335**,** 100-104.

ALVAREZ, L., ESPAILLAT, A., HERMOSO, J. A., DE PEDRO, M. A. & CAVA, F. 2014. PG remodeling by the coordinated action of multispecific enzymes. *Microb Drug Resist,* 20**,** 190-8.

ALYAHYA, S. A., ALEXANDER, R., COSTA, T., HENRIQUES, A. O., EMONET, T. & JACOBS-WAGNER, C. 2009. RodZ, a component of the bacterial core morphogenic apparatus. *Proc Natl Acad Sci U S A,* 106**,** 1239-1244.

ATRIH, A., ZOLLNER, P., ALLMAIER, G. & FOSTER, S. J. 1996. Structural analysis of *Bacillus subtilis* 168 endospore PG and its role during differentiation. *J Bacteriol,* 178**,** 6173-6183.

BARRETEAU, H., KOVAC, A., BONIFACE, A., SOVA, M., GOBEC, S. & BLANOT, D. 2008. Cytoplasmic steps of PG biosynthesis. *FEMS Microbiol Rev,* 32**,** 168-207.

BARRY, C. E., BOSHOFF, H. I., DARTOIS, V., DICK, T., EHRT, S., FLYNN, J., SCHNAPPINGER, D., WILKINSON, R. J. & YOUNG, D. 2009. The spectrum of latent tuberculosis: rethinking the biology and intervention strategies. *Nature Reviews Microbiology,* 7**,** 845-855.

BENSON, T. E., MARQUARDT, J. L., MARQUARDT, A. C., ETZKORN, F. A. & WALSH, C. T. 1993. Overexpression, purification, and mechanistic study of UDP-N-acetylenolpyruvylglucosamine reductase. *Biochemistry,* 32**,** 2024-2030.

BENTO, C. F., RENNA, M., GHISLAT, G., PURI, C., ASHKENAZI, A., VICINANZA, M., MENZIES, F. M. & RUBINSZTEIN, D. C. 2016. Mammalian autophagy: how does it work? *Annual review of biochemistry,* 85**,** 685-713.

BERENDT, S., LEHNER, J., ZHANG, Y. V., RASSE, T. M., FORCHHAMMER, K. & MALDENER, I. 2012. Cell wall amidase AmiC1 is required for cellular communication and heterocyst development in the *Cyanobacterium anabaena* PCC 7120 but not for filament integrity. *J Bacteriol,* 194**,** 5218-5227.

BERNHARDT, T. G. & DE BOER, P. A. 2003. The *Escherichia coli* amidase AmiC is a periplasmic septal ring component exported via the twin-arginine transport pathway. *Mol Microbiol,* 48**,** 1171-1182.

BERTSCHE, U., BREUKINK, E., KAST, T. & VOLLMER, W. 2005. In vitro murein PG synthesis by dimers of the bifunctional transglycosylase-transpeptidase PBP1B from *Escherichia coli*. *J Biol Chem,* 280**,** 38096-38101.

BEUKES, G. M. 2014. *The role of resuscitation promoting factors in PG hydrolysis and reactivation from dormancy in Mycobacterium smegmatis.* MSc Med, University of the Witwatersrand.

BLACKMAN, S. A., SMITH, T. J. & FOSTER, S. J. 1998. The role of autolysins during vegetative growth of *Bacillus subtilis* 168. *Microbiology,* 144 (Pt 1)**,** 73-82.

BLOKPOEL, M. C., MURPHY, H. N., O'TOOLE, R., WILES, S., RUNN, E. S., STEWART, G. R., YOUNG, D. B. & ROBERTSON, B. D. 2005. Tetracycline-inducible gene regulation in mycobacteria. *Nucleic Acids Research,* 33**,** e22-e22.

BORN, P., BREUKINK, E. & VOLLMER, W. 2006. In vitro synthesis of cross-linked murein and its attachment to sacculi by PBP1A from *Escherichia coli*. *J Biol Chem,* 281**,** 26985-26993.

BOTELLA, H., YANG, G., OUERFELLI, O., EHRT, S., NATHAN, C. F. & VAUBOURGEIX, J. 2017. Distinct Spatiotemporal Dynamics of PG Synthesis between *Mycobacterium smegmatis* and *Mycobacterium tuberculosis*. *mBio,* 8**,** e01183-17.

BÖTH, D., SCHNEIDER, G. & SCHNELL, R. 2011. PG remodeling in *Mycobacterium tuberculosis*: comparison of structures and catalytic activities of RipA and RipB. *Journal of Molecular Biology,* 413**,** 247-260.

BOUTTE, C. C., BAER, C. E., PAPAVINASASUNDARAM, K., LIU, W., CHASE, M. R., MENICHE, X., FORTUNE, S. M., SASSETTI, C. M., IOERGER, T. R. & RUBIN, E. J. 2016. A cytoplasmic PG amidase homologue controls mycobacterial cell wall synthesis. *Elife,* 5.

BRENNAN, P. J. 2003. Structure, function, and biogenesis of the cell wall of *Mycobacterium tuberculosis*. *Tuberculosis,* 83**,** 91-97.

BROWN, E. D., VIVAS, E. I., WALSH, C. T. & KOLTER, R. 1995. MurA (MurZ), the enzyme that catalyses the first committed step in PG biosynthesis, is essential in *Escherichia coli*. *Journal of Bacteriology,* 177**,** 4194-4197.

BURGERS, P., KORNBERG, A. & SAKAKIBARA, Y. 1981. The dnaN gene codes for the beta subunit of DNA polymerase III holoenzyme of *Escherichia coli*. *Proceedings of the National Academy of Sciences,* 78**,** 5391-5395.

CABRÉ, E. J., SÁNCHEZ-GOROSTIAGA, A., CARRARA, P., ROPERO, N., CASANOVA, M., PALACIOS, P., STANO, P., JIMÉNEZ, M., RIVAS, G. & VICENTE, M. 2013. Bacterial division proteins FtsZ and ZipA induce vesicle shrinkage and cell membrane invagination. *Journal of Biological Chemistry,* 288**,** 26625-26634.

CAMINERO, J. A., SOTGIU, G., ZUMLA, A. & MIGLIORI, G. B. 2010. Best drug treatment for multidrug-resistant and extensively drug-resistant tuberculosis. *The Lancet infectious diseases,* 10**,** 621-629.

CAVA, F. & DE PEDRO, M. A. 2014. PG plasticity in bacteria: emerging variability of the murein sacculus and their associated biological functions. *Current opinion in microbiology,* 18**,** 46-53.

CHAMAILLARD, M., HASHIMOTO, M., HORIE, Y., MASUMOTO, J., QIU, S., SAAB, L., OGURA, Y., KAWASAKI, A., FUKASE, K. & KUSUMOTO, S. 2003. An essential role for NOD1 in host recognition of bacterial PG containing diaminopimelic acid. *Nature immunology,* 4**,** 702-707.

CHAPUT, C., ECOBICHON, C., CAYET, N., GIRARDIN, S. E., WERTS, C., GUADAGNINI, S., PRÉVOST, M.-C., MENGIN-LECREULX, D., LABIGNE, A. & BONECA, I. G. 2006. Role of AmiA in the morphological transition of *Helicobacter pylori* and in immune escape. *PLoS Pathog,* 2**,** e97.

CHEN, Y., HUANG, H., OSAWA, M. & ERICKSON, H. P. 2017. ZipA and FtsA* stabilise FtsZ-GDP miniring structures. *Scientific reports,* 7**,** 3650.

CHUDI, I. P. 2010. Healthcare problems in developing countries. *Medical Practice and Reviews,* 1**,** 9-11.

CLOUD, K. A. & DILLARD, J. P. 2004. Mutation of a single lytic transglycosylase causes aberrant septation and inhibits cell separation of *Neisseria gonorrhoeae*. *Journal of bacteriology,* 186**,** 7811-7814.

COHEN GONSAUD, M., BARTHE, P., BAGNERIS, C., HENDERSON, B., WARD, J., ROUMESTAND, C. & KEEP, N. H. 2005. The structure of a resuscitation-promoting factor domain from *Mycobacterium tuberculosis* shows homology to lysozymes. *Nature Structural and Molecular Biology,* 12**,** 270-273.

CONRAD, W. H., OSMAN, M. M., SHANAHAN, J. K., CHU, F., TAKAKI, K. K., CAMERON, J., HOPKINSON-WOOLLEY, D., BROSCH, R. & RAMAKRISHNAN, L. 2017. Mycobacterial ESX-1 secretion system mediates host cell lysis through bacterium contact-dependent gross membrane disruptions. *Proceedings of the National Academy of Sciences,* 114**,** 1371-1376.

COULOMBE, F., DIVANGAHI, M., VEYRIER, F., DE LÉSÉLEUC, L., GLEASON, J. L., YANG, Y., KELLIHER, M. A., PANDEY, A. K., SASSETTI, C. M. & REED, M. B. 2009. Increased NOD2-mediated recognition of *N*-glycolyl muramyl dipeptide. *Journal of Experimental Medicine,* 206**,** 1709-1716.

CROFTON, J. & MITCHISON, D. 1948. Streptomycin resistance in pulmonary tuberculosis. *British medical journal,* 2**,** 1009-1015.

DAFFE, M. & ETIENNE, G. 1999. The capsule of *Mycobacterium tuberculosis* and its implications for pathogenicity. *Tubercle and lung disease,* 79**,** 153-169.

DANIEL, R. A. & ERRINGTON, J. 2003. Control of cell morphogenesis in bacteria: two distinct ways to make a rod-shaped cell. *Cell,* 113**,** 767-776.

DE LORENZO, S., ALFFENAAR, J. W., SOTGIU, G., CENTIS, R., D'AMBROSIO, L., TIBERI, S., BOLHUIS, M. S., VAN ALTENA, R., VIGGIANI, P. & PIANA, A. 2013. Efficacy and safety of meropenem–clavulanate added to linezolid-containing regimens in the treatment of MDR-/XDR-TB. *European Respiratory Journal,* 41**,** 1386-1392.

DE SOUZA, G. A., LEVERSEN, N. A., MÅLEN, H. & WIKER, H. G. 2011. Bacterial proteins with cleaved or uncleaved signal peptides of the general secretory pathway. *Journal of proteomics,* 75**,** 502-510.

DE STEENWINKEL, J. E., DE KNEGT, G. J., TEN KATE, M. T., VAN BELKUM, A., VERBRUGH, H. A., KREMER, K., VAN SOOLINGEN, D. & BAKKER-WOUDENBERG, I. A. 2010. Time–kill kinetics of anti-tuberculosis drugs, and emergence of resistance, in relation to metabolic activity of *Mycobacterium tuberculosis*. *Journal of antimicrobial chemotherapy,* 65**,** 2582-2589.

DERETIC, V. 2014. Autophagy in tuberculosis. *Cold Spring Harbor perspectives in medicine,* 4**,** a018481.

DERETIC, V., SAITOH, T. & AKIRA, S. 2013. Autophagy in infection, inflammation and immunity. *Nature Reviews Immunology,* 13**,** 722-737.

DERRICK, S. C. & MORRIS, S. L. 2007. The ESAT6 protein of *Mycobacterium tuberculosis* induces apoptosis of macrophages by activating caspase expression. *Cellular microbiology,* 9**,** 1547-1555.

DESHPANDE, R., KHALILI, H., PERGOLIZZI, R. G., MICHAEL, S. D. & CHANG, M. D. Y. 1997. Estradiol down-regulates LPS-induced cytokine production and NFkB activation in murine macrophages. *American journal of reproductive immunology,* 38**,** 46-54.

DIACON, A. H., PYM, A., GROBUSCH, M. P., DE LOS RIOS, J. M., GOTUZZO, E., VASILYEVA, I., LEIMANE, V., ANDRIES, K., BAKARE, N. & DE MAREZ, T. 2014. Multidrug-resistant tuberculosis and culture conversion with bedaquiline. *New England Journal of Medicine,* 371**,** 723-732.

DOMINGUEZ-ESCOBAR, J., CHASTANET, A., CREVENNA, A. H., FROMION, V., WEDLICH-SOLDNER, R. & CARBALLIDO-LOPEZ, R. 2011. Processive movement of MreB-associated cell wall biosynthetic complexes in bacteria. *Science,* 333**,** 225-228.

DOWNING, K. J., MISCHENKO, V. V., SHLEEVA, M. O., YOUNG, D. I., YOUNG, M., KAPRELYANTS, A. S., APT, A. S. & MIZRAHI, V. 2005. Mutants of *Mycobacterium tuberculosis* lacking three of the five rpf-like genes are defective for growth in vivo and for resuscitation in vitro. *Infection and immunity,* 73**,** 3038-3043.

DRIKS, A. 2002. Overview: development in bacteria: spore formation in *Bacillus subtilis*. *Cellular and Molecular Life Sciences,* 59**,** 389-391.

DURAND-HEREDIA, J., RIVKIN, E., FAN, G., MORALES, J. & JANAKIRAMAN, A. 2012. Identification of ZapD as a cell division factor that promotes the assembly of FtsZ in *Escherichia coli*. *Journal of bacteriology,* 194**,** 3189-3198.

DZIARSKI, R. 2004. PG recognition proteins (PGRPs). *Molecular immunology,* 40**,** 877-886.

EBERSBACH, G., GALLI, E., MØLLER-JENSEN, J., LÖWE, J. & GERDES, K. 2008. Novel coiled-coil cell division factor ZapB stimulates Z-ring assembly and cell division. *Molecular microbiology,* 68**,** 720-735.

EGAN, A. J., CLEVERLEY, R. M., PETERS, K., LEWIS, R. J. & VOLLMER, W. 2016. Regulation of bacterial cell wall growth. *The FEBS Journal,* 284**,** 851-867.

EGAN, A. J. & VOLLMER, W. 2013. The physiology of bacterial cell division. *Annals of the New York Academy of Sciences,* 1277**,** 8-28.

EHRT, S., GUO, X. V., HICKEY, C. M., RYOU, M., MONTELEONE, M., RILEY, L. W. & SCHNAPPINGER, D. 2005a. Controlling gene expression in mycobacteria with anhydrotetracycline and Tet repressor. *Nucleic acids research,* 33**,** e21-e21.

EHRT, S., GUO, X. V., HICKEY, C. M., RYOU, M., MONTELEONE, M., RILEY, L. W. & SCHNAPPINGER, D. 2005b. Controllong gene expression in mycobacteria with anhydrotetracycline and Tet repressor. *Nucleic Acids Res,* 33**,** e21.

EHRT, S. & SCHNAPPINGER, D. 2009. Mycobacterial survival strategies in the phagosome: defence against host stresses. *Cellular microbiology,* 11**,** 1170-1178.

ERRINGTON, J. 1993. *Bacillus subtilis* sporulation: regulation of gene expression and control of morphogenesis. *Microbiological reviews,* 57**,** 1-33.

ERRINGTON, J. 2015. Bacterial morphogenesis and the enigmatic MreB helix. *Nat Rev Microbiol,* 13**,** 241-248.

ESKANDARIAN, H. A., ODERMATT, P. D., VEN, J. X., HANNEBELLE, M. T., NIEVERGELT, A. P., DHAR, N., MCKINNEY, J. D. & FANTNER, G. E. 2017. Division site selection linked to inherited cell surface wave troughs in mycobacteria. *Nature microbiology,* 2**,** 17094.

FAIRN, G. D. & GRINSTEIN, S. 2012. How nascent phagosomes mature to become phagolysosomes. *Trends in immunology,* 33**,** 397-405.

FENTON, A. K. & GERDES, K. 2013. Direct interaction of FtsZ and MreB is required for septum synthesis and cell division in *Escherichia coli*. *The EMBO journal,* 32**,** 1953-1965.

FERGUSON, J. S., VOELKER, D. R., MCCORMACK, F. X. & SCHLESINGER, L. S. 1999. Surfactant protein D binds to *Mycobacterium tuberculosis* Bacilli and Lipoarabinomannan via carbohydrate-lectin interactions resulting in reduced phagocytosis of the bacteria by macrophages. *The Journal of immunology,* 163**,** 312-321.

FISCHER, K. E. & BREMER, E. 2012. Activity of the osmotically regulated yqiHIK promoter from *Bacillus subtilis* is controlled at a distance. *J Bacteriol,* 194**,** 5197-208.

FLEURIE, A., LESTERLIN, C., MANUSE, S., ZHAO, C., CLUZEL, C., LAVERGNE, J.-P., FRANZ-WACHTEL, M., MACEK, B., COMBET, C. & KURU, E. 2014. MapZ marks the division sites and positions FtsZ-rings in Streptococcus pneumoniae. *Nature,* 516**,** 259-262.

FUKATA, M., VAMADEVAN, A. S. & ABREU, M. T. Toll-like receptors (TLRs) and Nod-like receptors (NLRs) in inflammatory disorders. Seminars in immunology, 2009. Elsevier, 242-253.

GALLI, E. & GERDES, K. 2012. FtsZ-ZapA-ZapB interactome of *Escherichia coli*. *Journal of bacteriology,* 194**,** 292-302.

GARCIA, D. L. & DILLARD, J. P. 2006. AmiC functions as an *N*-acetylmuramyl-l-alanine amidase necessary for cell separation and can promote autolysis in *Neisseria gonorrhoeae*. *Journal of bacteriology,* 188**,** 7211-7221.

GARCIA, D. L. & DILLARD, J. P. 2008. Mutations in ampG or ampD affect PG fragment release from *Neisseria gonorrhoeae*. *Journal of bacteriology,* 190**,** 3799-3807.

GARNER, E. C., BERNARD, R., WANG, W., ZHUANG, X., RUDNER, D. Z. & MITCHISON, T. 2011. Coupled, circumferential motions of the cell wall synthesis machinery and MreB filaments in *B. subtilis*. *Science,* 333**,** 222-225.

GAYNOR, C. D., MCCORMACK, F. X., VOELKER, D. R., MCGOWAN, S. E. & SCHLESINGER, L. S. 1995. Pulmonary surfactant protein A mediates enhanced phagocytosis of *Mycobacterium tuberculosis* by a direct interaction with human macrophages. *The Journal of Immunology,* 155**,** 5343-5351.

GERONDAKIS, S., GROSSMANN, M., NAKAMURA, Y., POHL, T. & GRUMONT, R. 1999. Genetic approaches in mice to understand Rel/NF-kB and IkB function: transgenics and knockouts. *Oncogene,* 18**,** 6888-6895.

GINDA, K., BEZULSKA, M., ZIÓŁKIEWICZ, M., DZIADEK, J., ZAKRZEWSKA-CZERWIŃSKA, J. & JAKIMOWICZ, D. 2013. ParA of *Mycobacterium smegmatis* co-ordinates chromosome segregation with the cell cycle and interacts with the polar growth determinant DivIVA. *Molecular microbiology,* 87**,** 998-1012.

GIRARDIN, S. E., BONECA, I. G., CARNEIRO, L. A., ANTIGNAC, A., JÉHANNO, M., VIALA, J., TEDIN, K., TAHA, M.-K., LABIGNE, A. & ZÄTHRINGER, U. 2003a. Nod1 detects a unique muropeptide from gram-negative bacterial PG. *Science,* 300**,** 1584-1587.

GIRARDIN, S. E., BONECA, I. G., VIALA, J., CHAMAILLARD, M., LABIGNE, A., THOMAS, G., PHILPOTT, D. J. & SANSONETTI, P. J. 2003b. Nod2 is a general sensor of PG through muramyl dipeptide (MDP) detection. *J Biol Chem,* 278**,** 8869-72.

GOLA, S., MUNDER, T., CASONATO, S., MANGANELLI, R. & VICENTE, M. 2015. The essential role of SepF in mycobacterial division. *Molecular microbiology,* 97**,** 560-576.

GOLDEN, J. W. & YOON, H. S. 2003. Heterocyst development in Anabaena. *Curr Opin Microbiol,* 6**,** 557-63.

GOMEZ, J. E. & BISHAI, W. R. 2000. *whmD* is an essential mycobacterial gene required for proper septation and cell division. *Proceedings of the National Academy of Sciences,* 97**,** 8554-8559.

GOODELL, E. 1985. Recycling of murein by *Escherichia coli*. *Journal of bacteriology,* 163**,** 305-310.

GOODELL, E. W. & SCHWARZ, U. 1985. Release of cell wall peptides into culture medium by exponentially growing *Escherichia coli*. *Journal of bacteriology,* 162**,** 391-397.

GOTTFRIED, R. S. 2010. *Black death*, Simon and Schuster.

GRAY, P., DUNNE, A., BRIKOS, C., JEFFERIES, C. A., DOYLE, S. L. & O'NEILL, L. A. 2006. MyD88 adapter-like (Mal) is phosphorylated by Bruton's tyrosine kinase during TLR2 and TLR4 signal transduction. *J Biol Chem,* 281**,** 10489-95.

GRIFFIN, J. E., GAWRONSKI, J. D., DEJESUS, M. A., IOERGER, T. R., AKERLEY, B. J. & SASSETTI, C. M. 2011. High-resolution phenotypic profiling defines genes essential for mycobacterial growth and cholesterol catabolism. *PLoS Pathog,* 7**,** e1002251.

GROSSET, J. 2003. *Mycobacterium tuberculosis* in the extracellular compartment: an underestimated adversary. *Antimicrobial agents and chemotherapy,* 47**,** 833-836.

GUINN, K. M., HICKEY, M. J., MATHUR, S. K., ZAKEL, K. L., GROTZKE, J. E., LEWINSOHN, D. M., SMITH, S. & SHERMAN, D. R. 2004. Individual RD1-region genes are required for export of ESAT6/CFP-10 and for virulence of *Mycobacterium tuberculosis*. *Molecular microbiology,* 51**,** 359-370.

GUPTA, S., COHEN, K. A., WINGLEE, K., MAIGA, M., DIARRA, B. & BISHAI, W. R. 2014. Efflux inhibition with verapamil potentiates bedaquiline in *Mycobacterium tuberculosis*. *Antimicrobial agents and chemotherapy,* 58**,** 574-576.

HALE, C. A. & DE BOER, P. A. 1997. Direct binding of FtsZ to ZipA, an essential component of the septal ring structure that mediates cell division in *E. coli*. *Cell,* 88**,** 175-185.

HALE, C. A., SHIOMI, D., LIU, B., BERNHARDT, T. G., MARGOLIN, W., NIKI, H. & DE BOER, P. A. 2011. Identification of *Escherichia coli* ZapC (YcbW) as a component of the division apparatus that binds and bundles FtsZ polymers. *Journal of bacteriology,* 193**,** 1393-1404.

HASHIMOTO, M., OOIWA, S. & SEKIGUCHI, J. 2012. Synthetic lethality of the lytE cwlO genotype in *Bacillus subtilis* is caused by lack of D, L-endopeptidase activity at the lateral cell wall. *Journal of bacteriology,* 194**,** 796-803.

HAYASHI, J. M., LUO, C.-Y., MAYFIELD, J. A., HSU, T., FUKUDA, T., WALFIELD, A. L., GIFFEN, S. R., LESZYK, J. D., BAER, C. E. & BENNION, O. T. 2016. Spatially distinct and metabolically active membrane domain in mycobacteria. *Proceedings of the National Academy of Sciences,* 113**,** 5400-5405.

HAYASHI, J. M., RICHARDSON, K., MELZER, E. S., SANDLER, S. J., ALDRIDGE, B. B., SIEGRIST, M. S. & MORITA, Y. S. 2018. Stress-Induced Reorganisation of the Mycobacterial Membrane Domain. *mBio,* 9**,** e01823-17.

HEIDRICH, C., TEMPLIN, M. F., URSINUS, A., MERDANOVIC, M., BERGER, J., SCHWARZ, H., DE PEDRO, M. A. & HOLTJE, J. V. 2001. Involvement of *N*-acetylmuramyl-L-alanine amidases in cell separation and antibiotic-induced autolysis of *Escherichia coli*. *Mol Microbiol,* 41**,** 167-78.

HEIDRICH, C., URSINUS, A., BERGER, J., SCHWARZ, H. & HÖLTJE, J.-V. 2002. Effects of multiple deletions of murein hydrolases on viability, septum cleavage, and sensitivity to large toxic molecules in *Escherichia coli*. *Journal of bacteriology,* 184**,** 6093-6099.

HEMPEL, A. M., WANG, S.-B., LETEK, M., GIL, J. A. & FLÄRDH, K. 2008. Assemblies of DivIVA mark sites for hyphal branching and can establish new zones of cell wall growth in *Streptomyces coelicolor*. *Journal of bacteriology,* 190**,** 7579-7583.

HERSHKOVITZ, I., DONOGHUE, H. D., MINNIKIN, D. E., BESRA, G. S., LEE, O. Y., GERNAEY, A. M., GALILI, E., ESHED, V., GREENBLATT, C. L. & LEMMA, E. 2008. Detection and molecular characterisation of 9000-year-old *Mycobacterium tuberculosis* from a Neolithic settlement in the Eastern Mediterranean. *PloS one,* 3**,** e3426.

HETT, E. C., CHAO, M. C., DENG, L. L. & RUBIN, E. J. 2008. A mycobacterial enzyme essential for cell division synergises with resuscitation-promoting factor. *PLoS Pathog,* 4**,** e1000001.

HETT, E. C., CHAO, M. C. & RUBIN, E. J. 2010. Interaction and modulation of two antagonistic cell wall enzymes of mycobacteria. *PLoS pathogens,* 6**,** e1001020.

HETT, E. C., CHAO, M. C., STEYN, A. J., FORTUNE, S. M., DENG, L. L. & RUBIN, E. J. 2007. A partner for the resuscitation-promoting factors of *Mycobacterium tuberculosis*. *Mol Microbiol,* 66**,** 658-68.

HETT, E. C. & RUBIN, E. J. 2008. Bacterial growth and cell division: a mycobacterial perspective. *Microbiology and Molecular Biology Reviews,* 72**,** 126-156.

HORCAJO, P., DE PEDRO, M. A. & CAVA, F. 2012. PG plasticity in bacteria: stress-induced PG editing by noncanonical D-amino acids. *Microb Drug Resist,* 18**,** 306-13.

HOUBEN, E. N., NGUYEN, L. & PIETERS, J. 2006. Interaction of pathogenic mycobacteria with the host immune system. *Current opinion in microbiology,* 9**,** 76-85.

HUMANN, J. & LENZ, L. L. 2009. Bacterial PG-degrading enzymes and their impact on host muropeptide detection. *Journal of innate immunity,* 1**,** 88-97.

INOHARA, N. & NUNEZ, G. 2003. NODs: intracellular proteins involved in inflammation and apoptosis. *Nature Reviews Immunology,* 3**,** 371-382.

INOHARA, N., OGURA, Y., FONTALBA, A., GUTIERREZ, O., PONS, F., CRESPO, J., FUKASE, K., INAMURA, S., KUSUMOTO, S. & HASHIMOTO, M. 2003. Host Recognition of Bacterial Muramyl Dipeptide Mediated through NOD2 implications for crohn′ s disease. *Journal of Biological Chemistry,* 278**,** 5509-5512.

JACOBS, C., JORIS, B., JAMIN, M., KLARSOV, K., VAN BEEUMEN, J., MENGIN-LECREULX, D., VAN HEIJENOORT, J., PARK, J. T., NORMARK, S. & FRERE, J. M. 1995. AmpD, essential for both beta-lactamase regulation and cell wall recycling, is a novel cytosolic *N*-acetylmuramyl-L-alanine amidase. *Mol Microbiol,* 15**,** 553-559.

JARLIER, V. & NIKAIDO, H. 1994. Mycobacterial cell wall: structure and role in natural resistance to antibiotics. *FEMS microbiology letters,* 123**,** 11-18.

JONES-LÓPEZ, E. C., NAMUGGA, O., MUMBOWA, F., SSEBIDANDI, M., MBABAZI, O., MOINE, S., MBOOWA, G., FOX, M. P., REILLY, N. & AYAKAKA, I. 2013. Cough Aerosols of *Mycobacterium tuberculosis* Predict New Infection. A Household Contact Study. *American journal of respiratory and critical care medicine,* 187**,** 1007-1015.

JORGENSON, M. A., CHEN, Y., YAHASHIRI, A., POPHAM, D. L. & WEISS, D. S. 2014. The bacterial septal ring protein RlpA is a lytic transglycosylase that contributes to rod shape and daughter cell separation in *Pseudomonas aeruginosa*. *Molecular microbiology,* 93**,** 113-128.

JUSTICE, S. S., HUNSTAD, D. A., CEGELSKI, L. & HULTGREN, S. J. 2008. Morphological plasticity as a bacterial survival strategy. *Nature Reviews Microbiology,* 6**,** 162-168.

KANA, B. D., GORDHAN, B. G., DOWNING, K. J., SUNG, N., VOSTROKTUNOVA, G., MACHOWSKI, E. E., TSENOVA, L., YOUNG, M., KAPRELYANTS, A. & KAPLAN, G. 2008. The resuscitation-promoting factors of *Mycobacterium tuberculosis* are required for virulence and resuscitation from dormancy but are collectively dispensable for growth in vitro. *Molecular microbiology,* 67**,** 672-684.

KANG, C.-M., ABBOTT, D. W., PARK, S. T., DASCHER, C. C., CANTLEY, L. C. & HUSSON, R. N. 2005. The *Mycobacterium tuberculosis* serine/threonine kinases PknA and PknB: substrate identification and regulation of cell shape. *Genes & development,* 19**,** 1692-1704.

KANG, C.-M., NYAYAPATHY, S., LEE, J.-Y., SUH, J.-W. & HUSSON, R. N. 2008. Wag31, a homologue of the cell division protein DivIVA, regulates growth, morphology and polar cell wall synthesis in mycobacteria. *Microbiology,* 154**,** 725-735.

KANNEGANTI, T. D., LAMKANFI, M. & NUNEZ, G. 2007. Intracellular NOD-like receptors in host defense and disease. *Immunity,* 27**,** 549-59.

KARLEN, A. 1996. *Man and microbes: disease and plagues in history and modern times*, Simon and Schuster.

KESHAVJEE, S. & FARMER, P. E. 2012. Tuberculosis, drug resistance, and the history of modern medicine. *New England Journal of Medicine,* 367**,** 931-936.

KHALILGHARIBI, N., BAUM, B. & MIODOWNIK, M. 2012. Evolution of Cell Division.

KIESER, K. J., BOUTTE, C. C., KESTER, J. C., BAER, C. E., BARCZAK, A. K., MENICHE, X., CHAO, M. C., REGO, E. H., SASSETTI, C. M. & FORTUNE, S. M. 2015. Phosphorylation of the PG synthase PonA1 governs the rate of polar elongation in mycobacteria. *PLoS pathogens,* 11**,** e1005010.

KIM, J., KUNDU, M., VIOLLET, B. & GUAN, K.-L. 2011. AMPK and mTOR regulate autophagy through direct phosphorylation of Ulk1. *Nature cell biology,* 13**,** 132-141.

KLÖCKNER, A., OTTEN, C., DEROUAUX, A., VOLLMER, W., BÜHL, H., DE BENEDETTI, S., MÜNCH, D., JOSTEN, M., MÖLLEKEN, K. & SAHL, H.-G. 2014. AmiA is a penicillin target enzyme with dual activity in the intracellular pathogen *Chlamydia pneumoniae*. *Nature communications,* 5.

KORSAK, D., LIEBSCHER, S. & VOLLMER, W. 2005. Susceptibility to antibiotics and β-lactamase induction in murein hydrolase mutants of *Escherichia coli*. *Antimicrobial agents and chemotherapy,* 49**,** 1404-1409.

KRUSE, T., BORK-JENSEN, J. & GERDES, K. 2005. The morphogenetic MreBCD proteins of *Escherichia coli* form an essential membrane-bound complex. *Mol Microbiol,* 55**,** 78-89.

LAVOLLAY, M., ARTHUR, M., FOURGEAUD, M., DUBOST, L., MARIE, A., VEZIRIS, N., BLANOT, D., GUTMANN, L. & MAINARDI, J.-L. 2008. The PG of stationary-phase *Mycobacterium tuberculosis* predominantly contains cross-links generated by L, D-transpeptidation. *Journal of bacteriology,* 190**,** 4360-4366.

LAVOLLAY, M., FOURGEAUD, M., HERRMANN, J.-L., DUBOST, L., MARIE, A., GUTMANN, L., ARTHUR, M. & MAINARDI, J.-L. 2011. The PG of Mycobacterium abscessus is predominantly cross-linked by L, D-transpeptidases. *Journal of bacteriology,* 193**,** 778-782.

LEAVER, M. & ERRINGTON, J. 2005. Roles for MreC and MreD proteins in helical growth of the cylindrical cell wall in *Bacillus subtilis*. *Mol Microbiol,* 57**,** 1196-209.

LEMAITRE, B., REICHHART, J. M. & HOFFMANN, J. A. 1997. Drosophila host defense: differential induction of antimicrobial peptide genes after infection by various classes of microorganisms. *Proc Natl Acad Sci U S A,* 94**,** 14614-14619.

LEVIN, B. R., PERROT, V. & WALKER, N. 2000. Compensatory mutations, antibiotic resistance and the population genetics of adaptive evolution in bacteria. *Genetics,* 154**,** 985-997.

LIN, P. L. & FLYNN, J. L. 2010. Understanding latent tuberculosis: a moving target. *The Journal of Immunology,* 185**,** 15-22.

LIU, J., BARRY, C. E., BESRA, G. S. & NIKAIDO, H. 1996. Mycolic acid structure determines the fluidity of the mycobacterial cell wall. *Journal of Biological Chemistry,* 271**,** 29545-29551.

LIU, Z., MUKHERJEE, A. & LUTKENHAUS, J. 1999. Recruitment of ZipA to the division site by interaction with FtsZ. *Molecular microbiology,* 31**,** 1853-1861.

LOMOVSKAYA, O., WARREN, M. S., LEE, A., GALAZZO, J., FRONKO, R., LEE, M., BLAIS, J., CHO, D., CHAMBERLAND, S. & RENAU, T. 2001. Identification and characterisation of inhibitors of multidrug resistance efflux pumps in *Pseudomonas aeruginosa*: novel agents for combination therapy. *Antimicrobial agents and chemotherapy,* 45**,** 105-116.

LONGCHAMP, P. F., MAUEL, C. & KARAMATA, D. 1994. Lytic enzymes associated with defective prophages of *Bacillus subtilis*: sequencing and characterisation of the region comprising the *N*-acetylmuramoyl-L-alanine amidase gene of prophage PBSX. *Microbiology,* 140 (Pt 8)**,** 1855-67.

LOOSE, M. & MITCHISON, T. J. 2014. The bacterial cell division proteins FtsA and FtsZ self-organize into dynamic cytoskeletal patterns. *Nature cell biology,* 16**,** 38-46.

LOW, H. H., MONCRIEFFE, M. C. & LÖWE, J. 2004. The crystal structure of ZapA and its modulation of FtsZ polymerisation. *Journal of molecular biology,* 341**,** 839-852.

LÖWE, J. & AMOS, L. A. 1998. Crystal structure of the bacterial cell-division protein FtsZ. *Nature,* 391**,** 203-206.

MACHOWSKI, E. E., SENZANI, S., EALAND, C. & KANA, B. D. 2014. Comparative genomics for mycobacterial PG remodelling enzymes reveals extensive genetic multiplicity. *BMC microbiology,* 14**,** 75.

MAEDA, Y. T., NAKADAI, T., SHIN, J., URYU, K., NOIREAUX, V. & LIBCHABER, A. 2012. Assembly of MreB filaments on liposome membranes: a synthetic biology approach. *ACS Synth Biol,* 1**,** 53-9.

MARRAKCHI, H., LANÉELLE, M.-A. & DAFFÉ, M. 2014. Mycolic acids: structures, biosynthesis, and beyond. *Chemistry & biology,* 21**,** 67-85.

MARTEYN, B. S., KARIMOVA, G., FENTON, A. K., GAZI, A. D., WEST, N., TOUQUI, L., PREVOST, M.-C., BETTON, J.-M., POYRAZ, O. & LADANT, D. 2014. ZapE is a novel cell division protein interacting with FtsZ and modulating the Z-ring dynamics. *MBio,* 5**,** e00022-14.

MARTINELLI, D. J. & PAVELKA, M. S. 2016. The RipA and RipB PG endopeptidases are individually nonessential to *Mycobacterium smegmatis*. *Journal of bacteriology,* 198**,** 1464-1475.

MASSEY, T. H., MERCOGLIANO, C. P., YATES, J., SHERRATT, D. J. & LÖWE, J. 2006. Double-stranded DNA translocation: structure and mechanism of hexameric FtsK. *Molecular cell,* 23**,** 457-469.

MATTHEYSES, A. L., SIMON, S. M. & RAPPOPORT, J. Z. 2010. Imaging with total internal reflection fluorescence microscopy for the cell biologist. *J Cell Sci,* 123**,** 3621-3628.

MCCOY, A. J., SANDLIN, R. C. & MAURELLI, A. T. 2003. In vitro and in vivo functional activity of Chlamydia MurA, a UDP-*N*-acetylglucosamine enolpyruvyl transferase involved in PG synthesis and fosfomycin resistance. *J Bacteriol,* 185**,** 1218-28.

MCPHERSON, D. C. & POPHAM, D. L. 2003. PG synthesis in the absence of class A penicillin-binding proteins in *Bacillus subtilis*. *J Bacteriol,* 185**,** 1423-31.

MCSHANE, H. 2005. Co-infection with HIV and TB: double trouble. *International journal of STD & AIDS,* 16**,** 95-101.

MEISNER, J., MONTERO LLOPIS, P., SHAM, L. T., GARNER, E., BERNHARDT, T. G. & RUDNER, D. Z. 2013. FtsEX is required for CwlO PG hydrolase activity during cell wall elongation in *Bacillus subtilis*. *Molecular microbiology,* 89**,** 1069-1083.

MELLY, M. A., MCGEE, Z. A. & ROSENTHAL, R. S. 1984. Ability of monomeric PG fragments from *Neisseria gonorrhoeae* to damage human fallopian-tube mucosa. *Journal of Infectious Diseases,* 149**,** 378-386.

MENICHE, X., OTTEN, R., SIEGRIST, M. S., BAER, C. E., MURPHY, K. C., BERTOZZI, C. R. & SASSETTI, C. M. 2014. Subpolar addition of new cell wall is directed by DivIVA in mycobacteria. *Proc Natl Acad Sci U S A,* 111**,** E3243-51.

MESTRE, O., HURTADO-ORTIZ, R., DOS VULTOS, T., NAMOUCHI, A., CIMINO, M., PIMENTEL, M., NEYROLLES, O. & GICQUEL, B. 2013. High throughput phenotypic selection of *Mycobacterium tuberculosis* mutants with impaired resistance to reactive oxygen species identifies genes important for intracellular growth. *Plos One,* 8**,** e53486.

MIR, M., ASONG, J., LI, X., CARDOT, J., BOONS, G.-J. & HUSSON, R. N. 2011. The extracytoplasmic domain of the *Mycobacterium tuberculosis* Ser/Thr kinase PknB binds specific muropeptides and is required for PknB localisation. *PLoS pathog,* 7**,** e1002182.

MIZUNO, M., MASUDA, S., TAKEMARU, K., HOSONO, S., SATO, T., TAKEUCHI, M. & KOBAYASHI, Y. 1996. Systematic sequencing of the 283 kb 210 degrees-232 degrees region of the *Bacillus subtilis* genome containing the skin element and many sporulation genes. *Microbiology,* 142 (Pt 11)**,** 3103-3111.

MOHAMMADI, T., VAN DAM, V., SIJBRANDI, R., VERNET, T., ZAPUN, A., BOUHSS, A., DIEPEVEEN-DE BRUIN, M., NGUYEN-DISTÈCHE, M., DE KRUIJFF, B. & BREUKINK, E. 2011. Identification of FtsW as a transporter of lipid-linked cell wall precursors across the membrane. *The EMBO journal,* 30**,** 1425-1432.

MORGENSTEIN, R. M., BRATTON, B. P., NGUYEN, J. P., OUZOUNOV, N., SHAEVITZ, J. W. & GITAI, Z. 2015. RodZ links MreB to cell wall synthesis to mediate MreB rotation and robust morphogenesis. *Proc Natl Acad Sci U S A,* 112**,** 12510-12515.

MORITA, Y. S., VELASQUEZ, R., TAIG, E., WALLER, R. F., PATTERSON, J. H., TULL, D., WILLIAMS, S. J., BILLMAN-JACOBE, H. & MCCONVILLE, M. J. 2005. Compartmentalisation of lipid biosynthesis in mycobacteria. *Journal of Biological Chemistry,* 280**,** 21645-21652.

MORRIS, S., BAI, G. H., SUFFYS, P., PORTILLO-GOMEZ, L., FAIRCHOK, M. & ROUSE, D. 1995. Molecular mechanisms of multiple drug resistance in clinical isolates of *Mycobacterium tuberculosis*. *Journal of Infectious Diseases,* 171**,** 954-960.

MUKAMOLOVA, G. V., MURZIN, A. G., SALINA, E. G., DEMINA, G. R., KELL, D. B., KAPRELYANTS, A. S. & YOUNG, M. 2006. Muralytic activity of Micrococcus luteus Rpf and its relationship to physiological activity in promoting bacterial growth and resuscitation. *Molecular microbiology,* 59**,** 84-98.

MUKHERJEE, A., SAEZ, C. & LUTKENHAUS, J. 2001. Assembly of an FtsZ mutant deficient in GTPase activity has implications for FtsZ assembly and the role of the Z-ring in cell division. *Journal of bacteriology,* 183**,** 7190-7197.

MURRAY, H. & ERRINGTON, J. 2008. Dynamic control of the DNA replication initiation protein DnaA by Soj/ParA. *Cell,* 135**,** 74-84.

MURRAY, T., POPHAM, D. L. & SETLOW, P. 1996. Identification and characterisation of pbpC, the gene encoding *Bacillus subtilis* penicillin-binding protein 3. *J Bacteriol,* 178**,** 6001-5.

NATARAJ, V., VARELA, C., JAVID, A., SINGH, A., BESRA, G. S. & BHATT, A. 2015. Mycolic acids: deciphering and targeting the Achilles' heel of the tubercle bacillus. *Molecular microbiology,* 98**,** 7-16.

NELSON, D. E., GHOSH, A. S., PAULSON, A. L. & YOUNG, K. D. 2002. Contribution of membrane-binding and enzymatic domains of penicillin-binding protein 5 to maintenance of uniform cellular morphology of *Escherichia coli*. *J Bacteriol,* 184**,** 3630-9.

NELSON, D. E. & YOUNG, K. D. 2000. Penicillin-binding protein 5 affects cell diameter, contour, and morphology of *Escherichia coli*. *J Bacteriol,* 182**,** 1714-21.

NELSON, D. E. & YOUNG, K. D. 2001. Contributions of PBP 5 and DD-carboxypeptidase penicillin-binding proteins to maintenance of cell shape in *Escherichia coli*. *J Bacteriol,* 183**,** 3055-64.

NIKITUSHKIN, V. D., DEMINA, G. R., SHLEEVA, M. O. & KAPRELYANTS, A. S. 2013. PG fragments stimulate resuscitation of "non-culturable" mycobacteria. *Antonie Van Leeuwenhoek,* 103**,** 37-46.

NISA, S., BLOKPOEL, M. C., ROBERTSON, B. D., TYNDALL, J. D., LUN, S., BISHAI, W. R. & O'TOOLE, R. 2010. Targeting the chromosome partitioning protein ParA in tuberculosis drug discovery. *Journal of antimicrobial chemotherapy,* 65**,** 2347-2358.

NUGROHO, F. A., YAMAMOTO, H., KOBAYASHI, Y. & SEKIGUCHI, J. 1999. Characterisation of a new sigma-K-dependent PG hydrolase gene that plays a role in *Bacillus subtilis* mother cell lysis. *J Bacteriol,* 181**,** 6230-7.

ORME, I. & GONZALEZ-JUARRERO, M. 2007. Animal models of *M. tuberculosis* infection. *Current protocols in microbiology***,** 10A. 5.1-10A. 5.29.

ORTIZ, C., NATALE, P., CUETO, L. & VICENTE, M. 2016. The keepers of the ring: regulators of FtsZ assembly. *FEMS microbiology reviews,* 40**,** 57-67.
OSAWA, M., ANDERSON, D. E. & ERICKSON, H. P. 2008. Reconstitution of contractile FtsZ-rings in liposomes. *Science,* 320**,** 792-794.
OUELLETTE, S. P., KARIMOVA, G., SUBTIL, A. & LADANT, D. 2012. Chlamydia co-opts the rod shape-determining proteins MreB and Pbp2 for cell division. *Molecular microbiology,* 85**,** 164-178.
PALANIYAR, N., DZIARSKI, R. & GUPTA, D. 2010. Review: Mammalian PG recognition proteins (PGRPs) in innate immunity. *Innate immunity,* 16**,** 168-174.
PARISH, T. & STOKER, N. G. 2000. Use of a flexible cassette method to generate a double unmarked *Mycobacterium tuberculosis tlyA plcABC* mutant by gene replacement. *Microbiology,* 146 (Pt 8)**,** 1969-1975.
PARK, S. T., KANG, C.-M. & HUSSON, R. N. 2008. Regulation of the SigH stress response regulon by an essential protein kinase in *Mycobacterium tuberculosis*. *Proceedings of the National Academy of Sciences,* 105**,** 13105-13110.
PARRISH, N. M., DICK, J. D. & BISHAI, W. R. 1998. Mechanisms of latency in *Mycobacterium tuberculosis*. *Trends in microbiology,* 6**,** 107-112.
PATTERSON, K. D. & PYLE, G. F. 1991. The geography and mortality of the 1918 influenza pandemic. *Bulletin of the History of Medicine,* 65**,** 4.
PAZOS, M., NATALE, P. & VICENTE, M. 2013. A Specific Role for the ZipA Protein in Cell Division stabilisation of the FtsZ protein. *Journal of Biological Chemistry,* 288**,** 3219-3226.
PETERS, N. T., DINH, T. & BERNHARDT, T. G. 2011. A fail-safe mechanism in the septal ring assembly pathway generated by the sequential recruitment of cell separation amidases and their activators. *J Bacteriol,* 193**,** 4973-4983.
PIGGOT, P. J. & HILBERT, D. W. 2004. Sporulation of *Bacillus subtilis*. *Curr Opin Microbiol,* 7**,** 579-86.
PILHOFER, M., AISTLEITNER, K., BIBOY, J., GRAY, J., KURU, E., HALL, E., BRUN, Y. V., VANNIEUWENHZE, M. S., VOLLMER, W. & HORN, M. 2013. Discovery of chlamydial PG reveals bacteria with murein sacculi but without FtsZ. *Nature communications,* 4.
POLLOCK, J. J., NGUYEN-DISTÈCHE, M., GHUYSEN, J. M., COYETTE, J., LINDER, R., SALTON, M. R., KIM, K. S., PERKINS, H. R. & REYNOLDS, P. 1974. Fractionation of the DD-Carboxypeptidase-Transpeptidase Activities Solubilised from Membranes of *Escherichia coli* K12, Strain 44. *The FEBS Journal,* 41**,** 439-446.
PONPUAK, M., DAVIS, A. S., ROBERTS, E. A., DELGADO, M. A., DINKINS, C., ZHAO, Z., VIRGIN, H. W., KYEI, G. B., JOHANSEN, T. & VERGNE, I. 2010. Delivery of cytosolic components by autophagic adaptor protein p62 endows autophagosomes with unique antimicrobial properties. *Immunity,* 32**,** 329-341.
POPHAM, D. L. 2002. Specialised PG of the bacterial endospore: the inner wall of the lockbox. *Cell Mol Life Sci,* 59**,** 426-433.
POPHAM, D. L., HELIN, J., COSTELLO, C. E. & SETLOW, P. 1996. Muramic lactam in PG of *Bacillus subtilis* spores is required for spore outgrowth but not for spore dehydration or heat resistance. *Proc Natl Acad Sci U S A,* 93**,** 15405-15410.
POPHAM, D. L. & SETLOW, P. 1995. Cloning, nucleotide sequence, and mutagenesis of the *Bacillus subtilis ponA* operon, which codes for penicillin-binding protein (PBP) 1 and a PBP-related factor. *J Bacteriol,* 177**,** 326-335.
PRISIC, S., DANKWA, S., SCHWARTZ, D., CHOU, M. F., LOCASALE, J. W., KANG, C.-M., BEMIS, G., CHURCH, G. M., STEEN, H. & HUSSON, R. N. 2010. Extensive phosphorylation with overlapping specificity by *Mycobacterium tuberculosis* serine/threonine protein kinases. *Proceedings of the National Academy of Sciences,* 107**,** 7521-7526.
RAVIGLIONE, M. & SULIS, G. 2016. Tuberculosis 2015: burden, challenges and strategy for control and elimination. *Infectious disease reports,* 8.

RAYCHAUDHURI, D. 1999. ZipA is a MAP–Tau homolog and is essential for structural integrity of the cytokinetic FtsZ-ring during bacterial cell division. *The EMBO Journal,* 18**,** 2372-2383.

RAYCHAUDHURI, D. & PARK, J. T. 1992. *Escherichia coli* cell-division gene ftsZ encodes a novel GTP-binding protein. *Nature,* 359**,** 251-254.

RAYMAN, M. K. & MACLEOD, R. A. 1975. Interaction of Mg-2+ with PG and its relation to the prevention of lysis of a marine pseudomonad. *Journal of bacteriology,* 122**,** 650-659.

REGAMEY, A. & KARAMATA, D. 1998. The *N*-acetylmuramoyl-L-alanine amidase encoded by the *Bacillus subtilis* 168 prophage SP beta. *Microbiology,* 144 (Pt 4)**,** 885-893.

REZWAN, M., LANEELLE, M. A., SANDER, P. & DAFFE, M. 2007. Breaking down the wall: fractionation of mycobacteria. *J Microbiol Methods,* 68**,** 32-39.

RICO, A. I., GARCÍA-OVALLE, M., PALACIOS, P., CASANOVA, M. & VICENTE, M. 2010. Role of *Escherichia coli* FtsN protein in the assembly and stability of the cell division ring. *Molecular microbiology,* 76**,** 760-771.

ROCABOY, M., HERMAN, R., SAUVAGE, E., REMAUT, H., MOONENS, K., TERRAK, M., CHARLIER, P. & KERFF, F. 2013. The crystal structure of the cell division amidase AmiC reveals the fold of the AMIN domain, a new PG binding domain. *Mol Microbiol*.

ROTHSCHILD, B. & MARTIN, L. 2003. Frequency of pathology in a large natural sample from Natural Trap Cave with special remarks on erosive disease in the Pleistocene. *Reumatismo,* 55**,** 58-65.

RUSSELL-GOLDMAN, E., XU, J., WANG, X., CHAN, J. & TUFARIELLO, J. M. 2008. A *Mycobacterium tuberculosis* Rpf double-knockout strain exhibits profound defects in reactivation from chronic tuberculosis and innate immunity phenotypes. *Infection and immunity,* 76**,** 4269-4281.

RUSSELL, D. G., CARDONA, P.-J., KIM, M.-J., ALLAIN, S. & ALTARE, F. 2009. Foamy macrophages and the progression of the human tuberculosis granuloma. *Nature immunology,* 10**,** 943-948.

SANTI, I., DHAR, N., BOUSBAINE, D., WAKAMOTO, Y. & MCKINNEY, J. D. 2013. Single-cell dynamics of the chromosome replication and cell division cycles in mycobacteria. *Nat Commun,* 4**,** 2470.

SANTI, I. & MCKINNEY, J. D. 2015. Chromosome organisation and replisome dynamics in *Mycobacterium smegmatis*. *MBio,* 6**,** e01999-14.

SASSETTI, C. M. & RUBIN, E. J. 2003. Genetic requirements for mycobacterial survival during infection. *Proceedings of the National Academy of Sciences,* 100**,** 12989-12994.

SCHEFFERS, D. J. & DRIESSEN, A. J. 2002. Immediate GTP hydrolysis upon FtsZ polymerisation. *Molecular microbiology,* 43**,** 1517-1521.

SCHLESINGER, L. 1993. Macrophage phagocytosis of virulent but not attenuated strains of *Mycobacterium tuberculosis* is mediated by mannose receptors in addition to complement receptors. *The Journal of Immunology,* 150**,** 2920-2930.

SEKIGUCHI, J., AKEO, K., YAMAMOTO, H., KHASANOV, F. K., ALONSO, J. C. & KURODA, A. 1995. Nucleotide sequence and regulation of a new putative cell wall hydrolase gene, cwlD, which affects germination in *Bacillus subtilis*. *J Bacteriol,* 177**,** 5582-5589.

SEMU, M., FENTA, T. G., MEDHIN, G. & ASSEFA, D. 2017. Effectiveness of isoniazid preventative therapy in reducing incidence of active tuberculosis among people living with HIV/AIDS in public health facilities of Addis Ababa, Ethiopia: a historical cohort study. *BMC infectious diseases,* 17**,** 5.

SENZANI, S. 2014. *Analysis of PG degrading amidases in Mycobacterium smegmatis*. MSc Med, University of the Witwatersrand.

SENZANI, S., LI, D., BHASKAR, A., EALAND, C., CHANG, J., RIMAL, B., LIU, C., KIM, S. J., DHAR, N. & KANA, B. 2017. An Amidase_3 domain-containing *N*-acetylmuramyl-L-alanine amidase is required for mycobacterial cell division. *Scientific Reports,* 7**,** 1140.

SHAH, I. M., LAABERKI, M.-H., POPHAM, D. L. & DWORKIN, J. 2008. A eukaryotic-like Ser/Thr kinase signals bacteria to exit dormancy in response to PG fragments. *Cell,* 135**,** 486-496.

SHIOMI, D., TOYODA, A., AIZU, T., EJIMA, F., FUJIYAMA, A., SHINI, T., KOHARA, Y. & NIKI, H. 2013. Mutations in cell elongation genes *mreB, mrdA* and *mrdB* suppress the shape defect of RodZ-deficient cells. *Mol Microbiol,* 87**,** 1029-1044.

SHLEEVA, M., SALINA, E. & KAPRELYANTS, A. 2010. Dormant forms of mycobacteria. *Microbiology,* 79**,** 1-12.

SIEGER, B. & BRAMKAMP, M. 2015. Interaction sites of DivIVA and RodA from *Corynebacterium glutamicum*. *Frontiers in microbiology,* 5**,** 738.

SINGH, B., GHOSH, J., ISLAM, N. M., DASGUPTA, S. & KIRSEBOM, L. A. 2010. Growth, cell division and sporulation in mycobacteria. *Antonie Van Leeuwenhoek,* 98**,** 165-177.

SINGH, J. K., MAKDE, R. D., KUMAR, V. & PANDA, D. 2007. A membrane protein, EzrA, regulates assembly dynamics of FtsZ by interacting with the C-terminal tail of FtsZ. *Biochemistry,* 46**,** 11013-11022.

SINGH, R., KAUSHIK, S., WANG, Y., XIANG, Y., NOVAK, I., KOMATSU, M., TANAKA, K., CUERVO, A. M. & CZAJA, M. J. 2009. Autophagy regulates lipid metabolism. *Nature,* 458**,** 1131-1135.

SINGH, S. K., SAISREE, L., AMRUTHA, R. N. & REDDY, M. 2012. Three redundant murein endopeptidases catalyse an essential cleavage step in PG synthesis of *Escherichia coli* K12. *Molecular microbiology,* 86**,** 1036-1051.

SMITH, I. 2003. *Mycobacterium tuberculosis* pathogenesis and molecular determinants of virulence. *Clinical microbiology reviews,* 16**,** 463-496.

SMITH, J., MANORANJAN, J., PAN, M., BOHSALI, A., XU, J., LIU, J., MCDONALD, K. L., SZYK, A., LARONDE-LEBLANC, N. & GAO, L.-Y. 2008. Evidence for pore formation in host cell membranes by ESX-1-secreted ESAT6 and its role in *Mycobacterium marinum* escape from the vacuole. *Infection and immunity,* 76**,** 5478-5487.

SMITH, T. J., BLACKMAN, S. A. & FOSTER, S. J. 2000. Autolysins of *Bacillus subtilis*: multiple enzymes with multiple functions. *Microbiology,* 146 (Pt 2)**,** 249-262.

SMITH, T. J. & FOSTER, S. J. 1995. Characterisation of the involvement of two compensatory autolysins in mother cell lysis during sporulation of *Bacillus subtilis* 168. *J Bacteriol,* 177**,** 3855-62.

SNAPPER, S. B., MELTON, R. E., MUSTAFA, S., KEISER, T. & JACOBS JR, W. R., JR. 1990. Isolation and Characterisation of efficient vector transformation mutants of *Mycobactrium smegmatis*. *Mol Microbiol,* 4**,** 1911-1919.

SONG, T., DOVE, S. L., LEE, K. H. & HUSSON, R. N. 2003. RshA, an anti-sigma factor that regulates the activity of the mycobacterial stress response sigma factor SigH. *Molecular microbiology,* 50**,** 949-959.

STAPLETON, M. R., HORSBURGH, M. J., HAYHURST, E. J., WRIGHT, L., JONSSON, M., TARKOWSKI, A., KOKAI-KUN, J. F., MOND, J. J. & FOSTER, S. J. 2007. Characterisation of IsaA and SceD, two putative lytic transglycosylases of *Staphylococcus aureus*. *Journal of bacteriology,* 189**,** 7316-7325.

SUGAI, M., KOMATSUZAWA, H., AKIYAMA, T., HONG, Y.-M., OSHIDA, T., MIYAKE, Y., YAMAGUCHI, T. & SUGINAKA, H. 1995. Identification of endo-beta-*N*-acetylglucosaminidase and *N*-acetylmuramyl-L-alanine amidase as cluster-dispersing enzymes in *Staphylococcus aureus*. *Journal of bacteriology,* 177**,** 1491-1496.

SUMARYATI, S., NEGRUTIU, I. & JACOBS, M. 1992. Characterisation and regeneration of salt-and water-stress mutants from protoplast culture of *Nicotiana plumbaginifolia* (Viviani). *Theoretical and applied genetics,* 83**,** 613-619.

SZWEDZIAK, P., WANG, Q., FREUND, S. M. & LÖWE, J. 2012. FtsA forms actin-like protofilaments. *The EMBO journal,* 31**,** 2249-2260.

TAKEDA, K. & AKIRA, S. 2005. Toll-like receptors in innate immunity. *Int Immunol,* 17**,** 1-14.

TAKEUCHI, O., TAKEDA, K., HOSHINO, K., ADACHI, O., OGAWA, T. & AKIRA, S. 2000. Cellular responses to bacterial cell wall components are mediated through MyD88-dependent signaling cascades. *Int Immunol,* 12**,** 113-117.

TAN, T., LEE, W. L., ALEXANDER, D. C., GRINSTEIN, S. & LIU, J. 2006. The ESAT6/CFP-10 secretion system of *Mycobacterium marinum* modulates phagosome maturation. *Cellular microbiology,* 8**,** 1417-1429.

TEMPLIN, M. F., URSINUS, A. & HÖLTJE, J. V. 1999. A defect in cell wall recycling triggers autolysis during the stationary growth phase of *Escherichia coli*. *The EMBO Journal,* 18**,** 4108-4117.

TREUNER-LANGE, A., AGUILUZ, K., DER DOES, C., GÓMEZ-SANTOS, N., HARMS, A., SCHUMACHER, D., LENZ, P., HOPPERT, M., KAHNT, J. & MUÑOZ-DORADO, J. 2013. PomZ, a ParA-like protein, regulates Z-ring formation and cell division in *Myxococcus xanthus*. *Molecular microbiology,* 87**,** 235-253.

TUFARIELLO, J. M., MI, K., XU, J., MANABE, Y. C., KESAVAN, A. K., DRUMM, J., TANAKA, K., JACOBS, W. R. & CHAN, J. 2006. Deletion of the *Mycobacterium tuberculosis* resuscitation-promoting factor Rv1009 gene results in delayed reactivation from chronic tuberculosis. *Infection and immunity,* 74**,** 2985-2995.

TYPAS, A., BANZHAF, M., GROSS, C. A. & VOLLMER, W. 2011. From the regulation of PG synthesis to bacterial growth and morphology. *Nat Rev Microbiol,* 10**,** 123-136.

UEHARA, T., PARZYCH, K. R., DINH, T. & BERNHARDT, T. G. 2010. Daughter cell separation is controlled by cytokinetic ring-activated cell wall hydrolysis. *EMBO J,* 29**,** 1412-1422.

VAN DEN ENT, F. & LÖWE, J. 2000. Crystal structure of the cell division protein FtsA from *Thermotoga maritima*. *The EMBO journal,* 19**,** 5300-5307.

VAN DER WEL, N., HAVA, D., HOUBEN, D., FLUITSMA, D., VAN ZON, M., PIERSON, J., BRENNER, M. & PETERS, P. J. 2007. *M. tuberculosis* and *M. leprae* translocate from the phagolysosome to the cytosol in myeloid cells. *Cell,* 129**,** 1287-1298.

VAN TEEFFELEN, S., WANG, S., FURCHTGOTT, L., HUANG, K. C., WINGREEN, N. S., SHAEVITZ, J. W. & GITAI, Z. 2011. The bacterial actin MreB rotates, and rotation depends on cell-wall assembly. *Proc Natl Acad Sci U S A,* 108**,** 15822-15827.

VILA, J., MARTÍ, S. & SÁNCHEZ-CÉSPEDES, J. 2007. Porins, efflux pumps and multidrug resistance in *Acinetobacter baumannii*. *Journal of Antimicrobial Chemotherapy,* 59**,** 1210-1215.

VOLLMER, W., JORIS, B., CHARLIER, P. & FOSTER, S. 2008. Bacterial PG (murein) hydrolases. *FEMS microbiology reviews,* 32**,** 259-286.

WACHI, M. & MATSUHASHI, M. 1989. Negative control of cell division by *mreB*, a gene that functions in determining the rod shape of *Escherichia coli* cells. *Journal of bacteriology,* 171**,** 3123-3127.

WANG, X. & LUTKENHAUS, J. 1993. The FtsZ protein of *Bacillus subtilis* is localised at the division site and has GTPase activity that is dependent upon FtsZ concentration. *Molecular microbiology,* 9**,** 435-442.

WAYNE, L. 1994. Dormancy of *Mycobacterium tuberculosis* and latency of disease. *European Journal of Clinical Microbiology & Infectious Diseases,* 13**,** 908-914.

WEATHERSPOON-GRIFFIN, N., ZHAO, G., KONG, W., KONG, Y., ANDREWS-POLYMENIS, H., MCCLELLAND, M. & SHI, Y. 2011. The CpxR/CpxA two-component system up-regulates two Tat-dependent PG amidases to confer bacterial resistance to antimicrobial peptide. *Journal of Biological Chemistry,* 286**,** 5529-5539.

WEBBER, M. & PIDDOCK, L. 2003. The importance of efflux pumps in bacterial antibiotic resistance. *Journal of Antimicrobial Chemotherapy,* 51**,** 9-11.

WEI, Y., HAVASY, T., MCPHERSON, D. C. & POPHAM, D. L. 2003. Rod shape determination by the *Bacillus subtilis* class B penicillin-binding proteins encoded by pbpA and pbpH. *J Bacteriol,* 185**,** 4717-4726.

WEIBULL, C. 1953. The isolation of protoplasts from *Bacillus megaterium* by controlled treatment with lysozyme. *Journal of bacteriology,* 66**,** 688.

WELLS, W. F. 1934. On air-borne infection. Study II. Droplets and droplet nuclei. *American Journal of Hygiene,* 20**,** 611-618.

WHITE, C. L., KITICH, A. & GOBER, J. W. 2010. Positioning cell wall synthetic complexes by the bacterial morphogenetic proteins MreB and MreD. *Mol Microbiol,* 76**,** 616-633.

WHO 2016a. Global tuberculosis report 2016.
WHO 2016b. World Health Statistics: Monitering Health for sustainable development goals.
WILLEMSE, J., BORST, J. W., DE WAAL, E., BISSELING, T. & VAN WEZEL, G. P. 2011. Positive control of cell division: FtsZ is recruited by SsgB during sporulation of Streptomyces. *Genes & development,* 25**,** 89-99.
WILLIAMS, M. J., KANA, B. D. & MIZRAHI, V. 2011. Functional analysis of molybdopterin biosynthesis in mycobacteria identifies a fused molybdopterin synthase in *Mycobacterium tuberculosis*. *Journal of bacteriology,* 193**,** 98-106.
WURIE, F. B., LAWN, S. D., BOOTH, H., SONNENBERG, P. & HAYWARD, A. C. 2016. Bioaerosol production by patients with tuberculosis during normal tidal breathing: implications for transmission risk. *Thorax,* 71**,** 549-554.
XU, J., LAINE, O., MASCIOCCHI, M., MANORANJAN, J., SMITH, J., DU, S. J., EDWARDS, N., ZHU, X., FENSELAU, C. & GAO, L. Y. 2007. A unique Mycobacterium ESX-1 protein co-secretes with CFP-10/ESAT6 and is necessary for inhibiting phagosome maturation. *Molecular microbiology,* 66**,** 787-800.
YAKHNINA, A. A., MCMANUS, H. R. & BERNHARDT, T. G. 2015. The cell wall amidase AmiB is essential for *Pseudomonas aeruginosa* cell division, drug resistance and viability. *Molecular microbiology,* 97**,** 957-973.
YAMAMOTO, M., SATO, S., HEMMI, H., SANJO, H., UEMATSU, S., KAISHO, T., HOSHINO, K., TAKEUCHI, O., KOBAYASHI, M., FUJITA, T., TAKEDA, K. & AKIRA, S. 2002. Essential role for TIRAP in activation of the signalling cascade shared by TLR2 and TLR4. *Nature,* 420**,** 324-329.
YANG, D. C., PETERS, N. T., PARZYCH, K. R., UEHARA, T., MARKOVSKI, M. & BERNHARDT, T. G. 2011. An ATP-binding cassette transporter-like complex governs cell-wall hydrolysis at the bacterial cytokinetic ring. *Proc Natl Acad Sci U S A,* 108**,** E1052-60.
ZAFFAGNINI, G. & MARTENS, S. 2016. Mechanisms of selective autophagy. *Journal of molecular biology,* 428**,** 1714-1724.
ZHENG, Z., OMAIRI-NASSER, A., LI, X., DONG, C., LIN, Y., HASELKORN, R. & ZHAO, J. 2017. An amidase is required for proper intercellular communication in the filamentous *cyanobacterium Anabaena sp. PCC 7120*. *Proceedings of the National Academy of Sciences***,** 201621424.
ZUMLA, A., HAFNER, R., LIENHARDT, C., HOELSCHER, M. & NUNN, A. 2012. Advancing the development of tuberculosis therapy. *Nature Reviews Drug Discovery,* 11**,** 171-172.
ZUMLA, A., NAHID, P. & COLE, S. T. 2013. Advances in the development of new tuberculosis drugs and treatment regimens. *Nature reviews Drug discovery,* 12**,** 388-404.